



Universidade do Minho
Escola de Engenharia

**Immobilization of eco-friendly nanoparticles on different materials:
towards promising nanoplatforms for removal of pollutants from water**

Verónica Patrícia Moreira da Rocha

**Immobilization of eco-friendly
nanoparticles on different materials:
towards promising nanoplatforms for
removal of pollutants from water**



Universidade do Minho

Escola de Engenharia

Verónica Patrícia Moreira da Rocha

Immobilization of eco-friendly nanoparticles on different materials: towards promising nanoplatforms for removal of pollutants from water

Doctoral Thesis

Chemical and Biological Engineering

Work developed under supervision of

Professor Doctor Maria Teresa de Jesus Simões Campos Tavares

Professor Doctor Maria Isabel Pontes Correia Neves

DIREITOS DE AUTOR E CONDIÇÕES DE UTILIZAÇÃO DO TRABALHO POR TERCEIROS

Este é um trabalho académico que pode ser utilizado por terceiros desde que respeitadas as regras e boas práticas internacionalmente aceites, no que concerne aos direitos de autor e direitos conexos.

Assim, o presente trabalho pode ser utilizado nos termos previstos na licença abaixo indicada.

Caso o utilizador necessite de permissão para poder fazer um uso do trabalho em condições não previstas no licenciamento indicado, deverá contactar o autor, através do RepositóriUM da Universidade do Minho.

Licença concedida aos utilizadores deste trabalho



Atribuição-NãoComercial-SemDerivações

CC BY-NC-ND

<https://creativecommons.org/licenses/by-nc-nd/4.0/>

ACKNOWLEDGEMENTS

Chegou ao fim uma das etapas mais enriquecedoras e desafiantes, e por isso quero expressar os meus sinceros agradecimentos a todas as pessoas que contribuíram para a realização deste trabalho e para o meu crescimento pessoal.

Às minhas orientadoras, Professora Teresa Tavares e Professora Isabel Correia Neves, agradeço pela orientação, partilha de conhecimentos, ajuda, incentivo e por depositarem a vossa confiança no desenvolvimento deste trabalho. Muito obrigada por me darem a oportunidade de crescer a nível profissional e pessoal.

Agradeço ao Professor Pier Parpot, Professora Cristina Aguiar, Professora Sandra Franco, Eduardo Coelho, Raquel Bertão, Rita Silva e Luciana Pereira pela colaboração, apoio experimental e constante disponibilidade demonstrada. Um obrigada muito especial ao Pedro Santos, por todo o apoio a nível laboratorial, pelo constante incentivo e disponibilidade, sou muito grata por fazeres parte da minha vida.

Agradeço ao Centro de Engenharia Biológica e ao Centro de Química, ao corpo docente, técnico e de investigação. Um especial agradecimento à Engenheira Madalena Vieira, Sandra Souto, Aline Barros, Maura Silva, Raquel Pereira, Manuel Santos e Vitória Maciel por toda a ajuda prestada.

Aos colegas do Laboratório de Engenharia Química que me acompanharam nesta etapa: Bruna, Helena, Filomena, Jéssica, Jandira, Ziva, Idalina, Vítor, Mihaela e Valéria agradeço por todos os momentos de boa disposição e inter-ajuda.

Pela amizade incondicional, apoio, carinho e por me acolherem da melhor forma, agradeço aos amigos que Braga me trouxe: Lara, Elisa, Pedro Santos, Zlatina, Mariana, Fábio, Maria Antónia, Pedro Silva, Óscar e Isilda.

Por fim, agradeço aos meus pilares, a minha família e aos amigos de sempre. Obrigada por tudo e por tanto.

STATEMENT OF INTEGRITY

I hereby declare having conducted this academic work with integrity. I confirm that I have not used plagiarism or any form of undue use of information or falsification of results along the process leading to its elaboration.

I further declare that I have fully acknowledged the Code of Ethical Conduct of the University of Minho.

RESUMO

Imobilização de nanopartículas ecológicas em diferentes materiais: rumo a nanoplataformas promissoras para remoção de poluentes da água

A síntese verde de nanopartículas metálicas (NPM) através de extratos de plantas é um método alternativo com várias vantagens, tais como ser sustentável, económico e amigo do ambiente. Embora a síntese verde atenuar o impacto ambiental da produção de NPM, esta ainda apresenta limitações. O desenvolvimento de um método amigo do ambiente para a síntese de NPM com boa dispersão e estabilidade e a sua imobilização em suportes sustentáveis é altamente desejável. Nesta tese, foi desenvolvida uma nanoplataforma constituída por nanopartículas de prata (NPAg) suportadas em materiais sustentáveis para a remoção de poluentes da água. Inicialmente, diferentes extratos aquosos foram estudados de forma a selecionar o melhor extrato para sintetizar NPAg. Foi confirmada a capacidade dos extratos aquosos de folhas de eucalipto, chá verde e chá preto para sintetizar NPAg. Estas NPAg apresentaram efeito inibitório contra bactérias, sendo as NPAg sintetizadas com extrato aquoso de folhas de eucalipto (NPAg-Euc), as melhores nanopartículas com esta atividade. Posteriormente a sua atividade fotocatalítica foi confirmada pela degradação do corante carmim de índigo, como poluente modelo. Depois de selecionado o extrato aquoso para a obtenção de NPAg, foi otimizado e caracterizado o processo biosintético da produção de NPAg-Euc. Os melhores resultados foram obtidos com síntese a 50 °C e um rácio 1:2 de metal:extrato. Catequina, ácido elágico, rutina, ácido gálico, quercetina e kaempferol foram identificadas como biomoléculas envolvidas no processo de síntese de NPAg-Euc. Na remediação ambiental as NPAg-Euc otimizadas exibiram uma eficiente atividade antibacteriana e fotocatalítica. De forma a facilitar a recuperação, aumentar a estabilidade e dispersão das NPAg-Euc, materiais sustentáveis como argilas e resíduos foram aplicados como suportes. O compósito de NPAg-Euc/Caulim mostrou excelentes resultados na degradação do corante carmim de índigo, do herbicida atrazina e do antibiótico sulfametoxazol. Os resultados aqui apresentados contribuem para alargar a aplicação de NPM verdes na remediação ambiental bem como o uso de materiais sustentáveis como suportes para NPM.

Palavras-chave: Química verde; Nanopartículas ecológicas; Suportes sustentáveis; Atividade antibacteriana; Atividade fotocatalítica.

ABSTRACT

Immobilization of eco-friendly nanoparticles on different materials: towards promising nanoplatforms for removal of pollutants from water

The green synthesis of metallic nanoparticles (MNP) using plant extracts is an alternative production method with several advantages, such as being sustainable, competitive and environmental friendly. Although green synthesis mitigates the environmental impact of MNP production, it still has limitations. The development of an environmental friendly method for the synthesis of MNP with good dispersion and stability, and their immobilization on sustainable supports is highly desirable. In this thesis, a nanoplatform consisting of silver nanoparticles (AgNP) supported on sustainable materials was developed for the removal of pollutants from water. Initially, different aqueous extracts were studied in order to select the best extract for AgNP synthesis. The ability of aqueous extracts of eucalyptus leaves (ELE), green tea (GTE) and black tea (BTE) to synthesize NPAg was confirmed. These AgNP showed an inhibitory effect against bacteria, and the AgNP synthesized with aqueous ELE (ELE-AgNP) were the best ones with this activity. Their photocatalytic activity was subsequently confirmed in the degradation of the indigo carmine dye, as a model pollutant. After selecting the aqueous extract for the production of AgNP, the biosynthetic process for the production of ELE-AgNP was optimized and characterized. The best results were obtained with synthesis at 50 °C and a 1:2 metal:extract ratio. Catechin, ellagic acid, rutin, gallic acid, quercetin and kaempferol were identified as biomolecules involved in the ELE-AgNP synthesis process. In environmental remediation, the optimized ELE-AgNP exhibited efficient antibacterial and photocatalytic activity. In order to facilitate the recovery, to increase the stability and dispersion of the ELE-AgNP, sustainable materials such as clays and solid wastes were tested as supports. The ELE-AgNP/Kaolin composite showed excellent results in the degradation of the indigo carmine dye, the herbicide atrazine and the antibiotic sulphamethoxazole. The results presented here contribute to broadening the application of green MNP in environmental remediation as well as the use of sustainable materials as supports for MNP.

Keywords: Green Chemistry; Eco-friendly nanoparticles; Sustainable supports; Antibacterial activity; Photocatalytic activity.

TABLE OF CONTENTS

ACKNOWLEDGEMENTS.....	iii
RESUMO	v
ABSTRACT	vi
LIST OF FIGURES	x
LIST OF TABLES.....	xiii
LIST OF ABBREVIATIONS AND ACRONYMS.....	xiv
SCIENTIFIC OUTPUT	xvi
CHAPTER 1 RESEARCH MOTIVATION AND THESIS OUTLINE.....	1
1.1 THESIS MOTIVATION AND RESEARCH AIMS	2
1.2 OUTLINE OF THE THESIS	3
1.3 REFERENCES	4
CHAPTER 2 LITERATURE REVIEW.....	7
2.1 WASTEWATER TREATMENT	8
2.2 NANOTECHNOLOGY	9
2.3 BIO-INSPIRED FABRICATION OF METAL NANOPARTICLES	12
2.3.1 Adverse effects of suspension nanoparticles.....	14
2.4 SUPPORTED METAL NANOPARTICLES AS A GREEN APPROACH	15
2.4.1 Synthetic supports	16
2.4.2 Sustainable supports	18
2.5 ECONOMIC AND ENVIRONMENTAL PERSPECTIVE	38
2.6 REFERENCES	40
CHAPTER 3 VALORIZATION OF PLANT BY-PRODUCTS IN THE BIOSYNTHESIS OF SILVER NANOPARTICLES 58	
3.1 INTRODUCTION	59
3.2 MATERIALS AND METHODS.....	60

3.2.1	Chemicals	60
3.2.2	Preparation of plant extracts	61
3.2.3	Chemical characterization of plant extracts.....	61
3.2.4	Biofabrication of AgNP	63
3.2.5	Characterization of AgNP	63
3.2.6	Antibacterial activity	63
3.2.7	Photocatalytic activity.....	64
3.2.8	Statistical Analysis	64
3.3	RESULTS AND DISCUSSION	65
3.3.1	Selection and characterization of aqueous plant extracts.....	65
3.3.2	Green synthesis of AgNP.....	69
3.3.3	Antibacterial activity of aqueous extracts and AgNP	75
3.3.4	Photocatalytic activity of ELE-AgNP.....	77
3.3.5	Cost estimation of AgNP biofabrication.....	81
3.4	CONCLUSIONS.....	83
3.5	REFERENCES	83
CHAPTER 4	EXPLORATION OF GREEN SILVER NANOPARTICLES USING EUCALYPTUS LEAVES EXTRACT	
	90	
4.1	OPTIMIZATION AND CHARACTERIZATION OF BIOSYNTHETIC PROCESS	91
4.1.1	INTRODUCTION.....	91
4.1.2	MATERIALS AND METHODS	91
4.1.3	RESULTS AND DISCUSSION	94
4.1.4	CONCLUSIONS.....	109
4.1.5	REFERENCES	110
4.2	ANTIBACTERIAL AND PHOTOCATALYTIC BEHAVIOR OF OPTIMIZED AgNP	116
4.2.1	INTRODUCTION.....	116

4.2.2	MATERIALS AND METHODS	117
4.2.3	RESULTS AND DISCUSSION	119
4.2.4	CONCLUSIONS.....	124
4.2.5	REFERENCES	124
CHAPTER 5 RECYCLING OF SUSTAINABLE MATERIALS AS SUPPORTS FOR GREEN SILVER NANOPARTICLES 128		
5.1	INTRODUCTION	129
5.2	MATERIAL AND METHODS.....	131
5.2.1	Chemicals	131
5.2.2	Biosynthesis of AgNP/composite.....	132
5.2.3	Characterization of the nanocomposites	132
5.2.4	Photocatalytic activity.....	132
5.2.5	Statistical analysis.....	134
5.3	RESULTS AND DISCUSSION	134
5.3.1	Influence of biosynthesis experimental parameters for AgNP/kaolin on the rate of degradation 140	
5.3.2	Evaluation of photocatalytic performance.....	146
5.3.3	Effect of spectrum, wavelength and intensity of visible light.....	149
5.4	CONCLUSIONS	150
5.5	REFERENCES	151
CHAPTER 6 GENERAL CONCLUSIONS AND FUTURE PERSPECTIVES..... 155		
6.1	GENERAL CONCLUSIONS	156
6.2	FUTURE WORK	160

LIST OF FIGURES

Figure 2-1. Approaches applied to the synthesis of metal nanoparticles (MNP): Adapted from [22].	10
Figure 2-2. Bio-resources: bacteria, fungi, yeast, algae and plants and some examples of sustainable materials: clays, sands, rocks, activated carbon and residues from forest.	12
Figure 2-3. Green approaches for the synthesis of metal nanoparticles (MNP) supported on solid materials. .	16
Figure 3-1. Total phenolic content (TPC) (A) and Total flavonoids content (TFC) (B) of plant extracts. Values are expressed as mean \pm SD. Different lowercase letters show significant differences ($p < 0.05$) between extraction conditions for the same plant by-products. Different capital letters show significant differences ($p < 0.05$) between plant extracts for the same extraction conditions.	67
Figure 3-2. Changes in the color of the colloidal solutions indicate the formation of silver nanoparticles (AgNP): (A) 1. Silver nitrate (AgNO_3) solution; 2. Addition of eucalyptus leaves extract (ELE) to AgNO_3 solution at zero time (start of reaction) and 3. After 1 h of reaction at 50 °C (end of reaction). (B) UV-visible spectra of AgNP synthesized by aqueous extracts from eucalyptus leaves (ELE-AgNP), green tea (GTE-AgNP) and black tea (BTE-AgNP).	70
Figure 3-3. SEM images of AgNP synthesized by eucalyptus leaves (ELE), green tea (GTE) and black tea (BTE) extracts: (A) ELE-AgNP (B) GTE-AgNP (C) BTE-AgNP.	71
Figure 3-4. EDX spectra of (A) ELE-AgNP (B) GTE-AgNP (C) BTE-AgNP.	72
Figure 3-5. FTIR of extracts from (A) eucalyptus leaves (ELE), (B) green tea (GTE) and (C) black tea (BTE) and biosynthesized AgNP: (A) ELE-AgNP, (B) GTE-AgNP and (C) BTE-AgNP.	74
Figure 3-6. Schematic illustration of the mechanism of plant-mediated synthesis of silver nanoparticles (AgNP): Adapted from [62].	75
Figure 3-7. (A) Degradation efficiency of indigo carmine (IC) dye by biosynthesized ELE-AgNP and (B) pseudo-first-order reaction kinetics for IC decolorization by ELE-AgNP 0.5 g.L ⁻¹ ($R^2=0.9192$) and ELE-AgNP 1 g.L ⁻¹ ($R^2=0.9513$).	79
Figure 3-8. Flowchart for the preparation of 1 g of green AgNP.	81
Figure 4-1. Schematic representation of the synthesis of AgNP using eucalyptus leaves extract (ELE).	93
Figure 4-2. Evaluation of (A) optical properties by UV-Vis, (B) functional structure by FTIR and (C-E) surface morphology and texture by SEM of AgNP biosynthesized with eucalyptus leaves extract (ELE) at different synthesis conditions: (C) $\text{AgNP}_{\text{RT};1;1}$ at 30.00 k x magnification, (D) $\text{AgNP}_{50^\circ\text{C};1;1}$ at 100 000 x magnification and (E) $\text{AgNP}_{50^\circ\text{C};1;2}$ at 100 000 x magnification.	96
Figure 4-3. Survey XPS spectra of (A) $\text{AgNP}_{\text{RT};1;1}$ and (B) $\text{AgNP}_{50^\circ\text{C};1;1}$	97

Figure 4-4. High resolution XPS spectra of (A) C 1s and (B) O 1s from AgNP _{50°C:1:1} . High resolution XPS spectra of Ag 3d region for (C) AgNP _{RT:1:1} and (D) AgNP _{50°C:1:1} and Auger spectra for (E) AgNP _{RT:1:1} and (F) AgNP _{50°C:1:1} ...	100
Figure 4-5. Thermogravimetric analysis of (A) AgNP _{50°C:1:1} and (B) AgNP _{50°C:1:2} ; (C) Zeta potential evaluation during 3 months and (D) XRD pattern exhibiting the fcc structure of AgNP _{50°C:1:2}	102
Figure 4-6. GC-MS chromatogram of aqueous eucalyptus leaves extract (ELE).....	104
Figure 4-7. Phenolic profile of eucalyptus leaves obtained after aqueous extraction by HPLC-MS.....	107
Figure 4-8. Antibacterial activity of AgNP _{50°C:1:2} at range concentration 1-10 mg.mL ⁻¹ . The symbol * shows significant differences (p < 0.05) between inhibition zone of the same concentration of AgNP in different bacteria.	119
Figure 4-9. Evaluation of photocatalytic efficiency of AgNP _{50°C:1:2} under different irradiations (A) Indigo Carmine (IC) dye, (B) Decolorization efficiency vs time and (C) ln (C/C ₀) vs time.....	121
Figure 4-10. UV-visible spectra of Indigo Carmine (IC) degradation in the the presence of AgNP _{50°C:1:2} under (A) Visible irradiation, (B) UV irradiation and (C) Sunlight.....	122
Figure 4-11. Germination test results. (A) Ultrapure water, (B) IC solution at 10 mg.L ⁻¹ untreated, (C) IC solution after 120 min of photodegradation in the presence of AgNP _{50°C:1:2} under: UV light irradiation, (D) visible light irradiation and (E) direct sunlight irradiation.	123
Figure 5-1. Radiance spectra of the different visible light emitted by LED lamps.	134
Figure 5-2. FTIR spectra of (A) different clays (kaolin, vermiculite, bentonite and sepiolite) and (B) pistachio shell used as a sustainable supports for AgNP.....	137
Figure 5-3. Evaluation of photocatalytic efficiency of AgNP/kaolin and AgNP/pistachio synthesized with 2 g of kaolin or pistachio shell with 100 mL de AgNO ₃ and 100 mL of ELE at RT: (A) Decolorization efficiency (%) vs time and (B) ln (C/C ₀) vs time.....	139
Figure 5-4. Photocatalytic efficiency of AgNP/kaolin composites synthesized with different volumes of AgNO ₃ and ELE, at 50 °C and RT: (A and C) Decolorization efficiency (%) vs time and (B and D) ln (C/C ₀) vs time.	141
Figure 5-5. Evaluation of optical properties by UV-Vis of AgNP/kaolin composites synthesized at (A) 50 °C and (B) RT.....	142
Figure 5-6. Images of TEM of AgNP/kaolin _{50:50 50°C} (A-B) and AgNP/kaolin _{50:50 RT} (C-D) with different scales.	143
Figure 5-7. Survey XPS spectra of (A) AgNP/kaolin _{50:50 RT} and (B) AgNP/kaolin _{50:50 50 °C}	144
Figure 5-8. Photocatalytic degradation of IC dye with AgNP/kaolin _{50:50 RT} in the absence and presence of scavengers (EDTA-2Na, IPA and BQ) under visible light irradiation.	147

Figure 5-9. Photocatalytic efficiency of AgNP/kaolin_{50:50 RT} on the degradation of both organic compounds: (A) Photocatalytic efficiency *vs* time and (B) $\ln(C/C_0)$ *vs* time..... 148

Figure 5-10. FTIR spectra of AgNP/kaolin_{50:50 RT} before and after the photodegradation of ATZ, SMX and IC.... 149

LIST OF TABLES

Table 2-1. Natural materials as supports for biogenic MNP with applications in wastewater treatment.	23
Table 2-2. Waste materials as supports for biogenic MNP with applications in wastewater treatment.	30
Table 2-3. Biochar and activated carbon as supports for biogenic MNP, with applications in wastewater treatment.....	35
Table 3-1. Antioxidant activity of selected plant aqueous extracts.....	68
Table 3-2. Inhibition zones of the aqueous plant extracts and AgNP against Gram-positive and Gram-negative bacterial strains.	77
Table 3-3. Comparative performance of silver nanoparticles (AgNP) and their composites for photodegradation of indigo carmine (IC) dye.	80
Table 3-4. Estimation cost of preparation of 1 g of AgNP.....	82
Table 4-1. Binding energies (BE) and the amount of the elements (wt%) from the XPS resolution spectra in the C 1s, O 1s, Cl 2p, N 1s and Ag 3d regions of the samples.....	98
Table 4-2. Kinetic energies (KE), Auger Parameter (AP) and the contribution of the silver species in the Ag 3d region of the samples.....	101
Table 4-3. Identification of the volatile compounds present in aqueous extract of eucalyptus leaves (ELE)...	105
Table 4-4. Concentration of volatile compounds identified by GC-MS.	106
Table 4-5. HPLC-MS fragmentation profile and abundance of phenolic compounds identified in eucalyptus leaves extract (ELE) before and after AgNP synthesis.	108
Table 4-6. Values of decolorization efficiency (%), kinetic constant ($k = \text{min}^{-1}$) and linear correlation coefficient (R^2) for IC photodegradation under UV, visible and sunlight irradiation.	122
Table 5-1. Physicochemical properties of selected pollutants [21].	131
Table 5-2. Screening tests of IC photodegradation with AgNP/composites synthesized in identical conditions (2 g of sustainable material with 20 mL de AgNO_3 and 20 mL of ELE at 50 °C).	136
Table 5-3. Experimental conditions tested for the synthesis of AgNP/kaolin composite.	140
Table 5-4. Binding energies (BE) and the relative amount of the surface elements (wt%) from the XPS spectra in the Si 2p, Al 2p, Cl 2p, O 1s, C 1s, Ag 3d and Fe 2p regions of AgNP/kaolin samples.	145
Table 5-5. Spectrum, wavelength and intensity of visible light on the decolorization efficiency and mineralization of IC dye using AgNP/kaolin _{50:50 RT} as photocatalyst.....	150

LIST OF ABBREVIATIONS AND ACRONYMS

ABTS – 2,2'-Azino-bis(3-ethylbenzothiazoline-6-sulfonic acid) diammonium salt

AgNP – Silver nanoparticles

ANOVA – Analysis of Variance

AOP – Advanced oxidation processes

AP – Auger parameter

ATZ – Atrazine

ATR – Attenuated total reflectance

BE – Binding energy

BET – Brunauer-Emmett-Teller model

BQ – 1,4-benzoquinone

BTE – Black tea extract

CE – Catechin equivalents

CTAB – Cetyltrimethylammonium bromide

DPPH – 2,2-Di(4-tert-octylphenyl)-1-picrylhydrazyl

EDX – Energy-dispersive X-ray spectroscopy

EDTA-2Na - Ethylenediaminetetraacetic acid disodium salt dehydrate

ELE – Eucalyptus leaves extract

FAO – Food and Agriculture Organization

FRAP – Ferric reducing antioxidant power

FTIR – Fourier transform infrared spectroscopy

GAE – Gallic acid equivalents

GC-MS – Gas chromatography linked with mass spectrometry

GO – Graphene oxide

GTE – Green tea extract

IC – Indigo carmine

IPA – Isopropyl Alcohol

k – apparent rate constant

KE – Kinetic energy

LED – Light emitting diode
MNP – Metal nanoparticles
MONP – Metal oxide nanoparticles
NP – Nanoparticles
nZVI – Nano zerovalent iron
PSf – Polysulfone
PVDF – Polyvinylidene fluoride
rGO – Reduced graphene oxide
RE – Rutin equivalents
ROS – Reactive Oxygen Species
RT – Room temperature
SD – Standard deviation
SEM – Scanning electron microscopy
SDG – Sustainable development goals
SMX – Sulfamethazaxole
SPR – Surface plasmon resonance
TE – Trolox equivalents
TFC – Total flavonoid content
TGA – Thermogravimetric Analysis
TPC – Total phenolic content
TPTZ – 2,4,6-Tris(2-pyridyl)-s-triazine
Trolox – 6-Hydroxy-2,5,7,8-tetramethylchromane-2-carboxylic acid
TUD – Technische Universiteit Delft
WWTP – Wastewater treatment plants
UHPLC-DAD – Ultra-high performance liquid chromatography with diode array detector
UV – Ultraviolet
UV-vis – Ultraviolet-visible spectroscopy
XPS – X-ray photoelectron spectroscopy
XRD – X-Ray Diffraction

SCIENTIFIC OUTPUT

According to the 2nd paragraph of the article 8 of the Portuguese Decree-Law no. 388/70, the scientific outputs of this thesis are listed below.

The results presented in this thesis have been partially published elsewhere.

Published manuscripts under de scope of the activity of Chemical Engineering Lab:

Rocha, V., Ferreira-Santos, P., Genisheva, Z., Coelho, E., Neves, I.C., Tavares, T., 2023, Unveiling the environmental remediation action promoted by silver nanoparticles biosynthesized by eucalyptus leaves extract. *Journal of Water Process Engineering*. <https://doi.org/10.1016/j.jwpe.2023.104431>

Silva, B., **Rocha, V.**, Lago, A., Costa, F., Tavares, T., 2021, Rehabilitation of a complex industrial wastewater containing heavy metals and organic solvents using low cost permeable bio-barriers – from lab-scale to pilot-scale. *Separation and Purification Technology*. <https://doi.org/10.1016/j.seppur.2021.118381>

Silva, B., Martins, M., Rosca, M., **Rocha, V.**, Lago, A., Neves, I. C., Tavares, T., 2020, Waste-based biosorbents as cost-effective alternatives to commercial adsorbents for the retention of fluoxetine from water. *Separation and Purification Technology*, <https://doi.org/10.1016/j.seppur.2019.116139>

Costa, F., Lago, A., Barros, Ó., **Rocha, V.**, Vipotnik, Z., Silva, B., Tavares, T., 2020, Chapter 14 - Retention of organic micro-pollutants by sorption processes, *Current Developments in Biotechnology and Bioengineering*, <https://doi.org/10.1016/B978-0-12-819594-9.00014-0>

Costa, F., Lago, A., **Rocha, V.**, Barros, Ó., Costa, L., Vipotnik, Z., Silva, B., Tavares, T., 2019, A Review on Biological Processes for Pharmaceuticals Wastes Abatement—A Growing Threat to Modern Society. *Environmental Science & Technology* <https://doi.org/10.1021/acs.est.8b06977>

Barros, O., Costa, L., Costa, F., Lago, A., **Rocha, V.**, Vipotnik, Z., Silva, B., Tavares, T., 2019, Recovery of rare earth elements from wastewater towards a circular economy. *Molecules*, <https://doi.org/10.3390/molecules24061005>

Manuscripts under submission:

Rocha, V., Lago, A., Silva, B., Barros, Ó., Neves, I.C., Tavares, T., Immobilization of biogenic metal nanoparticles on sustainable materials - green approach applied to wastewater treatment: a systematic review – under revision in the Environmental Science: Nano

Rocha, V., Ferreira-Santos, P., Aguiar, C., Neves, I.C., Tavares, T., Valorization of plant by-products in the green synthesis of silver nanoparticles with antibacterial and catalytic applications – under revision in the Colloids & Surfaces B: Biointerfaces

Rocha, V., Franco, S., Bertão, A.R., Neves, I.C., Tavares, T., Recycling of natural and waste materials as supports for green-AgNP as efficient catalysts in photodegradation of organic pollutants – under revision in the Environmental Research

Lago, A.; **Rocha, V.**; Barros, Ó., Silva, B., Tavares, T., Bacterial biofilm attachment to sustainable carriers as a clean-up strategy for wastewater treatment: a review – under revision in Journal of Water Process Engineering

Oral communications in conferences:

Rocha V., Neves I.C., Tavares T., Green fabrication of silver nanoparticles using *Eucalyptus spp.* leaves extract and their application in wastewater remediation. July 2022. 5th International Conference EWaS – Naples, Italy.

Silva, B., **Rocha, V.**, Lago, A., Tavares, T. Valorization of spent coffee grounds as biosorbent for the retention of fluoxetine from water – a cost-effective alternative to activated carbon. October 2018. 13th International Chemical and Biological Engineering Conference. Aveiro, Portugal.

Posters in conferences:

Lago, A., **Rocha, V.**, Costa, F., Silva, B., Tavares, T. Rehabilitation of water contaminated with an organic solvent by an aerobic bacterium: tolerance and bioremoval assays. July 2019. 5th International Congress on Water, Waste and Energy Management. Paris, France.

CHAPTER 1 RESEARCH MOTIVATION AND THESIS OUTLINE

This chapter presents the background information supporting this work, as well as its objectives. This PhD thesis was carried out at Centre of Biological Engineering (CEB) at the Department of Biologic Engineering and Centre of Chemistry (CQ-UM) at the Department of Chemistry of the University of Minho. The thesis is divided in 6 chapters. Chapters 1, 2 and 6 correspond to the research motivation, state of the art and main conclusions and suggestions for future work, respectively. The main core of the text (Chapters 3 to 5) is based on 3 scientific papers, under revision in refereed Journals. The outline of the thesis is also presented.

1.1 THESIS MOTIVATION AND RESEARCH AIMS

The continuous growth of global population, rapid industrialization and urbanization result in an increasing demand of chemicals, materials and energy [1]. The release of unwanted wastes into the environment from numerous anthropogenic sources has been inevitably accompanied by a weaker quality of environmental systems [2]. Currently, there is a growing focus on the environmental pollution issue. The escalating pollution levels in soil, water and air, emerge as a major concern, particularly when it comes to water. The pollution of water sources is a pressing problem given its limited availability. Recognizing its significance, the United Nations has prioritized water quality as a crucial objective among the 17 sustainable development goals (SDG) outlined in the 2030 Agenda for Sustainable Development. These goals aim to mitigate poverty, preserve biodiversity, address climate change and enhance the well-being of individuals worldwide [3,4]. There is an urgent need for the development of sustainable, efficient and cost-effective materials/methods for the elimination or effective reduction of pollutants and microorganisms in wastewater and drinking water [5].

Nanotechnology is becoming an increasingly significant tool to achieve the SDG, in particular in the areas of environmental protection and circular economy and offers many opportunities and alternatives for the development of the next-generation water treatment processes [6,7]. Metal nanoparticles (MNP) often display high specific surface area, high surface free energy, relevant reactive sites, fast dissolution and various discontinuous properties such as supermagnetism, localized surface plasmon resonance (SPR) and quantum confinement effect [8]. Generally, MNP are synthesized by various physical and chemical techniques but the biosynthesis of MNP has attracted interest in recent years. Among other bio-resources, plant extracts have shown their effectiveness in such biosynthesis [9,10].

The advanced oxidation processes (AOP) are an alternative approach to eliminate pollutants from aqueous environments that consist of several groups of technologies that have been used with high efficiency in the treatment of water and wastewater [11]. Among them, photocatalysis has demonstrated considerable potential as an environmental friendly, low-cost and sustainable treatment technique [12]. This oxidation treatment approach has been demonstrated to be effective in eliminating microorganisms and organic pollutants from wastewater and does not generate additional waste, since the produced radicals degrade the organic pollutants indiscriminately [13].

One of the most important drawbacks of many reported photocatalytic systems is related to their small particle size, often present as MNP [14]. The use of powder MNP in photocatalytic reactors causes a non-uniform pore distribution/low surface area and formation of a colloidal dispersion with water, which makes reusability difficult [15,16]. The immobilization of MNP onto a support is a convenient alternative to attenuate the problems of powder filtration and catalyst recovery [17]. In this context, the usage of techniques that facilitates the reuse of spent catalyst will come a long way in making the photocatalysis processes eco-friendlier [18]. Therefore, the immobilization of MNP can eliminate costly and impractical post-treatment recovery of spent photocatalysts in large-scale operations.

Motivated by that, the ultimate goal of the work developed in this thesis is the development of an efficient nanocomposite based on eco-friendly nanoparticles supported on natural materials to be used as a heterogeneous catalyst for removing pollutants from water, thus, defining a clean technology that may rehabilitate water without resort to dangerous chemicals and with low waste generation.

The key challenges are:

- Is it possible to make the green synthesis of MNP more sustainable?
- Is it possible to understand the different parameters' influence in the synthesis of green MNP?
- Is it possible to develop nanocomposites with natural materials and maintain their effective photocatalytic properties?
- How do different sustainable materials behave as supports for green MNP?

Answering these challenges are the main objectives of this PhD thesis. To do so, green silver nanoparticles (AgNP), using different plant by-products, were developed and characterized regarding their optical, morphological and thermal properties; the antibacterial and catalytic activity was assessed; the selection of natural and low-cost or waste materials to function as supports for AgNP was also performed.

1.2 OUTLINE OF THE THESIS

Based on the previously described main objectives and following the research aims, this thesis was organized in 6 chapters.

The context, motivation and research aims of the thesis are presented in **Chapter 1**.

Chapter 2 provides the state of the art of the overarching topic of the thesis, nanotechnology, bio-inspired fabrication of metal nanoparticles and the development of supported metal nanoparticles, as well as the economic and environmental perspective.

Chapters 3 to 5 report, analyse and discuss the main results obtained.

Specifically, **Chapter 3** explores the importance of the selection of plant extracts and their chemical characterization before the synthesis of AgNP. The importance of previous optimization of the extraction process is emphasized, guaranteeing the extraction's efficiency and reducing energetic costs through a more sustainable process. In this chapter, the biosynthesized AgNP show their multifunction properties as antibacterial and photocatalyst.

Chapter 4 goes into further detail about the optimization and the characterization of the biosynthetic process of AgNP using aqueous extract from *Eucalyptus globulus* leaves, a raw material very common in Portugal, as well as the identification of some biomolecules involved in the AgNP synthesis. This chapter was divided in two subchapters. Subchapter 4.1 describes the results of the optimization of biosynthetic process. In turn, subchapter 4.2 includes the results of the antibacterial and photocatalytic behavior assessment of optimized AgNP against pathogenic bacteria and of the photocatalysis for the degradation of the indigo carmine under ultraviolet light, visible light and sunlight irradiation.

In **Chapter 5**, the recycling of natural and waste materials as solid supports for AgNP synthesized *in situ* using eucalyptus leaves extract and assessment of the influence of different synthesis parameters to make the process more sustainable, efficient and cost-effective are presented. Additionally, the photocatalytic ability to promote the degradation of Indigo Carmine dye, of the herbicide atrazine and of the antibiotic sulfamethoxazole under visible light is presented.

Finally, **Chapter 6** presents the main findings of this PhD thesis and suggests future lines of work in this research topic.

1.3 REFERENCES

- [1] P. Rani, V. Kumar, P.P. Singh, A.S. Matharu, W. Zhang, K.-H. Kim, J. Singh, M. Rawat, Highly stable AgNPs prepared via a novel green approach for catalytic and photocatalytic removal of biological and non-biological pollutants, *Environ. Int.* 143 (2020) 105924. <https://doi.org/https://doi.org/10.1016/j.envint.2020.105924>.

- [2] H. Ali, E. Khan, I. Ilahi, *Environmental Chemistry and Ecotoxicology of Hazardous Heavy Metals: Environmental Persistence, Toxicity, and Bioaccumulation*, *J. Chem.* 2019 (2019) 6730305. <https://doi.org/10.1155/2019/6730305>.
- [3] S. Axon, D. James, *The UN Sustainable Development Goals: How can sustainable chemistry contribute? A view from the chemical industry*, *Curr. Opin. Green Sustain. Chem.* 13 (2018) 140–145. <https://doi.org/https://doi.org/10.1016/j.cogsc.2018.04.010>.
- [4] United Nations, *Sustainable Development Goals*, (2016). <https://sustainabledevelopment.un.org/sdgs> (accessed June 24, 2023).
- [5] M.O. Alfred, M.O. Omorogie, O. Bodede, R. Moodley, A. Ogunlaja, O.G. Adeyemi, C. Günter, A. Taubert, I. Iermak, H. Eckert, I.D.A. Silva, A.S.S. de Camargo, A. de Jesus Motheo, S.M. Clarke, E.I. Unuabonah, *Solar-active clay-TiO₂ nanocomposites prepared via biomass assisted synthesis: Efficient removal of ampicillin, sulfamethoxazole and artemether from water*, *Chem. Eng. J.* 398 (2020) 125544. <https://doi.org/https://doi.org/10.1016/j.cej.2020.125544>.
- [6] L. Pokrajac, A. Abbas, W. Chrzanowski, G.M. Dias, B.J. Eggleton, S. Maguire, E. Maine, T. Malloy, J. Nathwani, L. Nazar, A. Sips, J. Sone, A. van den Berg, P.S. Weiss, S. Mitra, *Nanotechnology for a Sustainable Future: Addressing Global Challenges with the International Network4Sustainable Nanotechnology*, *ACS Nano.* 15 (2021) 18608–18623. <https://doi.org/10.1021/acsnano.1c10919>.
- [7] L. Zhao, J. Deng, P. Sun, J. Liu, Y. Ji, N. Nakada, Z. Qiao, H. Tanaka, Y. Yang, *Nanomaterials for treating emerging contaminants in water by adsorption and photocatalysis: Systematic review and bibliometric analysis*, *Sci. Total Environ.* 627 (2018) 1253–1263. <https://doi.org/10.1016/j.scitotenv.2018.02.006>.
- [8] E. Friehs, Y. AlSalka, R. Jonczyk, A. Lavrentieva, A. Jochums, J.-G. Walter, F. Stahl, T. Scheper, D. Bahnemann, *Toxicity, phototoxicity and biocidal activity of nanoparticles employed in photocatalysis*, *J. Photochem. Photobiol. C Photochem. Rev.* 29 (2016) 1–28. <https://doi.org/10.1016/J.JPHOTOCHEMREV.2016.09.001>.
- [9] A.M. El Shafey, *Green synthesis of metal and metal oxide nanoparticles from plant leaf extracts and their applications: A review*, *Green Process. Synth.* 9 (2020) 304–339. <https://doi.org/doi:10.1515/gps-2020-0031>.
- [10] S. Jadoun, R. Arif, N.K. Jangid, R.K. Meena, *Green synthesis of nanoparticles using plant extracts: a review*, *Environ. Chem. Lett.* 19 (2021) 355–374. <https://doi.org/10.1007/s10311-020-01074-x>.
- [11] M. Malakootian, A. Shahesmaeili, M. Faraji, H. Amiri, S. Silva Martinez, *Advanced oxidation processes for the removal of organophosphorus pesticides in aqueous matrices: A systematic review and meta-analysis*, *Process Saf. Environ. Prot.* 134 (2020) 292–307. <https://doi.org/10.1016/J.PSEP.2019.12.004>.
- [12] M.N. Chong, B. Jin, C.W.K. Chow, C. Saint, *Recent developments in photocatalytic water treatment technology: A review*, *Water Res.* 44 (2010) 2997–3027. <https://doi.org/https://doi.org/10.1016/j.watres.2010.02.039>.
- [13] O. Samuel, M.H.D. Othman, R. Kamaludin, H. Dzinun, A. Imtiaz, T. Li, T. El-badawy, A.U. Khan, M.H. Puteh, E. Yuliwati, T.A. Kurniawan, *Photocatalytic degradation of recalcitrant aromatic hydrocarbon compounds in oilfield-produced water: A critical review*, *J. Clean. Prod.* 415 (2023) 137567. <https://doi.org/https://doi.org/10.1016/j.jclepro.2023.137567>.
- [14] M. Akkari, P. Aranda, A. Mayoral, M. García-Hernández, A. Ben Haj Amara, E. Ruiz-Hitzky,

- Sepiolite nanoplatform for the simultaneous assembly of magnetite and zinc oxide nanoparticles as photocatalyst for improving removal of organic pollutants, *J. Hazard. Mater.* 340 (2017) 281–290. <https://doi.org/10.1016/J.JHAZMAT.2017.06.067>.
- [15] A. Mishra, A. Mehta, S. Kainth, S. Basu, Effect of different plasmonic metals on photocatalytic degradation of volatile organic compounds (VOCs) by bentonite/M-TiO₂ nanocomposites under UV/visible light, *Appl. Clay Sci.* 153 (2018). <https://doi.org/10.1016/j.clay.2017.11.040>.
- [16] H. Dong, G. Zeng, L. Tang, C. Fan, C. Zhang, X. He, Y. He, An overview on limitations of TiO₂-based particles for photocatalytic degradation of organic pollutants and the corresponding countermeasures, *Water Res.* 79 (2015) 128–146. <https://doi.org/10.1016/j.watres.2015.04.038>.
- [17] M. Sboui, M.F. Nsib, A. Rayes, M. Swaminathan, A. Houas, TiO₂-PANI/Cork composite: A new floating photocatalyst for the treatment of organic pollutants under sunlight irradiation, *J. Environ. Sci.* 60 (2017) 3–13. <https://doi.org/https://doi.org/10.1016/j.jes.2016.11.024>.
- [18] B. Srikanth, R. Goutham, R. Badri Narayan, A. Ramprasath, K.P. Gopinath, A.R. Sankaranarayanan, Recent advancements in supporting materials for immobilised photocatalytic applications in waste water treatment, *J. Environ. Manage.* 200 (2017) 60–78. <https://doi.org/https://doi.org/10.1016/j.jenvman.2017.05.063>.

CHAPTER 2 LITERATURE REVIEW

The application of the principles of green chemistry to the synthesis of metal nanoparticles (MNP) is a new emerging issue concerning sustainability. Together with the green nanotechnology, this is an evolving approach with innovative, reliable and sustainable solutions for applications in all fields of life. Those principles may be used on greener bio-inspired materials applied for the synthesis of MNP as well as for their immobilization on solid supports. This chapter provides a short survey of the topics related to the broad areas of this thesis, covering the available literature on the green fabrication of MNP from different bio-resources, ranging from micro- to macromolecular levels (bacteria, fungi, yeasts, algae and plants). These resources serve dual roles as both reducing and capping agents, facilitating the immobilization of biogenic MNP onto sustainable materials to improve their performance applied to wastewater treatment.



This chapter was adapted from:

Rocha, V., Lago, A., Silva, B., Barros, Ó, Neves, I.C., Tavares, T., *Immobilization of biogenic metal nanoparticles on sustainable materials - green approach applied to wastewater treatment: a systematic review* (under revision).

2.1 WASTEWATER TREATMENT

Environmental pollution is mainly caused due to the discharge of untreated or partially treated industrial waste into aquatic ecosystems [1]. Industrial effluents are a major concern as a threat to human health and the wastewater from various industries contains harmful and carcinogenic inorganic and organic contaminants [2]. The conventional wastewater treatment for these industries includes physicochemical (adsorption, sedimentation, coagulation and precipitation, chemical oxidation and membrane filtration) and biological (bacteria, fungi and algae metabolic degradation) methods [3]. Conventional techniques of wastewater treatment require a high energy input and their environmental impact is controversial [3]. Many efforts have been made over the last decades to reduce environmental pollution by developing suitable and sustainable treatment methods for pollutant removal [4]. However, new treatment technologies and infrastructures more environment eco-friendly are needed to provide high-quality water.

The AOP are employed to increase the efficiency reached by conventional wastewater treatments and fulfill the required limits set by various environmental regulations to deal with persistent pollutants present in low concentrations [5]. AOP are unselective processes based on the production of highly reactive radicals, which will destroy the pollutants into less complex compounds, followed by their complete mineralization that being the ideal scenario [6]. Many oxidant species are produced in the AOP, such as hydroxyl radicals ($\cdot\text{OH}$), superoxide radical anions ($\text{O}_2^{\cdot-}$), hydroperoxyl radical (HO_2^{\cdot}), hydrogen peroxide (H_2O_2), solvated electrons (e^-), hydrogen radicals ($\text{H}\cdot$), amongst others [7]. The most common radical generators/catalyst systems for AOP include Fenton's reagent involving iron species (Fe^{2+} or Fe^{3+}) and hydrogen peroxide (H_2O_2), ozone (O_3), ultraviolet (UV) radiation, $\text{H}_2\text{O}_2/\text{UV}$, $\text{H}_2\text{O}_2/\text{O}_3$, $\text{H}_2\text{O}_2/\text{O}_3/\text{UV}$, Fenton combined processes (ultrasound/electro/photo Fenton with addition of H_2O_2 and Fe^{2+}) and Photocatalysts/UV or visible or solar radiation [8].

Photocatalysis is one of the most promising technologies for the ecological degradation of pollutants present in wastewater [9]. This technology necessitates a semiconductor capable of producing radical species when activated by light. Photodegradation of wastewater pollutants using solar light may become an economically viable process, in particular for large-scale aqueous-phase applications [4]. Therefore, considerable effort has been applied to extend the photo-response of semiconductors into visible light region ($\sim 43\%$ of solar spectrum) [10]. The use of solar energy to degrade pollutants by

photocatalysis represents an economic and sustainable alternative to classical methods. The ideal photocatalyst would be nontoxic, stable, inexpensive, easily available and highly photoactive. Diverse nanomaterials such as carbon dots [11], MNPs [12], metal oxide nanoparticles (MONP) [13] have been used on the photocatalytic degradation of pollutants.

2.2 NANOTECHNOLOGY

The recent era of materials science and technology has observed the emergence of a new field of knowledge *viz.* nanotechnology [14]. Nanotechnology is an evolving field with the creation and utilization of materials with structural features of bulk materials with at least one dimension in the nanoscale [15]. Over the past few years, researchers have been developing and characterizing unique nanostructural morphologies such as nanowires, nanotubes, nanospheres, NP, etc., with several practical applications in engineering, materials science, chemistry, physics and biology [16]. Among the enormous variety of nanostructured materials that have emerged, MNP are considered the basic building blocks of nanotechnology and act as bridges between bulk materials and atomic or molecular structures [17,18]. The nanostructured materials find their pioneering applications in diverged areas ranging from medicine, agriculture, electronic elements fabrication, environmental waste remediation to several industrial domains [19]. MNP have gained prominence in technological advancements due to their tunable physicochemical characteristics such as melting point, wettability, electrical and thermal conductivity, catalytic activity, light absorption and scattering and surface area to volume ratio resulting in enhanced performance over their bulk counterparts [20].

The fabrication of MNP can be broadly categorized into two approaches: top-down and bottom-up (**Figure 2-1**) [21].

The top-down approach involves crushing or cutting the bulk materials into fine particles at the nanoscale, using processes such as arc discharge, ball milling, pulsed laser ablation, etc [15,20]. In the bottom-up approach, MNP are formed by assembling atom by atom, molecule by molecule or cluster by cluster [15,23]. This last approach includes numerous methods of synthesis: coprecipitation, chemical reduction of metal salts, electrochemical and green synthesis methods [22,24]. In the chemical synthesis of MNP, the chemical reduction of metal ions from salt solution in the presence of strong bases (reducing agents), sodium borohydride or sodium hydroxide is achieved, followed by the

addition of a stabilizing agent, also called the capping agent [25]. However, the reagents employed as reducing agents and the solvents used to dissolve the stabilizers are commonly toxic substances that have adverse and deleterious health and environmental effects [26,27]. The physical MNP synthesis is mainly a top-down approach in which the material is reduced in size by various physical approaches [28]. These conventional methods of MNP synthesis have various limitations such as the need of a huge amount of energy, the specific and costly equipment, the production of flammable hydrogen gas and the use of toxic chemicals such as sodium borohydride, organic solvents and, stabilizing and dispersing agents [29].

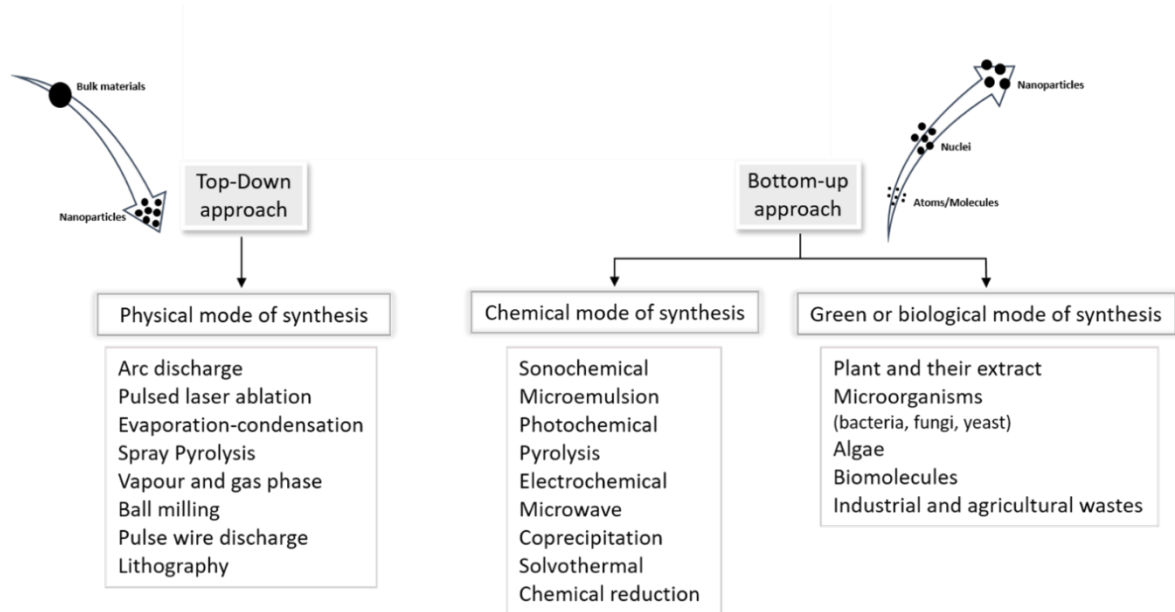


Figure 2-1. Approaches applied to the synthesis of metal nanoparticles (MNP): Adapted from [22].

In recent years, MNP appear as a new innovative tool with excellent potential for wastewater treatment through more effective strategies than previously explored ones [30]. The development of an environmental friendly, renewable, easy-to-implement and cost-effective means of MNP synthesis has become one of the foremost demands in the field of environmental remediation [31]. The bio-inspired fabrication is cost-effective, easy to implement, reduces the chemical load into the environment and eliminates unnecessary processing during synthesis [32,33].

Although the green synthesis mitigates the environmental impact in production of MNP, these biogenic procedures still suffer from certain limitations. In the last years, solid materials have been used as supports for MNP to prevent agglomeration and to overcome the obstacles associated with

stability and recovery. Additionally, the accumulation of MNP in the environment, after their intended use, also generates persistent MNP waste [34]. The development of an environmental friendly method for the synthesis of MNP with good dispersion and stability and their immobilization on effective and sustainable supports is highly desirable and it have progressively focused on green materials applied as support for MNP for sustainable development [35,36]. The interest in sustainable materials applied to support the biosynthesized MNP in the field of wastewater treatment became attractive.

The simultaneous use of bio-resources and sustainable materials as reducing/capping agents and supporting materials to obtain supported MNP is a significant green approach applied to wastewater treatment. Bearing this in mind, the present chapter consists in a survey of the literature currently available on the performance increase of biogenic MNP applied to wastewater treatment.

This chapter focused on biogenic MNP immobilized on sustainable materials is divided into two different goals:

- (i) Green fabrication of MNP from different bio-resources ranging from micro- to macromolecular levels (bacteria, fungi, yeasts, algae and plants (**Figure 2-2**)- acting as reducing and capping agents and a brief overview of the adverse effects of suspensions of MNP, emphasizing the need for solid-supported MNP;
- (ii) Immobilization of biogenic MNP on sustainable materials derived from earth-abundant and renewable materials (clays, natural zeolites, sediments, sands, rocks and volcanic glass), residues from food, industry and agro-forestry activities, activated carbon or biochar derived from wastes and their use as green nanocomposites with diverse applications for removal or degradation of various pollutants or disinfection of water (**Figure 2-2**).

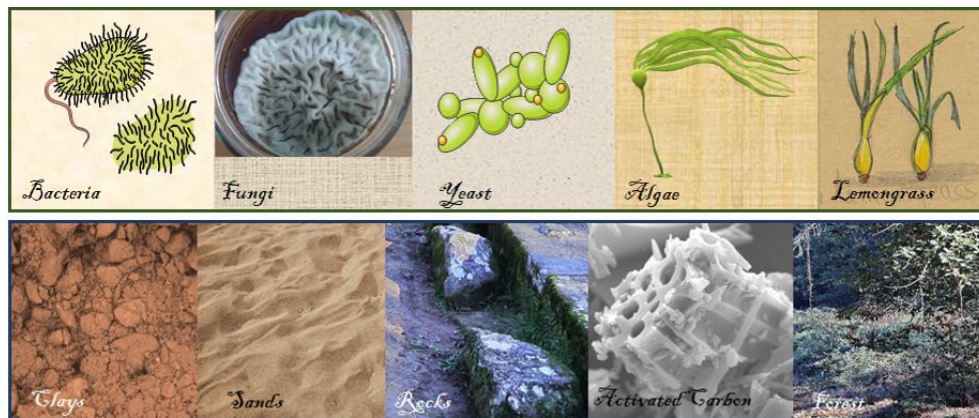


Figure 2-2. Bio-resources: bacteria, fungi, yeast, algae and plants and some examples of sustainable materials: clays, sands, rocks, activated carbon and residues from forest.

2.3 BIO-INSPIRED FABRICATION OF METAL NANOPARTICLES

In recent years, interest has grown for the implementation of environment friendly and economic remediation methods that guarantee low secondary impacts. Several green methods have been proposed and implemented for MNP synthesis. This field has received great attention due to its capability to design alternative, harmless, energy-efficient and less toxic routes towards the synthesis of these MNP. These routes have been associated with the rational utilization of various substances, and limited use of toxic precursors consequently reducing the quantity of impurities and by-products [37].

The bio-inspired fabrication of MNP involves the use of prokaryotic/eukaryotic cells or extracted biomolecules that act as reducing, stabilizing and capping agents [22]. The green synthetic processes comprise the use of either microorganisms such as bacteria [19,38], fungi [39,40] and yeasts [41,42], as well as algae [43,44] and plant biomass or plant extract [45,46].

Generically, microorganisms are endowed with excellent potential for adapting and surviving extreme conditions (pH, temperature, pressure and nutrient availability) due to their genetic biodiversity and thereby, they develop robust survival mechanisms [22]. Some metal ions are essential for their nutrition, whereas some others are reduced and/or oxidized to provide metabolic energy to counter non-essential toxic metal ions and thus microorganisms have developed a genetic and proteomic response for survival [33]. In the microbial cell-mediated synthesis of MNP, the formation of NP major routes are intracellular and extracellular processes that include bioaccumulation, precipitation,

biomineralization and biosorption, through which metal ions are reduced to MNP in the presence of cellular biomolecules [47,48]. Intracellular synthesis involves the formation of MNP within the cells by the transportation of metal ions across cell membranes. This process requires tolerance of microbial cells towards bio-reduction and the presence of aggregated MNP in the intercellular space may interrupt metabolic activities. The extracellular synthesis of MNP involves the formation of NP on the external layer of the cell membrane or most commonly, the extracellular MNP are synthesized using cell-free extracts of microbial cells [19]. The yeast-mediated synthesis of MNP has been found to be a cellular detoxification mechanism. Until now, there is no evidence to support the fact that yeast employs MNP in its metabolism [22]. Microbial cells are able to reduce a varied range of metal ions such as silver (Ag) [49], gold (Au) [50], iron (Fe) [51], copper (Cu) [52], cobalt (Co) [53], selenium (Se) [54], palladium (Pd) [55], lead (Pb) [56], zinc (Zn) [57] and titanium (Ti) [58] to their corresponding MNP and MONP.

Algae are economically and ecologically significant eukaryotic organisms that are increasingly being used as green bio-factories in the field of nanotechnology due to their high resilience to toxicity, coupled with high metal bio-accumulating and reducing capabilities [22]. The biological pathway for the synthesis of MNP is initiated by the adsorption of metallic ions on the algae cells surface. The metal ion is then synthesized either extracellularly or intracellularly (after influx through transmembrane protein by diffusion) by enzymatic machinery involving cytoplasm, thylakoid and membrane organelles [59]. Several studies have been performed to prepare a variety of MNP through algae, such as CuNP [60], AuNP [61], AgNP [62], ZnNP [63] and FeNP [64].

Plants have been reported to contain a huge variety of biomolecules that work in harmony to obstruct cellular components from oxidative damage, thereby resulting in metal ion reduction to MNP [22]. The first work on plants employed in the synthesis of MNP used *Medicago sativa* (alfalfa) which was able to synthesize AuNP and AgNP [65]. Since then, more attention has been scattered on plants. Most of the studies deal with the production of MNP by plants that are known to be more stable than MNP synthesized by microorganisms [66]. Biosynthesis can be achieved by plant tissues, extract of leaves, stems, roots, fruits, bark peels and flowers, being from a sustainable perspective, i.e. the utilization of renewable feedstock as precursor material.

2.3.1 Adverse effects of suspension nanoparticles

Suspension of MNP have been widely applied on the removal and/or degradation of various poisonous aqueous pollutants or on the disinfection of water. However, the accumulation of MNP in the environment, after their intended use, also generates persistent pollution and can provoke harmful effects on living organisms [34].

The MNP disposal by incineration or by land fill processes leads to the accumulation of the NP in land or in subaquatic sediments or to the dispersion in the atmosphere [67]. Shi *et al.* [68] studied the outcome of titanium dioxide (TiO₂) NP in wastewater treatment plants (WWTP) and although a part of the NP (>74%) was removed by the activated sludge, a significant concentration of them (27 to 43 µg.L⁻¹) was found in the effluents, which is higher than natural background levels (less than 5 µg.L⁻¹). After being released into the environment, the MNP can suffer different transformations such as agglomeration, sedimentation, oxidation, reduction, sulphidation, photochemical and biological mediated reactions [69–72].

The toxicity effects of citrate-coated AgNP in adult zebrafish *in vivo* are reported by Osborne *et al.* [73]. The authors show that the particle size and dissolution of Ag⁺ ions and subsequent reduction (Ag) from AgNP determined the toxic impact in the grills and intestines of zebrafish. Martin *et al.* [74] studied the effect of AgNP on a boreal lake, where the Ag accumulation was monitored in the tissues of yellow perch (*Perca flavescens*) and of northern pike (*Esox lucius*). It was found that both species accumulated Ag in their tissues during 2 years following exposure, with higher concentration detected in the liver. Toxic effects of AgNP of different sizes and surface functionalities were further investigated by Hou *et al.* [75] on aquatic crustacean *Daphnia magna*. Shi *et al.* [68] also report the presence of Ti in various fish tissues.

Studies to evaluate the phytotoxic impacts of suspended MNP have been also reported by Yin *et al.* [76] and showed that exposure of grass *Lolium multiflorum* to AgNP caused accumulation of Ag in the root and shoot, inhibiting seedling growth. Real *et al.* [77] studied the effect of wheat plants exposed to Ag in its different forms (AgNP, Ag₂SNP and Ag⁺ ions). Various chemical transformations were observed on the epidermis and inside of the roots after the exposure.

The wide application of MNP is limited by many obstacles such as the difficulty of manipulating the suspension, the ultimate health risks of the dissipation of MNP into the environment and instability of

size due to aggregation [78]. Synthesis of MNP on a solid support has emerged as a forthcoming solution that may prevent the accumulation of MNP waste in the ecosystem through a recycling process [34].

2.4 SUPPORTED METAL NANOPARTICLES AS A GREEN APPROACH

The bio-inspired fabrication of MNP on solid supports has emerged as a novel strategy for the sustainable development of nanotechnology. The easy recovery and reuse of the supported MNP avoid their accumulation into the environment and provide stability to the MNP. It further prevents aggregation and leaching of metal ions and thus reduces the expected toxicity of MNP [34]. Moreover, MNP powder is widely used in laboratory experiments for wastewater treatment, but for large-scale water treatment, immobilized MNP are much more desired [79,80].

A credible support-based material candidate should have high charge carrier mobility and thermal stability, high specific surface area, as well as a biocompatible nature [81–84]. Moreover, they should not be strong oxidant materials to restrict the production of harmful disinfectant by-products. The nature of the support will influence the performance kinetic and the leaching rate of the MNP [85]. Generally, supporting the MNP either by the usual chemical process or by the green methods into suitable carriers enhances the surface area, adsorption capacity and mechanical stability [86,87].

The attachment of MNP to the supporting medium can be performed by:

- (1) *in-situ* fabrication that involves the formation of a bond between metallic ions and the negatively charged of the functional groups of the supporting material, with the gradual reduction of the first that starts nucleating on the solid support (**Figure 2-3**);
- (2) *ex-situ* fabrication which includes the mixing of freshly pre-synthesized MNP with the supporting material by an electrostatic interaction between them (**Figure 2-3**) [34,88,89].

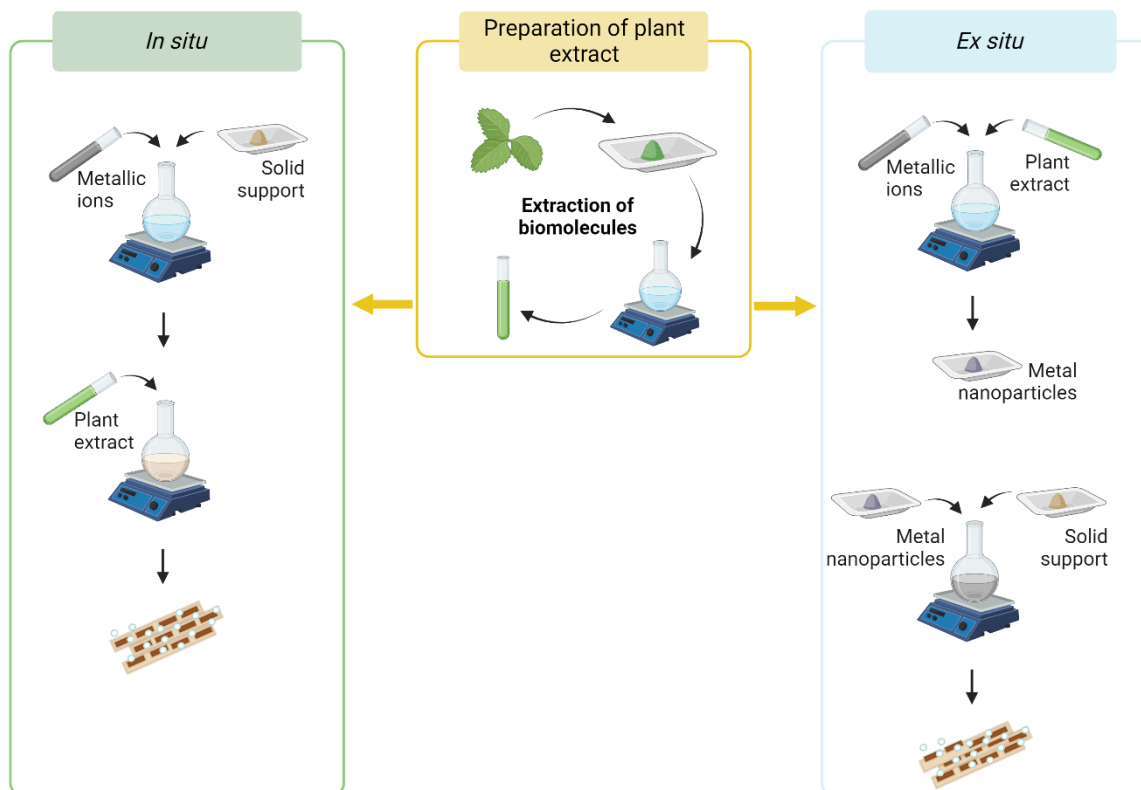


Figure 2-3. Green approaches for the synthesis of metal nanoparticles (MNP) supported on solid materials.

2.4.1 Synthetic supports

Different types of solid supports can be used for the immobilization of biogenic MNP and the most common are polymer-based membranes [90,91], glass [92], silica gel [93], commercial activated carbon [94], synthetic zeolites [95–97], resins [98], graphene oxide (GO) [99] and reduced graphene oxide (rGO) [100,101].

Amongst the different available synthetic supports, polymer-based membranes have received special attention due to their open structure and high internal surface area which ensure a high MNP loading and easy active site accessibility [102]. Hennebel *et al.* [90] described the degradation process of diatrizoate, a highly recalcitrant iodinated contrast medium, by using biogenic PdNP immobilized on polyvinylidene fluoride (PVDF) and on polysulfone (PSf) membranes. Arif *et al.* [91] studied the application of TiO₂NP synthesized through a green route using a PVDF polymer embedded in an extract of *Cajanus cajan* to develop a photocatalytic membrane. This membrane supporting biogenic TiO₂ acted

as a synergistic separation to reject chromium (Cr^{6+}) and further reduce the ion toxicity by photocatalytic reduction of the concentrated Cr^{6+} , achieving > 90% rejection and > 85% reduction of Cr^{6+} .

Zeolites acting as supports have been receiving considerable attention due to their high specific surface area, high catalytic activity, high thermal stability and exceptional structural properties with uniform distribution of pores and channels [97]. Nizam *et al.* [95] reported the use of biosynthesized magnetic iron (III) oxide (Fe_2O_3) NP immobilized on 13X zeolite ($\text{Fe}_2\text{O}_3/\text{MS}$) in the photocatalytic degradation of methylene blue. The results demonstrated excellent performance of $\text{Fe}_2\text{O}_3/\text{MS}$ on the photodegradation of the dye, with 99% of efficiency achieved in 150 min. The authors observed an enhanced photocatalytic performance of $\text{Fe}_2\text{O}_3/\text{MS}$ when compared to the pure synthesized Fe_2O_3 NP. Rostami-Vartooni *et al.* [96] investigated the use of magnetically recoverable $\text{Fe}_3\text{O}_4/\text{HZSM-5}$ as support for AgNP, synthesized in the presence of *Juglans regia L.* leaf extract. The authors found that the Ag/ $\text{Fe}_3\text{O}_4/\text{HZSM-5}$ nanocomposite showed high activity for the reduction of methyl orange and 4-nitrophenol, being reused three times without loss of activity. Also, Tajbakhsh *et al.* [97] studied the efficiency of Ag/HZSM-5 nanocomposite for the reduction of different organic dyes such as methylene blue, congo red, rhodamine B and 4-nitrophenol. The green synthesized Ag/HZSM-5 nanocomposite prepared using *Euphorbia heterophylla* leaf extract was found to be an efficient nanocatalyst with high regeneration potential.

Another class of graphene materials, GO and rGO, have been extensively used as promising supports for the immobilization of green MNP. These materials have many advantages such as large specific surface area, high adsorption capacity, good electrical conductivity and mechanical stability [100,103]. Naghdi *et al.* [99] reported the use of *Cuscuta reflexa* leaf extract for the biosynthesis of the Cu/GO/ MnO_2 nanocomposite as a heterogeneous catalyst for the reduction of 4-nitrophenol, 2,4-dinitrophenylhydrazine, congo red, methyl orange, methylene blue and rhodamine B. These authors reported a high catalytic activity of Cu/GO/ MnO_2 nanocomposite (100% of degradation attained instantly) as a recyclable heterogeneous catalyst for the reduction of all organic dyes and nitro compounds tested. Xue *et al.* [100] evaluated the use of rGO supported bimetallic Fe/NiNP (Fe/Ni-rGO) for the simultaneous removal of Rifampicin and Pb^{2+} from aqueous solution. It is stated that Fe/Ni-rGO nanocomposites prepared by green synthesis using green tea extract were effective for the removal of mixed Pb^{2+} and Rifampicin, being the removal efficiencies 81.9% and 94.3%, respectively. Ranjith *et al.* [101] synthesized a hybrid rGO- $\text{TiO}_2/\text{Co}_3\text{O}_4$ nanocomposite and studied the photocatalytic

degradation of methylene blue and crystal violet. The results revealed that the presence of rGO significantly induced the higher photocatalytic ability and the degradation of both dyes was more extensive under visible light irradiation.

For the sake of comparison and although the selected support is not a common material, the work of Harjati *et al.* [104] should be referred as they were able to synthesize green Fe₂O₃ supported on TUD-1 (a mesoporous material from Technische Universiteit Delft), using *Parkia speciosa hassk* pod extract as bioreductor agent. The support, in fact, is a three-dimensional mesoporous silicate synthesized in 2001 by Telalović *et al.* [105], with high specific surface area and with Brønsted acidic behaviour. These biosynthesized Fe₂O₃NP were immobilized on TUD-1 via the sol-gel method and their photocatalytic activity on bromophenol blue and methyl violet degradation was assessed.

Most of these nanocomposites were developed with expensive and sometimes not-readily available materials, which makes it difficult to scale-up their production to technologically relevant amounts. Alternative and sustainable supports have been recently employed on the preparation of supported MNP.

2.4.2 Sustainable supports

From the perspective of circular economy and green development, the application of natural materials, organic wastes, activated carbon or biochar, as solid supports for biogenic MNP, in the treatment of wastewater is the most attractive path for environmental researchers to incorporate the principles of Green Chemistry.

Recently, several works in immobilized green MNP for environmental pollution remediation have diverted their focus on the direct or indirect immobilization of MNP on a number of sustainable materials. There is a variety of sustainable materials, meaning materials in high abundance and renewable, agro-forest, food and industrial residues, which can either be utilized in pristine or in modified structures for supporting MNP. In this section, an exhaustive overview of the application of sustainable materials supporting biogenic MNP is presented, as well as their application in wastewater treatment for the degradation of various pollutants and for the inactivation of some microorganisms.

2.4.2.1 Natural materials

Green synthesis of MNP supported on natural materials (clay minerals, natural zeolites, sediments, sands, rocks and volcanic glass) forms an innovative approach for the preparation of these nanocomposites. These materials are widespread and abundant on earth and can be purchased at a low cost. Some can also be obtained as waste from exploitation deposits or from processing and purification processes. These accessible starting materials ensure that a reasonable quantity can be obtained and that there is a potential for up-scaling [106]. **Table 2-1** summarizes the works that highlight the ability of natural materials to act as stable supports for the immobilization of biogenic MNP for environmental pollution abatement.

Clays are layered phyllosilicate minerals that occur naturally in the earth's crust and are important constituents of soils [107]. These inorganic materials have gained significant interest as solid support for MNP due to their natural abundance, non-toxic nature, porosity, low cost, layered morphology, chemical inertness and mechanical stability [108,109]. Kaolin, which is one of the most common clay minerals, is low-cost, easily available, biogenic and has high thermal and mechanical stability [110]. These properties make it a significant candidate for MNP solid support. Alfred *et al.* [106] developed an alternative method for biofabrication of kaolinite-TiO₂ nanocomposites doped with ZnWO₄ with effective activity on the photodegradation of arthemether, ampicillin and sulfamethoxazole in water. These nanocomposites were prepared by biomass assisted synthesis routes, using *Carica papaya* seeds or *Musa paradisiaca* peels. The authors performed a pre-screening to evaluate the influence of TiO₂ and the impact of the different biomasses on the photocatalytic efficiency of the nanocomposites. The results showed that the presence of both the biomass and TiO₂ are crucial for the photocatalytic efficiency of the nanocomposites. The nanocomposite prepared from *Musa paradisiaca* peels at 500 °C showed the highest efficiency for the degradation of the substrates in water, due to its relatively small particle size (62 nm), high porosity and consequent large surface area, with a high number of active sites needed for photocatalysis [106].

Recently, Rakhshan *et al.* [111] produced three-component Ag/AgCl/kaolinite bionanocomposite and a four-component Ag/AgCl/Fe₃O₄/kaolinite using the aqueous extract of *Teucrium polium*. Both showed relevant catalytic activity for the reduction of 4-nitrophenol to 4-aminophenol, with a surplus for the four-component nanocomposite that can be easily separated with the aid of an external magnet.

Kaolin was used as support for nano zerovalent iron (nZVI) synthesized via a green method using leaf extract of *Ruellia tuberosa* as a reducing agent [112]. The synthesized green nanocomposite was used for the degradation of reactive black 5 with high decolorization efficiency in an acidic medium.

Montmorillonite is a very promising support for the preparation of nanocomposites, due to its particular characteristics such as high ion exchange capacity, swelling, intercalation and layered nanostructure that make it as suitable solid support for the green synthesis of MNP [78,113–117]. Yang *et al.* [114] successfully prepared a nanocomposite of nZVI/montmorillonite using a low-cost and environment friendly green synthesis via tea leaves extract. Although few studies propose the nanocomposites formation mechanism, the authors suggest that during the synthesis with green tea extract, the unique structure of montmorillonite with isolated exchangeable cations of Fe(III) results in nZVI particles formation, covered by organic matter (green tea extract) in the clay interlayer associated with negative charges [114]. The bio-synthesized composite showed a great removal capacity of Cr⁶⁺ and sufficient mobility under different soil conditions. Also, Sohrabnezhad and Seifi used montmorillonite to support green bimetallic Ag/ZnONP [115]. The attachment of MNP on the surface of montmorillonite and the presence of aluminum atoms in this clay structure, not only prevent the loss of photocatalyst during recovery but also assists electron-hole separation during the photocatalytic process [115].

Bentonite is a member of the smectite family, which is found in many countries and is originated from the activities of volcanoes [118]. This clay has an ordered structure, uniform pore volume, high exchange capacity, high specific surface area, thermal, chemical and mechanical stability and it is low-cost, which makes it promising support [119]. Bentonite is widely used as support for green MNP such as AgNP [120,121], CuNP [122,123], SnO₂NP [118], PdNP [124], ZnONP [125], nZVINP [119,126–130], bimetallic nZVI/CuNP [109], Ag/Fe₃O₄ and Pd/Fe₃O₄NP [131], Fe/PdNP [132] and Fe/NiNP [133]. The efficiency of tetracycline adsorption by green nZVI/CuNP in suspension and by bentonite supported green nZVI/Cu using pomegranate rind extract was studied by Gopal *et al.* [109]. The aggregation of bimetal NP was reduced and their dispersion onto bentonite increased. The increased surface area could be assigned to the certainty of bentonite as a supporting material that effectively reduces the aggregation of nZVI/CuNP and leads to equal distribution of bimetal NP on its surface [106]. Issaabadi *et al.* [122] described the preparation of bentonite/CuNP using the aqueous extract of the leaves of *Thymus vulgaris* as reducing agent and efficient stabilizer and studied the catalytic

efficiency of the nanocomposite in the degradation of methylene blue and congo red. They observed that the *Thymus vulgaris* leaf extract allows a fast and convenient preparation of the bentonite/CuNP and can reduce Cu^{2+} ions into CuNP without severe conditions and are efficient in the degradation. All the syntheses using green tea extract to produce bentonite supporting nZVI [126–129], were performed at RT. The biofabrication performed by Hassan *et al.* [128] was carried out in a short reaction period (15 min), but NaOH solution was added to adjust the pH, which makes the process less sustainable.

Zeolites are a particular group of aluminosilicate and microporous materials that have very good adsorbing properties. The microporous structure with varying pore diameter can retain the substances to be separated depending on their molecular size and thus acting as molecular sieves. This attribute of zeolites qualifies them as reliable, cost-effective and eco-friendly supports for binding the MNP [134]. Natural zeolites have been used as sustainable supports for biogenic MNP such as AgNP [135,136], CuNP [137,138], PdNP [139] and nZVINP [140]. In a recent study, the green nZVINP dispersed onto zeolite produced by eucalyptus leaf extracts were applied to concurrently eliminate ammonia and phosphate from aqueous solutions [140]. This nanocomposite eliminated 43.3% of NH_4^+ and 99.8% of PO_4^{3-} , at a primary concentration of 10 mg.L^{-1} each of the 2 co-existing ions. After optimization, the conditions for maximum adsorption capacity of the produced material for NH_4^+ and PO_4^{3-} were 3.47 and 38.91 mg.g^{-1} , respectively.

Other natural materials such as sand [141], sediments [142], rocks [143,144] and volcanic glass [145–147] have also been reported as solid supports for green MNP. Perlites are small pebbles of natural glass which contain a small amount of occluded water and are found in volcanic deposits [148]. The reduction of nitroarenes and organic dyes in water was evaluated using green PdNP dispersed on perlite [147]. The green Pd/perlite nanocomposite can be recovered and recycled several times without significant loss of activity. Likewise, Nasrollahzadeh *et al.* [146] used perlite to immobilize CuNP synthesized using an aqueous extract of the leaves of *E. esula L.* The *ex situ* fabrication involves the mixing of freshly pre-synthesized CuNP along with perlite during 15 h. The particles exhibited spherical morphology with a low tendency to agglomeration. The CuNP/perlite shows favorable activity and separability on the catalytic reduction of 4-nitrophenol and can be reused several times without a decrease in the catalytic activity.

The *in situ* fabrication is widely used to synthesize composites since it warrants more uniformity of the NP on the support. Only two studies were performed *ex situ* using natural materials as solid support and both reported a low tendency of NP to agglomerate [140,146].

Table 2-1. Natural materials as supports for biogenic MNP with applications in wastewater treatment.

Support	Biogenic MNP	Bioreductor	Immobilization method	Shape and size	Wastewater application and recyclability	Ref.
Kaolin	nZVI	<i>Ruellia tuberosa</i> leaves extract	<i>In situ</i> with stirring	Spherical 20-40 nm	Adsorption of reactive black 5 5 cycles	[112]
	TiO ₂ /ZnWO ₄	<i>Carica papaya</i> seeds and <i>musa paradisiaca</i> peels biomass	<i>In situ</i> with mechanical grinding for 15 min and calcined	Spherical 62-257 nm	Photocatalytic degradation of ampicillin, sulfamethoxazole and artemether 5 cycles	[106]
	Ag/AgCl	<i>Teucrium polium</i> extract	<i>In situ</i> with stirring for 24 h	Spherical 19-22 nm	Catalytic reduction of 4-nitrophenol n.r.	[111]
Montmorillonite	Ag	<i>Sida acuta</i> leaves extract	<i>In situ</i> with stirring at RT for 24 h	n.r. 15-20 nm	Adsorption of methylene blue n.r.	[117]
	nZVI	Green tea extract	<i>In situ</i> with stirring	Spherical 15-30 nm	Adsorption of Cr ⁶⁺ n.r.	[114]
	Ag/ZnO	<i>Urtica dioica</i> leaves extract	<i>In situ</i> with stirring at 80°C for 4 h	Spherical 2-4 nm	Photocatalytic degradation of methylene blue 4 cycles	[115]
Bentonite	Ag	<i>Euphorbia larica</i> extract	<i>In situ</i> with constant stirring at 80°C for 4 h	Spherical 32 nm	Catalytic reduction of 4-nitrophenol, congo red, methylene blue and rhodamine B 5 cycles	[120]
	Fe Ag	Different extracts	<i>In situ</i> with stirring for 30 min or overnight	n.r.	Adsorption of chlorfenapyr n.r.	[121]

Cu	<i>Thymus vulgaris</i> leaves extract	<i>In situ</i> with constant stirring at 80°C for 4 h	Spherical 23-94 nm	Catalytic reduction of methylene blue and congo red 5 cycles	[122]
			Spherical 56 nm	Catalytic reduction of 4-nitrophenol 5 cycles	[123]
SnO ₂	<i>Ziziphus jujuba</i> fruit extract	<i>In situ</i> with vigorously stirring at RT for 30 min and calcined	Spherical 18 nm	Photocatalytic degradation of methylene blue and eriochrome black T 3 cycles	[118]
Pd	<i>Gardenia taitensis</i> leaves extract	<i>In situ</i> with constant stirring at 80°C for 4 h	Spherical 76–97 nm	Catalytic reduction of Cr (VI), 4-nitrophenol and 2,4- dinitrophenylhydrazine 5 cycles	[124]
ZnO	<i>Jujube</i> fruit extract	<i>In situ</i> with constant stirring at 80°C for 5 h and calcinated	Spherical 10-40 nm	Photocatalytic degradation of methylene blue and eriochrome black-T 3 cycles	[125]
nZVI	Green tea extract	<i>In situ</i> with constant stirring at RT	Spherical 40-60 nm	Adsorption of phosphate n.r.	[126]
			n.r. 40-80 nm	Adsorption of Cr ⁶⁺ n.r.	[127]
			Irregular spherical <50 nm	Fenton-like oxidation of reactive blue 238 n.r.	[128]
			n.r. 50-60 nm	Adsorption of malachite green 2 cycles	[129]
	<i>Eucalyptus</i> leaves extract	<i>In situ</i> with stirring for 3 h	Irregular 10-60 nm	Catalytic reduction of 4-nitrophenol 5 cycles	[119]
	Black tea extract	<i>In situ</i> with constant stirring at RT for 15 min	Irregular spherical <50 nm	Fenton-like oxidation of reactive blue 238 n.r.	[130]

	nZVI-Cu	Pomegranate rind extract	<i>In situ</i> with continuous purged of nitrogen gas and continuous stirring	Spherical 60 nm	Adsorption of tetracycline 3 cycles	[109]
	Ag/Fe ₃ O ₄ Pd/Fe ₃ O ₄	<i>Salix aegyptiaca</i> leaves extract	<i>In situ</i> with stirring at RT for 1 h	Spherical 15-65 nm	Catalytic reduction of rhodamine B, methylene blue and methyl orange 4 cycles	[131]
	Fe/Pd	Pomegranate peel extract	<i>In situ</i> with nitrogen gas atmosphere	Mostly spherical 20-60 nm	Adsorption of tetracycline 3 cycles	[132]
	Fe/Ni			Spherical 70 nm	Adsorption of tetracycline and Cu ²⁺ 4 cycles	[133]
Sand	Fe/Ni	<i>Punica granatum</i> peel extract	<i>In situ</i> with orbital shaker for 1 h	Spherical 161 nm	Adsorption of tetracycline 4 cycles	[141]
Silty	nZVI	Green tea leaves extract	<i>In situ</i> with stirring for 1 h	Cubical 100 nm	Adsorption of phenol n.r.	[142]
Diatomite	Ag	<i>Alocasia macrorrhiza</i> leaves extract	<i>In situ</i> with stirring at 80°C for 4 h	Spherical 32 nm	Catalytic reduction of 2,4-dinitrophenylhydrazine, nigrosin, 4-nitrophenol, methyl orange and congo red 5 cycles	[143]
	Pt	<i>Cinnamomum camphora</i> leaves extract	<i>In situ</i> with stirring at 90°C for 1 h	n.r. 3.5 nm	Catalytic oxidation of benzene n.r.	[144]
Perlite	Ag	<i>Hamamelis virginiana</i> leaves extract	<i>In situ</i> with stirring at 60°C for 1 h	Spherical 8-25 nm	Catalytic reduction of 4-nitrophenol and congo red 4 cycles	[145]
	Cu	<i>Euphorbia esula L.</i> leaves extract	<i>Ex situ</i> with stirring at 100°C for 15 h	Spherical 32 nm	Catalytic reduction of 4-nitrophenol 3 cycles	[146]
	Pd	<i>Euphorbia neriifolia L.</i> leaves extract	<i>In situ</i> with continuous stirring and heated	Spherical <18 nm	Catalytic reduction of 2,4-dinitrophenylhydrazine, 4- nitrophenol, rhodamine B, methyl orange and congo red 5 cycles	[147]

		under reflux conditions for 3 h			
Clinoptilolite	Ag	<i>Vaccinium macrocarpon</i> fruit extract	<i>In situ</i> with constant stirring at 60–70°C for 30 min	Spherical 15-30 nm	Catalytic reduction of rhodamine B, methylene blue, methyl orange and congo red 6 cycles [135]
	CuO	<i>Rheum palmatum L.</i> root extract	<i>In situ</i> with constant stirring at 70°C for 10 min	Spherical 30 nm	Catalytic reduction of 4-nitrophenol, rhodamine B, methylene blue and methyl orange 5 cycles [137]
Natrolite	Ag	<i>Euphorbia prolifera</i> leaves extract	<i>In situ</i> with stirring at 60°C for 2 h	Semispherical 15 nm	Catalytic reduction of 4-nitrophenol, rhodamine B, methylene blue, methyl orange and congo red 7 cycles [136]
	Cu	<i>Anthemis xylopoda</i> flowers extract	<i>In situ</i> with stirring at 100°C for 15 h	Spherical 20 nm	Catalytic reduction of 4-nitrophenol, congo red and methylene blue 5 cycles [138]
	Pd	<i>Piper longum</i> fruit extract	<i>In situ</i> with stirring at 100°C for 15 h	Spherical 12.5 nm	Catalytic reduction of 4-nitrophenol, rhodamine B, methylene blue, methyl orange and congo red 7 cycles [139]
Natural zeolite	nZVI	<i>Eucalyptus</i> leaves extract	<i>Ex situ</i> with stirring	Spherical 60 nm	Adsorption of ammonia and phosphate n.r. [140]

Nano zerovalent iron (nZVI); room temperature (RT); not reported (n.r.)

2.4.2.2 Waste materials

In recent years, there has been a tremendous upsurge of interest in the application of waste materials for the removal of pollutants from aqueous media and focused on the application of waste materials as supports for biogenic MNP. Some residues from food, industry and agro-forestry have been reported as good supports for biogenic MNP. **Table 2-2** summarizes the studies that highlight the ability of waste materials to act as stable supports for the immobilization of biogenic MNP for environmental pollution abatement.

Eggshell waste is among the most abundant waste materials coming from food processing industries and it is mainly composed of calcium carbonate (CaCO_3) [149]. The eggshell waste have been applied as reliable support for biosynthesized $\text{Cu/Fe}_2\text{O}_3\text{NP}$ [150], $\text{SnO}_2/\text{ZnONP}$ [151], PdNP [152], CuNP [153], AgNP [154] and ZnONP [155]. Nasrollahzadeh *et al.* [150] used for the first time waste materials as support for biogenic MNP with catalytic activity for pollutant reduction. These authors produced Cu/eggshell, $\text{Fe}_3\text{O}_4/\text{eggshell}$ and $\text{Cu/Fe}_3\text{O}_4/\text{eggshell}$ nanocomposites from waste chicken eggshells using aqueous extract of the leaves of *Orchis mascula L.*, as a stabilizing and reducing agent. The immobilization of Cu and $\text{Fe}_3\text{O}_4\text{NP}$ increased the specific surface area, the number of pores on the surface of the eggshell and the catalytic activity compared with the MNP in suspension. Also, eggshell was used as economic and environmental friendly support for the preparation of the supported PdNP through the green and simple *in situ* reduction method using barberry fruit extract as a reducing and stabilizing agent [152]. The authors observed that PdNP were immobilized on the eggshell surface, which indicates the perfect combination of the PdNP and eggshell.

The eggshell membrane is the innermost portion of the eggshell and is mainly composed of a thin inner and a thick outer membrane which includes proteins such as collagen, sialoprotein, osteopontin, and a small amount of saccharides with an interwoven fibrous structure [156]. The use of eggshell membrane as support for biogenic MNP was found for MnO_2NP [157], ZnSNP [156] and AuNP [158]. Wang *et al.* [157] used eggshell membrane acting as both support and reducing agent for MnO_2NP . The clean eggshell membrane were cut into slices, soaked into potassium permanganate solution, and stirred at RT. This nanocomposite showed a good capacity for decontamination of tetracycline hydrochloride and can be separated easily from the bulk solution by taking the membrane out to stop the degradation, instead of centrifugation or filtration. Zhang *et al.* [156] proposed a mechanism to

explain the production of ZnS supported on eggshell membrane. The authors show that when the membrane of the eggshell is immersed into Zn-precursor solution, Zn^{2+} can be tightly adsorbed by negative functional groups on the glycoprotein mantle of the eggshell membrane. By consecutive soaking of the new eggshell membrane into Na_2S solution, S^{2-} is moved toward active positions to achieve *in situ* nucleation of the ZnS nanocrystallites. With the repetition of this cycle, the ZnSNP self-assembled spheroid-like nanocrystallites on the eggshell membrane do grow.

Agriculture wastes can be used as supports for biogenic MNP, as is the case of the shells of almonds [159,160], walnuts [35], peaches [30], pistachios [161,162], hazelnuts [163], wheat bran and rice bran [121] and seeds of Russian olives [164]. The catalytic performance of green PdNP supported on modified almond shells was studied [153]. The surface of almond shells was chemically modified using captopril and it was observed that the surface to volume ratio increased and the immobilized NP were more stable. Walnut shell is a low-cost, easily available biomaterial, which has an intrinsic pore structure and is composed of cellulose, hemicelluloses and lignin [165]. This material was used for the first time by Bordbar and Mortazavimanesh [35], in the *in situ* fabrication of PdNP by reduction of Pd ions adsorbed on the surface of the walnut shell using the aqueous extract of the leaves of *E. arvense L.* as a reducing agent. These nanocomposites showed high catalytic activity in the reduction of 4-nitrophenol, congo red, methylene blue and rhodamine B in the presence of aqueous $NaBH_4$ at RT. Also, the pistachio shell powder is an effective support for immobilization and dispersion of CuNP using pistachio hull extract [162]. The nanocomposite of CuNP/pistachio shell has shown high catalytic activity in the reduction of organic dyes and could be easily recovered and reused several cycles.

Forestry wastes such as coconut palm spathe have been used as support for green $Fe-TiO_2$ NP and used for photocatalytic degradation of cypermethrin, reaching more than 80% degradation [166].

Natural seashell waste was utilized to support AgNP by a simple and green method using *B. persicum* seeds extract [167]. The AgNP/seashell nanocomposite showed a great catalytic reduction of different organic dyes. Also, Rostami-Vartooni used seashell waste to support CuONP using *Rumex crispus* seeds extract as a chelating and capping agent [168]. This nanocomposite was reused five times for 100% reduction of 4-nitrophenol.

Luffa sponge is the dried vascular bundle from the fruit of a widely distributed cucurbit and it is an environmental friendly and pollution-free support, with a large specific surface area and was used to immobilize ZnONP to remove trypan blue azo dye [169]. The ZnONP were obtained by using the

peroxidase enzyme from *Euphorbia amygdaloides* plants and then were immobilized on the fiber of the luffa sponge by incubation in an ultrasonic bath for 30 min. The optimum removal of the dye was found at pH 7 and the equilibrium was attained within 30 min.

The reuse efficiency is demonstrated in most studies. It should be noted that the highest recyclability is found in studies that use wastes as solid supports for NP. Some composites were reused several times (10 fold) without any significant loss in the activity [153,158,159]. The process of separation from the reaction mixture varies between centrifugation [158,159], filtration [153] and external magnetic separation [110].

Table 2-2. Waste materials as supports for biogenic MNP with applications in wastewater treatment.

Support	Biogenic MNP	Bioreductor	Immobilization method	Shape and size	Wastewater application and recyclability	Ref.
Eggshell	Cu Fe ₃ O ₄ Cu/Fe ₃ O ₄	<i>Orchis mascula L.</i> leaves extract	<i>In situ</i> with vigorously shaking at 70°C for 3 h	Spherical 5–15 nm	Catalytic reduction of 4-nitrophenol, rhodamine B, methylene blue, methyl orange and congo red 7 cycles	[150]
	Pd	Barberry fruit extract	<i>In situ</i> with vigorous stirring and refluxed for 3 h	Spherical <20 nm	Catalytic reduction of 4-nitrophenol, methylene blue, methyl orange and congo red 6 cycles	[152]
	SnO ₂ /ZnO	Teucrium polium leaves extract	<i>In situ</i> with vigorously stirring at 70°C for 8 h	Spherical 20-25 nm	Adsorption of Hg ²⁺ 3 cycles	[151]
	CuO	Pomegranate peel extract	<i>Ex situ</i> with reflux condition at 80°C for 24 h	Spherical 30 nm	Adsorption of aromatic compound from crude oil 10 cycles Catalytic reduction of 4-nitrophenol 6 cycles	[153]
	Ag	<i>Cacumen platycladi</i> extract	<i>In situ</i> with impregnation for 6h and reacted for 48 h	Spherical 60 nm	Catalytic reduction of 4-nitrophenol 5 cycles Antibacterial activity against <i>E. coli</i> and <i>S. aureus</i> n.a.	[154]
	ZnO	<i>Ferulago macrocarpa</i> extract	<i>In situ</i> with stirring for 24 h and calcined	Spherical 25 nm	Photocatalytic degradation of diazinon n.r. Antibacterial activity against both human and fish pathogenic bacterial n.a.	[155]

Membrane of eggshell	MnO ₂	Membrane of eggshell	<i>In situ</i> with stirring at RT for 35 min	Spherical 4.8 nm	Adsorption of tetracycline n.r.	[157]
	ZnS		<i>In situ</i> with liquid impregnation method	Spherical 40 nm	Photocatalytic degradation of methyl orange 4 cycles	[156]
	Au		<i>Lagerstroemia speciosa</i> leaves extract	<i>In situ</i> with impregnation for 3 h	Spherical 20 nm	Catalytic reduction of 4-nitrophenol 10 cycles
Almond shell	Pd	Almond hull extract	<i>In situ</i> with stirring at 100°C	Spherical <20 nm	Catalytic reduction of methylene blue, methyl orange and rhodamine 6G 10 cycles	[159]
	Ag	<i>Ruta graveolens</i> sleeves extract	<i>In situ</i> with stirring at 70°C for 2 h	Spherical 10-15 nm	Catalytic reduction of 4-nitrophenol, rhodamine B and methylene blue 5 cycles	[160]
Walnut shell	Pd	<i>Equisetum arvense</i> L. leaves extract	<i>In situ</i> with vigorously shaking at 70°C for 3 h	Spherical 5–12 nm	Catalytic reduction of 4-nitrophenol, rhodamine B, methylene blue, methyl orange and congo red 7 cycles	[35]
Peach kernel shell	Ag	<i>Achillea millefolium</i> L. extract	<i>In situ</i> with reflux conditions at 70°C for 1.5 h	Spherical <20 nm	Catalytic reduction of 4-nitrophenol, methyl orange and methylene blue 5 cycles	[30]
Seashell	Ag	<i>Bunium persicum</i> seeds extract	<i>In situ</i> with stirring at 70°C for 1 h	Spherical 11 nm	Catalytic reduction of 4-nitrophenol, methylene blue, methyl orange and congo red 5 cycles	[167]
	CuO	<i>Rumex crispus</i> seeds extract	<i>In situ</i> with stirring at 60°C for 20 min and calcination	Spherical 8–60 nm	Catalytic reduction of 4-nitrophenol and congo red 5 cycles	[168]
Pistachio shell	Ag	<i>Cichorium intybus</i> L. leaves extract	<i>In situ</i> with stirring at 75°C for 2 h	Spherical 20-50 nm	Catalytic reduction of 4-nitrophenol, methylene blue, methyl orange and congo red 5 cycles	[161]
	Cu	<i>Pistacia Vera</i> L. hull extract	<i>In situ</i> with sonicator bath at 60 °C	Spherical 15–45 nm	Catalytic reduction of 4-nitrophenol, rhodamine B, methylene blue and methyl orange 5 cycles	[162]

Hazelnut shell	Ag	<i>Origanum vulgare</i> leaves extract	<i>In situ</i> with stirring at 70°C for 2 h	Spherical <30 nm	Catalytic reduction of methyl orange and congo red 5 cycles	[163]
Wheat bran	Fe Ag	Different extracts	<i>In situ</i> with stirring for 30 min or overnight	n.r.	Adsorption of chlorfenapyr n.r.	[121]
Rice bran						
Coconut palm spathe	Fe-TiO ₂	<i>Cymbopogon citratus</i> aqueous extract	<i>Ex situ</i> with doctor blade technique	Spherical 13-16 nm	Photocatalytic degradation of cypermethrin n.r.	[166]
<i>Elaeagnus angustifolia</i> seed	Ag@AgCl	<i>Elaeagnus angustifolia</i> leaves extract	<i>In situ</i> with stirring at 60°C	Spherical 40 nm	Photocatalytic degradation of methylene blue 3 cycles	[164]
Luffa sponge	Zn	Peroxidase enzymes from <i>Euphorbia amygdaloides</i>	<i>Ex situ</i> with ultrasonic batch during 30 min and lyophilized	n.a 20 nm	Adsorption of trypan blue n.r.	[169]

Room temperature (RT); not reported (n.r.); not applicable (n.a.)

2.4.2.3 Activated carbon and biochar

Among various types of sustainable supports, carbon-based materials derived from bio-resources are also utilized as suitable supports for biogenic MNP. Biochar and activated carbon are pyrogenic carbonaceous materials that are produced by thermochemical conversion of carbonaceous feedstock (pyrolysis or/and activation) [170]. **Table 2-3** summarizes the studies that highlight the ability of biochar and activated carbon to act as stable supports for the immobilization of biogenic MNP for environmental pollution abatement.

Biochar is an attractive and low-cost carbon-rich material derived from biomass and produced by pyrolysis under limited oxygen or by hydrothermal carbonization at high pressure. In order to produce biochar the pyrolysis temperature generally ranges from 300 to 1000 °C [171]. A variety of raw materials have been tested as precursors of biochar such as carbonaceous materials from sewage sludge [172], invasive plants [173], jackfruit peel [174], oak wood [175], banana peel [176], kenaf bar [177], green tea [178] and rambutan peel [179], to serve as support for biogenic MNP. The synthesis of a novel biochar-supported nZVI through a green method with green tea aqueous extract has been reported by Liu *et al.* [177]. The nanocomposite showed high performance on the simultaneous removal of Cu²⁺ and bisphenol A by a combination of biochar/nZVI with persulfate system, reaching removals of 96% and 98% within 60 min, respectively. The authors proposed a possible reaction mechanism for the synergistic reduction and oxidation. For Cu²⁺ removal process, Cu²⁺ species could be firstly adsorbed and then suffers co-precipitation and complexation processes, being reduced into Cu⁺ and Cu⁰ species at the end through one electron reduction process. For the bisphenol A removal process, this could also be adsorbed on the biochar/nZVI surface, while Fe²⁺ would be released from the nanocomposite under acidic conditions which could activate the persulfate system for the production of SO₄²⁻. Subsequently, bisphenol A could be degraded into a series of products such as p-isopropenyl phenol, 4-isopropylphenol, 4-hydroxyacetophenone, p-hydroquinone, fumaric acid and 2-hydroxypropionic acid. The synthesis of a green biochar/iron oxide composite, using a facile approach involving banana peel extract and biochar from the same banana peel, was achieved with an enhanced adsorption ability for methylene blue (862 mg.g⁻¹) [176]. The authors proposed a mechanism in which the banana peel biochar with reductive biomolecules reacts with FeSO₄ to form biochar/nZVI

composite. Formerly, under the action of dissolved oxygen in water, nZVI is oxidized and hydrolyzed to form biochar/Fe₃O₄ composite.

Also, Jing *et al.* [173] synthesized ZnONP using *S. alterniflora* extract loaded on biochar derived from *S. alterniflora* by a one-step carbonization method and showed 98.38% photocatalytic degradation of malachite green. Nayak *et al.* [174] fabricated a novel biocompatible nanocomposite by ultrasonication-assisted extraction of natural polysaccharides from mushrooms followed by their use in the synthesis of biogenic magnetite NP immobilized onto the biochar of jackfruit peel with a good adsorption capacity for phosphate (7.95 mg.g⁻¹) and nitrate (5.26 mg.g⁻¹).

Activated carbon is produced from environmental wastes with high carbon content [180]. Lignocellulosic and coal materials such as tree [181], jute stick [182], flamboyant pods [183], palm coconut [184], lemon pomace [185], corn straws [186], worn tires [187,188], pomegranate peel [189], sawdust [190], spent mushroom compost [191] and spent filters from home filtration systems [192] have been used as raw materials planned for the manufacture of activated carbon to act as support for biogenic MNP.

The preparation of an efficient heterogeneous nanocomposite based on the immobilization of biogenic SnO₂NP on activated carbon from *Corchorus olitorius* stems was reported and showed excellent photocatalytic activity towards degradation of naproxen [182]. Taha *et al.* [192] have reported the green synthesis of Ag-, ZnO- and Ag/ZnONP with posterior immobilization on activated carbon from the spent filters from home filtration systems and evaluated the antibacterial and the catalytic activity of the synthesized nanocomposites. The results showed that AgNP loaded on activated carbon have the best catalytic activity compared to the other nanocomposites, which was attributed to the good dispersion of AgNP on the surface of activated carbon.

Table 2-3. Biochar and activated carbon as supports for biogenic MNP, with applications in wastewater treatment.

Support	Biogenic MNP	Bioreductor	Immobilization method	Shape and size	Wastewater application and recyclability	Ref.
Biochar from carbonaceous material from sewage sludge	Ag	<i>Camellia sinensis</i> leaves extract	<i>In situ</i> with stirring for 12 h	Non-spherical 26 nm	Catalytic reduction of methylene blue n.r.	[172]
Biochar from <i>Spartina alterniflora</i>	ZnO	<i>Spartina alterniflora</i> extract	<i>Ex situ</i> with a water bath at 80 °C for 2 h and carbonized	Near-rodlike 25-40 nm	Photocatalytic degradation of malachite green n.r.	[173]
Biochar from jackfruit peel	Fe	Polysaccharide extract from mushroom	<i>Ex situ</i> with microwave irradiation	Spherical 100 nm	Adsorption of phosphate and nitrate 5 cycles	[174]
Biochar from oak wood	nZVI	Tea polyphenol	<i>In situ</i> with stirring for 30 min	Spherical 90-200 nm	Adsorption of Cr ⁶⁺ n.r.	[175]
Biochar from banana peel	Fe	Banana peel extract	<i>In situ</i> with continuous sonication for 1.5 h	Irregular n.r.	Adsorption of methylene blue 5 cycles	[176]
Biochar from kenaf bar	nZVI	Green tea extract	<i>In situ</i> with N ₂ atmosphere	Spherical 100 nm	Catalytic reduction and oxidation of Cu ²⁺ and bisphenol A 3 cycles	[177]
Biochar from green tea residues				n.r.	Adsorption of p-nitrophenol 5 cycles	[178]
Biochar from <i>N. lappaceum</i> peel	Fe	<i>Nephelium lappaceum</i> peel extract	<i>In situ</i> with stirring at RT for 30 min	Spherical 20-80 nm	Adsorption of organochlorine pesticides 5 cycles	[179]
Activated carbon from <i>Hildegardia barteri</i> leaves	Ag	<i>Ocimum gratissimum</i> leaves extract	<i>Ex situ</i> with stirring for 2 h	Spherical 22-43 nm	Adsorption of congo red 5 cycles	[181]

Activated carbon from <i>Corchorus olitorius</i> stems	SnO ₂	<i>Saccharum officinarum</i> juice	<i>In situ</i> with constant stirring for 15 min and autoclaved	Irregular 3 nm	Photocatalytic degradation of naproxen 5 cycles	[182]
Activated carbon from <i>Delonix regia</i>	ZnO	<i>Tithonia diversifolia</i> leaves extract	<i>Ex situ</i> with stirring at 150°C for 1 h	Spherical 9-29 nm	Adsorption of methylene blue 5 cycles	[183]
Activated carbon from palm coconut shell	Cu	<i>Moringa oleifera</i> leaves extract	<i>In situ</i> with stirring at RT for 36 h	n.r. 66-61	Adsorption of nitrate n.r.	[184]
Activated carbon from lemon pomace	Fe/Zn	Lemon leaves extract	<i>In situ</i> with stirring for 3 h	Spherical 126 nm	Fenton-like oxidation of reactive red 2 n.r.	[185]
Activated carbon from corn straws	S-nZVI	Green tea extract	<i>In situ</i> with stirring for 2 h under nitrogen-flowing atmosphere	n.r.	Adsorption of Pb ²⁺ n.r.	[186]
Activated carbon from worn tires	ZnO	Walnut peel extract	<i>Ex situ</i> with stirring for 2 h	Spherical 31-35 nm	Adsorption of eosin Y and erythrosine B 5 cycles	[188]
		Walnut shell extract	<i>Ex situ</i> with stirring for 10 h	n.r.	Adsorption of reactive blue 19 and reactive black-5 n.r.	[187]
Activated carbon from pomegranate peel	nZVI	Pomegranate peel extract	<i>Ex situ</i> with stirring for 2 h and placed in the oven for 10 h at 95 °C	Non-uniform 11-35 nm	Adsorption of furfural 5 cycles	[189]
Activated carbon from sawdust	Cu	Green tea extract	<i>Ex situ</i> with stirring for 12 h at RT and then heated at 80°C	n.r. 200 nm	Adsorptive of acridine orange n.r.	[190]

Activated carbon from spent mushroom compost	Ag	Corncob extract	<i>Ex situ</i> with magnetic stirring and sonication	Spherical 10-25 nm	Adsorption of levofloxacin n.r. Antibacterial activity against both <i>E. coli</i> and <i>S. aureus</i> n.a.	[191]
Activated carbon from the spent home filtration system filters	Ag ZnO Ag/ZnO	<i>Azadirachta indica</i> leaves extract	<i>Ex situ</i> with vigorous stirring overnight at RT	Spherical 20-300 nm	Catalytic reduction of 4-nitrophenol n.r. Antibacterial activity against 16 pathogenic bacteria n.a.	[192]

Nano zerovalent iron (nZVI); room temperature (RT); not reported (n.r.); not applicable (n.a.)

2.5 ECONOMIC AND ENVIRONMENTAL PERSPECTIVE

In order to guarantee the highest quality drinking water, it is necessary to introduce new advanced technologies in this area. The ability to integrate different properties, resulting in multifunctional systems, is a major benefit for the use of NP as compared with traditional water technology [193]. In fact, the development of sustainable, efficient and cost-effective methods for the elimination or effective reduction of pollutants and microorganisms in wastewater and drinking water is highly required [106].

Recently, the application of bio-resources for the development of green methods for the synthesis of MNP has gained widespread attention. Using non-toxic, biocompatible and environmentally benign methods for synthesis of MNP associated with sustainable materials that may be recovered and reused became of great interest. Various high-value products may be obtained with low economic and environmental impact and nature provides many useful materials with hidden potential to be applied in innovative processes. This environmental approach has been reflected in an increased interest in clay minerals because they are abundant, easily found everywhere and present unique properties to act as MNP supports. They have a significant ability to immobilize pollutants, either by adsorption or ion exchange mechanisms and usually present excellent mechanical stability [109]. Among the more than four thousand known minerals, only a small part has been tested as a support for green NP. Clays such as sepiolite [194], rectorite [195], chrysotile [196], halloysite [197], hectorite [198] are found in the literature as sustainable supports for commercial MNP or chemically synthesized MNP.

Amongst natural materials, cork (the bark of the evergreen oak *Quercus suber* L.) is a particularly interesting and promising option not yet found as support for biogenic MNP [199,200]. The use of cork is sustainable, as the tree is not harmed during the harvesting of the bark (the harvesting is performed every 9-13 years) [201].

Wastes have been used as valuable and environmental friendly support for the immobilization of biogenic MNP. The concept of utilization of waste materials as a vector of circular economy introduces alternatives to maximize the reuse and recycling of wastes within the wastewater treatment process [202]. At present, large quantities of wastes are discharged as the end of the line, resulting in considerable environmental issues. Food waste in the world is estimated at 1.6 billion tons per year as a result of population growth [202]. For example, eggshell is one of the most common forms of food waste with a worldwide production of 50,000 t per year [149]. According to Food and Agriculture

Organization (FAO) reports, almost 30 million tons of biomass from pistachio nuts are discarded annually in landfills by the pistachio nut processing industry [162]. According to Caruso *et al.* [203] more than 50% of fishing is thrown away as wastes resulting in around 20 million tons of residues being discarded worldwide each year from fisheries.

These wastes if not appropriately handled, will produce large quantities of greenhouse gases to be released into the atmosphere [204]. Mostly, waste materials from the different sectors are disposed of by allowing them to rot at the source or in stockpiles [202]. This lack of proper treatment of wastes severely affects the ecosystems [205]. Furthermore, there are numerous wastes that can be applied as sustainable supports such as kitchen wipe sponge [206], palm trunk [207], industrial waste (lithium silicon powder) [208], fly ash [209], wood [210] and aloe vera [211]. The use of wastes as sustainable supports for biogenic MNP only implies washing, drying and crushing. In addition, activated carbon and biochar have been produced from wastes as precursors, making this approach an effective and economically valuable solution for environmental pollution. Activated carbon has been identified as one of the most promising materials of the 21st century used in chemical industries thanks to its unique properties, including morphology, high mechanical strength, adsorption capacity, durability and good chemical stability however, it is expensive [212]. There is a research effort to design and prepare affordable materials that may act as an alternative to the commercially available activated carbon [189].

Alternative supports including sustainable natural biopolymers such as cellulose, chitosan, alginate, dextran and starch have been recently employed for the preparation of supported MNP [213]. Biopolymers offer several advantages compared to traditional supports including low toxicity and cost, high biocompatibility, availability and abundance as well as delivering unique functions as per their use [214].

These natural or cheap precursor materials, therefore, ensure that a reasonable quantity of nanocomposite can be produced and that there is a potential for up scaling. This is a condition that is not typically the case in current nanocomposites because they are prepared from rather expensive reagents and often through more complex processes that are not generally amenable for developing countries [106].

The circular economy nowadays is the goal for research that seeks improvement in sustainable development. It aims at minimizing human and industrial pollution by turning waste and by-products

into added value products [215]. From the perspective of circular economy and green development, the simultaneous utilization of low-cost materials and/or reuse of natural or organic waste materials as support for green MNP in the treatment of wastewater is one of the most thrust area for researchers and environmental scientists [205]. This synergistic effect will enhance the reusability of material and eliminate the generation of secondary pollutants.

2.6 REFERENCES

- [1] A.K. Singh, R. Chandra, Pollutants released from the pulp paper industry: Aquatic toxicity and their health hazards, *Aquat. Toxicol.* 211 (2019) 202–216. <https://doi.org/10.1016/J.AQUATOX.2019.04.007>.
- [2] K. Saravanakumar, V. Muthuraj, Fabrication of sphere like plasmonic Ag/SnO₂ photocatalyst for the degradation of phenol, *Opt. - Int. J. Light Electron Opt.* 131 (2017) 754–763. <https://doi.org/https://doi.org/10.1016/j.ijleo.2016.11.127>.
- [3] R. Toczyłowska-Mamińska, Limits and perspectives of pulp and paper industry wastewater treatment – A review, *Renew. Sustain. Energy Rev.* 78 (2017) 764–772. <https://doi.org/10.1016/j.rser.2017.05.021>.
- [4] M.E. Borges, M. Sierra, E. Cuevas, R.D. García, P. Esparza, Photocatalysis with solar energy: Sunlight-responsive photocatalyst based on TiO₂ loaded on a natural material for wastewater treatment, *Sol. Energy.* 135 (2016) 527–535. <https://doi.org/10.1016/j.solener.2016.06.022>.
- [5] R. Dewil, New perspectives for Advanced Oxidation Processes, *J. Environ. Manage.* 195 (2017) 93–99. <https://doi.org/10.1016/J.JENVMAN.2017.04.010>.
- [6] C. Teodosiu, A.-F. Gilca, G. Barjoveanu, S. Fiore, Emerging pollutants removal through advanced drinking water treatment: A review on processes and environmental performances assessment, *J. Clean. Prod.* 197 (2018) 1210–1221. <https://doi.org/10.1016/J.JCLEPRO.2018.06.247>.
- [7] A.R. Ribeiro, O.C. Nunes, M.F.R. Pereira, A.M.T. Silva, An overview on the advanced oxidation processes applied for the treatment of water pollutants defined in the recently launched Directive 2013/39/EU, *Environ. Int.* 75 (2015) 33–51. <https://doi.org/10.1016/J.ENVINT.2014.10.027>.
- [8] X. Wang, Y. Mao, S. Tang, H. Yang, Y.F. Xie, Disinfection byproducts in drinking water and regulatory compliance: A critical review, *Front. Environ. Sci. Eng.* 9 (2015) 3–15. <https://doi.org/10.1007/s11783-014-0734-1>.
- [9] R. A. Osawa, B. T. Barrocas, O. C. Monteiro, M.C. Oliveira, M.H. Florêncio, Photocatalytic degradation of cyclophosphamide and ifosfamide: Effects of wastewater matrix, transformation products and in silico toxicity prediction, *Sci. Total Environ.* 692 (2019) 503–510. <https://doi.org/10.1016/J.SCITOTENV.2019.07.247>.
- [10] C. Wang, J. Zhai, H. Jiang, D. Liu, L. Zhang, CdS/Ag₂S nanocomposites photocatalyst with enhanced visible light photocatalysis activity, *Solid State Sci.* 98 (2019) 106020. <https://doi.org/10.1016/J.SOLIDSTATESCIENCES.2019.106020>.

- [11] J. Wen, L. Zhou, Q. Tang, X. Xiao, S. Sun, Photocatalytic degradation of organic pollutants by carbon quantum dots functionalized g-C₃N₄: A review, *Ecotoxicol. Environ. Saf.* 262 (2023) 115133. <https://doi.org/https://doi.org/10.1016/j.ecoenv.2023.115133>.
- [12] Q. Xiao, E. Jaatinen, H. Zhu, Direct photocatalysis for organic synthesis by using plasmonic-metal nanoparticles irradiated with visible light., *Chem. Asian J.* 9 (2014) 3046–3064. <https://doi.org/10.1002/asia.201402310>.
- [13] U. Qumar, J.Z. Hassan, R.A. Bhatti, A. Raza, G. Nazir, W. Nabgan, M. Ikram, Photocatalysis vs adsorption by metal oxide nanoparticles, *J. Mater. Sci. Technol.* 131 (2022) 122–166. <https://doi.org/https://doi.org/10.1016/j.jmst.2022.05.020>.
- [14] A. Parmar, G. Kaur, S. Kapil, V. Sharma, M.K. Choudhary, S. Sharma, Novel biogenic silver nanoparticles as invigorated catalytic and antibacterial tool: A cleaner approach towards environmental remediation and combating bacterial invasion, *Mater. Chem. Phys.* 238 (2019) 121861. <https://doi.org/https://doi.org/10.1016/j.matchemphys.2019.121861>.
- [15] R.M. Tripathi, S.J. Chung, Biogenic nanomaterials: Synthesis, characterization, growth mechanism, and biomedical applications, *J. Microbiol. Methods.* 157 (2019) 65–80. <https://doi.org/https://doi.org/10.1016/j.mimet.2018.12.008>.
- [16] A. Rastogi, P. Singh, F.A. Haraz, A. Barhoum, Chapter 19 - Biological synthesis of nanoparticles: an environmentally benign approach, in: A. Barhoum, A.S.B.T.-F. of N. Hamdy Makhoul (Eds.), *Micro Nano Technol.*, Elsevier, 2018: pp. 571–604. <https://doi.org/https://doi.org/10.1016/B978-0-323-51255-8.00023-9>.
- [17] A. Si, K. Pal, S. Kralj, G.S. El-Sayyad, F.G. de Souza, T. Narayanan, Sustainable preparation of gold nanoparticles via green chemistry approach for biogenic applications, *Mater. Today Chem.* 17 (2020) 100327. <https://doi.org/https://doi.org/10.1016/j.mtchem.2020.100327>.
- [18] D. Sharma, S. Kanchi, K. Bisetty, Biogenic synthesis of nanoparticles: A review, *Arab. J. Chem.* 12 (2019) 3576–3600. <https://doi.org/https://doi.org/10.1016/j.arabjc.2015.11.002>.
- [19] J. Annamalai, S.B. Ummalyma, A. Pandey, T. Bhaskar, Recent trends in microbial nanoparticle synthesis and potential application in environmental technology: a comprehensive review., *Environ. Sci. Pollut. Res. Int.* 28 (2021) 49362–49382. <https://doi.org/10.1007/s11356-021-15680-x>.
- [20] J. Jeevanandam, A. Barhoum, Y.S. Chan, A. Dufresne, M.K. Danquah, Review on nanoparticles and nanostructured materials: history, sources, toxicity and regulations, *Beilstein J. Nanotechnol.* 9 (2018) 1050–1074. <https://doi.org/10.3762/bjnano.9.98>.
- [21] E.L. Hu, D.T. Shaw, Synthesis and Assembly BT - Nanostructure Science and Technology: R&D Status and Trends in Nanoparticles, Nanostructured Materials, and Nanodevices, in: R.W. Siegel, E. Hu, D.M. Cox, H. Goronkin, L. Jelinski, C.C. Koch, J. Mendel, M.C. Roco, D.T. Shaw (Eds.), Springer Netherlands, Dordrecht, 1999: pp. 15–33. https://doi.org/10.1007/978-94-015-9185-0_2.
- [22] A. Rana, K. Yadav, S. Jagadevan, A comprehensive review on green synthesis of nature-inspired metal nanoparticles: Mechanism, application and toxicity, *J. Clean. Prod.* 272 (2020) 122880. <https://doi.org/https://doi.org/10.1016/j.jclepro.2020.122880>.
- [23] M. Shah, D. Fawcett, S. Sharma, S.K. Tripathy, G.E.J. Poinern, Green Synthesis of Metallic Nanoparticles via Biological Entities., *Mater. (Basel, Switzerland)*. 8 (2015) 7278–7308. <https://doi.org/10.3390/ma8115377>.
- [24] P. Praveen Kumar, M. Laxmi Deepak Bhatlu, K. Sukanya, S. Karthikeyan, N. Jayan, Synthesis

- of magnesium oxide nanoparticle by eco friendly method (green synthesis) – A review, *Mater. Today Proc.* (2020). <https://doi.org/https://doi.org/10.1016/j.matpr.2020.08.726>.
- [25] C.J. Murphy, T.K. Sau, A.M. Gole, C.J. Orendorff, J. Gao, L. Gou, S.E. Hunyadi, T. Li, Anisotropic Metal Nanoparticles: Synthesis, Assembly, and Optical Applications, *J. Phys. Chem. B.* 109 (2005) 13857–13870. <https://doi.org/10.1021/jp0516846>.
- [26] L.P. Silva, I.G. Reis, C.C. Bonatto, Green Synthesis of Metal Nanoparticles by Plants: Current Trends and Challenges BT - Green Processes for Nanotechnology: From Inorganic to Bioinspired Nanomaterials, in: V.A. Basiuk, E. V Basiuk (Eds.), Springer International Publishing, Cham, 2015: pp. 259–275. https://doi.org/10.1007/978-3-319-15461-9_9.
- [27] S. Mohammadinejad, H. Almasi, M. Esmaili, Simultaneous green synthesis and in-situ impregnation of silver nanoparticles into organic nanofibers by *Lythrum salicaria* extract: Morphological, thermal, antimicrobial and release properties., *Mater. Sci. Eng. C. Mater. Biol. Appl.* 105 (2019) 110115. <https://doi.org/10.1016/j.msec.2019.110115>.
- [28] A. Gour, N.K. Jain, Advances in green synthesis of nanoparticles, *Artif. Cells, Nanomedicine, Biotechnol.* 47 (2019) 844–851. <https://doi.org/10.1080/21691401.2019.1577878>.
- [29] A. Saravanan, P.S. Kumar, S. Karishma, D.-V.N. Vo, S. Jeevanantham, P.R. Yaashikaa, C.S. George, A review on biosynthesis of metal nanoparticles and its environmental applications, *Chemosphere.* 264 (2021) 128580. <https://doi.org/https://doi.org/10.1016/j.chemosphere.2020.128580>.
- [30] B. Khodadadi, M. Bordbar, M. Nasrollahzadeh, *Achillea millefolium* L. extract mediated green synthesis of waste peach kernel shell supported silver nanoparticles: Application of the nanoparticles for catalytic reduction of a variety of dyes in water, *J. Colloid Interface Sci.* 493 (2017) 85–93. <https://doi.org/https://doi.org/10.1016/j.jcis.2017.01.012>.
- [31] P. Rani, V. Kumar, P.P. Singh, A.S. Matharu, W. Zhang, K.-H. Kim, J. Singh, M. Rawat, Highly stable AgNPs prepared via a novel green approach for catalytic and photocatalytic removal of biological and non-biological pollutants, *Environ. Int.* 143 (2020) 105924. <https://doi.org/https://doi.org/10.1016/j.envint.2020.105924>.
- [32] I. Khan, K. Saeed, I. Khan, Nanoparticles: Properties, applications and toxicities, *Arab. J. Chem.* 12 (2019) 908–931. <https://doi.org/https://doi.org/10.1016/j.arabjc.2017.05.011>.
- [33] G. Marslin, K. Siram, Q. Maqbool, R.K. Selvakesavan, D. Kruszka, P. Kachlicki, G. Franklin, Secondary Metabolites in the Green Synthesis of Metallic Nanoparticles, *Mater. (Basel, Switzerland)*. 11 (2018) 940. <https://doi.org/10.3390/ma11060940>.
- [34] T. Parandhaman, M.D. Dey, S.K. Das, Biofabrication of supported metal nanoparticles: exploring the bioinspiration strategy to mitigate the environmental challenges, *Green Chem.* 21 (2019) 5469–5500. <https://doi.org/10.1039/C9GC02291K>.
- [35] M. Bordbar, N. Mortazavimanesh, Green synthesis of Pd/walnut shell nanocomposite using *Equisetum arvense* L. leaf extract and its application for the reduction of 4-nitrophenol and organic dyes in a very short time, *Environ. Sci. Pollut. Res.* 24 (2017) 4093–4104. <https://doi.org/10.1007/s11356-016-8183-y>.
- [36] A. Kumar, G. Sharma, M. Naushad, A.H. Al-Muhtaseb, A. García-Peñas, G.T. Mola, C. Si, F.J. Stadler, Bio-inspired and biomaterials-based hybrid photocatalysts for environmental detoxification: A review, *Chem. Eng. J.* 382 (2020) 122937. <https://doi.org/https://doi.org/10.1016/j.cej.2019.122937>.
- [37] H. Duan, D. Wang, Y. Li, Green chemistry for nanoparticle synthesis, *Chem. Soc. Rev.* 44

- (2015) 5778–5792. <https://doi.org/10.1039/C4CS00363B>.
- [38] A. Dieudonné, D. Pignol, S. Prévéral, Magnetosomes: biogenic iron nanoparticles produced by environmental bacteria., *Appl. Microbiol. Biotechnol.* 103 (2019) 3637–3649. <https://doi.org/10.1007/s00253-019-09728-9>.
- [39] E.A. Adebayo, M.A. Azeez, M.B. Alao, A.M. Oke, D.A. Aina, Fungi as veritable tool in current advances in nanobiotechnology., *Heliyon.* 7 (2021) e08480. <https://doi.org/10.1016/j.heliyon.2021.e08480>.
- [40] K. He, G. Chen, G. Zeng, Z. Huang, Z. Guo, T. Huang, M. Peng, J. Shi, L. Hu, Applications of white rot fungi in bioremediation with nanoparticles and biosynthesis of metallic nanoparticles., *Appl. Microbiol. Biotechnol.* 101 (2017) 4853–4862. <https://doi.org/10.1007/s00253-017-8328-z>.
- [41] A. Roychoudhury, Yeast-mediated Green Synthesis of Nanoparticles for Biological Applications, *Indian J. Pharm. Biol. Res.* 8 (2020) 26–31. <https://doi.org/10.30750/ijpbr.8.3.4>.
- [42] X. Zhang, Y. Qu, W. Shen, J. Wang, H. Li, Z. Zhang, S. Li, J. Zhou, Biogenic synthesis of gold nanoparticles by yeast *Magnusiomyces ingens* LH-F1 for catalytic reduction of nitrophenols, *Colloids Surfaces A Physicochem. Eng. Asp.* 497 (2016) 280–285. <https://doi.org/https://doi.org/10.1016/j.colsurfa.2016.02.033>.
- [43] A. Mukherjee, D. Sarkar, S. Sasmal, A Review of Green Synthesis of Metal Nanoparticles Using Algae., *Front. Microbiol.* 12 (2021) 693899. <https://doi.org/10.3389/fmicb.2021.693899>.
- [44] S.-N. Li, R. Wang, S.-H. Ho, Algae-mediated biosystems for metallic nanoparticle production: From synthetic mechanisms to aquatic environmental applications, *J. Hazard. Mater.* 420 (2021) 126625. <https://doi.org/https://doi.org/10.1016/j.jhazmat.2021.126625>.
- [45] R.G. Saratale, G.D. Saratale, H.S. Shin, J.M. Jacob, A. Pugazhendhi, M. Bhisare, G. Kumar, New insights on the green synthesis of metallic nanoparticles using plant and waste biomaterials: current knowledge, their agricultural and environmental applications., *Environ. Sci. Pollut. Res. Int.* 25 (2018) 10164–10183. <https://doi.org/10.1007/s11356-017-9912-6>.
- [46] S. Jadoun, R. Arif, N.K. Jangid, R.K. Meena, Green synthesis of nanoparticles using plant extracts: a review, *Environ. Chem. Lett.* 19 (2021) 355–374. <https://doi.org/10.1007/s10311-020-01074-x>.
- [47] A.M. El Shafey, Green synthesis of metal and metal oxide nanoparticles from plant leaf extracts and their applications: A review, *Green Process. Synth.* 9 (2020) 304–339. <https://doi.org/doi:10.1515/gps-2020-0031>.
- [48] A. Singh, S.B. Ummalyama, D. Sahoo, Bioremediation and biomass production of microalgae cultivation in river watercontaminated with pharmaceutical effluent., *Bioresour. Technol.* 307 (2020) 123233. <https://doi.org/10.1016/j.biortech.2020.123233>.
- [49] A. Sharma, A. Sagar, J. Rana, R. Rani, Green synthesis of silver nanoparticles and its antibacterial activity using fungus *Talaromyces purpureogenus* isolated from *Taxus baccata* Linn., *Micro Nano Syst. Lett.* 10 (2022) 2. <https://doi.org/10.1186/s40486-022-00144-9>.
- [50] X. Pei, Y. Qu, W. Shen, H. Li, X. Zhang, S. Li, Z. Zhang, X. Li, Green synthesis of gold nanoparticles using fungus *Mariannaea* sp. HJ and their catalysis in reduction of 4-nitrophenol, *Environ. Sci. Pollut. Res.* 24 (2017) 21649–21659. <https://doi.org/10.1007/s11356-017-9684-z>.
- [51] S. Mahanty, M. Bakshi, S. Ghosh, S. Chatterjee, S. Bhattacharyya, P. Das, S. Das, P. Chaudhuri,

- Green Synthesis of Iron Oxide Nanoparticles Mediated by Filamentous Fungi Isolated from Sundarban Mangrove Ecosystem, India, *Bionanoscience*. 9 (2019) 637–651. <https://doi.org/10.1007/s12668-019-00644-w>.
- [52] S.E.-D. Hassan, A. Fouda, A.A. Radwan, S.S. Salem, M.G. Barghoth, M.A. Awad, A.M. Abdo, M.S. El-Gamal, Endophytic actinomycetes *Streptomyces* spp mediated biosynthesis of copper oxide nanoparticles as a promising tool for biotechnological applications., *J. Biol. Inorg. Chem. JBIC a Publ. Soc. Biol. Inorg. Chem.* 24 (2019) 377–393. <https://doi.org/10.1007/s00775-019-01654-5>.
- [53] A.S. Vijayanandan, R.M. Balakrishnan, Biosynthesis of cobalt oxide nanoparticles using endophytic fungus *Aspergillus nidulans*., *J. Environ. Manage.* 218 (2018) 442–450. <https://doi.org/10.1016/j.jenvman.2018.04.032>.
- [54] H. Zhang, H. Zhou, J. Bai, Y. Li, J. Yang, Q. Ma, Y. Qu, Biosynthesis of selenium nanoparticles mediated by fungus *Mariannaea* sp. HJ and their characterization, *Colloids Surfaces A Physicochem. Eng. Asp.* 571 (2019) 9–16. <https://doi.org/https://doi.org/10.1016/j.colsurfa.2019.02.070>.
- [55] J. Li, G. Ma, H. Liu, H. Liu, Yeast cells carrying metal nanoparticles, *Mater. Chem. Phys.* 207 (2018) 373–379. <https://doi.org/https://doi.org/10.1016/j.matchemphys.2018.01.001>.
- [56] S. Seshadri, K. Saranya, M. Kowshik, Green synthesis of lead sulfide nanoparticles by the lead resistant marine yeast, *Rhodospiridium diobovatum*, *Biotechnol. Prog.* 27 (2011) 1464–1469. <https://doi.org/https://doi.org/10.1002/btpr.651>.
- [57] J.L. Sharma, V. Dhayal, R.K. Sharma, White-rot fungus mediated green synthesis of zinc oxide nanoparticles and their impregnation on cellulose to develop environmental friendly antimicrobial fibers., *3 Biotech.* 11 (2021) 269. <https://doi.org/10.1007/s13205-021-02840-6>.
- [58] M. Peiris, T. Gunasekara, P.M. Jayaweera, S. Fernando, TiO₂ Nanoparticles from Baker's Yeast: A Potent Antimicrobial., *J. Microbiol. Biotechnol.* 28 (2018) 1664–1670. <https://doi.org/10.4014/jmb.1807.07005>.
- [59] N. Shabnam, P. Pardha-Saradhi, Photosynthetic electron transport system promotes synthesis of Au-nanoparticles, *PLoS One.* 8 (2013) e71123–e71123. <https://doi.org/10.1371/journal.pone.0071123>.
- [60] A. Arya, K. Gupta, T.S. Chundawat, D. Vaya, Biogenic Synthesis of Copper and Silver Nanoparticles Using Green Alga *Botryococcus braunii* and Its Antimicrobial Activity., *Bioinorg. Chem. Appl.* 2018 (2018) 7879403. <https://doi.org/10.1155/2018/7879403>.
- [61] N. Abdel-Raouf, N.M. Al-Enazi, I.B.M. Ibraheem, Green biosynthesis of gold nanoparticles using *Galaxaura elongata* and characterization of their antibacterial activity, *Arab. J. Chem.* 10 (2017) S3029–S3039. <https://doi.org/https://doi.org/10.1016/j.arabjc.2013.11.044>.
- [62] R.A. Hamouda, M.H. Hussein, R.A. Abo-Elmagd, S.S. Bawazir, Synthesis and biological characterization of silver nanoparticles derived from the cyanobacterium *Oscillatoria limnetica*., *Sci. Rep.* 9 (2019) 13071. <https://doi.org/10.1038/s41598-019-49444-y>.
- [63] M.S. Alsaggaf, A.M. Diab, B.E.F. ElSaied, A.A. Tayel, S.H. Moussa, Application of ZnO Nanoparticles Phycosynthesized with *Ulva fasciata* Extract for Preserving Peeled Shrimp Quality., *Nanomater.* (Basel, Switzerland). 11 (2021). <https://doi.org/10.3390/nano11020385>.
- [64] D.M.S.A. Salem, M.M. Ismail, H.R.Z. Tadros, Evaluation of the antibiofilm activity of three

- seaweed species and their biosynthesized iron oxide nanoparticles (Fe₃O₄-NPs), *Egypt. J. Aquat. Res.* 46 (2020) 333–339. <https://doi.org/https://doi.org/10.1016/j.ejar.2020.09.001>.
- [65] J.L. Gardea-Torresdey, E. Gomez, J.R. Peralta-Videa, J.G. Parsons, H. Troiani, M. Jose-Yacamán, Alfalfa Sprouts: A Natural Source for the Synthesis of Silver Nanoparticles, *Langmuir*. 19 (2003) 1357–1361. <https://doi.org/10.1021/la020835i>.
- [66] S. Baker, D. Rakshith, K.S. Kavitha, P. Santosh, H.U. Kavitha, Y. Rao, S. Satish, Plants: Emerging as Nanofactories towards Facile Route in Synthesis of Nanoparticles, *Bioimpacts*. 3 (2013) 111–117. <https://doi.org/10.5681/bi.2013.012>.
- [67] P. Wang, N.W. Menzies, H. Chen, X. Yang, S.P. McGrath, F.-J. Zhao, P.M. Kopittke, Risk of Silver Transfer from Soil to the Food Chain Is Low after Long-Term (20 Years) Field Applications of Sewage Sludge, *Environ. Sci. Technol.* 52 (2018) 4901–4909. <https://doi.org/10.1021/acs.est.8b00204>.
- [68] X. Shi, Z. Li, W. Chen, L. Qiang, J. Xia, M. Chen, L. Zhu, P.J.J. Alvarez, Fate of TiO₂ nanoparticles entering sewage treatment plants and bioaccumulation in fish in the receiving streams, *NanoImpact*. 3–4 (2016) 96–103. <https://doi.org/https://doi.org/10.1016/j.impact.2016.09.002>.
- [69] Q. Abbas, B. Yousaf, Amina, M.U. Ali, M.A.M. Munir, A. El-Naggar, J. Rinklebe, M. Naushad, Transformation pathways and fate of engineered nanoparticles (ENPs) in distinct interactive environmental compartments: A review, *Environ. Int.* 138 (2020) 105646. <https://doi.org/https://doi.org/10.1016/j.envint.2020.105646>.
- [70] C. Lei, Y. Sun, D.C.W. Tsang, D. Lin, Environmental transformations and ecological effects of iron-based nanoparticles, *Environ. Pollut.* 232 (2018) 10–30. <https://doi.org/https://doi.org/10.1016/j.envpol.2017.09.052>.
- [71] B. Nowack, J.F. Ranville, S. Diamond, J.A. Gallego-Urrea, C. Metcalfe, J. Rose, N. Horne, A.A. Koelmans, S.J. Klaine, Potential scenarios for nanomaterial release and subsequent alteration in the environment., *Environ. Toxicol. Chem.* 31 (2012) 50–59. <https://doi.org/10.1002/etc.726>.
- [72] D.M. Mitrano, P. Limpiteprakan, S. Babel, B. Nowack, Durability of nano-enhanced textiles through the life cycle: releases from landfilling after washing, *Environ. Sci. Nano*. 3 (2016) 375–387. <https://doi.org/10.1039/C6EN00023A>.
- [73] O.J. Osborne, S. Lin, C.H. Chang, Z. Ji, X. Yu, X. Wang, S. Lin, T. Xia, A.E. Nel, Organ-Specific and Size-Dependent Ag Nanoparticle Toxicity in Gills and Intestines of Adult Zebrafish, *ACS Nano*. 9 (2015) 9573–9584. <https://doi.org/10.1021/acs.nano.5b04583>.
- [74] J.D. Martin, P.C. Frost, H. Hintelmann, K. Newman, M.J. Paterson, L. Hayhurst, M.D. Rennie, M.A. Xenopoulos, V. Yargeau, C.D. Metcalfe, Accumulation of Silver in Yellow Perch (*Perca flavescens*) and Northern Pike (*Esox lucius*) From a Lake Dosed with Nanosilver., *Environ. Sci. Technol.* 52 (2018) 11114–11122. <https://doi.org/10.1021/acs.est.8b03146>.
- [75] J. Hou, Y. Zhou, C. Wang, S. Li, X. Wang, Toxic Effects and Molecular Mechanism of Different Types of Silver Nanoparticles to the Aquatic Crustacean *Daphnia magna*., *Environ. Sci. Technol.* 51 (2017) 12868–12878. <https://doi.org/10.1021/acs.est.7b03918>.
- [76] L. Yin, Y. Cheng, B. Espinasse, B.P. Colman, M. Auffan, M. Wiesner, J. Rose, J. Liu, E.S. Bernhardt, More than the ions: the effects of silver nanoparticles on *Lolium multiflorum*., *Environ. Sci. Technol.* 45 (2011) 2360–2367. <https://doi.org/10.1021/es103995x>.

- [77] A.E. Pradas Del Real, V. Vidal, M. Carriere, H. Castillo-Michel, C. Levard, P. Chaurand, G. Sarret, Ag nanoparticles and wheat roots: a complex interplay, *Environ. Sci. Technol.* 51 (2017). <https://doi.org/10.1021/acs.est.7b00422>.
- [78] M.S. Abdel-Aziz, K.S. Abou-El-Sherbini, E.M.A. Hamzawy, M.H.A. Amr, S. El-Dafrawy, Green Synthesis of Silver Nano-particles by *Macroccoccus bovicus* and Its Immobilization onto Montmorillonite Clay for Antimicrobial Functionality, *Appl. Biochem. Biotechnol.* 176 (2015) 2225–2241. <https://doi.org/10.1007/s12010-015-1710-3>.
- [79] V. Porley, N. Robertson, 6 - Substrate and support materials for photocatalysis, in: R. Boukherroub, S.B. Ogale, N.B.T.-N.P. Robertson (Eds.), *Micro Nano Technol.*, Elsevier, 2020: pp. 129–171. <https://doi.org/https://doi.org/10.1016/B978-0-12-817836-2.00006-5>.
- [80] R. Oblak, M. Kete, U.L. Štangar, M. Tasbihi, Alternative support materials for titania photocatalyst towards degradation of organic pollutants, *J. Water Process Eng.* 23 (2018) 142–150. <https://doi.org/https://doi.org/10.1016/j.jwpe.2018.03.015>.
- [81] W. Zou, B. Gao, Y.S. Ok, L. Dong, Integrated adsorption and photocatalytic degradation of volatile organic compounds (VOCs) using carbon-based nanocomposites: A critical review, *Chemosphere.* 218 (2019) 845–859. <https://doi.org/https://doi.org/10.1016/j.chemosphere.2018.11.175>.
- [82] M.A. Mohd Adnan, N. Muhd Julkapli, M.N.I. Amir, A. Maamor, Effect on different TiO₂ photocatalyst supports on photodecolorization of synthetic dyes: a review, *Int. J. Environ. Sci. Technol.* 16 (2019) 547–566. <https://doi.org/10.1007/s13762-018-1857-x>.
- [83] N.M. Ainali, D. Kalaronis, E. Evgenidou, D.N. Bikiaris, D.A. Lambropoulou, Insights into Biodegradable Polymer-Supported Titanium Dioxide Photocatalysts for Environmental Remediation, *Macromol . 1* (2021). <https://doi.org/10.3390/macromol1030015>.
- [84] A.Y. Shan, T.I.M. Ghazi, S.A. Rashid, Immobilisation of titanium dioxide onto supporting materials in heterogeneous photocatalysis: A review, *Appl. Catal. A Gen.* 389 (2010) 1–8. <https://doi.org/https://doi.org/10.1016/j.apcata.2010.08.053>.
- [85] M.J. Ndolomingo, N. Bingwa, R. Meijboom, Review of supported metal nanoparticles: synthesis methodologies, advantages and application as catalysts, *J. Mater. Sci.* 55 (2020) 6195–6241. <https://doi.org/10.1007/s10853-020-04415-x>.
- [86] K. Vikrant, C.M. Park, K.-H. Kim, S. Kumar, E.-C. Jeon, Recent advancements in photocatalyst-based platforms for the destruction of gaseous benzene: Performance evaluation of different modes of photocatalytic operations and against adsorption techniques, *J. Photochem. Photobiol. C Photochem. Rev.* 41 (2019) 100316. <https://doi.org/https://doi.org/10.1016/j.jphotochemrev.2019.08.003>.
- [87] V. Tan, L. Vinh, Supported-Metal Oxide Nanoparticles-Potential Photocatalysts, in: 2020. <https://doi.org/10.5772/intechopen.93238>.
- [88] J.Y. Xu, X.C. Lei, R. Yang, Z.Z. Fan, In Situ Formation of Carbon Nanomaterials on Bulk Metallic Materials, *J. Nanomater.* 2014 (2014) 690630. <https://doi.org/10.1155/2014/690630>.
- [89] P. Tabrizian, W. Ma, A. Bakr, M.S. Rahaman, pH-sensitive and magnetically separable Fe/Cu bimetallic nanoparticles supported by graphene oxide (GO) for high-efficiency removal of tetracyclines, *J. Colloid Interface Sci.* 534 (2019) 549–562. <https://doi.org/https://doi.org/10.1016/j.jcis.2018.09.034>.
- [90] T. Hennebel, S. De Corte, L. Vanhaecke, K. Vanherck, I. Forrez, B. De Gussemme, P. Verhagen, K. Verbeken, B. Van der Bruggen, I. Vankelecom, N. Boon, W. Verstraete, Removal of diatrizoate

- with catalytically active membranes incorporating microbially produced palladium nanoparticles., *Water Res.* 44 (2010) 1498–1506. <https://doi.org/10.1016/j.watres.2009.10.041>.
- [91] Z. Arif, N.K. Sethy, P.K. Mishra, B. Verma, Green approach for the synthesis of ultrafiltration photocatalytic membrane for tannery wastewater: modeling and optimization, *Int. J. Environ. Sci. Technol.* 17 (2020) 3397–3410. <https://doi.org/10.1007/s13762-020-02719-8>.
- [92] J.A. Mazumder, M. Perwez, R. Noori, M. Sardar, Development of sustainable and reusable silver nanoparticle-coated glass for the treatment of contaminated water., *Environ. Sci. Pollut. Res. Int.* 26 (2019) 23070–23081. <https://doi.org/10.1007/s11356-019-05647-4>.
- [93] A.H. Gemeay, E.F. Aboelfetoh, R.G. El-sharkawy, Immobilization of Green Synthesized Silver Nanoparticles onto Amino-Functionalized Silica and Their Application for Indigo Carmine Dye Removal, *Water, Air, & Soil Pollut.* 229 (2017) 1–17.
- [94] M. Bilal, S. Khan, J. Ali, M. Ismail, M.I. Khan, A.M. Asiri, S.B. Khan, Biosynthesized silver supported catalysts for disinfection of *Escherichia coli* and organic pollutant from drinking water, *J. Mol. Liq.* 281 (2019) 295–306. <https://doi.org/https://doi.org/10.1016/j.molliq.2019.02.087>.
- [95] A. Nizam, V.G. Warriar, J. Devasia, N. Ganganagappa, Magnetic iron oxide nanoparticles immobilized on microporous molecular sieves as efficient porous catalyst for photodegradation, transesterification and esterification reactions, *J. Porous Mater.* (2021). <https://doi.org/10.1007/s10934-021-01150-9>.
- [96] A. Rostami-Vartooni, A. Moradi-Saadatmand, Green synthesis of magnetically recoverable Fe₃O₄/HZSM-5 and its Ag nanocomposite using *Juglans regia* L. leaf extract and their evaluation as catalysts for reduction of organic pollutants, *IET Nanobiotechnology.* 13 (2019) 407–415. <https://doi.org/https://doi.org/10.1049/iet-nbt.2018.5089>.
- [97] M. Tajbakhsh, H. Alinezhad, M. Nasrollahzadeh, T.A. Kamali, Green synthesis of the Ag/HZSM-5 nanocomposite by using *Euphorbia heterophylla* leaf extract: A recoverable catalyst for reduction of organic dyes, *J. Alloys Compd.* 685 (2016) 258–265. <https://doi.org/https://doi.org/10.1016/j.jallcom.2016.05.278>.
- [98] A. Toli, C. Mystrioti, I. Avgoustidis, N. Papassiopi, Fixed-bed flow experiments with supported green nZVI for the remediation of contaminated waters: Effect of pH and background solution composition, *Chemosphere.* 279 (2021) 130472. <https://doi.org/https://doi.org/10.1016/j.chemosphere.2021.130472>.
- [99] S. Naghdi, M. Sajjadi, M. Nasrollahzadeh, K.Y. Rhee, S.M. Sajadi, B. Jaleh, *Cuscuta reflexa* leaf extract mediated green synthesis of the Cu nanoparticles on graphene oxide/manganese dioxide nanocomposite and its catalytic activity toward reduction of nitroarenes and organic dyes, *J. Taiwan Inst. Chem. Eng.* 86 (2018) 158–173. <https://doi.org/https://doi.org/10.1016/j.jtice.2017.12.017>.
- [100] C. Xue, W. Cai, X. Weng, G. Owens, Z. Chen, A one step synthesis of hybrid Fe/Ni-rGO using green tea extract for the removal of mixed contaminants, *Chemosphere.* 284 (2021) 131369. <https://doi.org/https://doi.org/10.1016/j.chemosphere.2021.131369>.
- [101] R. Ranjith, V. Renganathan, S.-M. Chen, N.S. Selvan, P.S. Rajam, Green synthesis of reduced graphene oxide supported TiO₂/Co₃O₄ nanocomposite for photocatalytic degradation of methylene blue and crystal violet, *Ceram. Int.* 45 (2019) 12926–12933. <https://doi.org/https://doi.org/10.1016/j.ceramint.2019.03.219>.

- [102] S. Lewis, V. Smuleac, A. Montague, L. Bachas, D. Bhattacharyya, Iron-Functionalized Membranes for Nanoparticle Synthesis and Reactions, *Sep. Sci. Technol.* 44 (2009) 3289–3311. <https://doi.org/10.1080/01496390903212805>.
- [103] M.F.R. Samsudin, A. Mahmood, S. Sufian, Enhanced photocatalytic degradation of wastewater over RGO-TiO₂/BiVO₄ photocatalyst under solar light irradiation, *J. Mol. Liq.* 268 (2018) 26–36. <https://doi.org/https://doi.org/10.1016/j.molliq.2018.05.012>.
- [104] F. Harjati, P.W. Citradewi, G. Purwiandono, I. Fatimah, Green synthesis of hematite/TUD-1 nanocomposite as efficient photocatalyst for bromophenol blue and methyl violet degradation, *Arab. J. Chem.* 13 (2020) 8395–8410. <https://doi.org/https://doi.org/10.1016/j.arabjc.2020.05.032>.
- [105] S. Telalović, A. Ramanathan, G. Mul, U. Hanefeld, TUD-1: synthesis and application of a versatile catalyst, carrier, material..., *J. Mater. Chem.* 20 (2010) 642–658. <https://doi.org/10.1039/B904193A>.
- [106] M.O. Alfred, M.O. Omorogie, O. Bodede, R. Moodley, A. Ogunlaja, O.G. Adeyemi, C. Günter, A. Taubert, I. Iermak, H. Eckert, I.D.A. Silva, A.S.S. de Camargo, A. de Jesus Motheo, S.M. Clarke, E.I. Unuabonah, Solar-active clay-TiO₂ nanocomposites prepared via biomass assisted synthesis: Efficient removal of ampicillin, sulfamethoxazole and artemether from water, *Chem. Eng. J.* 398 (2020) 125544. <https://doi.org/https://doi.org/10.1016/j.cej.2020.125544>.
- [107] C. de S.F. Gomes, J.B.P. Silva, Minerals and clay minerals in medical geology, *Appl. Clay Sci.* 36 (2007) 4–21. <https://doi.org/https://doi.org/10.1016/j.clay.2006.08.006>.
- [108] C. Li, N. Zhu, S. Yang, X. He, S. Zheng, Z. Sun, D.D. Dionysiou, A review of clay based photocatalysts: Role of phyllosilicate mineral in interfacial assembly, microstructure control and performance regulation, *Chemosphere.* 273 (2021) 129723. <https://doi.org/https://doi.org/10.1016/j.chemosphere.2021.129723>.
- [109] G. Gopal, H. Sankar, C. Natarajan, A. Mukherjee, Tetracycline removal using green synthesized bimetallic nZVI-Cu and bentonite supported green nZVI-Cu nanocomposite: A comparative study, *J. Environ. Manage.* 254 (2020) 109812. <https://doi.org/https://doi.org/10.1016/j.jenvman.2019.109812>.
- [110] T. Baran, M. Nasrollahzadeh, Facile fabrication of magnetically separable palladium nanoparticles supported on modified kaolin as a highly active heterogeneous catalyst for Suzuki coupling reactions, *J. Phys. Chem. Solids.* 146 (2020) 109566. <https://doi.org/https://doi.org/10.1016/j.jpcs.2020.109566>.
- [111] N. Rakhshan, M. Mansournia, F. Jookar Kashi, Plant Extract-Strategy Using Teucrium Polium Stems to Green Synthesize Ag/AgCl Bionanocomposite Imprinted on Fe₃O₄/kaolinite and Potentials in Catalytic and Chemosensor Applications, *Arab. J. Chem.* (2022) 103719. <https://doi.org/https://doi.org/10.1016/j.arabjc.2022.103719>.
- [112] U. Khunjan, P. Kasikamphaiboon, Green Synthesis of Kaolin-Supported Nanoscale Zero-Valent Iron Using Ruellia tuberosa Leaf Extract for Effective Decolorization of Azo Dye Reactive Black 5, *Arab. J. Sci. Eng.* 46 (2021) 383–394. <https://doi.org/10.1007/s13369-020-04831-w>.
- [113] F. Moradi, S. Sedaghat, S. Arab-Salmanabadi, O. Moradi, Biosynthesis of silver-montmorillonite nanocomposites using *Ocimum Basilicum* and *Teucrium Polium*; a comparative study, *Mater. Res. Express.* 6 (2019) 125008. <https://doi.org/10.1088/2053-1591/ab5474>.
- [114] J. Yang, S. Wang, N. Xu, Z. Ye, H. Yang, X. Huangfu, Synthesis of montmorillonite-supported nano-zero-valent iron via green tea extract: Enhanced transport and application for hexavalent

- chromium removal from water and soil, *J. Hazard. Mater.* 419 (2021) 126461. <https://doi.org/https://doi.org/10.1016/j.jhazmat.2021.126461>.
- [115] S. Sohrabnezhad, A. Seifi, The green synthesis of Ag/ZnO in montmorillonite with enhanced photocatalytic activity, *Appl. Surf. Sci.* 386 (2016) 33–40. <https://doi.org/https://doi.org/10.1016/j.apsusc.2016.05.102>.
- [116] S. Sohrabnezhad, M. Rassa, A. Seifi, Green synthesis of Ag nanoparticles in montmorillonite, *Mater. Lett.* 168 (2016) 28–30. <https://doi.org/https://doi.org/10.1016/j.matlet.2016.01.025>.
- [117] N. Choudhary, V.K. Yadav, K.K. Yadav, A.I. Almohana, S.F. Almojil, G. Gnanamoorthy, D.-H. Kim, S. Islam, P. Kumar, B.-H. Jeon, Application of Green Synthesized MMT/Ag Nanocomposite for Removal of Methylene Blue from Aqueous Solution, *Water* . 13 (2021). <https://doi.org/10.3390/w13223206>.
- [118] M. Honarmand, M. Golmohammadi, A. Naeimi, Green synthesis of SnO₂-bentonite nanocomposites for the efficient photodegradation of methylene blue and eriochrome black-T, *Mater. Chem. Phys.* 241 (2020) 122416. <https://doi.org/https://doi.org/10.1016/j.matchemphys.2019.122416>.
- [119] K. Sravanthi, D. Ayodhya, P.Y. Swamy, Green synthesis, characterization and catalytic activity of 4-nitrophenol reduction and formation of benzimidazoles using bentonite supported zero valent iron nanoparticles, *Mater. Sci. Energy Technol.* 2 (2019) 298–307. <https://doi.org/https://doi.org/10.1016/j.mset.2019.02.003>.
- [120] S.M. Sajadi, K. Kolo, S.M. Hamad, S.A. Mahmud, A.A. Barzinjy, S.M. Hussein, Green Synthesis of the Ag/Bentonite Nanocomposite Using *Euphorbia larica* Extract: A Reusable Catalyst for Efficient Reduction of Nitro Compounds and Organic Dyes, *ChemistrySelect*. 3 (2018) 12274–12280. <https://doi.org/https://doi.org/10.1002/slct.201802707>.
- [121] A.A. Romeh, R.A. Ibrahim Saber, Green nano-phytoremediation and solubility improving agents for the remediation of chlorfenapyr contaminated soil and water, *J. Environ. Manage.* 260 (2020) 110104. <https://doi.org/https://doi.org/10.1016/j.jenvman.2020.110104>.
- [122] Z. Issaabadi, M. Nasrollahzadeh, S.M. Sajadi, Green synthesis of the copper nanoparticles supported on bentonite and investigation of its catalytic activity, *J. Clean. Prod.* 142 (2017) 3584–3591. <https://doi.org/https://doi.org/10.1016/j.jclepro.2016.10.109>.
- [123] A. Rostami-Vartooni, M. Alizadeh, M. Bagherzadeh, Green synthesis, characterization and catalytic activity of natural bentonite-supported copper nanoparticles for the solvent-free synthesis of 1-substituted 1H-1,2,3,4-tetrazoles and reduction of 4-nitrophenol, *Beilstein J. Nanotechnol.* 6 (2015) 2300–2309.
- [124] M. Nasrollahzadeh, S.M. Sajadi, M. Maham, I. Kohsari, Biosynthesis, characterization and catalytic activity of the Pd/bentonite nanocomposite for base- and ligand-free oxidative hydroxylation of phenylboronic acid and reduction of chromium (VI) and nitro compounds, *Microporous Mesoporous Mater.* 271 (2018) 128–137. <https://doi.org/https://doi.org/10.1016/j.micromeso.2018.05.045>.
- [125] M. Golmohammadi, M. Honarmand, A. Esmaeili, Biosynthesis of ZnO nanoparticles supported on bentonite and the evaluation of its photocatalytic activity, *Mater. Res. Bull.* 149 (2022) 111714. <https://doi.org/https://doi.org/10.1016/j.materresbull.2021.111714>.
- [126] A. Soliemanzadeh, M. Fekri, Synthesis of clay-supported nanoscale zero-valent iron using green tea extract for the removal of phosphorus from aqueous solutions, *Chinese J. Chem. Eng.* 25

- (2017) 924–930. <https://doi.org/https://doi.org/10.1016/j.cjche.2016.12.006>.
- [127] A. Soliemanzadeh, M. Fekri, The application of green tea extract to prepare bentonite-supported nanoscale zero-valent iron and its performance on removal of Cr(VI): Effect of relative parameters and soil experiments, *Microporous Mesoporous Mater.* 239 (2017) 60–69. <https://doi.org/https://doi.org/10.1016/j.micromeso.2016.09.050>.
- [128] A.K. Hassan, G.Y. Al-Kindi, D. Ghanim, Green synthesis of bentonite-supported iron nanoparticles as a heterogeneous Fenton-like catalyst: Kinetics of decolorization of reactive blue 238 dye, *Water Sci. Eng.* 13 (2020) 286–298. <https://doi.org/https://doi.org/10.1016/j.wse.2020.12.001>.
- [129] R. Abbassi, A.K. Yadav, N. Kumar, S. Huang, P.R. Jaffe, Modeling and optimization of dye removal using “green” clay supported iron nano-particles, *Ecol. Eng.* 61 (2013) 366–370. <https://doi.org/https://doi.org/10.1016/j.ecoleng.2013.09.040>.
- [130] G. Al Kindi, A. Hassan, D. Yahya, H. Alhaidri, The nanoparticles zero-valent synthesis by black tea extract to remove rb 238 using synthetic and natural wastewater by packed bed reactor, *IOP Conf. Ser. Earth Environ. Sci.* 779 (2021) 12092. <https://doi.org/10.1088/1755-1315/779/1/012092>.
- [131] A. Rostami-Vartooni, L. Rostami, M. Bagherzadeh, Green synthesis of Fe₃O₄/bentonite-supported Ag and Pd nanoparticles and investigation of their catalytic activities for the reduction of azo dyes, *J. Mater. Sci. Mater. Electron.* 30 (2019) 21377–21387. <https://doi.org/10.1007/s10854-019-02514-3>.
- [132] G. Gopal, R. KVG, S. M, L.A.A. J, N. Chandrasekaran, A. Mukherjee, Green synthesized Fe/Pd and in-situ Bentonite-Fe/Pd composite for efficient tetracycline removal, *J. Environ. Chem. Eng.* 8 (2020) 104126. <https://doi.org/https://doi.org/10.1016/j.jece.2020.104126>.
- [133] G. Gopal, C. Natarajan, A. Mukherjee, Synergistic removal of tetracycline and copper (II) by in-situ B-Fe/Ni nanocomposite—A novel and an environmentally sustainable green nanomaterial, *Environ. Technol. Innov.* 25 (2022) 102187. <https://doi.org/https://doi.org/10.1016/j.eti.2021.102187>.
- [134] B. Srikanth, R. Goutham, R. Badri Narayan, A. Ramprasath, K.P. Gopinath, A.R. Sankaranarayanan, Recent advancements in supporting materials for immobilised photocatalytic applications in waste water treatment, *J. Environ. Manage.* 200 (2017) 60–78. <https://doi.org/https://doi.org/10.1016/j.jenvman.2017.05.063>.
- [135] B. Khodadadi, M. Bordbar, A. Yeganeh-Faal, M. Nasrollahzadeh, Green synthesis of Ag nanoparticles/clinoptilolite using Vaccinium macrocarpon fruit extract and its excellent catalytic activity for reduction of organic dyes, *J. Alloys Compd.* 719 (2017) 82–88. <https://doi.org/https://doi.org/10.1016/j.jallcom.2017.05.135>.
- [136] A. Hatamifard, M. Nasrollahzadeh, S.M. Sajadi, Biosynthesis, characterization and catalytic activity of an Ag/zeolite nanocomposite for base- and ligand-free oxidative hydroxylation of phenylboronic acid and reduction of a variety of dyes at room temperature, *New J. Chem.* 40 (2016) 2501–2513. <https://doi.org/10.1039/C5NJ02909K>.
- [137] M. Bordbar, Z. Sharifi-Zarchi, B. Khodadadi, Green synthesis of copper oxide nanoparticles/clinoptilolite using Rheum palmatum L. root extract: high catalytic activity for reduction of 4-nitro phenol, rhodamine B, and methylene blue, *J. Sol-Gel Sci. Technol.* 81 (2017) 724–733. <https://doi.org/10.1007/s10971-016-4239-1>.
- [138] M. Nasrollahzadeh, S.M. Sajadi, M. Maham, H.R. Dasmeh, In situ green synthesis of Cu

- nanoparticles supported on natural Natrolite zeolite for the reduction of 4-nitrophenol, congo red and methylene blue, *IET Nanobiotechnology*. 11 (2017) 538–545. <https://doi.org/https://doi.org/10.1049/iet-nbt.2016.0143>.
- [139] A. Hatamifard, M. Nasrollahzadeh, J. Lipkowski, Green synthesis of a natrolite zeolite/palladium nanocomposite and its application as a reusable catalyst for the reduction of organic dyes in a very short time, *RSC Adv.* 5 (2015) 91372–91381. <https://doi.org/10.1039/C5RA18476B>.
- [140] Q. Xu, W. Li, L. Ma, D. Cao, G. Owens, Z. Chen, Simultaneous removal of ammonia and phosphate using green synthesized iron oxide nanoparticles dispersed onto zeolite, *Sci. Total Environ.* 703 (2020) 135002. <https://doi.org/https://doi.org/10.1016/j.scitotenv.2019.135002>.
- [141] K.V.G. Ravikumar, G. Debayan, P. Mrudula, N. Chandrasekaran, M. Amitava, In situ formation of bimetallic FeNi nanoparticles on sand through green technology: Application for tetracycline removal, *Front. Environ. Sci. Eng.* 14 (2019) 16. <https://doi.org/10.1007/s11783-019-1195-3>.
- [142] S.T. Kadhum, G.Y. Alkindi, T.M. Albayati, Eco friendly adsorbents for removal of phenol from aqueous solution employing nanoparticle zero-valent iron synthesized from modified green tea bio-waste and supported on silty clay, *Chinese J. Chem. Eng.* 36 (2021) 19–28. <https://doi.org/https://doi.org/10.1016/j.cjche.2020.07.031>.
- [143] M. Nasrollahzadeh, E. Mehdipour, M. Maryami, Efficient catalytic reduction of nitroarenes and organic dyes in water by synthesized Ag/diatomite nanocomposite using *Alocasia macrorrhiza* leaf extract, *J. Mater. Sci. Mater. Electron.* 29 (2018) 17054–17066. <https://doi.org/10.1007/s10854-018-9802-9>.
- [144] Q. Li, G. Zhai, Y. Xu, T. Odoom-Wubah, L. Jia, J. Huang, D. Sun, Q. Li, Diatomite Supported Pt Nanoparticles as Efficient Catalyst for Benzene Removal, *Ind. Eng. Chem. Res.* 58 (2019) 14008–14015. <https://doi.org/10.1021/acs.iecr.9b02835>.
- [145] A. Rostami-Vartooni, M. Nasrollahzadeh, M. Alizadeh, Green synthesis of perlite supported silver nanoparticles using *Hamamelis virginiana* leaf extract and investigation of its catalytic activity for the reduction of 4-nitrophenol and Congo red, *J. Alloys Compd.* 680 (2016) 309–314. <https://doi.org/https://doi.org/10.1016/j.jallcom.2016.04.008>.
- [146] M. Nasrollahzadeh, S.M. Sajadi, A. Rostami-Vartooni, M. Bagherzadeh, R. Safari, Immobilization of copper nanoparticles on perlite: Green synthesis, characterization and catalytic activity on aqueous reduction of 4-nitrophenol, *J. Mol. Catal. A Chem.* 400 (2015) 22–30. <https://doi.org/https://doi.org/10.1016/j.molcata.2015.01.032>.
- [147] M. Maryami, M. Nasrollahzadeh, E. mehdipour, S.M. Sajadi, Green synthesis of the Pd/perlite nanocomposite using *Euphorbia neriifolia* L. leaf extract and evaluation of its catalytic activity, *Sep. Purif. Technol.* 184 (2017) 298–307. <https://doi.org/https://doi.org/10.1016/j.seppur.2017.05.003>.
- [148] H.B.W. Patterson, Chapter 6 - Filtration and Filters, in: G.R.B.T.-B. and P.F. and O. (Second E. List (Ed.), AOCs Press, 2009: pp. 159–188. <https://doi.org/https://doi.org/10.1016/B978-1-893997-91-2.50012-2>.
- [149] M. Baláž, E. V Boldyreva, D. Rybin, S. Pavlović, D. Rodríguez-Padrón, T. Mudrinić, R. Luque, State-of-the-Art of Eggshell Waste in Materials Science: Recent Advances in Catalysis, Pharmaceutical Applications, and Mechanochemistry., *Front. Bioeng. Biotechnol.* 8 (2020) 612567. <https://doi.org/10.3389/fbioe.2020.612567>.

- [150] M. Nasrollahzadeh, S.M. Sajadi, A. Hatamifard, Waste chicken eggshell as a natural valuable resource and environmentally benign support for biosynthesis of catalytically active Cu/eggshell, Fe₃O₄/eggshell and Cu/Fe₃O₄/eggshell nanocomposites, *Appl. Catal. B Environ.* 191 (2016) 209–227. <https://doi.org/https://doi.org/10.1016/j.apcatb.2016.02.042>.
- [151] M. Honarmand, M. Mirzadeh, M. Honarmand, Green synthesis of SnO(2)-ZnO-eggshell nanocomposites and study of their application in removal of mercury (II) ions from aqueous solution, *J. Environ. Heal. Sci. Eng.* 18 (2020) 1581–1593. <https://doi.org/10.1007/s40201-020-00576-8>.
- [152] M. Khazaei, A. Khazaei, M. Nasrollahzadeh, M.R. Tahsili, Highly efficient reusable Pd nanoparticles based on eggshell: Green synthesis, characterization and their application in catalytic reduction of variety of organic dyes and ligand-free oxidative hydroxylation of phenylboronic acid at room temperature, *Tetrahedron.* 73 (2017) 5613–5623. <https://doi.org/https://doi.org/10.1016/j.tet.2017.04.016>.
- [153] S.M. Sajadi, K. Kolo, S.M. Abdullah, S.M. Hamad, H.S. Khalid, A.T. Yassein, Green synthesis of highly recyclable CuO/ eggshell nanocomposite to efficient removal of aromatic containing compounds and reduction of 4-nitrophenol at room temperature, *Surfaces and Interfaces.* 13 (2018) 205–215. <https://doi.org/https://doi.org/10.1016/j.surfin.2018.08.006>.
- [154] X. Huang, L. Chang, Y. Lu, Z. Li, Z. Kang, X. Zhang, M. Liu, D.-P. Yang, Plant-mediated synthesis of dual-functional Eggshell/Ag nanocomposites towards catalysis and antibacterial applications, *Mater. Sci. Eng. C.* 113 (2020) 111015. <https://doi.org/https://doi.org/10.1016/j.msec.2020.111015>.
- [155] F. Lashkarizadeh, Green synthesis of ZnO/eggshell nanocomposite using ferulago macrocarpa extract and its photocatalytic and antimicrobial activity in water disinfection, *Inorg. Nano-Metal Chem.* (2021) 1–12. <https://doi.org/10.1080/24701556.2021.1983837>.
- [156] G. Zhang, C. Li, X. Zhang, X. Guo, Y. Liu, W. He, J. Liu, H. Wang, Y. Gao, Biogenic synthesis of photocatalytically active ZnS/ESM composites, *RSC Adv.* 4 (2014) 13569–13574. <https://doi.org/10.1039/C4RA00021H>.
- [157] Q. Wang, C. Ma, J. Tang, C. Zhang, L. Ma, Eggshell Membrane-Templated MnO₂ Nanoparticles: Facile Synthesis and Tetracycline Hydrochloride Decontamination, *Nanoscale Res. Lett.* 13 (2018) 255. <https://doi.org/10.1186/s11671-018-2679-y>.
- [158] W. Chang, S. Liu, A. Qileng, W. Liu, Y. Liu, In-situ synthesis of monodispersed Au nanoparticles on eggshell membrane by the extract of Lagerstroemia speciosa leaves for the catalytic reduction of 4-nitrophenol, *Mater. Res. Express.* 6 (2018) 15002. <https://doi.org/10.1088/2053-1591/aae2f0>.
- [159] M. Rashidi, M.R. Islami, A.M. Tikdari, Green synthesis of Pd nanoparticles supported on modified Nonpareil almond shell using almond hull extract: a beneficial nanocatalyst for convenient reduction of organic dyes, *J. Mater. Sci. Mater. Electron.* 30 (2019) 18111–18122. <https://doi.org/10.1007/s10854-019-02164-5>.
- [160] M. Bordbar, Biosynthesis of Ag/almond shell nanocomposite as a cost-effective and efficient catalyst for degradation of 4-nitrophenol and organic dyes, *RSC Adv.* 7 (2017) 180–189. <https://doi.org/10.1039/C6RA24977A>.
- [161] M. Bordbar, N. Mortazavimanesh, Biosynthesis of waste pistachio shell supported silver nanoparticles for the catalytic reduction processes, *IET Nanobiotechnology.* 12 (2018) 939–

945. <https://doi.org/https://doi.org/10.1049/iet-nbt.2017.0266>.
- [162] A. Taghizadeh, K. Rad-Moghadam, Green fabrication of Cu/pistachio shell nanocomposite using *Pistacia Vera L. hull*: An efficient catalyst for expedient reduction of 4-nitrophenol and organic dyes, *J. Clean. Prod.* 198 (2018) 1105–1119. <https://doi.org/https://doi.org/10.1016/j.jclepro.2018.07.042>.
- [163] B. Khodadadi, Hazelnut shell as a valuable bio-waste support for green synthesis of Ag NPs using *Origanum vulgare* leaf extract: Catalytic activity for reduction of methyl orange and Congo red, *Iran. J. Catal.* 7 (2017) 111–119.
- [164] M. Rashidi, M.R. Islami, Green synthesis of Ag@AgCl/*Elaeagnus angustifolia* seed nanocomposite using *Elaeagnus angustifolia* leaves: an amazing nanophotocatalyst with highly photocatalytic activity under sunlight irradiation, *Environ. Sci. Pollut. Res.* 27 (2020) 21455–21467. <https://doi.org/10.1007/s11356-020-08598-3>.
- [165] A. Güngör, I.K. Akbay, T. Özdemir, Waste walnut shell as an alternative bio-based filler for the EPDM: mechanical, thermal, and kinetic studies, *J. Mater. Cycles Waste Manag.* 21 (2019) 145–155. <https://doi.org/10.1007/s10163-018-0778-6>.
- [166] R.A. Solano Pizarro, A.P. Herrera Barros, Cypermethrin elimination using Fe-TiO₂ nanoparticles supported on coconut palm spathe in a solar flat plate photoreactor, *Adv. Compos. Lett.* 29 (2020) 2633366X20906164. <https://doi.org/10.1177/2633366X20906164>.
- [167] A. Rostami-Vartooni, M. Nasrollahzadeh, M. Alizadeh, Green synthesis of seashell supported silver nanoparticles using *Bunium persicum* seeds extract: Application of the particles for catalytic reduction of organic dyes, *J. Colloid Interface Sci.* 470 (2016) 268–275. <https://doi.org/https://doi.org/10.1016/j.jcis.2016.02.060>.
- [168] A. Rostami-Vartooni, Green synthesis of CuO nanoparticles loaded on the seashell surface using *Rumex crispus* seeds extract and its catalytic applications for reduction of dyes, *IET Nanobiotechnology.* 11 (2017) 349–359. <https://doi.org/https://doi.org/10.1049/iet-nbt.2016.0149>.
- [169] H. Nadaroglu, S. Cicek, A.A. Gungor, Removing Trypan blue dye using nano-Zn modified Luffa sponge, *Spectrochim. Acta Part A Mol. Biomol. Spectrosc.* 172 (2017) 2–8. <https://doi.org/https://doi.org/10.1016/j.saa.2016.08.052>.
- [170] N. Hagemann, K. Spokas, H.-P. Schmidt, R. Kägi, M.A. Böhler, T.D. Bucheli, Activated Carbon, Biochar and Charcoal: Linkages and Synergies across Pyrogenic Carbon's ABCs, *Water* . 10 (2018). <https://doi.org/10.3390/w10020182>.
- [171] A.K. Sakhiya, A. Anand, P. Kaushal, Production, activation, and applications of biochar in recent times, *Biochar.* 2 (2020) 253–285. <https://doi.org/10.1007/s42773-020-00047-1>.
- [172] A.-R. Vilchis-Nestor, J. Trujillo-Reyes, J.A. Colín-Molina, V. Sánchez-Mendieta, M. Avalos-Borja, Biogenic silver nanoparticles on carbonaceous material from sewage sludge for degradation of methylene blue in aqueous solution, *Int. J. Environ. Sci. Technol.* 11 (2014) 977–986. <https://doi.org/10.1007/s13762-013-0309-x>.
- [173] H. Jing, L. Ji, Z. Wang, J. Guo, S. Lu, J. Sun, L. Cai, Y. Wang, Synthesis of ZnO Nanoparticles Loaded on Biochar Derived from *Spartina alterniflora* with Superior Photocatalytic Degradation Performance, *Nanomater.* . 11 (2021). <https://doi.org/10.3390/nano11102479>.
- [174] A. Nayak, B. Bhushan, V. Gupta, S. Kotnala, Fabrication of microwave assisted biogenic magnetite-biochar nanocomposite: A green adsorbent from jackfruit peel for removal and recovery of nutrients in water sample, *J. Ind. Eng. Chem.* 100 (2021) 134–148.

- <https://doi.org/https://doi.org/10.1016/j.jiec.2021.05.028>.
- [175] Y. Zhang, X. Jiao, N. Liu, J. Lv, Y. Yang, Enhanced removal of aqueous Cr(VI) by a green synthesized nanoscale zero-valent iron supported on oak wood biochar, *Chemosphere*. 245 (2020) 125542. <https://doi.org/https://doi.org/10.1016/j.chemosphere.2019.125542>.
- [176] P. Zhang, D. O'Connor, Y. Wang, L. Jiang, T. Xia, L. Wang, D.C.W. Tsang, Y.S. Ok, D. Hou, A green biochar/iron oxide composite for methylene blue removal, *J. Hazard. Mater.* 384 (2020) 121286. <https://doi.org/https://doi.org/10.1016/j.jhazmat.2019.121286>.
- [177] C.-M. Liu, Z.-H. Diao, W.-Y. Huo, L.-J. Kong, J.-J. Du, Simultaneous removal of Cu²⁺ and bisphenol A by a novel biochar-supported zero valent iron from aqueous solution: Synthesis, reactivity and mechanism, *Environ. Pollut.* 239 (2018) 698–705. <https://doi.org/https://doi.org/10.1016/j.envpol.2018.04.084>.
- [178] B. Wang, C. Zhu, D. Ai, Z. Fan, Activation of persulfate by green nano-zero-valent iron-loaded biochar for the removal of p-nitrophenol: Performance, mechanism and variables effects, *J. Hazard. Mater.* 417 (2021) 126106. <https://doi.org/https://doi.org/10.1016/j.jhazmat.2021.126106>.
- [179] S. Batool, A.A. Shah, A.F. Abu Bakar, M.J. Maah, N.K. Abu Bakar, Removal of organochlorine pesticides using zerovalent iron supported on biochar nanocomposite from Nephelium lappaceum (Rambutan) fruit peel waste, *Chemosphere*. 289 (2022) 133011. <https://doi.org/https://doi.org/10.1016/j.chemosphere.2021.133011>.
- [180] A. Ahmad, T. Azam, 4 - Water Purification Technologies, in: A.M. Grumezescu, A.M.B.T.-B. and P.W. Holban (Eds.), Woodhead Publishing, 2019: pp. 83–120. <https://doi.org/https://doi.org/10.1016/B978-0-12-815272-0.00004-0>.
- [181] K.S. Obayomi, S. Yon Lau, D. Akubuo-Casmir, M. Diekola Yahya, M. Auta, A.S.M. Fazle Bari, A. Elizabeth Oluwadiya, O.V. Obayomi, M. Mahmudur Rahman, Adsorption of endocrine disruptive congo red onto biosynthesized silver nanoparticles loaded on *Hildegardia barteri* activated carbon, *J. Mol. Liq.* 352 (2022) 118735. <https://doi.org/https://doi.org/10.1016/j.molliq.2022.118735>.
- [182] S. Begum, M. Ahmaruzzaman, Biogenic synthesis of SnO₂/activated carbon nanocomposite and its application as photocatalyst in the degradation of naproxen, *Appl. Surf. Sci.* 449 (2018) 780–789. <https://doi.org/https://doi.org/10.1016/j.apsusc.2018.02.069>.
- [183] K.S. Obayomi, A.E. Oluwadiya, S.Y. Lau, A.O. Dada, D. Akubuo-Casmir, T.A. Adelani-Akande, A.S.M. Fazle Bari, S.O. Temidayo, M.M. Rahman, Biosynthesis of *Tithonia diversifolia* leaf mediated Zinc Oxide Nanoparticles loaded with flamboyant pods (*Delonix regia*) for the treatment of Methylene Blue Wastewater, *Arab. J. Chem.* 14 (2021) 103363. <https://doi.org/https://doi.org/10.1016/j.arabjc.2021.103363>.
- [184] C.R. Galan, M.F. Silva, D. Mantovani, R. Bergamasco, M.F. Vieira, Green synthesis of copper oxide nanoparticles impregnated on activated carbon using *Moringa oleifera* leaves extract for the removal of nitrates from water, *Can. J. Chem. Eng.* 96 (2018) 2378–2386. <https://doi.org/https://doi.org/10.1002/cjce.23185>.
- [185] Z. Oruç, M. Ergüt, D. Uzunoğlu, A. Özer, Green synthesis of biomass-derived activated carbon/Fe-Zn bimetallic nanoparticles from lemon (*Citrus limon* (L.) Burm. f.) wastes for heterogeneous Fenton-like decolorization of Reactive Red 2, *J. Environ. Chem. Eng.* 7 (2019) 103231. <https://doi.org/https://doi.org/10.1016/j.jece.2019.103231>.
- [186] J. Qu, Y. Liu, L. Cheng, Z. Jiang, G. Zhang, F. Deng, L. Wang, W. Han, Y. Zhang, Green synthesis

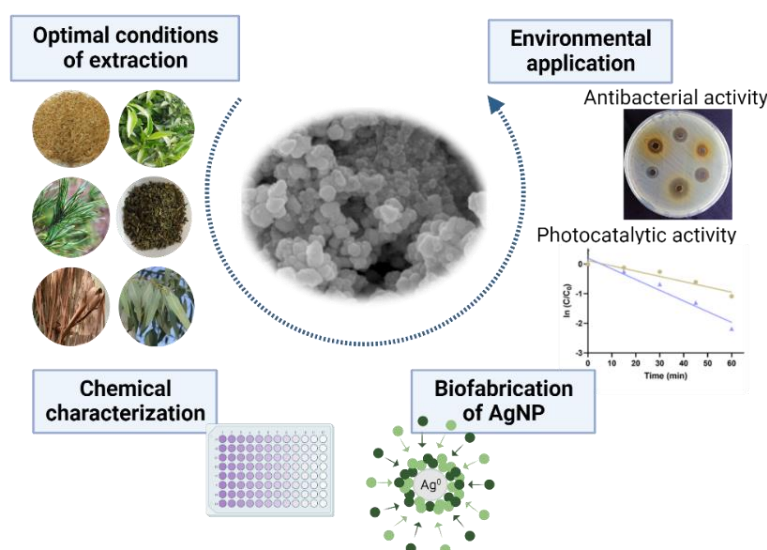
- of hydrophilic activated carbon supported sulfide nZVI for enhanced Pb(II) scavenging from water: Characterization, kinetics, isotherms and mechanisms., *J. Hazard. Mater.* 403 (2021) 123607. <https://doi.org/10.1016/j.jhazmat.2020.123607>.
- [187] Y. Rashtbari, S. Afshin, A. Hamzadeh, M. Abazari, Y. Poureshgh, M. Fazlzadeh, Application of powdered activated carbon coated with zinc oxide nanoparticles prepared using a green synthesis in removal of Reactive Blue 19 and Reactive Black-5: adsorption isotherm and kinetic models, *Desalin. Water Treat.* 179 (2020) 354–367.
- [188] Y. Rashtbari, S. Afshin, A. Hamzadeh, A. Gholizadeh, F.J. Ansari, Y. Poureshgh, M. Fazlzadeh, Green synthesis of zinc oxide nanoparticles loaded on activated carbon prepared from walnut peel extract for the removal of Eosin Y and Erythrosine B dyes from aqueous solution: experimental approaches, kinetics models, and thermodynamic studies., *Environ. Sci. Pollut. Res. Int.* 29 (2022) 5194–5206. <https://doi.org/10.1007/s11356-021-16006-7>.
- [189] Y. Rashtbari, F. Sher, S. Afshin, A. Hamzadeh, S. Ahmadi, O. Azhar, A. Rastegar, S. Ghosh, Y. Poureshgh, Green synthesis of zero-valent iron nanoparticles and loading effect on activated carbon for furfural adsorption, *Chemosphere.* 287 (2022) 132114. <https://doi.org/https://doi.org/10.1016/j.chemosphere.2021.132114>.
- [190] K. Chandrika, A. Chaudhary, T. Mareedu, U. Sirisha, M. Vangalapati, Adsorptive removal of acridine orange dye by green tea/copper-activated carbon nanoparticles (Gt/Cu-AC np), *Mater. Today Proc.* 44 (2021) 2283–2289. <https://doi.org/https://doi.org/10.1016/j.matpr.2020.12.391>.
- [191] Ş. Karadirek, H. Okkay, Ultrasound assisted green synthesis of silver nanoparticle attached activated carbon for levofloxacin adsorption, *J. Taiwan Inst. Chem. Eng.* 105 (2019) 39–49. <https://doi.org/https://doi.org/10.1016/j.jtice.2019.10.007>.
- [192] A. Taha, M. Ben Aissa, E. Da'na, Green Synthesis of an Activated Carbon-Supported Ag and ZnO Nanocomposite for Photocatalytic Degradation and Its Antibacterial Activities., *Molecules.* 25 (2020). <https://doi.org/10.3390/molecules25071586>.
- [193] M. Nasrollahzadeh, M. Sajjadi, S. Iravani, R.S. Varma, Green-synthesized nanocatalysts and nanomaterials for water treatment: Current challenges and future perspectives, *J. Hazard. Mater.* 401 (2021) 123401. <https://doi.org/https://doi.org/10.1016/j.jhazmat.2020.123401>.
- [194] B. Savun-Hekimoğlu, Z. Eren, N.H. Ince, Photocatalytic Destruction of Caffeine on Sepiolite-Supported TiO₂ Nanocomposite, *Sustain.* 12 (2020). <https://doi.org/10.3390/su122410314>.
- [195] S. Li, P. Zhou, W. Zhang, S. Chen, H. Peng, Effective photocatalytic decolorization of methylene blue utilizing ZnO/rectorite nanocomposite under simulated solar irradiation, *J. Alloys Compd.* 616 (2014) 227–234. <https://doi.org/https://doi.org/10.1016/j.jallcom.2014.07.102>.
- [196] Q. Liu, H. Peng, X. Tian, J. Guo, Synthesis of chrysotile based nanocomposites for tuning band gap and photocatalytic property, *Appl. Clay Sci.* 199 (2020) 105885. <https://doi.org/https://doi.org/10.1016/j.clay.2020.105885>.
- [197] U.A. Khan, J. Liu, J. Pan, H. Ma, S. Zuo, Y. Yu, A. Ahmad, S. Ullah, M. Iqbal, B. Li, Fabrication of flower-shaped hierarchical rGO QDs-Bi₂WO₆/EP floating photocatalyst: Eminent degradation kinetic under sun-like irradiation, *Appl. Surf. Sci.* 484 (2019) 341–353. <https://doi.org/https://doi.org/10.1016/j.apsusc.2019.04.092>.
- [198] D. Kibanova, M. Sleiman, J. Cervini-Silva, H. Destailats, Adsorption and photocatalytic oxidation

- of formaldehyde on a clay-TiO₂ composite, *J. Hazard. Mater.* 211–212 (2012) 233–239. <https://doi.org/https://doi.org/10.1016/j.jhazmat.2011.12.008>.
- [199] A. Quarta, R.M. Novais, S. Bettini, M. Iafisco, R.C. Pullar, C. Piccirillo, A sustainable multi-function biomorphic material for pollution remediation or UV absorption: Aerosol assisted preparation of highly porous ZnO-based materials from cork templates, *J. Environ. Chem. Eng.* 7 (2019) 102936. <https://doi.org/https://doi.org/10.1016/j.jece.2019.102936>.
- [200] N.H. Mohamad Idris, J. Rajakumar, K.Y. Cheong, B.J. Kennedy, T. Ohno, A. Yamakata, H.L. Lee, Titanium Dioxide/Polyvinyl Alcohol/Cork Nanocomposite: A Floating Photocatalyst for the Degradation of Methylene Blue under Irradiation of a Visible Light Source, *ACS Omega.* 6 (2021) 14493–14503. <https://doi.org/10.1021/acsomega.1c01458>.
- [201] H. Pereira, The Rationale behind Cork Properties: A Review of Structure and Chemistry, *BioResources.* 10 (2015). <https://doi.org/10.15376/biores.10.3.Pereira>.
- [202] N. Hossain, M.A. Bhuiyan, B.K. Pramanik, S. Nizamuddin, G. Griffin, Waste materials for wastewater treatment and waste adsorbents for biofuel and cement supplement applications: A critical review, *J. Clean. Prod.* 255 (2020) 120261. <https://doi.org/https://doi.org/10.1016/j.jclepro.2020.120261>.
- [203] N. Welter, J. Leichtweis, S. Silvestri, P.I.Z. Sánchez, A.C.C. Mejía, E. Carissimi, Preparation of a new green composite based on chitin biochar and ZnFe₂O₄ for photo-Fenton degradation of Rhodamine B, *J. Alloys Compd.* 901 (2022) 163758. <https://doi.org/https://doi.org/10.1016/j.jallcom.2022.163758>.
- [204] B. Richter, Knowledge and perception of food waste among German consumers, *J. Clean. Prod.* 166 (2017) 641–648. <https://doi.org/https://doi.org/10.1016/j.jclepro.2017.08.009>.
- [205] R. Bushra, S. Mohamad, Y. Alias, Y. Jin, M. Ahmad, Current approaches and methodologies to explore the perceptive adsorption mechanism of dyes on low-cost agricultural waste: A review, *Microporous Mesoporous Mater.* 319 (2021) 111040. <https://doi.org/https://doi.org/10.1016/j.micromeso.2021.111040>.
- [206] D. Nagarajan, S. Venkatanarasimhan, Copper(II) oxide nanoparticles coated cellulose sponge—an effective heterogeneous catalyst for the reduction of toxic organic dyes., *Environ. Sci. Pollut. Res. Int.* 26 (2019) 22958–22970. <https://doi.org/10.1007/s11356-019-05419-0>.
- [207] M. Sboui, M.F. Nsib, A. Rayes, T. Ochiai, A. Houas, Application of solar light for photocatalytic degradation of Congo red by a floating salicylic acid-modified TiO₂/palm trunk photocatalyst, *Comptes Rendus Chim.* 20 (2017) 181–189. <https://doi.org/https://doi.org/10.1016/j.crci.2015.12.007>.
- [208] Y. Chen, M. Ran, Z. Zhou, X. Han, H. Zhu, J. Gu, Lanthanum/titanium dioxide immobilized onto industrial waste with enhanced photocatalytic activity, and the degradation of dimethyl phthalate, *J. Clean. Prod.* 321 (2021) 129014. <https://doi.org/https://doi.org/10.1016/j.jclepro.2021.129014>.
- [209] G. Li, Q. Teng, B. Sun, Z. Yang, S. Liu, X. Zhu, Synthesis scaly Ag-TiO₂ loaded fly ash magnetic bead particles for treatment of xanthate wastewater, *Colloids Surfaces A Physicochem. Eng. Asp.* 624 (2021) 126795. <https://doi.org/https://doi.org/10.1016/j.colsurfa.2021.126795>.
- [210] L. Gao, W. Gan, S. Xiao, X. Zhan, J. Li, A robust superhydrophobic antibacterial Ag–TiO₂ composite film immobilized on wood substrate for photodegradation of phenol under visible-light illumination, *Ceram. Int.* 42 (2016) 2170–2179. <https://doi.org/https://doi.org/10.1016/j.ceramint.2015.10.002>.

- [211] B. Avinash, C.R. Ravikumar, M.R.A. Kumar, M.S. Santosh, C. Pratapkumar, H.P. Nagaswarupa, H.C.A. Murthy, V. V. Deshmukh, A.S. Bhatt, A.A. Jahagirdar, M.W. Alam, NiO bio-composite materials: Photocatalytic, electrochemical and supercapacitor applications, *Appl. Surf. Sci. Adv.* 3 (2021) 100049. <https://doi.org/https://doi.org/10.1016/j.apsadv.2020.100049>.
- [212] A.T. Adeleye, A.A. Akande, C.K. Odoh, M. Philip, T.T. Fidelis, P.I. Amos, O.O. Banjoko, Efficient synthesis of bio-based activated carbon (AC) for catalytic systems: A green and sustainable approach, *J. Ind. Eng. Chem.* 96 (2021) 59–75. <https://doi.org/https://doi.org/10.1016/j.jiec.2021.01.044>.
- [213] W.B. Ayinde, W.M. Gitari, M. Munkombwe, A. Samie, J.A. Smith, Green synthesis of AgMgOnHaP nanoparticles supported on chitosan matrix: Defluoridation and antibacterial effects in groundwater, *J. Environ. Chem. Eng.* 8 (2020) 104026. <https://doi.org/https://doi.org/10.1016/j.jece.2020.104026>.
- [214] B. Srikanth, R. Goutham, R. Badri Narayan, A. Ramprasath, K.P. Gopinath, A.R. Sankaranarayanan, Recent advancements in supporting materials for immobilised photocatalytic applications in waste water treatment, *J. Environ. Manage.* 200 (2017) 60–78. <https://doi.org/10.1016/J.JENVMAN.2017.05.063>.
- [215] I.H. Alsohaimi, A.M. Nassar, T.A. Seaf Elnasr, B. amar Cheba, A novel composite silver nanoparticles loaded calcium oxide stemming from egg shell recycling: A potent photocatalytic and antibacterial activities, *J. Clean. Prod.* 248 (2020) 119274. <https://doi.org/https://doi.org/10.1016/j.jclepro.2019.119274>.

CHAPTER 3 VALORIZATION OF PLANT BY-PRODUCTS IN THE BIOSYNTHESIS OF SILVER NANOPARTICLES

Biosynthesis based on natural compounds has emerged as a sustainable approach to the fabrication of MNP. The main goal of this chapter is to biosynthesize stable and multifunctional silver nanoparticles (AgNP) using different plant by-products as reducers and capping agents. The biosynthesized AgNP are characterized by UV/Vis and FTIR spectroscopies, SEM-EDX and zeta potential. The synthesized AgNP are evaluated as antibacterial agents against various pathogenic bacteria and as photocatalysts for the degradation of the indigo carmine (IC), a dye from the indigoid class that is extremely poisonous.



This chapter was adapted from:

Rocha, V., Ferreira-Santos, P., Aguiar, C., Neves, I.C., Tavares, T., *Valorization of plant by-products in the biosynthesis of silver nanoparticles with antibacterial and catalytic applications* (under revision)

3.1 INTRODUCTION

Metallic nanoparticles (MNP) are an unusual class of materials with distinctive properties and wide applications in numerous fields [1]. Surface plasmon resonance (SPR), a high surface-to-volume ratio, size, reconfigurable geometry, surface charge, wide band gap, generation of reactive oxygen species (ROS) and intrinsic stability are some of the characteristics of these MNP [2]. One of the most interesting examples of these nano-entities are AgNP due to their excellent conductivity, stability and multiple applications as catalysts, antiviral, antifungal and antibacterial agents [3–6]. There are several synthetic routes used for the fabrication of AgNP, mainly classified as physical or chemical. However, these methods present environmental toxicity, as they produce dangerous wastes and require harmful reducing and stabilizing agents [7].

Within the green methods, plant biodiversity allowed various new syntheses by using plant extracts to fabricate diverse MNP due to a rapid technique, simplicity and scalability of production [8–10]. Plants produce several primary and secondary metabolites including polyphenols (e.g., phenolic acids, flavonoids, tannins, stilbenes lignans and anthocyanins), amino acids, proteins, sugars, lipids, carbohydrates, alkaloids, terpenoids, quinines and saponins [2]. These biomolecules can act as surfactants, reducing and stabilizer agents in the biosynthesis of MNP.

Extracts obtained from bark, leaves, roots, flowers, seeds and fruits have been used to synthesize AgNP [11–17]. In 2003, the first synthesis of AgNP employing a plant extract (*Pelargonium graveolens*) was reported [18]. Up to now, many plant extracts including those from eucalyptus leaves [19], eucalyptus bark [20], orange peels [21], black plums [22], kidney beans [23], black tea [13] and green tea [24] among others have been successfully used to biosynthesize AgNP. There are some advantages of using plant extracts, namely the capping ability induced on the MNP by the polyphenol extract matrix, extending their reactivity and the decreased toxicity of the reducing agent compared to the toxicity of the chemicals utilized in other procedures. Additionally, due to the extracts' high water solubility, they can serve as a source of nutrients to promote complementary biodegradation and the natural product valorization, that in some situations are regarded as wastes with no additional value [25–28].

Extract-mediated AgNP have been used as an agent for effective environmental remediation, including the removal/degradation of biological and non-biological contaminants. Rani et al. [23] have shown the excellent photocatalytic, catalytic and antimicrobial properties of AgNP prepared using

kidney beans (*Phaseolus vulgaris*) extract as a reducing and stabilizer agent. AgNP showed a capacity of degradation of reactive red-141 dye and were effective against the bacteria *Bacillus subtilis* and *Escherichia coli*, showing antimicrobial activity [23]. Also, Mehwish *et al.* [26] showed the efficient sunlight photodegradation (> 75%) of organic dyes (methylene blue, orange red and 4-nitrophenol) and the excellent antimicrobial action against *Staphylococcus aureus*, *Escherichia coli*, *Salmonella enterica typhimurium* and *Pseudomonas aeruginosa*, all pathogenic bacteria, presented by AgNP biosynthesized using *Moringa oleifera* seed extract. Muthukumar *et al.* [29] synthesized AgNP with amaranth leaf extract as a reducing agent and proved their efficiency in the degradation of caffeine (99% at pH 9, in 15 h) and in the inactivation of *Escherichia coli*.

To date, only a few studies have reported comparative evaluations of the effect of different plant extracts on the synthesis of AgNP [14,30,31]. In the present chapter, a screening involving a range of different aqueous plant extracts obtained from *Eucalyptus globulus*, *Pinus pinaster*, *Citrus sinensis*, *Cedrus atlantica* and *Camellia sinensis* was performed to select the best extracts to synthesize highly stable AgNP. Optimal conditions of extraction (raw material, extraction time and temperature) were determined using as a basis the total phenolic and flavonoid content of each extract. The bioinspired synthesized AgNP were evaluated as antibacterial agents against various pathogenic bacteria and as alternative photocatalysts for the degradation of indigo carmine (IC) dye in aqueous solution under sunlight. For the first time, a complete cost analysis for the AgNP synthesis was carried out to evaluate its cost-effectiveness and scalability of production.

3.2 MATERIALS AND METHODS

3.2.1 Chemicals

Silver nitrate (AgNO₃) was obtained from PanReac AppliChem. IC dye (5,5'-indigodisulfonic acid sodium salt, C₁₆H₈N₂Na₂O₆S₂) was purchased from Sigma-Aldrich. The nutrient broth and agar for the antimicrobial assays were bought from Oxoid. All other analytical-grade chemicals were acquired from Sigma-Aldrich.

Ultrapure water was used in all experiments and solutions, obtained from a Milli-Q system (Millipore), with a resistivity of 18.2 MΩcm⁻¹.

3.2.2 Preparation of plant extracts

Eucalyptus bark and eucalyptus leaves (*Eucalyptus globulus*), pine needles (*Pinus pinaster*) and orange leaves (*Citrus sinensis*) were collected in Marco de Canaveses, Portugal. Cedar wood (*Cedrus atlantica*) was collected in Fez, Morocco. Green tea and black tea (*Camellia sinensis*) were purchased as commercial products (Tetley®) and were used as received. The collected plants were washed using distilled water to eliminate impurities adhered to leaves and dried in the shade for 7 days, then they were chopped and ground to a fine powder (< 1 mm) in a mechanical grinder. Dried plant powder (2 g) was subjected to a conventional solid-liquid extraction using a cylindrical reactor into a water bath with continuous shaking (200 rpm) and extracted with 20 mL of water. Extractions were performed at different temperatures (50 and 80 °C) and during different times (30 and 60 min). The obtained extracts were filtered through Whatman filter paper No. 1 and stored at 4 °C until use. All the experiments were done at least in triplicate.

3.2.3 Chemical characterization of plant extracts

3.2.3.1 Determination of total phenolic content (TPC) and total flavonoid content (TFC)

The TPC and TFC were used as selection criteria to choose the most promising extracts to synthesize highly stable AgNP.

The TPC of the aqueous extracts was accessed using the Folin-Ciocalteu colorimetric assay [32]. Briefly, the aqueous extract (0.1 mL) was combined with 0.3 mL of distilled water and 0.1 mL of Folin-Ciocalteu's phenol reagent. After waiting for 5 min, 0.5 mL of 8% sodium carbonate solution was added to the mixture and the volume was made up to 3 mL with distilled water. After 30 min of darkness for the reaction, the absorbance at 765 nm was measured in a spectrophotometric microplate reader (Synergy HT, BioTek Instruments, Inc., USA). Using a standard curve of gallic acid (10-500 mg.L⁻¹), R²=0.999, the TPC was calculated as mg of gallic acid equivalents (GAE) per gram of dry plant material (mg_{GAE}·g⁻¹).

The aluminium chloride (AlCl₃) colorimetric assay was used to quantify the TFC of extracts [33]. In brief, 0.5 mL of aqueous extract was mixed with 2 mL of distilled water and 0.15 mL of 5% sodium nitrite solution. After 6 min, 0.150 mL of 10% aluminium chloride solution was added and allowed to

stand further 6 min. Then, 2 mL of 4% sodium hydroxide solution was added and the final volume of the mixture was brought to 5 mL with distilled water. After thoroughly mixing the mixture, it was left to stand for 15 min and then the absorbance was measured at 510 nm. Using a standard curve of catechin (10-600 mg.L⁻¹, R²=0.999), the TFC was calculated as mg of catechin equivalents (CE) per gram of dry plant material (mg_{CE}.g⁻¹).

3.2.3.2 Determination of antioxidant activity

To examine the antioxidant capacity of the extracts, three independent methods were used: the ferric reducing antioxidant power (FRAP assay), the free radical scavenging activity (DPPH assay) and the radical cation decolorization (ABTS assay).

The FRAP assay was performed using the Benzie and Strain methodology [34] with some adjustments for the determination of the Fe(III)-reducing capacity of the extracts. In a 96-well microplate, 10 µL of the aqueous extract (properly diluted) was combined with 290 µL of FRAP reagent. The resulting reaction mixture was incubated at 37 °C for 15 min and the absorbance at 593 nm was measured. Based on a standard curve of FeSO₄.7H₂O (100-1250 µM, R²=0.999), the ability of the extracts to reduce Fe(III) was calculated as millimoles of ferrous equivalent per gram of dry plant material (mmol_{Fe(II)}}.g⁻¹).

The DPPH free radical scavenging activity was assessed using the method described by Ferreira-Santos *et al.* [35]. A 30 µL sample of the aqueous extract was combined with 270 µL of 150 µM 2,2-diphenyl-1-picrylhydrazyl (DPPH•) free radical (dissolved in methanol to an absorbance of 0.70 ± 0.01 at 515 nm). Solutions were left to stand for 1 h in the dark at RT, until complete reaction. Absorbance was measured at 515 nm using water as a blank. Trolox (6-hydroxy-2,5,7,8-tetramethylchroman-2-carboxylic acid) standard solution was used to perform a calibration curve (10-400 µM, R²=0.998). The DPPH values were recorded as millimoles of Trolox equivalent (TE) per gram of dry plant material (mmol_{TE}.g⁻¹).

The ABTS radical scavenging activity of extracts was assessed according to Ferreira-Santos *et al.* [35] using the ABTS reagent (2,2'-azino-bis(3-ethylbenzothiazoline-6-sulfonic acid) diammonium salt). Each sample was diluted and 10 µL of each was combined with 290 µL of ABTS^{•+} radical and incubated at RT for 1 h in the dark. Water was used as a blank to test the absorbance at 734 nm. A standard

solution of Trolox was used to build the calibration curve (30-800 μM , $R^2=0.996$) and results were expressed as millimoles of Trolox equivalent (TE) per gram of dry plant material ($\text{mmol}_{\text{TE}} \cdot \text{g}^{-1}$).

3.2.4 Biofabrication of AgNP

For the green synthesis of AgNP, 100 mL of selected extracts of eucalyptus leaves (ELE), green tea (GTE) and black tea (BTE) (10% w/v) were individually added dropwise to 100 mL of 60 mM AgNO_3 (with constant stirring at 50 °C during 1 h). Therefore, the mass of silver used was 0.6350 g which corresponds to 5.89 initial millimoles of silver. The reaction mixture gradually darkened in color, indicating the production of AgNP. Finally, the obtained suspensions of AgNP were separated by centrifugation at 10000 rpm for 30 min to remove the unreacted Ag^+ ions and extract residues. The precipitate was washed three times with ultrapure water and absolute ethanol and finally lyophilized.

3.2.5 Characterization of AgNP

A UV-Vis spectrophotometer (model V-630, JASCO) was used to evaluate the optical properties of biosynthesized AgNP at wavelengths between 350 and 700 nm. An ultra-high resolution field-emission scanning electron microscope (SEM, FEI Nova 200) with an integrated microanalysis X-ray system (EDX - Energy-dispersive X-ray spectroscopy, Pegasus X4M) with an acceleration voltage of 10 kV at 200 000 fold magnifications was used to analyze the powder AgNP. The role of aqueous extracts and their interaction with AgNP were investigated by Fourier Transform Infrared Spectroscopy with a diamond-composite attenuated total reflectance cell (FTIR-ATR, ALPHA II-Bruker spectrometer). The spectrum was recorded over the wavelength range from 4000 to 400 cm^{-1} , with a resolution of 4 cm^{-1} and 64 scans. The zeta potential of AgNP was accessed by dynamic light scattering (DLS, Malvern Panalytical) at 25 °C, 150 V, for the samples in double-distilled water.

3.2.6 Antibacterial activity

The antibacterial activity of selected extracts and biosynthesized AgNP was investigated against both Gram-negative bacteria, *Escherichia coli* (ATCC 25922), *Pseudomonas putida* S12 (ATCC 700801) and *Vibrio spp.* (CECT 7119), and Gram-positive bacteria, *Bacillus megaterium* (ATCC 14581), *Staphylococcus aureus* (ATCC 6538) and *Streptococcus equisimillis* (CECT 926). Nutrient broth medium was used for the cultivation of freshly growing bacteria (turbidity of 0.5 McFarland

suspension). Using sterilized cotton swabs, 100 μL of each cell suspension was spread on a nutrient agar surface. The agar medium was then punched with 6 mm diameter wells and filled with 50 μL of biosynthesized AgNP aqueous solutions (1 $\text{mg}\cdot\text{mL}^{-1}$) as well as with the respective aqueous extracts. Subsequently, the plates were maintained at 37 $^{\circ}\text{C}$ for 24 h and the antibacterial action was determined by measuring the diameter of the growth inhibition zone (or halo), in mm. Each test was performed in triplicate.

3.2.7 Photocatalytic activity

The photocatalytic capacity of biosynthesized AgNP to degrade IC dye was evaluated under sunlight. An aqueous solution of IC (10 $\text{mg}\cdot\text{L}^{-1}$) with 0.5 or 1 $\text{g}\cdot\text{L}^{-1}$ of AgNP was firstly placed in the dark for 30 min under magnetic stirring, to allow the equilibrium to be reached before starting the photocatalytic reaction. Thereafter, the solution was exposed to sunlight from 1 h to 3 h p.m. Centrifugation was used to separate the AgNP from the dye solution after exposure and a UV-Vis spectrophotometer was used to examine the supernatant at 610 nm. Control experiments with and without catalysts in dark and sunlight conditions were also executed to determine the effects of catalyst and sunlight *per se*. Each experiment was done in triplicate.

The IC dye degradation efficiency was determined as equation 3-1:

$$\text{Degradation efficiency (\%)} = \frac{C_0 - C_t}{C_0} \times 100 \quad (\text{Equation 3-1})$$

where C_0 is the initial solution concentration ($\text{mg}\cdot\text{L}^{-1}$) and C_t is the final solution concentration at time t ($\text{mg}\cdot\text{L}^{-1}$).

3.2.8 Statistical Analysis

All experiments were carried out on three independent replicates and results were expressed as mean \pm standard deviation (SD). The significance of the data was statistically determined with One-way ANOVA followed by Tukey's multiple comparisons test using GraphPad Prism[®] software (version 8.0). P values < 0.05 were considered to be statistically significant.

3.3 RESULTS AND DISCUSSION

3.3.1 Selection and characterization of aqueous plant extracts

Aqueous extraction from different plant by-products, like eucalyptus bark and leaves, pine needles, orange leaves, cedar wood, as well as commercial green and black tea, was carried out to assess the potential of resulting extracts for biosynthesizing AgNP. From the perspective of circular economy and green development, the use of natural and waste materials for the synthesis of MNP to be used in the treatment of wastewater is the most attractive one, according to the twelve principles of Green Chemistry [36]. The use of biowastes in chemical synthesis can help to clean up the environment while producing new functional materials [37].

The establishment of extraction conditions is important because an inadequate method for the recovery of bio-compounds can affect the content and the functional properties of obtained extracts to be involved in the synthesis of MNP [38,39]. Water was selected as the extraction solvent as it is the safest, cheapest and most environmental friendly solvent, and its efficiency has previously been reported in terms of phenolic compounds and other antioxidants extraction, using conventional or modern techniques [14,28,38,40].

For a clearer comparison between the obtained extracts, the TFC and TFC were determined for different extraction conditions. **Figure 3-1** shows the results obtained for each aqueous extract at different temperatures (50 and 80 °C) and times (30 and 60 min) of extraction. The extracts obtained from ELE (40.7 to 45.3 mg_{GAE}·g⁻¹), GTE (48.7 to 54.0 mg_{GAE}·g⁻¹) and BTE (37.6 to 45.2 mg_{GAE}·g⁻¹) are the ones with the highest TPC and those from cedar wood (1.4 to 2.2 mg_{GAE}·g⁻¹) have the lowest TPC, regardless the extraction conditions.

As it may be observed in **Figure 3-1A**, the TPC value of the extract obtained at 50 °C and 30 min is not statistically different ($p > 0.05$) from those of the extracts obtained within other conditions, except for pine needles extract obtained at 80 °C for 60 min, which presented a higher phenolic content (9.3 mg_{GAE}·g⁻¹). Several authors such as Machado *et al.* [41], optimized the extraction conditions (temperature, time) for leaves from 26 different tree species and concluded that the highest temperature (80 °C) presented the best results for the extraction of phenolic compounds, without significant degradation of these antioxidants. For some types of leaves, 20 min of extraction is sufficient to extract almost all of the antioxidants, being influenced by the temperature used in the process.

Moreover, Chandini *et al.* [40] demonstrated that extraction times higher than 40 min at 90 °C can degrade some phenolic compounds (*e.g.* flavins and catechins) in the BTE.

The profile of TFC (**Figure 3-1B**) is similar to the one of TPC and the highest values were reached for the GTE and the BTE with maximum values of 10.5 and 9.3 mg_{QE}·g⁻¹, respectively. The ELE only reached a maximum value of 3.7 mg_{QE}·g⁻¹, a value similar to eucalyptus bark and pine needles extracts. This is low value in comparison to the one described by Kuppusamy *et al.* [28], who obtained a TFC of 13.7±0.9 mg_{QE}·g⁻¹ (quercetin equivalents (QE) in mg per g of dry material) for eucalyptus leaves. On the other hand, Balčiūnaitienė *et al.* [30] obtained a lower TFC of 0.48±0.04 mg_{RE}·g⁻¹ (rutin equivalents (RE) in mg per g of dry plant material) for dry *Eucalyptus globulus* leaves. These differences may be due to the extraction conditions (boiled water, sample/solvent ratio, time, etc.), as well as to the provenance and storage conditions of the raw material.

Therefore, based on the high content of TPC and TFC, the ELE, GTE and BTE obtained at 50 °C for 30 min (extracts obtained with lower associated energy costs) were selected as promising candidates to synthesize AgNP. Similarly, Salgado *et al.* [42] studied the effect of phenolic compounds present in plant extracts on the synthesis of MNP and selected the extracts with higher phenolic content for the synthesis of iron oxide nanoparticles, including eucalyptus leaves extract.

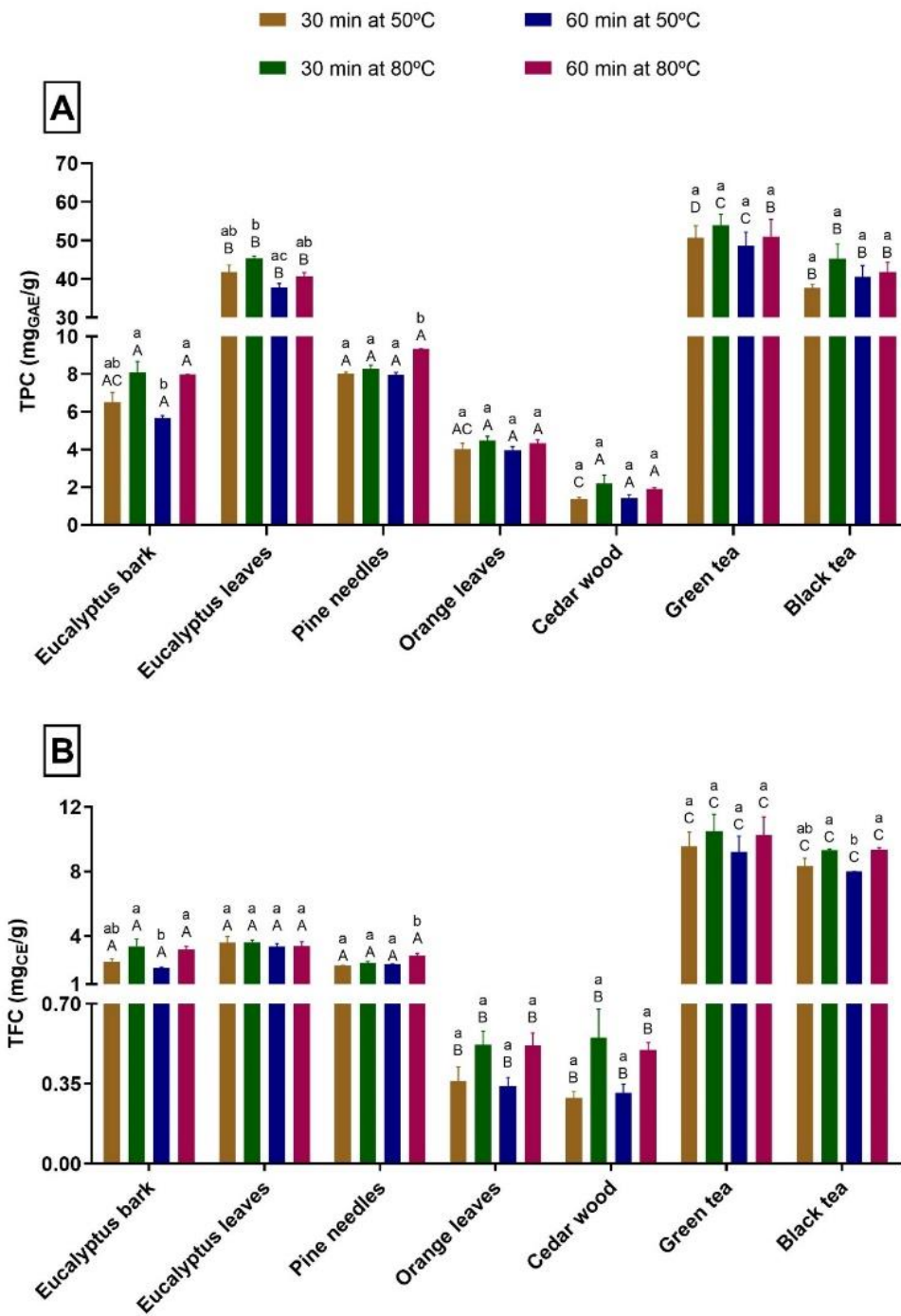


Figure 3-1. Total phenolic content (TPC) (A) and Total flavonoids content (TFC) (B) of plant extracts. Values are expressed as mean \pm SD. Different lowercase letters show significant differences ($p < 0.05$) between extraction conditions for the same plant by-products. Different capital letters show significant differences ($p < 0.05$) between plant extracts for the same extraction conditions.

There are many distinct compounds in plant extracts that function as antioxidants through different reaction mechanisms [30]. Therefore, it is strongly advised that at least two distinct methodologies be used to determine the antioxidant capacity of plant extracts [43]. In this study, three different methods were used to evaluate the antioxidant activity of the selected extracts from ELE, GTE and BTE (**Table 3-1**).

Table 3-1. Antioxidant activity of selected plant aqueous extracts.

Plant Extract	Eucalyptus leaves (ELE)	Green tea (GTE)	Black tea (BTE)
FRAP (mmol_{Fe(II)}·g⁻¹)	0.910±0.023 ^{ab}	1.188±0.052 ^A	0.770±0.118 ^B
ABTS (mmol_{TE}·g⁻¹)	1.909±0.167 ^A	3.099±0.102 ^B	2.034±0.343 ^A
DPPH (mmol_{TE}·g⁻¹)	2.550±0.090 ^A	3.080±0.047 ^B	2.310±0.150 ^A

Values are expressed as mean ± SD. Different capital letters show significant differences ($p < 0.05$) between plant extracts for the same antioxidant assay.

The ability of the ELE, GTE and BTE to reduce Fe³⁺ was evaluated using the FRAP method, and the results showed a reduction capacity of 0.910, 1.188 and 0.770 mmol_{Fe(II)}·g⁻¹, respectively. These data were higher than that reported for *Eucalyptus globulus* extract [42]. The free radical scavenging activity (DPPH and ABTS methods) are spectrophotometric methods employed for the assessment of the antioxidant activity of various compounds present in vegetables, beverages, foods or extracts. The DPPH method is based on the ability of antioxidants to reduce the stable free radical (2,2-diphenyl-1-picrylhydrazyl, DPPH*) to the respective hydrazine, and the ABTS test is based on the capacity of antioxidants to inhibit the radical cation ABTS** absorbance [44]. These tests are reliable, accurate, fast, simple and cost-effective ways to assess the capacity of natural antioxidants to scavenge free radicals. Regarding to the DPPH and ABTS results, the highest antioxidant capacity was attained for the GTE (about 3 mmol_{TE}·g⁻¹ by both methods), compared to ELE and BTE (**Table 3-1**). Martinez-Cabanas *et al.* [38] studied the antioxidant capacity of eleven plant extracts by the DPPH method and obtained a value above 5 mmol_{TE}·L⁻¹ for ELE (*Eucalyptus globulus*) and for GTE (*Camellia sinensis*), a lower activity compared to that obtained in the present work, 255.0 mmol_{TE}·L⁻¹ (2.550±0.090 mmol_{TE}·g

) for ELE, and $308.0 \text{ mmol}_{\text{TE}} \cdot \text{L}^{-1}$ ($3.080 \pm 0.047 \text{ mmol}_{\text{TE}} \cdot \text{g}^{-1}$) for GTE. These results show the positive correlation of antioxidant activity assessed by the DPPH, ABTS and FRAP tests with the TPC and TFC of plant extracts, indicating the contribution of these extracted biomolecules to the biological activity and it is in agreement with previous results [38,42,45].

3.3.2 Green synthesis of AgNP

AgNP were successfully synthesized by the reduction of AgNO_3 with the phenolic-rich aqueous extracts of eucalyptus leaves (ELE-AgNP), green tea (GTE-AgNP) and black tea (BTE-AgNP) previously obtained (50 °C for 30 min) and chemically characterized (**Figure 3-1** and **Table 3-1**).

The color change interpretation is considered the preliminary optical inference for the synthesis of AgNP. The addition of phenolic extracts to AgNO_3 solution at 50 °C (ratio of 1:1) transformed the color of the suspension from colorless to pale yellow, then to a dark brownish-red (**Figure 3-2A**). The appearance of brownish is due to the reduction of the AgNP, Ag^+ ions to Ag^0 by phenolic extract, evidenced by UV-visible spectroscopy (**Figure 3-2B**) [46]. SPR occurs when free electrons on the metal surface generate the surface plasmon, as a consequence of beaming MNP at a specific refraction angle and the intensity of the reflected light decreases [47]. The green AgNP exhibited SPR vibration bands at 474, 453 and 450 nm, confirming the synthesis of ELE-AgNP, GTE-AgNP and BTE-AgNP, respectively (**Figure 3-2B**) and this is in agreement with previous results [24,37].

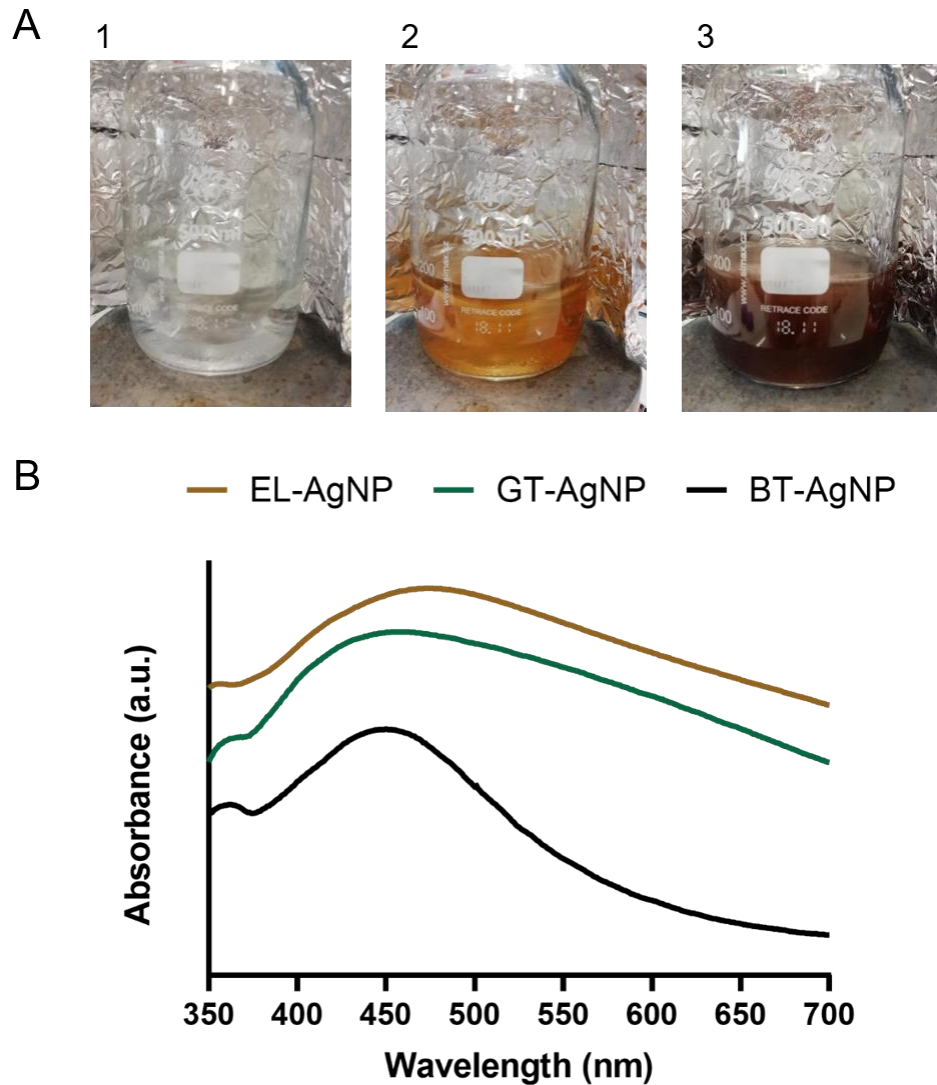


Figure 3-2. Changes in the color of the colloidal solutions indicate the formation of silver nanoparticles (AgNP): (A) 1. Silver nitrate (AgNO_3) solution; 2. Addition of eucalyptus leaves extract (ELE) to AgNO_3 solution at zero time (start of reaction) and 3. After 1 h of reaction at 50 °C (end of reaction). (B) UV–visible spectra of AgNP synthesized by aqueous extracts from eucalyptus leaves (ELE-AgNP), green tea (GTE-AgNP) and black tea (BTE-AgNP).

SEM was performed to investigate the surface morphology of the biosynthesized AgNP with different aqueous extracts. AgNP morphology is homogeneous with spherical particles (**Figure 3-3**). The size distribution is in the range of 29-136, 14-81 and 22-81 nm for the synthesized ELE-AgNP, GTE-AgNP and BTE-AgNP, respectively. The calculated average particle-size distribution (average of 25 particles)

suggests that the BTE-AgNP were the smallest ones (40.6 ± 16.0 nm), followed by the GTE-AgNP (47.1 ± 21.1 nm) and finally, by the largest ELE-AgNP (86.4 ± 28.2 nm). Devatha *et al.* [48] proposed that the amounts and types of phenolic compounds are two of the main reasons for the variability in the sizes of MNP. It was suggested that a high concentration of reductive biomolecules present in plant extracts leads to a rapid production of AgNP, followed by their subsequent growth via Ostwald reopening, which leads to an increase in the size of AgNP over time [23]. In this work, GTE showed the highest TPC (50.7 ± 3.1 mg_{GAE}.g⁻¹) and TFC (9.6 ± 0.9 mg_{CE}.g⁻¹), but ELE-AgNP presented the highest size (86.4 ± 28.2 nm), indicating the variability of the phenolic compounds in each extract.

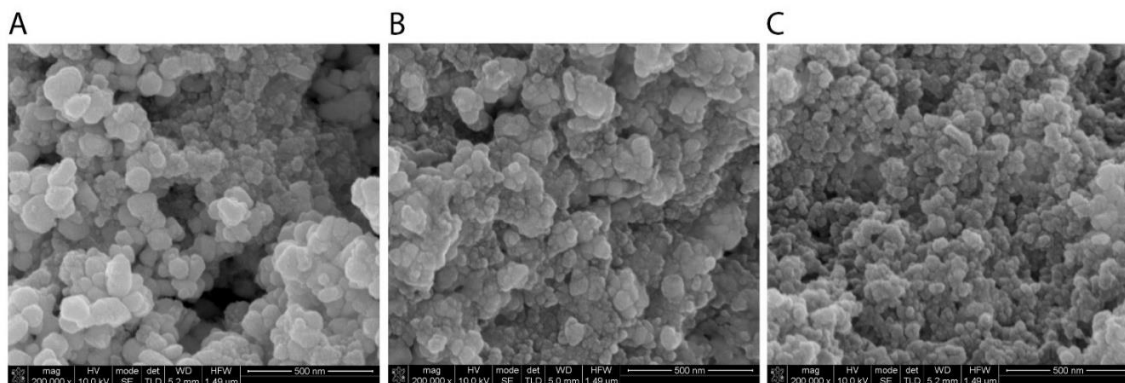


Figure 3-3. SEM images of AgNP synthesized by eucalyptus leaves (ELE), green tea (GTE) and black tea (BTE) extracts: (A) ELE-AgNP (B) GTE-AgNP (C) BTE-AgNP.

The EDX spectra of ELE-AgNP, GTE-AgNP and BTE-AgNP are shown in **Figure 3-4**. The presence of silver at 3 keV was detected, confirming the effective formation of AgNP, due to SPR metallic AgNP [49]. Other authors described that the formation of spherical-shaped AgNP provides a peak in the range of 2.5–3.5 keV [12], corroborating our results. Also, the presence of magnesium, oxygen and chloride, resulting from the organic compounds present in extracts was identified, being responsible for Ag ions reduction and stabilization of resultant nanoparticles [50,51]. Accordingly, wt (%) values determined in EDX analyses revealed that GTE-AgNP retained 83.2% of silver (4.90 mmol of Ag), ELE-AgNP retained 80.7% (4.75 mmol) and BTE-AgNP retained 77.5% of silver (4.56 mmol). These results are in concordance with the obtained by the FRAP method, indicating that the GTE shows stronger reducing activity, followed by ELE and BTE.

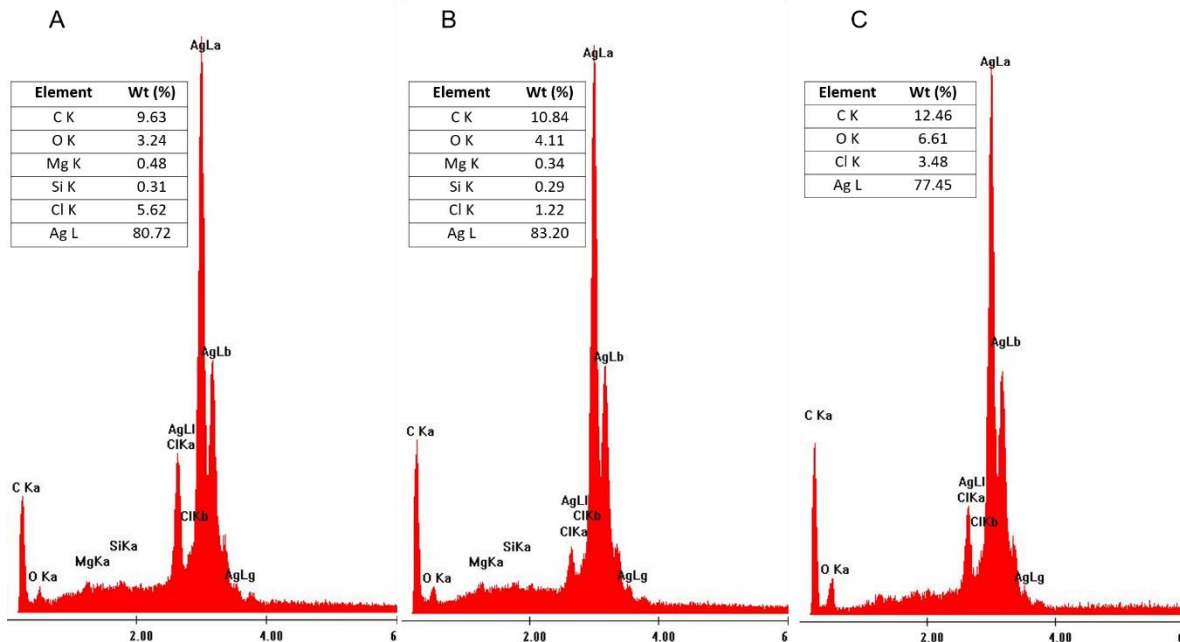


Figure 3-4. EDX spectra of (A) ELE-AgNP (B) GTE-AgNP (C) BTE-AgNP.

The number of atoms per nanoparticle (N) was calculated using a procedure described by Kalishwaralal *et al.* [52] and Rani *et al.* [23], equation 3-2:

$$N = \frac{\pi \rho D^3}{6M} N_A \quad \text{(Equation 3-2)}$$

where ρ is the density of the face-centered cubic crystalline (fcc) structure of silver (10.5 g.cm^{-3}), D is the average diameter of ELE-AgNP ($8.6 \times 10^6 \text{ cm}$), GTE-AgNP ($4.7 \times 10^6 \text{ cm}$) and BTE-AgNP ($4.1 \times 10^6 \text{ cm}$), M is the molar mass of silver (107.87 g) and N_A is the Avogadro's number, 6.023×10^{23} , assuming 100% conversion of all silver ions to AgNP. The N calculated was 19.5×10^6 (ELE-AgNP), 3.19×10^6 (GTE-AgNP) and 2.11×10^6 (BTE-AgNP), suggesting that ELE-AgNP have more silver atoms per nanoparticle with a high average diameter.

The molar concentration of AgNP (C) was calculated using equation 3-3 [23,52]:

$$C = \frac{N_T}{NVN_A} \quad \text{(Equation 3-3)}$$

where N_T is the total number of silver atoms (number of mol of silver ions quantified by EDX \times Avogadro's number), N is the average number of atoms per nanoparticle (equation 3-2) and V is the

total volume of solution used in the synthesis (0.2 L). Therefore, the molar concentration was 1.22 μM (ELE-AgNP), 7.68 μM (GTE-AgNP) and 10.8 μM (BTE-AgNP). These values show that the AgNP from ELE has a lower concentration than the other particles prepared with the leaves from the different teas.

Zeta potential is the physical property that measures the effective electric charge on the MNP surface and it is a crucial parameter for the stability characterization of AgNP in aqueous suspensions. The repulsive interaction between the particles is determined by the surface charge as the measured zeta potential values indicate the particles' tendency to agglomerate or to disperse [53]. The synthesized AgNP showed high zeta potential values of -31.8, -35.3 and -36.3 mV for ELE-AgNP, GTE-AgNP and BTE-AgNP, respectively compared to results obtained by other authors [24,31]. The high negative values indicate the coordination of anionic stabilizing agents and the stability of the AgNP colloidal solution as a result to electrostatic repulsion between the negative charges [31].

Figure 3-5 shows the FTIR spectra of aqueous extracts and of the respective biosynthesized AgNP. In the aqueous extracts, the bands between 3600 and 3000 cm^{-1} represent the O-H stretching vibration of the hydroxyl group (-OH) in polysaccharides and phenolic compounds and are assigned to secondary amides (-NH) [53]. The band situated at 2923 cm^{-1} is associated with the C-H characteristic stretching vibration from CH and CH_2 present in the aliphatic compounds [54]. The band at 1634 cm^{-1} represents the carbonyl group C=O stretch vibration of aromatic ketones, amine and carboxyl which are typically found in the proteins from plant extract [55]. The N-H functional groups of primary and secondary amides are responsible for the absorption band at 1515 cm^{-1} . The peak at 1492 cm^{-1} can be related to the C=C stretching of the aromatic ring of the lignin [56]. The intensity band located at 1422 cm^{-1} is related to the symmetric bending of the CH_2 which is present in comparable compounds such as cellulose, while the bands located at 1379 and 1320 cm^{-1} correspond to the bending vibration of C-O and C-H groups of the aromatic ring of the polysaccharides [57]. A band situated at 1062 cm^{-1} is attributed to the C-N stretching vibration band of aliphatic amines and the presence of a C-O stretching vibration was shown by the band at 1043 cm^{-1} . This band could be used to assign a primary, secondary or tertiary structure of alcohol, that establishes the existence of phenolic compounds or ether and hydroxyl groups in cellulose [58,59]. The bands at 922, 872, 765 and 608 cm^{-1} were associated to out of plane C-H bending vibrations in aromatics and alkenes [5]. All the identified bands are common in the spectra of the biosynthesized AgNP, especially in the case of ELE-

AgNP and BTE-AgNP. These results support that these functional groups play essential roles in the reduction of Ag⁺ ions to biosynthesize AgNP that is consistent with other works [58].

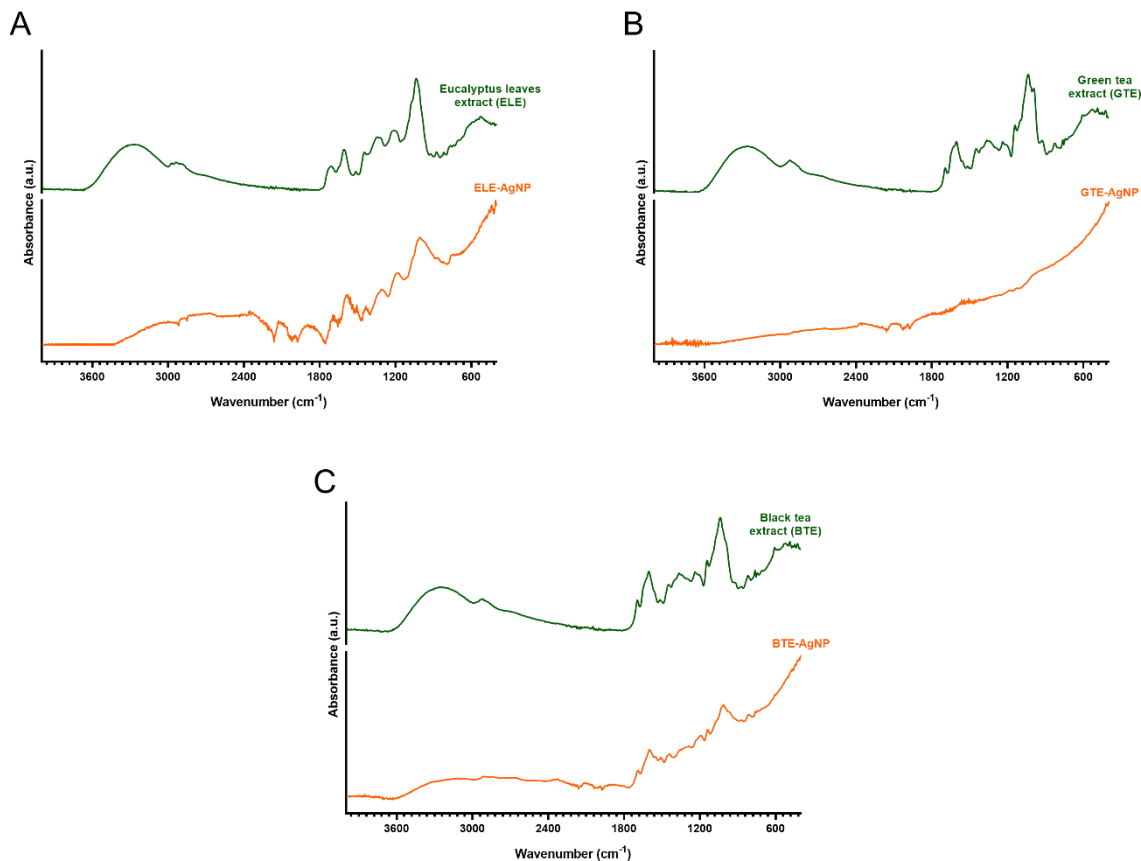


Figure 3-5. FTIR of extracts from (A) eucalyptus leaves (ELE), (B) green tea (GTE) and (C) black tea (BTE) and biosynthesized AgNP: (A) ELE-AgNP, (B) GTE-AgNP and (C) BTE-AgNP.

Although the use of plant extract in biosynthesis has been extensively studied, the mechanism of bio-reduction of metal ions remains unknown [60]. It has been proposed that the electrostatic trapping of silver ions on the surface of proteins in plant extract is the first step in silver bio-reduction [61]. The involvement of the secondary metabolites has also been proposed to have an implication in the reduction of metal ions that lead to nanoparticle formation and in supporting their subsequent stability [60].

Figure 3-6 displays the probable mechanism of plant-mediated synthesis of AgNP from AgNO₃ as suggested by Din and Rani [62]. It is proposed that the hydroxyl groups of the various biomolecules

present in the different extracts are primarily responsible for the reduction of silver ions (Ag^+) into zero metallic species (Ag^0). These Ag^0 nuclei formed rapidly undergo the phenomenon of coalescence, culminating in the formation of AgNP.

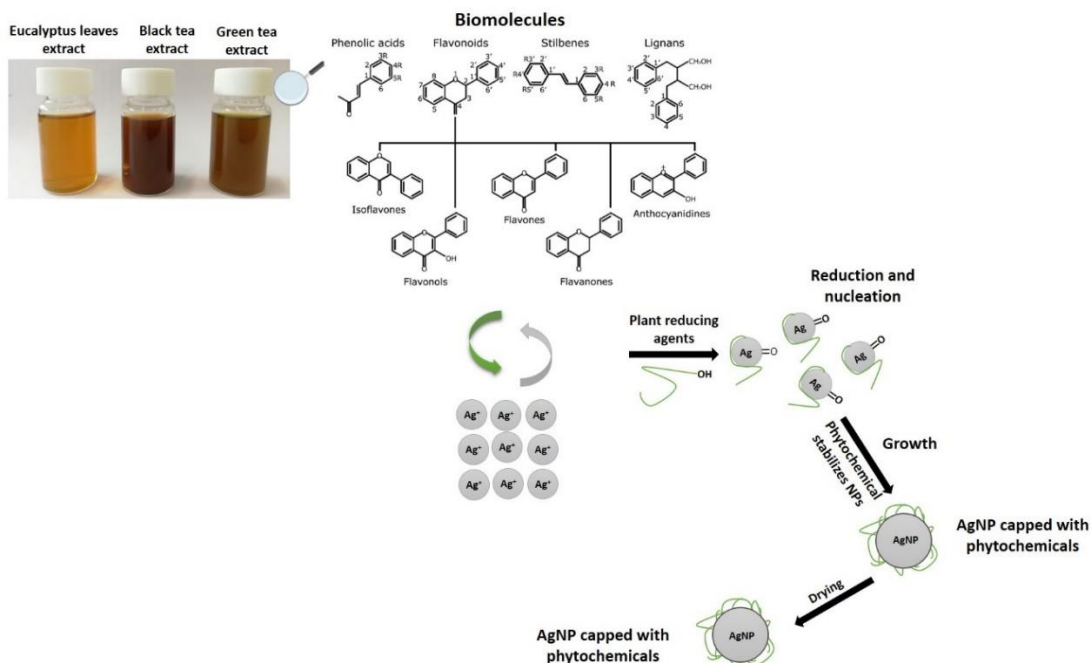


Figure 3-6. Schematic illustration of the mechanism of plant-mediated synthesis of silver nanoparticles (AgNP): Adapted from [62].

3.3.3 Antibacterial activity of aqueous extracts and AgNP

The antibacterial action of aqueous ELE, GTE and BTE and the respective biosynthesized AgNP was investigated against both Gram-negative (*P. putida*, *E. coli*, *Vibrio spp.*) and Gram-positive (*B. megaterium*, *S. aureus*, *S. equisimilis*) bacteria strains. The results of the inhibition zone (mm) are expressed in **Table 3-2**. The extracts were only effective against *Vibrio spp.* and the ELE showed the highest inhibition (11.5 ± 0.5 mm). In other studies, the application of *Eucalyptus globulus* extract showed an inhibition zone for *S. aureus* and *E. coli* [30]. However, the extracts were obtained with ethanol 70% (v/v), which may present different concentrations and profiles of bioactive compounds with antibacterial properties. In fact, ethanol is widely considered the ideal solvent for the extraction of phenolic compounds, although it is a flammable and costly solvent [33]. So, water was used in this work as the safest, cheapest and most environmental friendly extraction solvent.

The antibacterial action of the biosynthesized AgNP against the Gram-positive and Gram-negative bacteria can be appreciated in both cases. ELE-AgNP, GTE-AgNP and BTE-AgNP were potentially effective in suppressing bacterial growth within a range of inhibition zones from 7.3 ± 0.4 to 14 ± 1 mm. ELE-AgNP and BTE-AgNP exhibited significantly ($p < 0.05$) higher antimicrobial activity than the GTE-AgNP for all bacterial strains, but for *Vibrio spp.* and *B. megaterium*, for which ELE-AgNP showed higher inhibitory effect than BTE-AgNP. The inhibition zones of ELE-AgNP ranged between 10 ± 0 to 14 ± 1 mm. ELE-AgNP showed a higher inhibition against *Vibrio spp.* (14 ± 1 mm), *S. aureus* (13.5 ± 0.8 mm) and *S. equisimillis* (13.5 ± 0.5 mm). In the case of *Vibrio spp.*, this higher inhibition has the contribution of the ELE, since ELE also shows antibacterial activity (11.5 ± 0.5 mm), while the remaining the unique responsible for the effect is silver. Similar outcomes were obtained by Liaqat *et al.* [63] that reported antibacterial activity of AgNP biosynthesized by ELE against *E. coli* (8 ± 6 mm) and *S. aureus* (13.0 ± 0.3 mm). The inhibition zones of GTE-AgNP ranged between 7.3 ± 0.4 to 11.3 ± 0.8 mm and the highest inhibition was shown against *S. aureus* (11.3 ± 0.8 mm). Previous studies reported antibacterial activity from GTE mediated AgNP against *E. coli* and *S. aureus*, forming inhibition zones of 11 and 7 mm, respectively [55]. The inhibition zone of BTE-AgNP ranged between 8.8 ± 0.8 to 12.8 ± 0.4 mm. BTE-AgNP showed higher inhibition against *Vibrio spp.* (12 ± 0 mm), *S. aureus* (12.8 ± 0.4 mm) and *S. equisimillis* (12.5 ± 0.5 mm). The BTE is also active against *Vibrio spp.* (11 ± 0 mm), enhancing the inhibitory effect obtained by BTE-AgNP.

In general, the antibacterial action is higher against Gram-positive (*S. aureus* and *S. equisimillis*), likewise reported by other authors [64]. As suggested by Loo *et al.* [65], Gram-negative bacteria may be less vulnerable due to the positive charges of AgNP trapped and inhibited by lipopolysaccharides, thus making them less susceptible.

It is suggested that AgNP demonstrated enhanced toxicity towards bacterial strains due to the small size and large intake of AgNP by bacteria [10]. Although the detailed mechanism by which AgNP exhibits antibacterial action is not entirely known, various mechanisms of action have been documented in the bibliography. Due to their anchoring capabilities, AgNP have been demonstrated to induce structural changes in the bacterial membrane and eventual cell death as a result of their penetration into the cell wall [11,66]. Breakage of genetic material, inactivation of structural proteins and enzyme degradation by AgNP have been suggested as mechanisms of action too [67]. Another

proposed mechanism is based on the release of silver cations from AgNP and on their interaction which results in severe changes in the bacterial membrane structure, increasing its permeability [64].

This antibacterial screening confirmed that green AgNP possess efficient antimicrobial potential against bacteria and could be used as alternative disinfectants in wastewater remediation. The perfect disinfectant should be able to inactivate a wide range of microorganisms quickly, not corrosive, without producing any dangerous by-products, using little energy and being easy to use and store. It should also be able to be safely disposed [68].

Table 3-2. Inhibition zones of the aqueous plant extracts and AgNP against Gram-positive and Gram-negative bacterial strains.

Bacterial strains	Inhibition zone (mm)					
	Aqueous extracts			AgNP		
	Eucalyptus leaves (ELE)	Green tea (GTE)	Black tea (BTE)	ELE-AgNP	GTE-AgNP	BTE-AgNP
<i>E. coli</i>	n.d.	n.d.	n.d.	10±0.7 ^{aA}	7.8±0.4 ^{aA}	10.3±1.1 ^{aA}
Gram - <i>P. putida</i>	n.d.	n.d.	n.d.	10.8±0.4 ^{aA}	7.8±0.4 ^{aA}	10.5±0.5 ^{aA}
<i>Vibrio spp.</i>	11.5±0.5 ^a	10±0 ^b	10.5±0.5 ^b	14±1 ^{aB}	8.3±0.8 ^{aA}	12±0 ^{bB}
<i>S. aureus</i>	n.d.	n.d.	n.d.	13.5±0.8 ^{bB}	11.3±0.8 ^{bB}	12.8±0.4 ^{aB}
Gram + <i>B. megaterium</i>	n.d.	n.d.	n.d.	10.0±0 ^{aA}	7.3±0.4 ^{aA}	8.8±0.8 ^{cC}
<i>S. equisimilis</i>	n.d.	n.d.	n.d.	13.5±0.5 ^{bB}	7.8±0.8 ^{aA}	12.5±0.5 ^{aB}

not detected (n.d.); Values are expressed as mean (mm) ± SD; Different lowercase letters show significant differences ($p < 0.05$) between inhibition zone of aqueous extracts or AgNP for the same bacteria strain. Different capital letters show significant differences ($p < 0.05$) between bacterial strains for the same AgNP.

3.3.4 Photocatalytic activity of ELE-AgNP

Eucalyptus leaves a by-product (biowaste) of the lumber and cellulose industry, were considered a good source of bioactive compounds for the synthesis of AgNP. For this reason, the photocatalytic potential of biosynthesized ELE-AgNP was assessed by evaluating the photodegradation of a model dye compound, indigo carmine (IC) dye, under direct sunlight. IC is an anionic (acidic)-type dye and it is one of the oldest dyes still widely used in many industries especially in textile, food, cosmetics, pharmaceuticals and medical diagnostics [69,70]. It is a very toxic member of the indigoid dye class

and direct contact causes eye and skin irritation, as well as permanent damage to the cornea and conjunctiva [71].

Figure 3-7A illustrates the photocatalytic degradation of IC dye under different dosages of ELE-AgNP (0.5 and 1 g.L⁻¹). Control experiments were performed to verify the effectiveness of ELE-AgNP and the effects of direct sunlight on IC degradation. Degradation of IC was insignificant under direct sunlight and in the absence of AgNP. In addition, no significant changes were observed in the dye removal experiment conducted in the dark in the presence of ELE-AgNP. These findings indicate that the dye degradation should depend on both ELE-AgNP and sunlight. The degradation percentages of the IC dye are nearly 95 and 100% under natural sunlight after 75 min with 0.5 and 1 g.L⁻¹ of ELE-AgNP, respectively. The apparent kinetic parameters were estimated assuming that the degradation rate follows a pseudo-first-order kinetics represented by equation 3.4 (**Figure 3-7B**). The catalytic reaction kinetics were evaluated through the creation of a graph of normalized concentration (C_t/C_0) vs time.

$$\ln \frac{C_t}{C_0} = -k \cdot t \quad (\text{Equation 3-4})$$

where C_0 is the IC dye initial concentration, C_t is the concentration of IC dye at t (time) and k is the rate constant.

These kinetics assessment confirmed that the photocatalytic reaction follows a pseudo-first-order relationship, with an apparent rate constant (k) of 0.0178 and 0.03612 min⁻¹ using 0.5 and 1 g.L⁻¹ of ELE-AgNP, respectively. The dosage of 1 g.L⁻¹ led to the highest photocatalytic activity, indicating that the amount of catalyst influences the degradation rate, as more electron-pairs are formed which increases the rate of reaction [72].

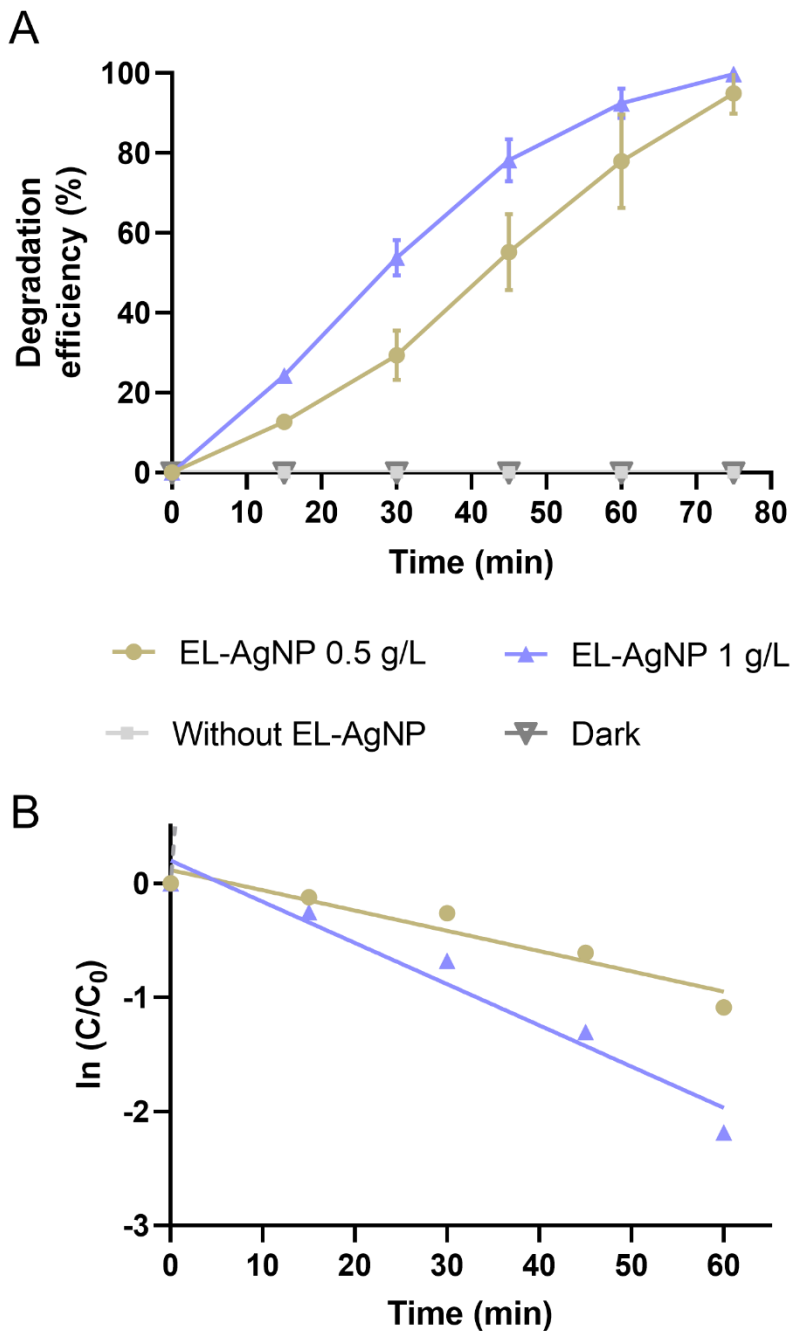


Figure 3-7. (A) Degradation efficiency of indigo carmine (IC) dye by biosynthesized E-LE-AgNP and (B) pseudo-first-order reaction kinetics for IC decolorization by E-LE-AgNP 0.5 g.L⁻¹ (R²=0.9192) and E-LE-AgNP 1 g.L⁻¹ (R²=0.9513).

The photocatalytic efficiency is affected by the type of catalyst, the nature of the pollutant and the experimental conditions (pollutant concentration, light power catalyst surface, pH, etc.) [73]. Although it is difficult to compare of the obtained results with those of the literature, as efficiency is a vital factor for the large scale of a photocatalyst, the photodegradation of IC with AgNP and other catalysts is presented (**Table 3-3**).

Table 3-3. Comparative performance of silver nanoparticles (AgNP) and their composites for photodegradation of indigo carmine (IC) dye.

Catalyst	Method of synthesis	Catalyst dosage (g.L ⁻¹)	IC concentration (mg.L ⁻¹)	Light source	Reaction time (min)	Degradation efficiency (%)	Degradation rate (min ⁻¹)	Ref.
Ag-ZnO	Sol-gel spin coating	n.r.	6.6	Simulated sunlight	360	85	0.004	[73]
Ag-CaO	Thermal	0.8	25	Sunlight	25	99.45	0.180	[74]
Ag-rGO	Hydrothermal	0.3	20	Sunlight	240	100	0.012	[75]
Ag-GO	Photochemical	1.0	10	Visible	420	54	0.003	[76]
Ag-TiO₂	Sol-gel	1.0	28	UV	240	100	0.044	[71]
Ag-PbMoO₄	Sonochemical	2.0	20	Simulated sunlight	120	n.a.	0.026	[77]
Ag	Green using <i>Flammulina velutipes</i> extract	0.7	20	UV	140	98.2	n.r.	[78]
Ag	Green using <i>Eucalyptus globulus</i> leaves extract	1.0	10	Sunlight	75	99.8	0.036	This work
	not reported (n.r.)							

These results encourage further efforts to recognize the potential of ELE-AgNP to photodegrade pollutants and the respective mechanism of photodegradation. Faisal *et al.* [78] tested the photodegradation of IC using green AgNP and obtained 98.2% dye within 140 min. A higher degradation rate was found for the Ag-TiO₂ composite (0.044 min⁻¹) [71], similar to our work (0.036 min⁻¹).

3.3.5 Cost estimation of AgNP biofabrication

Successful implementation of materials usage for the elimination of pollutants and microorganisms from water depends largely on the cost of the material production. The cost assessment of the synthesis of green AgNP is a very important step to evaluate its cost-effectiveness and scalability of production. The total cost of the biosynthesis of AgNP covers various items including collection, washing, drying and milling of plant material; preparation and filtration of plant extract; and synthesis, centrifugation, washing and lyophilization of AgNP. **Figure 3-8** shows the different steps performed to produce 1 g of AgNP as well as the input flows of energy, water and chemicals.

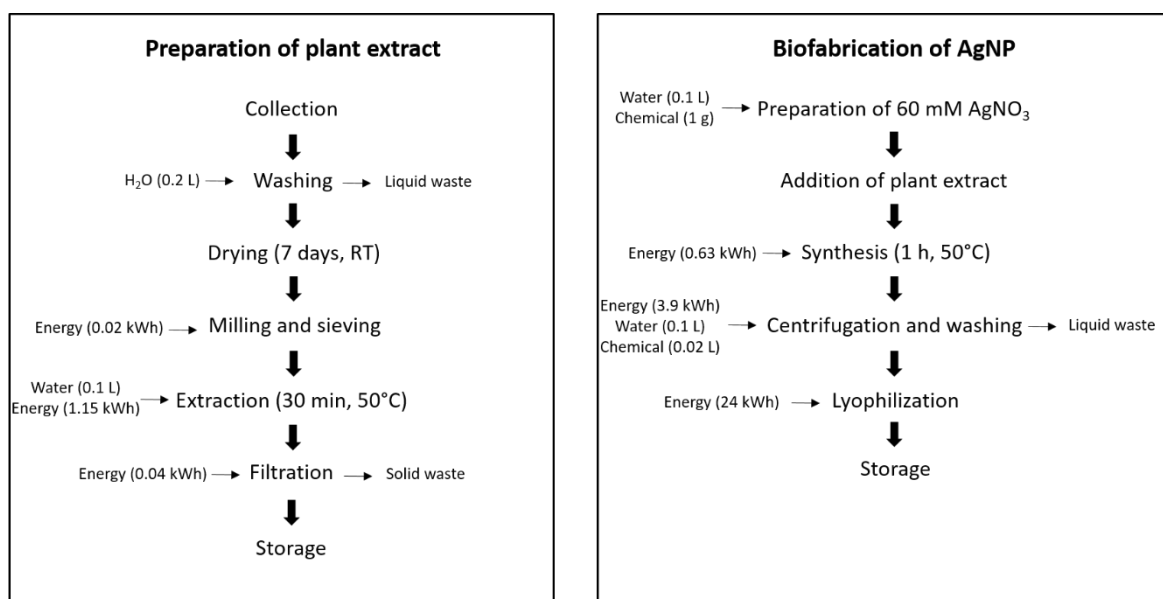


Figure 3-8. Flowchart for the preparation of 1 g of green AgNP.

The total cost involved in this process was evaluated by determining the cost of energy, water, metallic salt and ethanol required for the biofabrication of AgNP. The cost of each step and the total preparation cost for 1 g of AgNP are given in **Table 3-4**. The cost associated with the collection of eucalyptus leaves was not considered once it is locally and abundantly available and was acquired as a biowaste. Green and black tea were purchased as commercial products (Tetley®) and were used as received. The cost of material collection, energy, water and chemicals was defined considering average values practiced in Portugal.

Table 3-4. Estimation cost of preparation of 1 g of AgNP.

	Plant Costs (€·g⁻¹ AgNP)	Eucalyptus leaves	Green tea	Black tea
	Material collection	-	0.82	0.65
Energy consumption ^a	Milling and Sieving	0.002	-	-
	Extraction	0.184	0.184	0.184
	Filtration	0.007	0.007	0.007
	Synthesis	0.1	0.1	0.1
	Centrifugation	0.624	0.624	0.624
	Lyophilization	3.84	3.84	3.84
	Water consumption ^b	Plant washing, extraction process, AgNO ₃ solution and AgNP washing	0.0003	0.0003
Chemicals	Silver nitrate ^c	2.78	2.78	2.78
	Ethanol ^d	0.4	0.4	0.4
	Total cost (€·g⁻¹ AgNP)	7.94	8.76	8.59

^aConsidering an energy cost of 0.16 €·kWh⁻¹

^bConsidering a cost of 0.70 €·m⁻³ of deionized water

^cConsidering a cost of 69.60 €·25g⁻¹

^dConsidering a cost of 16.02 €·2.5L⁻¹

The total cost of the synthesis of green AgNP in the laboratory ranges 7.94-8.76 €·g⁻¹. The main items with a remarkable cost are the energy required in the lyophilization step and the silver nitrate. The commercial AgNP are currently priced between 18.48 €·g⁻¹ (Sigma-Aldrich, #576832) and 28.72 €·g⁻¹ (ThermoFischer Scientific, #045509.14), which illustrates the need to develop cheaper and scalable alternatives. This cost analysis reveals that the proposed green synthesis is comparatively very competitive.

3.4 CONCLUSIONS

The use of plant extracts for the biosynthesis of AgNP is an alternative green method of preparation due to its quick, ecological, non-pathogenic and inexpensive procedure. Different aqueous plant extracts, obtained from *Eucalyptus globulus*, *Pinus pinaster*, *Citrus sinensis*, *Cedrus atlantica* and *Camellia sinensis* by-products, were evaluated in order to select the best extract to synthesize stable AgNP. This study confirms the ability of ELE, GTE and BTE for the biosynthesis of AgNP. The resulting biosynthesized AgNP have antimicrobial activity against Gram-negative and Gram-positive bacteria, with ELE-AgNP being the nanostructure with the greatest antimicrobial action. The photocatalytic capacity of ELE-AgNP was proved by the total degradation of the IC dye after 75 min of reaction. The cost analysis demonstrated the potential of this green approach to enable the large-scale deployment of AgNP in a wide range of environmental applications.

3.5 REFERENCES

- [1] I. Khan, K. Saeed, I. Khan, Nanoparticles: Properties, applications and toxicities, Arab. J. Chem. 12 (2019) 908–931. <https://doi.org/https://doi.org/10.1016/j.arabjc.2017.05.011>.
- [2] M.T. Yarak, S. Zahed Nasab, I. Zare, M. Dahri, M. Moein Sadeghi, M. Koohi, Y.N. Tan, Biomimetic Metallic Nanostructures for Biomedical Applications, Catalysis, and Beyond, Ind. Eng. Chem. Res. 61 (2022) 7547–7593. <https://doi.org/10.1021/acs.iecr.2c00285>.
- [3] S.S. Salem, A. Fouda, Green Synthesis of Metallic Nanoparticles and Their Prospective Biotechnological Applications: an Overview., Biol. Trace Elem. Res. 199 (2021) 344–370. <https://doi.org/10.1007/s12011-020-02138-3>.
- [4] A.A. Yaqoob, K. Umar, M.N.M. Ibrahim, Silver nanoparticles: various methods of synthesis, size affecting factors and their potential applications—a review, Appl. Nanosci. 10 (2020) 1369–1378. <https://doi.org/10.1007/s13204-020-01318-w>.
- [5] N. Esmaili, P. Mohammadi, M. Abbaszadeh, H. Sheibani, Green synthesis of silver nanoparticles using Eucalyptus comadulensis leaves extract and its immobilization on magnetic nanocomposite (GO-Fe₃O₄/PAA/Ag) as a recoverable catalyst for degradation of organic dyes in water, Appl. Organomet. Chem. 34 (2020) e5547. <https://doi.org/https://doi.org/10.1002/aoc.5547>.
- [6] A.M. El Shafey, Green synthesis of metal and metal oxide nanoparticles from plant leaf extracts and their applications: A review, Green Process. Synth. 9 (2020) 304–339. <https://doi.org/doi:10.1515/gps-2020-0031>.
- [7] A. Saravanan, P.S. Kumar, S. Karishma, D.-V.N. Vo, S. Jeevanantham, P.R. Yaashikaa, C.S. George, A review on biosynthesis of metal nanoparticles and its environmental applications, Chemosphere. 264 (2021) 128580. <https://doi.org/https://doi.org/10.1016/j.chemosphere.2020.128580>.
- [8] N.T.T. Nguyen, L.M. Nguyen, T.T.T. Nguyen, R.K. Liew, D.T.C. Nguyen, T. Van Tran, Recent

- advances on botanical biosynthesis of nanoparticles for catalytic, water treatment and agricultural applications: A review, *Sci. Total Environ.* 827 (2022) 154160. <https://doi.org/https://doi.org/10.1016/j.scitotenv.2022.154160>.
- [9] K. Pyrzynska, A. Sentkowska, Biosynthesis of selenium nanoparticles using plant extracts, *J. Nanostructure Chem.* 12 (2022) 467–480. <https://doi.org/10.1007/s40097-021-00435-4>.
- [10] I. Ijaz, A. Bukhari, E. Gilani, A. Nazir, H. Zain, R. Saeed, S. Hussain, T. Hussain, A. Bukhari, Yasra Naseer, R. Aftab, Green synthesis of silver nanoparticles using different plants parts and biological organisms, characterization and antibacterial activity, *Environ. Nanotechnology, Monit. Manag.* 18 (2022) 100704. <https://doi.org/https://doi.org/10.1016/j.enmm.2022.100704>.
- [11] D.H. Nguyen, T.N.N. Vo, N.T. Nguyen, Y.C. Ching, T.T. Hoang Thi, Comparison of biogenic silver nanoparticles formed by *Momordica charantia* and *Psidium guajava* leaf extract and antifungal evaluation., *PLoS One.* 15 (2020) e0239360. <https://doi.org/10.1371/journal.pone.0239360>.
- [12] Taruna, J. Kaushal, J. Bhatti, P. Kumar, Green synthesis and physico-chemical study of silver nanoparticles extracted from a natural source *Luffa acutangula*, *J. Mol. Liq.* 224 (2016) 991–998. <https://doi.org/https://doi.org/10.1016/j.molliq.2016.10.065>.
- [13] F. Göll, A. Aygün, A. Seyrankaya, T. Gür, C. Yenikaya, F. Şen, Green synthesis and characterization of *Camellia sinensis* mediated silver nanoparticles for antibacterial ceramic applications, *Mater. Chem. Phys.* 250 (2020) 123037. <https://doi.org/https://doi.org/10.1016/j.matchemphys.2020.123037>.
- [14] A. Salayová, Z. Bedlovičová, N. Daneu, M. Baláž, Z. Lukáčová Bujňáková, Ľ. Balážová, Ľ. Tkáčiková, Green Synthesis of Silver Nanoparticles with Antibacterial Activity Using Various Medicinal Plant Extracts: Morphology and Antibacterial Efficacy, *Nanomater.* 11 (2021). <https://doi.org/10.3390/nano11041005>.
- [15] M.A. Asghar, E. Zahir, S.M. Shahid, M.N. Khan, M.A. Asghar, J. Iqbal, G. Walker, Iron, copper and silver nanoparticles: Green synthesis using green and black tea leaves extracts and evaluation of antibacterial, antifungal and aflatoxin B1 adsorption activity, *LWT.* 90 (2018) 98–107. <https://doi.org/https://doi.org/10.1016/j.lwt.2017.12.009>.
- [16] Y. Liu, X. Jin, Z. Chen, The formation of iron nanoparticles by *Eucalyptus* leaf extract and used to remove Cr(VI), *Sci. Total Environ.* 627 (2018) 470–479. <https://doi.org/https://doi.org/10.1016/j.scitotenv.2018.01.241>.
- [17] S. Ahmad, S. Munir, N. Zeb, A. Ullah, B. Khan, J. Ali, M. Bilal, M. Omer, M. Alamzeb, S.M. Salman, S. Ali, Green nanotechnology: a review on green synthesis of silver nanoparticles - an ecofriendly approach., *Int. J. Nanomedicine.* 14 (2019) 5087–5107. <https://doi.org/10.2147/IJN.S200254>.
- [18] S.S. Shankar, A. Ahmad, M. Sastry, Geranium Leaf Assisted Biosynthesis of Silver Nanoparticles, *Biotechnol. Prog.* 19 (2003) 1627–1631. <https://doi.org/https://doi.org/10.1021/bp034070w>.
- [19] M. Rabeea, M. Owaid, R. Muslim, Synthesis and characterization of silver nanoparticles by natural organic compounds extracted from *Eucalyptus* leaves and their role in the catalytic degradation of methylene blue dye, *Songklanakarin J. Sci. Technol.* 43 (2021) 14–23. <https://doi.org/10.14456/sjst-psu.2021.3>.
- [20] M. Das, Biosynthesis of Silver Nanoparticles Using Bark Extracts of *Eucalyptus tereticornis* Sm.

- and Study of Their Antimicrobial Properties, Proc. Natl. Acad. Sci. India Sect. B Biol. Sci. 91 (2021) 557–564. <https://doi.org/10.1007/s40011-021-01242-1>.
- [21] M.I. Skiba, V.I. Vorobyova, Synthesis of Silver Nanoparticles Using Orange Peel Extract Prepared by Plasmochemical Extraction Method and Degradation of Methylene Blue under Solar Irradiation, Adv. Mater. Sci. Eng. 2019 (2019) 8306015. <https://doi.org/10.1155/2019/8306015>.
- [22] A. Parmar, G. Kaur, S. Kapil, V. Sharma, M.K. Choudhary, S. Sharma, Novel biogenic silver nanoparticles as invigorated catalytic and antibacterial tool: A cleaner approach towards environmental remediation and combating bacterial invasion, Mater. Chem. Phys. 238 (2019) 121861. <https://doi.org/https://doi.org/10.1016/j.matchemphys.2019.121861>.
- [23] P. Rani, V. Kumar, P.P. Singh, A.S. Matharu, W. Zhang, K.-H. Kim, J. Singh, M. Rawat, Highly stable AgNPs prepared via a novel green approach for catalytic and photocatalytic removal of biological and non-biological pollutants, Environ. Int. 143 (2020) 105924. <https://doi.org/https://doi.org/10.1016/j.envint.2020.105924>.
- [24] A. Kharabi Masooleh, A. Ahmadikhah, A. Saidi, Green synthesis of stable silver nanoparticles by the main reduction component of green tea (*Camellia sinensis* L.), IET Nanobiotechnology. 13 (2019) 183–188. <https://doi.org/https://doi.org/10.1049/iet-nbt.2018.5141>.
- [25] M. Balamurugan, S. Saravanan, Green Synthesis of Silver Nanoparticles by using Eucalyptus Globulus Leaf Extract, J. Inst. Eng. Ser. A. 98 (2017) 461–467. <https://doi.org/10.1007/s40030-017-0236-9>.
- [26] H.M. Mehwish, M.S.R. Rajoka, Y. Xiong, H. Cai, R.M. Aadil, Q. Mahmood, Z. He, Q. Zhu, Green synthesis of a silver nanoparticle using *Moringa oleifera* seed and its applications for antimicrobial and sun-light mediated photocatalytic water detoxification, J. Environ. Chem. Eng. 9 (2021) 105290. <https://doi.org/https://doi.org/10.1016/j.jece.2021.105290>.
- [27] R.A. Radwan, Y.A. El-Sherif, M.M. Salama, A Novel Biochemical Study of Anti-Ageing Potential of Eucalyptus Camaldulensis Bark Waste Standardized Extract and Silver Nanoparticles, Colloids Surfaces B Biointerfaces. 191 (2020) 111004. <https://doi.org/https://doi.org/10.1016/j.colsurfb.2020.111004>.
- [28] S. Kuppusamy, P. Thavamani, M. Megharaj, R. Nirola, Y.B. Lee, R. Naidu, Assessment of antioxidant activity, minerals, phenols and flavonoid contents of common plant/tree waste extracts, Ind. Crops Prod. 83 (2016) 630–634. <https://doi.org/https://doi.org/10.1016/j.indcrop.2015.12.060>.
- [29] H. Muthukumar, S.K. Palanirajan, M.K. Shanmugam, P. Arivalagan, S.N. Gummadi, Photocatalytic degradation of caffeine and *E. coli* inactivation using silver oxide nanoparticles obtained by a facile green co-reduction method, Clean Technol. Environ. Policy. 24 (2022) 1087–1098. <https://doi.org/10.1007/s10098-021-02135-7>.
- [30] A. Balčiūnaitienė, M. Liaudanskas, V. Puzerytė, J. Viškelis, V. Janulis, P. Viškelis, E. Griškonis, V. Jankauskaitė, Eucalyptus globulus and Salvia officinalis Extracts Mediated Green Synthesis of Silver Nanoparticles and Their Application as an Antioxidant and Antimicrobial Agent., Plants (Basel, Switzerland). 11 (2022). <https://doi.org/10.3390/plants11081085>.
- [31] S. Paosen, J. Saising, A. Wira Septama, S. Piyawan Voravuthikunchai, Green synthesis of silver nanoparticles using plants from Myrtaceae family and characterization of their antibacterial activity, Mater. Lett. 209 (2017) 201–206. <https://doi.org/https://doi.org/10.1016/j.matlet.2017.07.102>.

- [32] V.L. Singleton, J.A. Rossi, Colorimetry of Total Phenolics with Phosphomolybdic-Phosphotungstic Acid Reagents, *Am. J. Enol. Vitic.* 16 (1965) 144 LP – 158. <http://www.ajevonline.org/content/16/3/144.abstract>.
- [33] P. Ferreira-Santos, Z. Genisheva, C. Botelho, J. Santos, C. Ramos, J.A. Teixeira, C.M.R. Rocha, Unravelling the Biological Potential of Pinus pinaster Bark Extracts, *Antioxidants* (Basel, Switzerland). 9 (2020) 334. <https://doi.org/10.3390/antiox9040334>.
- [34] I.F.F. Benzie, J.J.B.T.-M. in E. Strain, [2] Ferric reducing/antioxidant power assay: Direct measure of total antioxidant activity of biological fluids and modified version for simultaneous measurement of total antioxidant power and ascorbic acid concentration, in: *Oxid. Antioxidants Part A*, Academic Press, 1999: pp. 15–27. [https://doi.org/https://doi.org/10.1016/S0076-6879\(99\)99005-5](https://doi.org/https://doi.org/10.1016/S0076-6879(99)99005-5).
- [35] P. Ferreira-Santos, Z. Genisheva, R.N. Pereira, J.A. Teixeira, C.M.R. Rocha, Moderate Electric Fields as a Potential Tool for Sustainable Recovery of Phenolic Compounds from Pinus pinaster Bark, *ACS Sustain. Chem. Eng.* 7 (2019) 8816–8826. <https://doi.org/10.1021/acssuschemeng.9b00780>.
- [36] P. Anastas, N. Eghbali, *Green Chemistry: Principles and Practice*, *Chem. Soc. Rev.* 39 (2010) 301–312. <https://doi.org/10.1039/B918763B>.
- [37] T.I.J. Dugmore, J.H. Clark, J. Bustamante, J.A. Houghton, A.S. Matharu, Valorisation of Biowastes for the Production of Green Materials Using Chemical Methods, *Top. Curr. Chem.* 375 (2017) 46. <https://doi.org/10.1007/s41061-017-0133-8>.
- [38] M. Martínez-Cabanas, M. López-García, P. Rodríguez-Barro, T. Vilariño, P. Lodeiro, R. Herrero, J.L. Barriada, M.E. Sastre de Vicente, Antioxidant Capacity Assessment of Plant Extracts for Green Synthesis of Nanoparticles, *Nanomater.* 11 (2021). <https://doi.org/10.3390/nano11071679>.
- [39] L. Soltys, O. Olkhovyy, T. Tatarchuk, M. Naushad, Green Synthesis of Metal and Metal Oxide Nanoparticles: Principles of Green Chemistry and Raw Materials, *Magnetochemistry* . 7 (2021). <https://doi.org/10.3390/magnetochemistry7110145>.
- [40] S.K. Chandini, L. Jaganmohan Rao, R. Subramanian, Influence of extraction conditions on polyphenols content and cream constituents in black tea extracts, *Int. J. Food Sci. Technol.* 46 (2011) 879–886. <https://doi.org/https://doi.org/10.1111/j.1365-2621.2011.02576.x>.
- [41] S. Machado, S.L. Pinto, J.P. Grosso, H.P.A. Nouws, J.T. Albergaria, C. Delerue-Matos, Green production of zero-valent iron nanoparticles using tree leaf extracts, *Sci. Total Environ.* 445–446 (2013) 1–8. <https://doi.org/https://doi.org/10.1016/j.scitotenv.2012.12.033>.
- [42] P. Salgado, K. Márquez, O. Rubilar, D. Contreras, G. Vidal, The effect of phenolic compounds on the green synthesis of iron nanoparticles (FexOy-NPs) with photocatalytic activity, *Appl. Nanosci.* 9 (2019) 371–385. <https://doi.org/10.1007/s13204-018-0931-5>.
- [43] R.L. Prior, X. Wu, K. Schaich, Standardized Methods for the Determination of Antioxidant Capacity and Phenolics in Foods and Dietary Supplements, *J. Agric. Food Chem.* 53 (2005) 4290–4302. <https://doi.org/10.1021/jf0502698>.
- [44] P. Ferreira-Santos, Valorization of Natural Antioxidants for Nutritional and Health Applications, in: Z. Genisheva (Ed.), *IntechOpen, Rijeka, 2021: p. Ch. 28*. <https://doi.org/10.5772/intechopen.96111>.
- [45] M. Kędzierska-Matysek, M. Stryjecka, A. Teter, P. Skąłeczki, P. Domaradzki, M. Florek, Relationships between the Content of Phenolic Compounds and the Antioxidant Activity of Polish

- Honey Varieties as a Tool for Botanical Discrimination, *Molecules*. 26 (2021). <https://doi.org/10.3390/molecules26061810>.
- [46] Y. Mo, Y. Tang, S. Wang, J. Lin, H. Zhang, D. Luo, Green synthesis of silver nanoparticles using eucalyptus leaf extract, *Mater. Lett.* 144 (2015) 165–167. <https://doi.org/https://doi.org/10.1016/j.matlet.2015.01.004>.
- [47] C. Noguez, Surface Plasmons on Metal Nanoparticles: The Influence of Shape and Physical Environment, *J. Phys. Chem. C*. 111 (2007) 3806–3819. <https://doi.org/10.1021/jp066539m>.
- [48] C.P. Devatha, A.K. Thalla, S.Y. Katte, Green synthesis of iron nanoparticles using different leaf extracts for treatment of domestic waste water, *J. Clean. Prod.* 139 (2016) 1425–1435. <https://doi.org/https://doi.org/10.1016/j.jclepro.2016.09.019>.
- [49] M. Bilal, S. Khan, J. Ali, M. Ismail, M.I. Khan, A.M. Asiri, S.B. Khan, Biosynthesized silver supported catalysts for disinfection of *Escherichia coli* and organic pollutant from drinking water, *J. Mol. Liq.* 281 (2019) 295–306. <https://doi.org/https://doi.org/10.1016/j.molliq.2019.02.087>.
- [50] O.O. Oluwaniyi, H.I. Adegoke, E.T. Adesuji, A.B. Alabi, S.O. Bodede, A.H. Labulo, C.O. Oseghale, Biosynthesis of silver nanoparticles using aqueous leaf extract of *Thevetia peruviana* Juss and its antimicrobial activities, *Appl. Nanosci.* 6 (2016) 903–912. <https://doi.org/10.1007/s13204-015-0505-8>.
- [51] I. Alghoraibi, C. Soukkarieh, R. Zein, A. Alahmad, J.-G. Walter, M. Daghestani, Aqueous extract of *Eucalyptus camaldulensis* leaves as reducing and capping agent in biosynthesis of silver nanoparticles, *Inorg. Nano-Metal Chem.* 50 (2020) 895–902. <https://doi.org/10.1080/24701556.2020.1728315>.
- [52] K. Kalishwaralal, S. BarathManiKanth, S.R.K. Pandian, V. Deepak, S. Gurunathan, Silver nanoparticles impede the biofilm formation by *Pseudomonas aeruginosa* and *Staphylococcus epidermidis*, *Colloids Surfaces B Biointerfaces*. 79 (2010) 340–344. <https://doi.org/https://doi.org/10.1016/j.colsurfb.2010.04.014>.
- [53] Á. de J. Ruiz-Baltazar, S.Y. Reyes-López, M. de L. Mondragón-Sánchez, M. Estevez, A.R. Hernández-Martínez, R. Pérez, Biosynthesis of Ag nanoparticles using *Cynara cardunculus* leaf extract: Evaluation of their antibacterial and electrochemical activity, *Results Phys.* 11 (2018) 1142–1149. <https://doi.org/https://doi.org/10.1016/j.rinp.2018.11.032>.
- [54] S. Perugu, V. Nagati, M. Bhanoori, Green synthesis of silver nanoparticles using leaf extract of medicinally potent plant *Saraca indica*: a novel study, *Appl. Nanosci.* 6 (2016) 747–753. <https://doi.org/10.1007/s13204-015-0486-7>.
- [55] A. Bergal, G.H. Matar, M. Andaç, Olive and green tea leaf extracts mediated green synthesis of silver nanoparticles (AgNPs): comparison investigation on characterizations and antibacterial activity, *Bionanoscience*. 12 (2022) 307–321. <https://doi.org/10.1007/s12668-022-00958-2>.
- [56] C. Shanmugam, G. Sivasubramanian, B. Parthasarathi, K. Baskaran, R. Balachander, V.R. Parameswaran, Antimicrobial, free radical scavenging activities and catalytic oxidation of benzyl alcohol by nano-silver synthesized from the leaf extract of *Aristolochia indica* L.: a promenade towards sustainability, *Appl. Nanosci.* 6 (2016) 711–723. <https://doi.org/10.1007/s13204-015-0477-8>.
- [57] Á. de Jesús Ruiz-Baltazar, S.Y. Reyes-López, D. Larrañaga, M. Estévez, R. Pérez, Green

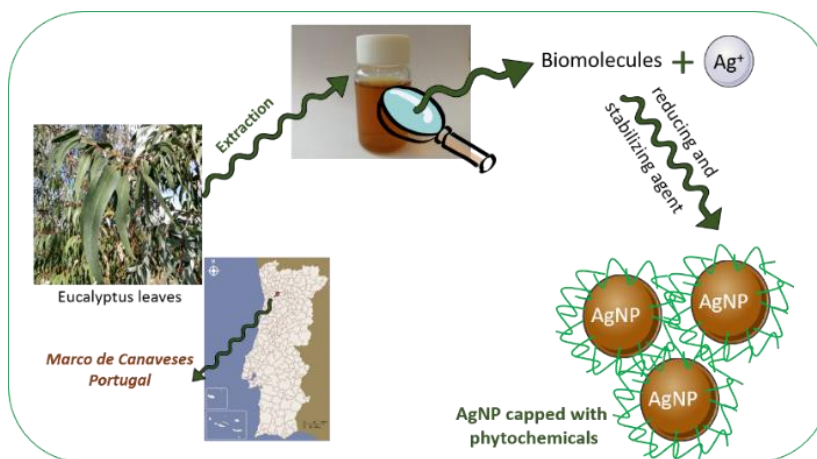
- synthesis of silver nanoparticles using a *Melissa officinalis* leaf extract with antibacterial properties, *Results Phys.* 7 (2017) 2639–2643. <https://doi.org/https://doi.org/10.1016/j.rinp.2017.07.044>.
- [58] X.N. Pham, H.T. Nguyen, N.T. Pham, Green Synthesis and Antibacterial Activity of HAp@Ag Nanocomposite Using *Centella asiatica* (L.) Urban Extract and Eggshell., *Int. J. Biomater.* 2020 (2020) 8841221. <https://doi.org/10.1155/2020/8841221>.
- [59] R. Manikandan, B. Manikandan, T. Raman, K. Arunagirinathan, N.M. Prabhu, M. Jothi Basu, M. Perumal, S. Palanisamy, A. Munusamy, Biosynthesis of silver nanoparticles using ethanolic petals extract of *Rosa indica* and characterization of its antibacterial, anticancer and anti-inflammatory activities, *Spectrochim. Acta Part A Mol. Biomol. Spectrosc.* 138 (2015) 120–129. <https://doi.org/https://doi.org/10.1016/j.saa.2014.10.043>.
- [60] T. Mustapha, N. Misni, N.R. Ithnin, A.M. Daskum, N.Z. Unyah, A Review on Plants and Microorganisms Mediated Synthesis of Silver Nanoparticles, Role of Plants Metabolites and Applications., *Int. J. Environ. Res. Public Health.* 19 (2022). <https://doi.org/10.3390/ijerph19020674>.
- [61] G. Marslin, K. Siram, Q. Maqbool, R.K. Selvakesavan, D. Kruszka, P. Kachlicki, G. Franklin, Secondary Metabolites in the Green Synthesis of Metallic Nanoparticles, *Mater. (Basel, Switzerland)*. 11 (2018) 940. <https://doi.org/10.3390/ma11060940>.
- [62] M. Imran Din, A. Rani, Recent Advances in the Synthesis and Stabilization of Nickel and Nickel Oxide Nanoparticles: A Green Adeptness., *Int. J. Anal. Chem.* 2016 (2016) 3512145. <https://doi.org/10.1155/2016/3512145>.
- [63] N. Liaqat, N. Jahan, Khalil-Ur-Rahman, T. Anwar, H. Qureshi, Green synthesized silver nanoparticles: Optimization, characterization, antimicrobial activity, and cytotoxicity study by hemolysis assay., *Front. Chem.* 10 (2022) 952006. <https://doi.org/10.3389/fchem.2022.952006>.
- [64] S. Pirtarighat, M. Ghannadnia, S. Baghshahi, Green synthesis of silver nanoparticles using the plant extract of *Salvia spinosa* grown in vitro and their antibacterial activity assessment, *J. Nanostructure Chem.* 9 (2019) 1–9. <https://doi.org/10.1007/s40097-018-0291-4>.
- [65] Y.Y. Loo, Y. Rukayadi, M.-A.-R. Nor-Khaizura, C.H. Kuan, B.W. Chieng, M. Nishibuchi, S. Radu, In Vitro Antimicrobial Activity of Green Synthesized Silver Nanoparticles Against Selected Gram-negative Foodborne Pathogens, *Front. Microbiol.* 9 (2018). <https://doi.org/10.3389/fmicb.2018.01555>.
- [66] M. SINGH, A.K. Mallick, M. BANERJEE, R. KUMAR, Loss of outer membrane integrity in Gram-negative bacteria by silver nanoparticles loaded with *Camellia sinensis* leaf phytochemicals: plausible mechanism of bacterial cell disintegration, *Bull. Mater. Sci.* 39 (2016) 1871–1878. <https://doi.org/10.1007/s12034-016-1317-5>.
- [67] M. Guzman, J. Dille, S. Godet, Synthesis and antibacterial activity of silver nanoparticles against gram-positive and gram-negative bacteria, *Nanomedicine Nanotechnology, Biol. Med.* 8 (2012) 37–45. <https://doi.org/https://doi.org/10.1016/j.nano.2011.05.007>.
- [68] H.S. Taher, R. Sayed, A. Loutfi, H. Abdulla, Construction of a domestic wastewater disinfection filter from biosynthesized and commercial nanosilver: a comparative study, *Ann. Microbiol.* 72 (2022) 31. <https://doi.org/10.1186/s13213-022-01688-2>.
- [69] S. Ammar, R. Abdelhedi, C. Flox, C. Arias, E. Brillas, Electrochemical degradation of the dye indigo carmine at boron-doped diamond anode for wastewaters remediation, *Environ. Chem.*

- Lett. 4 (2006) 229–233. <https://doi.org/10.1007/s10311-006-0053-2>.
- [70] D. Ahirwar, M. Bano, F. Khan, Synthesis of mesoporous TiO₂ and its role as a photocatalyst in degradation of indigo carmine dye, *J. Sol-Gel Sci. Technol.* 79 (2016) 228–237. <https://doi.org/10.1007/s10971-016-4039-7>.
- [71] M.F. Abdel Messih, M.A. Ahmed, A. Soltan, S.S. Anis, Facile approach for homogeneous dispersion of metallic silver nanoparticles on the surface of mesoporous titania for photocatalytic degradation of methylene blue and indigo carmine dyes, *J. Photochem. Photobiol. A Chem.* 335 (2017) 40–51. <https://doi.org/https://doi.org/10.1016/j.jphotochem.2016.11.001>.
- [72] M. Saeed, M. Muneer, A. ul Haq, N. Akram, Photocatalysis: an effective tool for photodegradation of dyes—a review, *Environ. Sci. Pollut. Res.* 29 (2022) 293–311. <https://doi.org/10.1007/s11356-021-16389-7>.
- [73] A. Khiari MickaëlAU - Lejeune, MichaëlAU - Lazar, FloricaAU - Hadjadj, Effects of Ag Nanoparticles on Zinc Oxide Photocatalytic Performance, *Coatings.* 11 (2021). <https://doi.org/10.3390/coatings11040400>.
- [74] I.H. Alsohaimi, A.M. Nassar, T.A. Seaf Elnasr, B. amar Cheba, A novel composite silver nanoparticles loaded calcium oxide stemming from egg shell recycling: A potent photocatalytic and antibacterial activities, *J. Clean. Prod.* 248 (2020) 119274. <https://doi.org/https://doi.org/10.1016/j.jclepro.2019.119274>.
- [75] P.P.A. Jose, M.S. Kala, N. Kalarikkal, S. Thomas, Silver-attached reduced graphene oxide nanocomposite as an eco-friendly photocatalyst for organic dye degradation, *Res. Chem. Intermed.* 44 (2018) 5597–5621. <https://doi.org/10.1007/s11164-018-3443-8>.
- [76] R.D. Martínez-Orozco, H.C. Rosu, S.-W. Lee, V. Rodríguez-González, Understanding the adsorptive and photoactivity properties of Ag-graphene oxide nanocomposites, *J. Hazard. Mater.* 263 (2013) 52–60. <https://doi.org/https://doi.org/10.1016/j.jhazmat.2013.07.056>.
- [77] G. Gyawali, R. Adhikari, B. Joshi, T.H. Kim, V. Rodríguez-González, S.W. Lee, Sonochemical synthesis of solar-light-driven Ag²PbMoO₄ photocatalyst, *J. Hazard. Mater.* 263 (2013) 45–51. <https://doi.org/https://doi.org/10.1016/j.jhazmat.2013.03.065>.
- [78] S. Faisal, M.A. Khan, H. Jan, S.A. Shah, Abdullah, S. Shah, M. Rizwan, Wajidullah, M.T. Akbar, Redaina, Edible mushroom (*Flammulina velutipes*) as biosource for silver nanoparticles: from synthesis to diverse biomedical and environmental applications, *Nanotechnology.* 32 (2020) 65101. <https://doi.org/10.1088/1361-6528/abc2eb>.

CHAPTER 4 EXPLORATION OF GREEN SILVER NANOPARTICLES USING EUCALYPTUS LEAVES EXTRACT

Eucalyptus leaves extract (ELE) contains biomolecules that can act as surfactants, stabilizers and/or reducing agents in the synthesis of AgNP. The main goal of this chapter described in two subchapters, is to optimize and to characterize a simple and low-cost green synthesis method to prepare stable AgNP using aqueous *Eucalyptus globulus* leaves extract, a regional raw material. Subchapter 4.1 describes the results of the optimization of biosynthetic process. The green-synthesized AgNP are characterized by UV/Vis and FTIR spectroscopies, SEM-EDX, zeta potential, TGA, XRD and XPS. The specific mechanism of biosynthesis of metal nanoparticles is still to be understood and different putative mechanisms for their synthesis are proposed.

In the subchapter 4.2, the results of the antibacterial and photocatalytic behavior assessment of optimized AgNP against pathogenic bacteria and as photocatalysts for the degradation of the IC under UV light, visible light and sunlight irradiation were described. The germination of corn kernels test is used to determine the toxicity of the treated IC solutions.



This chapter was adapted from:

Rocha, V., Ferreira-Santos, P., Genisheva, Z., Coelho, E., Neves, I.C., Tavares, T., *Unveiling the environmental remediation action promoted by silver nanoparticles biosynthesized by eucalyptus leaves extract*. Journal of Water Process Engineering. <https://doi.org/10.1016/j.jwpe.2023.104431>

4.1 OPTIMIZATION AND CHARACTERIZATION OF BIOSYNTHETIC PROCESS

4.1.1 INTRODUCTION

Eucalyptus, a genus in the *Myrtaceae* family, are the world's largest cultivated and natural hardwood flora [1]. Eucalyptus leaves extract (ELE) has a high content of polyphenols, flavonoids, tannins, terpenoids and monoterpenes that contribute to strong reducing ability [2]. In the first work on the ELE-mediated synthesis of MNP, Ramezani *et al.* [3] used an extract of *Eucalyptus camaldulensis* as a reducing and capping agent for the synthesis of AuNP with size ranging from 1.25 to 17.5 nm. Until now, ELE has been used to biosynthesize different MNP such as ZnONP [4], FeNP [5], AgNP [6], CuONP [7], MgONP [8], Fe/NiNP [9] and Fe/PdNP [10] to be used in environmental remediation. Recently, ZnONP were synthesized from the leaf extract of *Eucalyptus grandis* and applied in the efficient photodegradation of tartrazine dye and as antimicrobial agent [11]. In the presence of biosynthesized FeNP by ELE, approximately 100% of Cr⁶⁺ was adsorbed [5]. Also, bimetallic Fe/NiNP biosynthesized with ELE showed a high catalytic activity in the degradation of methyl orange dye [9].

The synthesis of MNP from extracts hampered reproducibility since the composition of the extracts was susceptible to change owing to a variety of environmental factors, it becomes challenging to identify the biomolecules responsible for production of MNP. In this context, the present subchapter aims to optimize and characterize the biosynthetic process of the green synthesis of AgNP using aqueous ELE from *Eucalyptus globulus*, a raw material from Portugal. The identification of the biomolecules involved in the AgNP synthesis was performed by HPLC-MS and GC-MS.

4.1.2 MATERIALS AND METHODS

4.1.2.1 Chemicals

Silver nitrate (AgNO₃) was obtained from PanReac. Other reagents were acquired from Sigma-Aldrich and utilized as received. Ultrapure water (Milli-Q system, Millipore) with a resistivity of 18.2 MΩ cm⁻¹ was used to prepare all aqueous solutions.

4.1.2.2 Preparation of eucalyptus leaves extract

Eucalyptus leaves from *Eucalyptus globulus* were picked in Marco de Canaveses, Portugal (41°06' 17.0"N 8°09'07.0"W) in September 2021. To remove impurities adhered, the collected fresh leaves were rinsed several times with distilled water and then dried at room temperature (RT) to constant weight. Dried leaves were chopped and ground to a fine powder (≤ 1 mm), in a mechanical grinder. Dried plant powder (25 g) was subjected to a conventional solid-liquid extraction using a cylindrical reactor into a water bath with shaking (200 rpm) and extracted with 250 mL of water at 50 °C for 30 min (previously optimized in Chapter 3). Whatman filter paper No. 1 was used to filter the extract and the filtrate was stored at 4 °C for further use.

To determine the extraction yield, a glass slide was weighed and then 1000 μ l of the ELE was dropped on it, the weight of the slide and its content after evaporation (105 °C/12 h) was recorded. The yield was calculated take into account the weight of the powder sample, measured (25 g) by equation 4-1:

$$\text{Yield (\%)} = \frac{\text{Weight of aqueous extract (g)}}{\text{Weight of the powdered extract (g)}} \times 100 \quad (\text{Equation 4-1})$$

4.1.2.3 Synthesis of AgNP using eucalyptus leaves aqueous extract: Preparation and characterization

Different amounts (100 and 200 mL) of ELE (10% w/v) were added dropwise to 100 mL of 60 mM AgNO₃ with constant stirring at different temperatures (RT and 50 °C) during 1 h. The resulting colored solution of AgNP was submitted for 30 min to centrifugation at 10,000 rpm in order to be separated. The resulting precipitate was washed twice with distilled water and ethanol and then lyophilized (**Figure 4-1**).

The biosynthesized AgNP with 100 mL of ELE at RT and 50 °C were labeled as AgNP_{RT-1:1} and AgNP_{50°C-1:1}, respectively, while the biosynthesized AgNP with 200 mL of ELE at 50 °C were labeled as AgNP_{50°C-1:2}.

1:2.

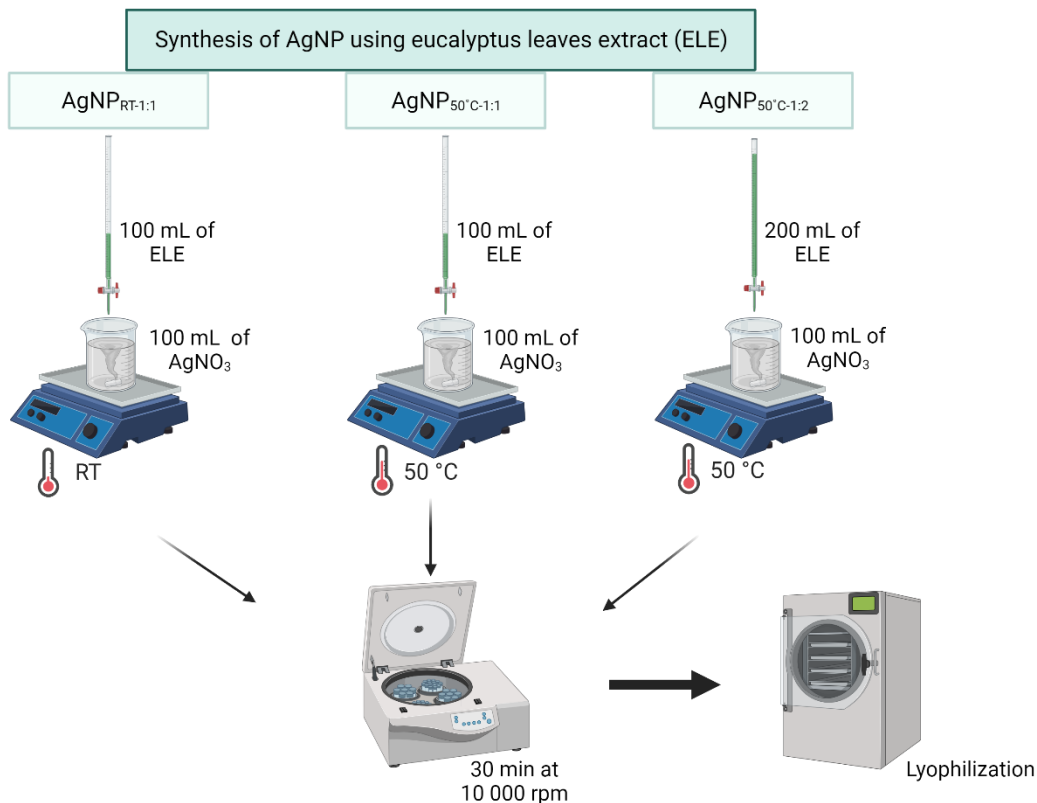


Figure 4-1. Schematic representation of the synthesis of AgNP using eucalyptus leaves extract (ELE).

The AgNP were characterized using a UV-Vis spectrophotometer, SEM-EDX, FTIR-ATR and DLS (detailed description in Chapter 3). X-ray photoelectron spectroscopy (XPS) of AgNP_{RT-1:1} and AgNP_{50°C-1:1} was made using an AXIS Supra X-ray photoelectron spectroscope (Kratos) equipped with aluminum $\text{K}\alpha$ monochromatized radiation at 1486.6 eV X-ray source, with ESCApe software. The measurement was performed in a Constant Analyzer Energy mode with a 15 mA of emission current and 160 eV pass energy for survey spectra and 40 eV pass energy for high-resolution spectra. Thermal gravimetric analysis (TGA) was done on a thermogravimetric analyzer (Perkin Elmer TGA 4000) and the samples were weighted in an alumina crucible in the equipment's scale. Analyses were performed from 25 to 800 °C at 10 °C.min⁻¹ under a nitrogen atmosphere (flow rate: 20 mL.min⁻¹). The percentage of weight loss and its derivative were shown as a function of temperature. The powdered synthesized AgNP were analyzed by X-ray diffraction (XRD) using a Bragg-Brentano diffractometer (Bruker D8 Advance DaVinci) and Cu-K α radiation 1.5406 Å over an angular range of 10 to 80°, at a 40 kV voltage and a 40 mA current.

4.1.2.4 Analytical methods for biomolecules identification

The identification of volatile compounds in the ELE carried out using gas chromatography linked with mass spectrometry (GC–MS), was made according to Coelho *et al.* [12].

The identification of the polyphenolic compounds was made by 1260 Infinity HPLC Series system (Agilent) equipped with MS/MS detector (8AB SCIEX Triple Quad 3500). Reverse-phase analytical column was used for molecule separation (Zorbax Eclipse XDB-C18, 2.1 × 100 mm, 1.8 μm). Mass spectra were recorded from 50 to 1100 m/z in negative mode. For processing the of chromatographic data a ChemStation and DataAnalysis software from Agilent were used. Water/formic acid 0.5% (v/v) (A) and acetonitrile/formic acid 0.5% (v/v) (B), were used as mobile phase. The solvent B elution gradient was as follows: from 0 min to 5 min, 2% eluent B, from 5 min to 14 min it linearly increased from 2% to 20%. Then from 14 min to 41 min it increased from 20% to 100% and at the end, the column was equilibrated at 2% for 5 min. The injection volume was 5 μL at a flow rate of 0.5 mL.min⁻¹.

The quantification of some phenolic compounds in aqueous ELE, before and after synthesis of AgNP, was performed using a Shimadzu Nexpera X2 ultra-performance liquid chromatography (UPLC) set-up, connected with Diode Array Detector (DAD) (Shimadzu, SPD-M20A), as described by Ferreira-Santos *et al.* [13]. All analyses were performed in triplicate.

4.1.3 RESULTS AND DISCUSSION

4.1.3.1 Optimization of the biosynthetic process of AgNP

The biosynthesis of AgNP is performed by reducing the Ag⁺ salt solution with the aqueous *Eucalyptus globulus* leaves extract, which was used both as a reducing and as a stabilizing agent (**Figure 4-1**). The leaves obtained from trees at Marco de Canaveses, North of Portugal, are a by-product (biowaste) of the lumber and cellulose industry. Several parameters influence the AgNP formation, such as reaction temperature and the concentration of the plant extracts [14,15]. Different temperatures (RT and 50 °C) and ratios between AgNO₃ and ELE (1:1 and 1:2) were tested. The color of the suspension progressively shifted to a dark brown, which indicated the formation of AgNP.

UV-Vis spectroscopy can be used as a useful method to recognize and characterize MNP [16]. The conduction electrons on the metal surface are set into their oscillations when MNP are exposed to light

excitation. The resonance attained between the light photons and frequencies of surface electron oscillations is localized surface plasmon resonance (SPR). The green AgNP were analyzed in the wavelength range from 350 to 700 nm by UV-Vis. An individual spectral fingerprint for a plasmonic NP with a specific shape and size is produced by the wavelength for maximum absorption (λ_{max}) and band width [17]. **Figure 4-2A** shows the optical spectra of AgNP, 1 h after the addition of the ELE at different synthesis conditions.

It can be seen in **Figure 4-2A** that both AgNP obtained at 50 °C presents the characteristic SPR, with a λ_{max} at 458 and 464 nm for AgNP_{50°C-1:1} and AgNP_{50°C-1:2}, respectively. These results confirm in a first approach, the successful synthesis of AgNP [18]. The broad peaks were also observed, indicating a broad size distribution. Similar results were obtained by other authors [16,19]. On the other hand, AgNP obtained at RT, AgNP_{RT-1:1}, do not show the characteristic SPR. Vimala *et al.* [20] studied the effect of reaction temperature on the synthesis of AgNP using *Couroupita guianensis* and showed that no AgNP could be formed under 37 °C during 60 min. Increasing the reaction temperature, the reduction rate also increases and, the majority of Ag ions are consumed during the formation of nuclei, blocking the secondary reduction process on the surface of the produced nuclei [21]. Several publications claim to have successfully synthesized green AgNP at RT, but the incubation time is always longer than 1 h [16,19].

It is not possible to observe the AgNP formed at RT from the SEM analyses (**Figure 4-2C**). This is in concordance with the obtained UV-Vis absorption spectra (**Figure 4-2A**). Nevertheless, the synthesis at 50 °C showed the formation of AgNP with different shapes and sizes. With a low amount of extract (AgNP_{50°C-1:1}), the particles are irregularly shaped with a size distribution ranging from 42.9 to 142.9 nm (**Figure 4-2D**). While, the higher amount of extract (AgNP_{50°C-1:2}) results in the formation of particles with more defined shapes, mostly spherical and the size distribution was in the range 58.0 to 101.4 nm (**Figure 4-2E**). The calculated average particle size (average of 25 particles) suggests that the AgNP_{50°C-1:1} have the largest one (84.1 ± 26.5 nm) and AgNP_{50°C-1:2} have the smallest one (73.6 ± 10.9 nm). Due to their high surface energy, AgNP have a propensity to aggregate [14], so rapid nucleation in a short period of time is necessary to obtain monodispersed AgNP and for that, almost all ionic species have to be reduced rapidly and simultaneously to metallic species, followed by conversion to stable nuclei to be grown [22]. Zayed and Eisa [22] showed the influence of the concentration of extract in the biosynthesis of AuNP. The authors concluded that whereas faster nucleation produced

monodisperse and smaller particles at the highest extract concentration, slower nucleation produced larger particles at the smallest extract volume, most likely as a result of a slower nucleation rate. Also, Baruah *et al.* [15] concluded that at high concentration of extract, sufficient reducing and capping agents become available which stabilize the growing nuclei and prevent the aggregation of particles. Pinto *et al.* [23] investigated the impact of different parameters on the morphology and size of AuNP and concluded that the concentration of extract plays a significant role.

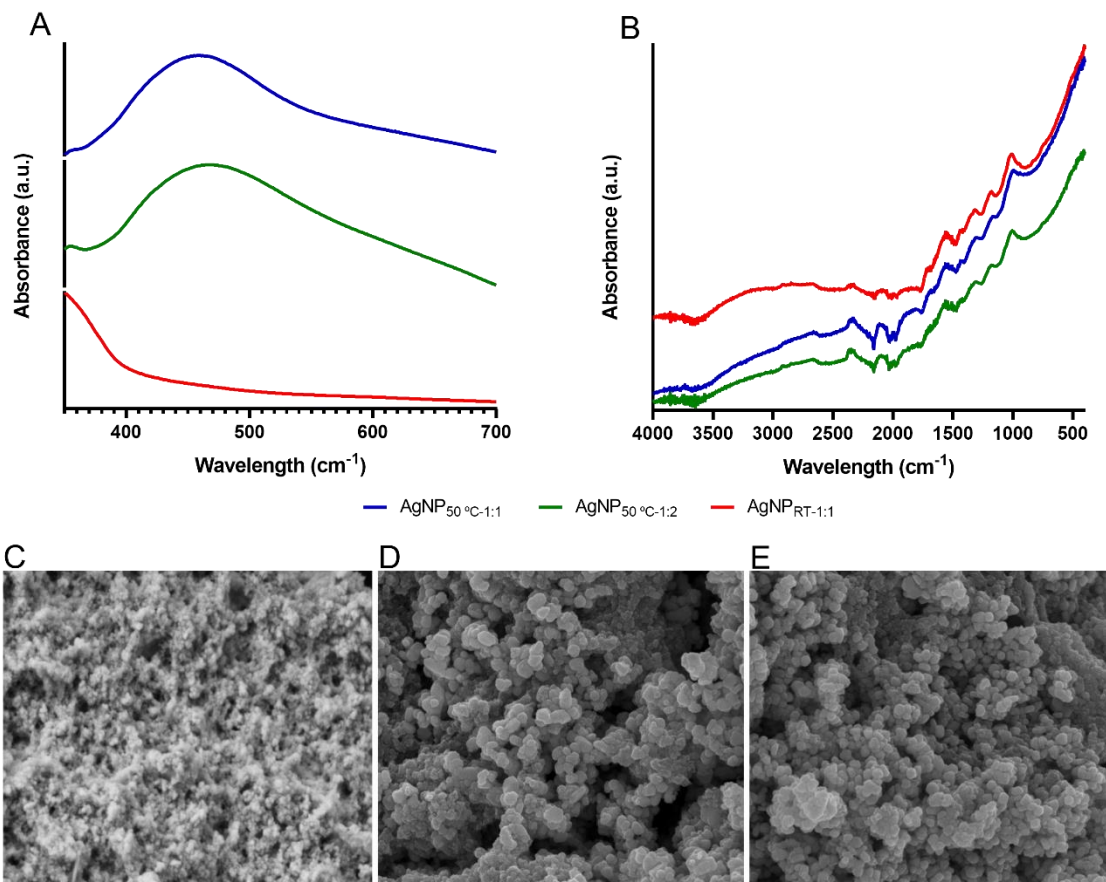


Figure 4-2. Evaluation of (A) optical properties by UV-Vis, (B) functional structure by FTIR and (C-E) surface morphology and texture by SEM of AgNP biosynthesized with eucalyptus leaves extract (ELE) at different synthesis conditions: (C) AgNP_{RT-1:1} at 30.00 k x magnification, (D) AgNP_{50°C-1:1} at 100 000 x magnification and (E) AgNP_{50°C-1:2} at 100 000 x magnification.

FTIR analysis intend to reveal the structural differences between AgNP obtained at different synthesis conditions. **Figure 4-2B** shows the representative spectra and clearly proves that no

differences result from those conditions of biosynthesis. The stretching vibration of the NH functional groups of the primary and secondary amines of amino acids, proteins and peptides is related with the large band at $2800\text{-}3500\text{ cm}^{-1}$ [24]. Additionally, the hydroxyl compounds (OH) stretching vibration in aliphatic and phenolic structures are ascribed to this band [25]. The bands observed at 1721 cm^{-1} and 1612 cm^{-1} correspond to C=O functional group of carboxylic acid and C=C stretching vibrations of an aromatic alkene, respectively. Primary and secondary amides with NH functional groups is related of the band at 1515 cm^{-1} [26]. The band at 1449 cm^{-1} is assigned to the C-H functional group of alkanes and the absorption bands in the region of $1357\text{-}1044\text{ cm}^{-1}$ represent the stretching of the C-O functional group of alcohols, carboxylic acids, esters and anhydrides [27]. The bands in the region of $922\text{-}608\text{ cm}^{-1}$ usually indicates the presence of out-of-plane C-H bending vibrations in alkenes and aromatics [28]. The presence of these bands confirms that the AgNP is coated by phytochemicals from the ELE.

The surface composition, the relative distribution of elements and their oxidation state that are present on the surface of the $\text{AgNP}_{\text{RT}:1:1}$ and $\text{AgNP}_{50^\circ\text{C}:1:1}$ were assessed by X-ray photoelectron spectroscopy (XPS) measurements. Both samples revealed the presence of oxygen, carbon, nitrogen and chloride in their survey XPS resolution spectra, as well as silver in the region of Ag 3d (**Figure 4-3**).

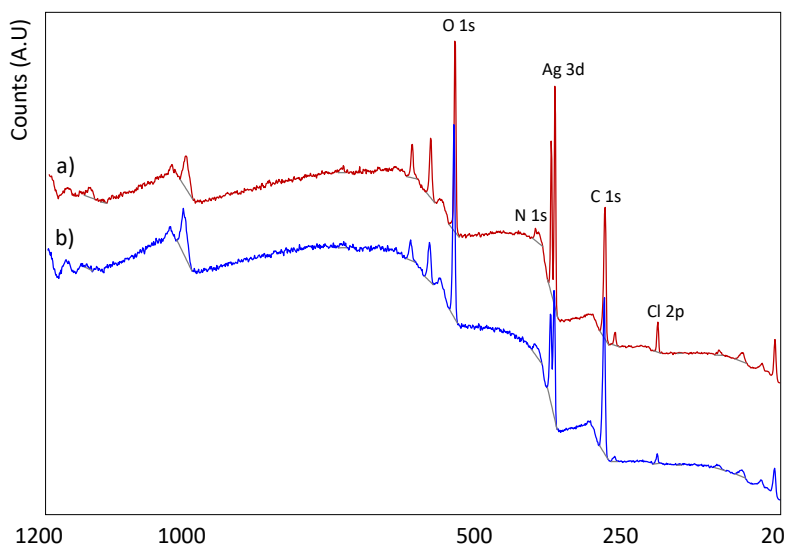


Figure 4-3. Survey XPS spectra of (A) $\text{AgNP}_{\text{RT}:1:1}$ and (B) $\text{AgNP}_{50^\circ\text{C}:1:1}$.

The binding energies (BE) of the elements as well as their amount (wt%) present on the surface, identified by XPS for both samples are shown in **Table 4-1**.

Table 4-1. Binding energies (BE) and the amount of the elements (wt%) from the XPS resolution spectra in the C 1s, O 1s, Cl 2p, N 1s and Ag 3d regions of the samples.

Sample		C 1s	O 1s	Cl 2p	N 1s	Ag 3d
AgNP _{RT-1:1}	BE (eV)	285.04	533.44	198.54	400.64	368.44
	wt%	39.82	20.02	5.82	2.34	32.00
AgNP _{50°C-1:1}	BE (eV)	286.40	533.80	198.50	400.30	368.90
	wt%	52.07	24.28	1.97	2.19	19.48

The values of the BE of the elements are similar between both samples, but the percentage of the elements are different, especially in the case of C 1s, Cl 2p and Ag 3d. The increase of the temperature in the preparation of AgNP affects the quantity of these elements on the surface. For AgNP_{50°C-1:1}, the amount of carbon increases and the amount of chlorine and silver decreases, in comparison with the sample produced at RT. The higher amounts of carbon and oxygen are due to the biomolecules such as phenolic acids, flavones, flavonoids and others from ELE. These findings suggest that elevated temperatures promote reactions among the biomolecule-derived compounds, leading to the formation of more complex structures. Moreover, the elements detected by the photoelectron peaks Cl 2p and N 1s can be attributed to compounds derived from biomolecules.

The main carbon peak occurred at 285.04 and 286.40 eV for AgNP_{RT-1:1} and AgNP_{50°C-1:1}, respectively. For both samples, a deconvolution of the C 1s peak revealed that carbon is present mainly as C-C, C-H, C-O and O=C-O groups from the biomolecules compounds, in accordance with the FTIR analysis. The O 1s peak was measured at 533.44 and 533.80 eV for AgNP_{RT-1:1} and AgNP_{50°C-1:1}, respectively and the deconvolution revealed that the oxygen atoms are linked to the C present in the biomolecules (**Figure 4-4A** and **B**).

Silver peak is measured at 368.44 and 368.90 eV for AgNP_{RT-1:1} and AgNP_{50°C-1:1}, respectively. In addition, silver amounts at the surface of each sample are different, with a decrease of Ag in the sample AgNP_{50°C-1:1} (**Table 4-1**).

The deconvolution of Ag 3d peak (**Figure 4-4C** and **D**) shows four peaks at the same BE for both samples, with an intense doublet corresponding to peak positions at 368.2 and 374.2 eV, for Ag 3d_{5/2} and Ag 3d_{3/2}, respectively, with energy separations ($E\Delta$) of 6 eV, typical of metallic silver. The other BE peaks located at 369.5 eV (Ag 3d_{5/2}) and 375.4 eV (Ag 3d_{3/2}) correspond to different silver species [29,30].

In order to identify the different silver species, the Auger spectra (**Figure 4-4E** and **F**) were obtained for both samples, since the peak of Ag 3d_{5/2} displays two BE values at 368.2 eV and 369.5 eV, being difficult to distinguish the different chemical states due to the small chemical shift of the silver BE [31]. The Auger spectra obtained for both samples are similar between them, with a complex form related to the Ag MNN regions with peaks assigned at different kinetic energy values. The sample AgNP_{50°C:1:1} shows the same six peaks at lower values of kinetic energy compared to AgNP_{RT:1:1}, with a contribution of different silver species. The presence of these species was defined by the Auger Parameter (AP) using BE (Ag 3d_{5/2}) + KE (Ag MNN), where BE is the binding energy of Ag 3d_{5/2} peak (eV) and Ag MNN (KE) is the Auger kinetic energy [31]. **Table 4-2** shows the values of kinetic energies, AP and the contribution of each silver species for both samples, according to the identification based on [30,32].

Different silver species were so identified as Ag, Ag⁺, AgO and Ag₂O and they are dependent on the temperature used in the preparation of the AgNP. For the sample AgNP_{RT:1:1}, Ag⁺ species is dominant with 64.3% contribution, suggesting that the reduction of silver is not completed at this temperature, followed by 20.2% of metallic Ag and 15.5% of AgO. The increase in temperature changes the oxidation state of the same silver species and the presence of the silver oxide is improved with 38.2% of AgO and Ag₂O, followed by only 19.3% of Ag⁺ and 42.6% of Ag. At 50 °C, the silver reduction occurs and this indicates that increasing the amount of extract in the synthesis of AgNP at 50 °C can be sufficient to reduce the Ag⁺ ions.

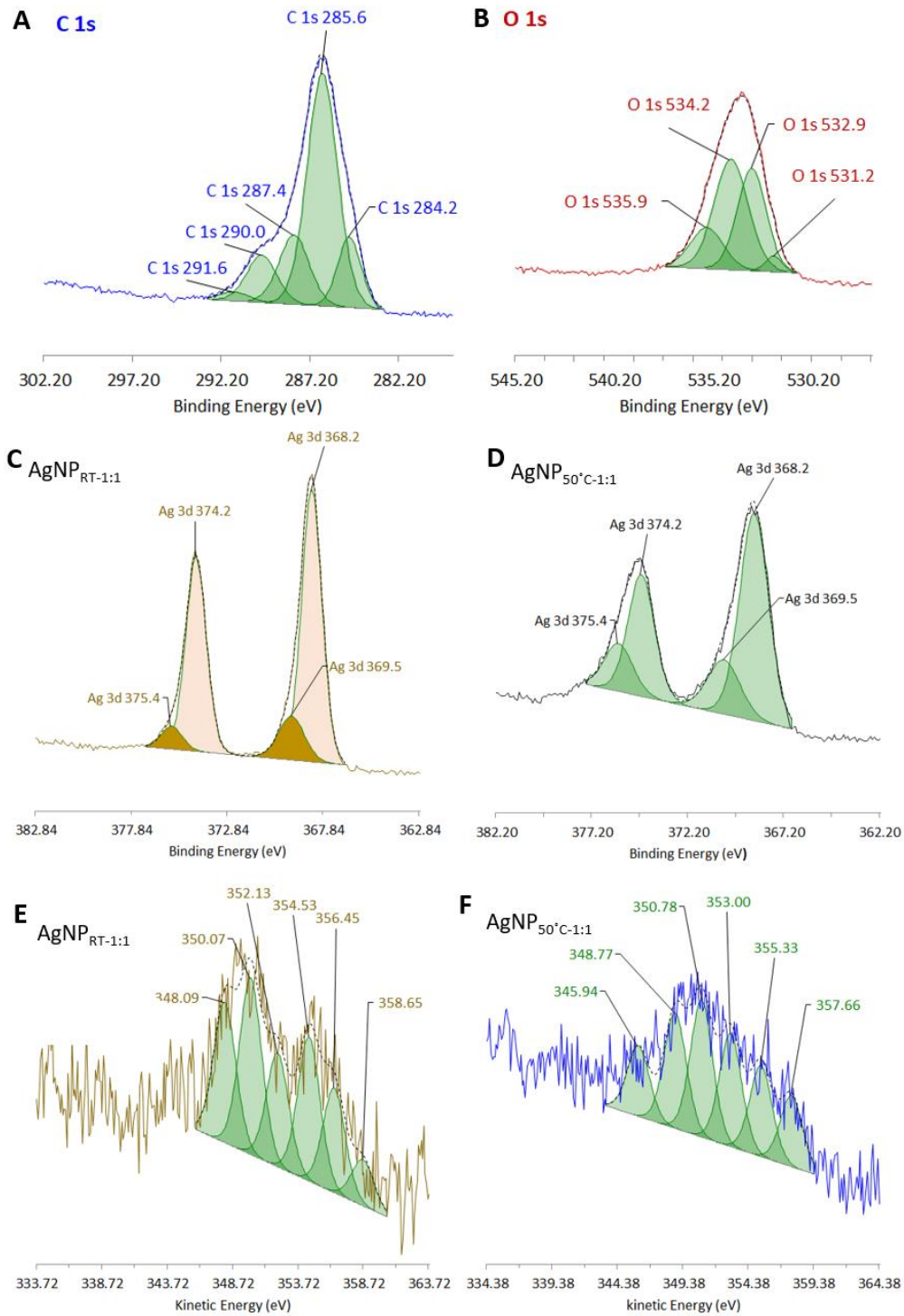


Figure 4-4. High resolution XPS spectra of (A) C 1s and (B) O 1s from AgNP_{50°C:1:1}. High resolution XPS spectra of Ag 3d region for (C) AgNP_{RT-1:1} and (D) AgNP_{50°C-1:1} and Auger spectra for (E) AgNP_{RT-1:1} and (F) AgNP_{50°C-1:1}.

Table 4-2. Kinetic energies (KE), Auger Parameter (AP) and the contribution of the silver species in the Ag 3d region of the samples.

Sample		AgNP_{RT-1:1}		
KE (eV)	AP	Contribution (%)	Silver species	
356.64	724.84	15.53	AgO	
354.11	722.31	17.35	Ag ⁺	
351.15	719.35	23.69	Ag ⁺	
348.78	716.98	23.21	Ag ⁺	
359.87	728.07	7.59	Ag	
345.99	714.19	12.63	Ag	

Sample		AgNP_{50°C-1:1}		
KE (eV)	AP	Contribution (%)	Silver species	
355.33	723.53	15.27	AgO	
353.00	721.20	18.90	Ag	
350.78	718.98	22.88	Ag ₂ O	
348.77	716.97	19.30	Ag ⁺	
357.66	725.86	23.10	Ag	
345.94	714.14	0.55	Ag	

The thermal degradation of the AgNP_{50°C-1:1} and AgNP_{50°C-1:2} was evaluated in order to understand the select effect of the amount of extract on the synthesis of AgNP (**Figure 4-5A e B**).

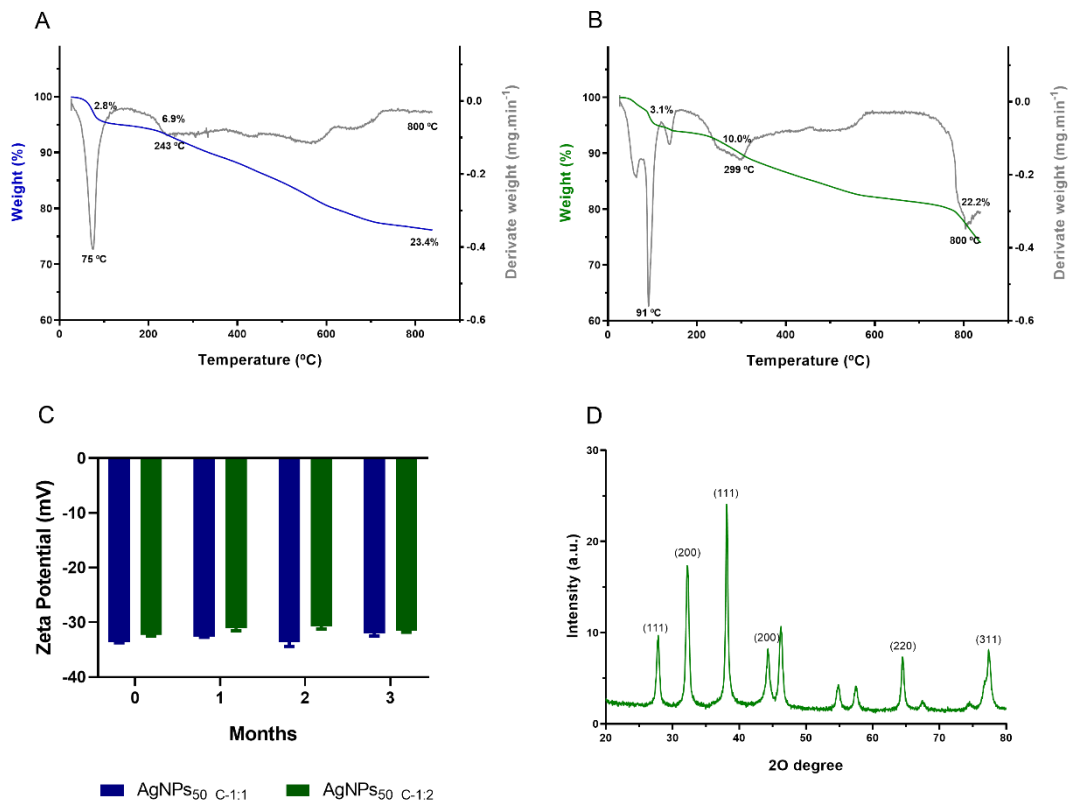


Figure 4-5. Thermogravimetric analysis of (A) AgNP_{50°C:1.1} and (B) AgNP_{50°C:1.2}; (C) Zeta potential evaluation during 3 months and (D) XRD pattern exhibiting the fcc structure of AgNP_{50°C:1.2}.

The first thermal event which occurred at temperatures of up to 75 °C and 91 °C showed 2.8% and 3.1% loss in weight of AgNP_{50°C:1.1} and AgNP_{50°C:1.2}, respectively. These weight losses are attributed to the loss of water that has been adsorbed, as well as the loss of volatile substances in the extract, demonstrating that these substances exist and serve as biosurfactants for the AgNP [8,33]. The second weight losses (approximately 7% and 10%), which occurred at 243 °C and 299 °C, were a result of the thermal degradation of bioactive molecules containing carbon found on the surface of AgNP [33]. The weight loss observed between 300 °C and 800 °C may be due to the thermal degradation of phytoconstituents present on the AgNP, including the degradation of resistant aromatic compounds and the release of oxygen molecules present on the surface of the particles [34,35]. Finally, transitions were observed at above 800 °C for AgNP_{50°C:1.2} and is close to the melting point of silver (961.78 °C). Thermal stability of AgNP_{50°C:1.1} and AgNP_{50°C:1.2} showed a weight loss less than 24% and 22%, respectively,

up to 800 °C. These results suggest that the amount of extract to biosynthesize AgNP does not influence their thermal properties.

Zeta potential determinations allow estimation of the surface charge, which can be used to assess the physical stability of MNP [36]. A large positive or negative value of the zeta potential points out a good physical stability of the nanoparticles, due to the electrostatic repulsion between them. The zeta potential of the green AgNP determined in water as a dispersant was evaluated for 3 months and the results are shown in **Figure 4-5C**, with the initial zeta potential values of -33.6 ± 0.2 mV and -32.3 ± 0.2 mV for AgNP_{50°C-1:1} and AgNP_{50°C-1:2}, respectively. These values indicate that AgNP have a negatively charged surface, which implies strong repellent forces among the particles leading to aggregation prevention and stabilization of the AgNP in the medium. After 3 months, zeta potential values of -32.0 ± 0.5 mV and -31.5 ± 0.3 mV for AgNP_{50°C-1:1} and AgNP_{50°C-1:2}, respectively, and proved that the NP were stable.

XRD analysis is a common technique used to investigate the crystal structure and size of MNP [1]. The XRD patterns of AgNP_{50°C-1:2} were recorded from 20° to 80° as shown in **Figure 4-5D**. The presence of the four distinct thin and narrow diffraction peaks in the XRD pattern indicates that synthesized AgNP are crystalline. These peaks at 38.10°, 44.29°, 64.44° and 77.38° are assigned to (1 1 1), (2 0 0), (2 2 0) and (3 1 1) *hkl* planes of face-centered cubic of AgNP_{50°C-1:2}, in agreement with other works (ICCD 00-001-1167 and JCPDS File N°:03-0921) [37,38]. Peaks at 27.84° and 32.19° are assigned to reflection planes of AgCl nanoparticles (ICCD 00-006-1480 and JCPDS File N°:00-031-1238) [39]. The other crystalline peaks (46.24° and 57.46°) are also observed and are due to the presence of organic compounds in the extracts [37,40,41].

The crystallinity of the biosynthesized AgNP is 83.26% and was calculated using the equation 4.2:

$$\text{Crystallinity (\%)} = \frac{\text{Area of crystalline peaks}}{\text{Area of all peaks (crystalline+amorphous)}} \quad (\text{Equation 4-2})$$

The average crystallite size of the synthesized NP was calculated using the Debye-Scherrer formula, equation 4.3:

$$D = \frac{K\lambda}{\beta_D \cos\theta} \quad (\text{Equation 4-3})$$

where K is the Scherrer constant (0.94), λ is the X-ray wavelength (1.5421 Å), $\beta_D = \sqrt{\beta_m^2 - \beta_\alpha^2}$ where β_m is the width of the XRD peak at half-height (FWHM) and β_α is a constant determined from the instrument broadening (2.74×10^{-3} rad) and θ is the Bragg angle [19]. From the Scherrer equation, the average crystallite size of AgNP_{50°C:1.2} is found to be 25.42 nm.

4.1.3.2 Identification of biomolecules in eucalyptus leaves extract

Eucalyptus globulus leaves extract was previously characterized chemically and selected as a promising candidate for the biosynthesis of AgNP in Chapter 3. ELE has been increasingly recognized as a rich source of bioactive molecules for the successful production of different NP [11,16,41]. In this work, the extraction yield was 18.4(± 0.1)% and similar results were obtained by Hassine *et al.* [42].

The biomolecules in the ELE were identified by different analytical techniques. It was possible to identify seventeen volatile compounds by GC-MS analysis of the aqueous ELE (**Figure 4-6** and

Table 4-3).

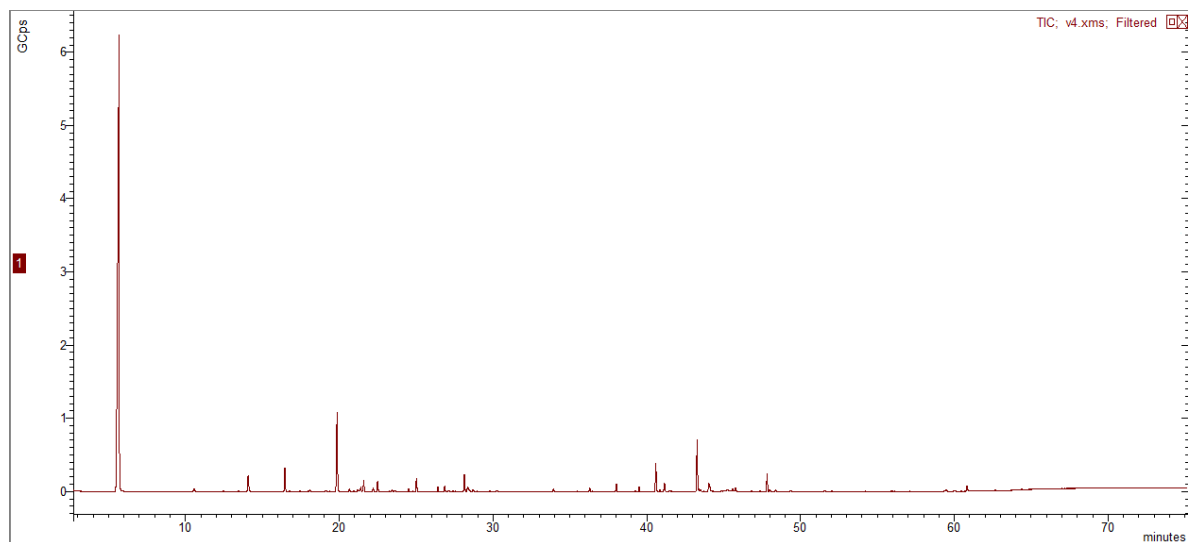


Figure 4-6. GC-MS chromatogram of aqueous eucalyptus leaves extract (ELE).

Table 4-3. Identification of the volatile compounds present in aqueous extract of eucalyptus leaves (ELE).

Peak	Rt (min)	Compound	Composition of the extract (%)	Research on compounds identification
1	5.690	1,8-cineole (eucalyptol)	72.30±0.92	[42,43,52,53,44–51]
2	9.071	6-methyl-5-hepten-2-one	<1	n.r.
3	10.562	(<i>Z</i>)-3-hexenol	<1	n.r.
4	12.475	<i>cis</i> -linalool furanic oxide	<1	n.r.
5	13.463	<i>trans</i> -linalool furanic oxide	<1	[50]
6	16.470	pinocarvone	2.14±0.08	[47,49,50]
7	17.456	fenchol	<1	[46,47,50]
8	17.977	caryophyllene	<1	[46,49,50,54,55]
9	18.100	terpinen-4-ol	<1	[46,49,51,52,55]
10	19.864	pinocarveol	7.85±0.20	[48,50,51,53]
11	21.594	α -terpineol	1.16±0.02	[5,44–46,49,50,52,55]
12	24.784	myrtenol	<1	[47,51,55]
13	25.025	<i>trans-p</i> -mentha-1(7),8-dien-2-ol	1.19±0.02	[45,50]
14	26.414	carveol	<1	[5]
15	26.863	<i>p</i> -cymen-8-ol	<1	[50]
16	28.142	<i>cis-p</i> -mentha-1(7),8-dien-2-ol	1.59±0.02	[45,50]
17	28.706	2-phenylethanol	<1	n.r.
18	33.936	ledol	<1	[43,46,50]

Retention time (Rt)

Most of the volatile compounds identified in the extract of these eucalyptus leaves were also described as constituents of other ELE. The major constituents of the *Eucalyptus globulus* leaves extract were 1,8-cineole or eucalyptol (72.3%), followed by pinocarveol (7.9%) and pinocarvone (2.1%). The concentration of other volatile compounds in such extract was less than 2% (**Table 4-4**).

Table 4-4. Concentration of volatile compounds identified by GC-MS.

Peak	Rt ^a (min)	Compound	Concentration (mg.L ⁻¹)
1	5.690	1,8-cineole (eucalyptol)	70.72±2.19
2	9.071	6-methyl-5-hepten-2-one	0.06±0.03
3	10.562	(<i>±</i>)-3-hexenol	0.42±0.00
4	12.475	<i>cis</i> -linalool furanic oxide	0.13±0.00
5	13.463	<i>trans</i> -linalool furanic oxide	0.09±0.00
6	16.470	pinocarvone	2.10±0.17
7	17.456	fenchol	0.08±0.00
8	17.977	caryophyllene	0.08±0.00
9	18.100	terpinen-4-ol	0.21±0.00
10	19.864	pinocarveol	7.69±0.54
11	21.594	α -terpineol	1.14±0.03
12	24.784	myrtenol	0.09±0.01
13	25.025	<i>trans-p</i> -mentha-1(7),8-dien-2-ol	1.17±0.07
14	26.414	carveol	0.47±0.03
15	26.863	<i>p</i> -cymen-8-ol	0.48±0.01
16	28.142	<i>cis-p</i> -mentha-1(7),8-dien-2-ol	1.56±0.09
17	28.706	2-phenylethanol	0.26±0.02
18	33.936	ledol	0.25±0.08

Retention time (Rt)

The compound 1,8-cineole was the most abundant, which is in good agreement with data reported by other studies [43,48,49]. Previous reports have shown the significance of these biomolecules in the synthesis of AgNP [17,56]. It was defended that sesquiterpenoids and monoterpenoids are the key donors for the synthesis of AgNP [57]. Wang *et al.* [45] identified the biomolecules of ELE involved in the formation of iron nanoparticles/reduced graphene oxide composites. The authors concluded that biomolecules such as 1,8-cineole, *trans-p*-mentha-1(7), α -terpineol, 8-dien-2-ol and *cis-p*-mentha-1(7), 8-dien-2-ol, due to their specific functional groups, hydroxyl (-OH) and carbonyl (-C=O), acted as

reducing agents. Liu *et al.* [5] also identified specific biomolecules involved in the synthesis of iron nanoparticles, such as carveol, as reducing agent and α -terpineol as capping agent. Ali *et al.* [52] demonstrated that terpenoids such as terpinen-4-ol and 1,8-cineole are involved in the formation of copper oxide nanoparticles. Based on these findings, it is forwarded that compounds such as (1) 1,8-cineol, (9) terpinen-4-ol, (10) α -terpineol, (13) *trans-p*-mentha-1(7), 8-dien-2-ol, (14) carveol and (16) *cis-p*-mentha-1(7) are identified in literature as biomolecules in ELE that may contribute for the biosynthesis of MNP.

The phenolic profile of eucalyptus leaves obtained after aqueous extraction (**Figure 4-7**) and the respective chemical identification are presented in **Table 4-5**. Fragmentation profiles were compared to the mass spectrometry database and literature, to identify the compounds. Twelve phenolic compounds were detected, including flavonoids and phenolic acids. Some phenolic compounds of the ELE before and after synthesis of AgNP_{50°C-12} were quantified by HPLC with UV detection and are expressed in mg.L⁻¹ (**Table 4-5**).

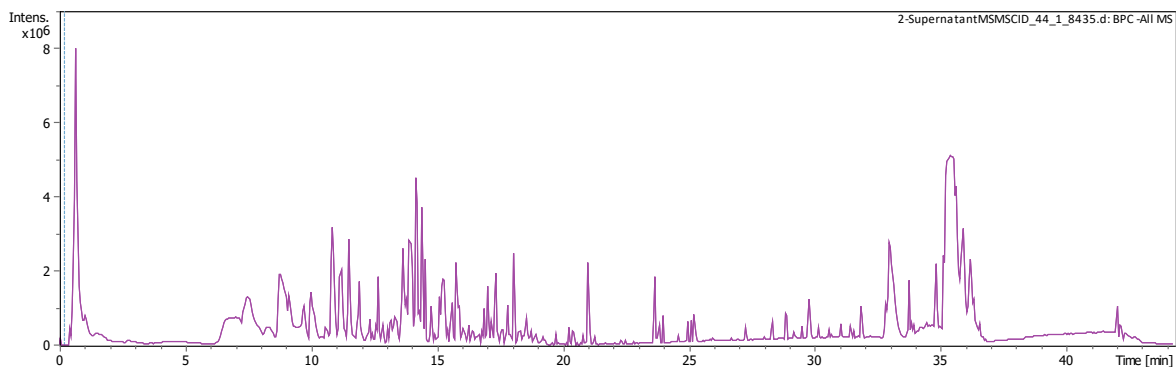


Figure 4-7. Phenolic profile of eucalyptus leaves obtained after aqueous extraction by HPLC-MS.

Table 4-5. HPLC-MS fragmentation profile and abundance of phenolic compounds identified in eucalyptus leaves extract (ELE) before and after AgNP synthesis.

Peak no.	Rt ^a (min)	[M-H] [m/z]	MSn product ions [m/z]	Compound	Quantification of phenolic compounds in eucalyptus leaves extract (ELE) [mg.L ⁻¹]		Research on compounds identification
					Before AgNP synthesis	After AgNP synthesis	
1	7.49	191	173, 111, 87, 85	quinic acid	-	-	[55]
2	8.33	353	191	chlorogenic acid	-	-	[55,58–62]
3	9.23	289	245, 205, 203, 125, 109	catechin	232.6±12.4	172.2±10.7	[61]
4	12.4	635	483, 465, 313, 211, 169	trigalloyl-glucoside	-	-	[63,64]
5	13.73	301	229, 185, 173, 157, 146	ellagic acid	250.1±3.6	209.0±2.2	[55,58,62,64]
6	13.83	610	301	rutin (quercetin-3-O-rutinoside)	266.3±3.5	239.8±1.8	[59,60]
7	13.93	169	125	gallic acid	165.7±2.1	79.6±0.8	[55,58,61,62,64,65]
8	14.65	433	243, 271, 300	quercetin 3-arabinoside	-	-	[55]
9	15.36	463	151, 179, 301	spiraeoside	-	-	n.r.
10	17.36	301	179, 165, 151, 121, 107	quercetin	2.4±0.2	2.100±0.003	[59,65]
11	18.64	395	305, 275, 247	8-glucosyl-5,7-dihydroxy-2-(1-methylpropyl)chromone	-	-	n.r.
12	18.69	285	-	kaempferol	17.2±1.0	11.9±0.8	[55,58]

Retention time (Rt); not reported (n.r.)

After synthesis of AgNP_{50°C, 12}, the amount of the compounds 3 (catechin), 5 (ellagic acid), 6 (rutin), 7 (gallic acid), 10 (quercetin) and 12 (kaempferol) decreased and this decline was more accentuated for gallic acid, kaempferol and catechin, with a reduction of 51, 31 and 26%, respectively. These compounds can be used as reducing and/or capping agents in the reaction as stated in current works on gallic acid metal-reducing potential [38,66,67]. Santos *et al.* [38] observed that the concentration of gallic acid diminished after the synthesis of AgNP with eucalyptus bark extract and concluded that phenolic compounds, in particular derivatives of gallic acid, are mainly responsible for the metal-ion reduction. It is forwarded that AgNP may be synthesized upon the development of a transitory complex between Ag⁺ ions and the phenolic hydroxyl groups of the gallic acid. Subsequently, through the oxidation process, it changes to quinone that generates AgNP [66,67]. Other previous studies have shown that kaempferol [68] and quercetin [68,69] were able to reduce metal ions such as Ag⁺. Based on the similarities between the AgNP synthesized using *Ocimum sanctum* leaves extract and pure quercetin in terms of optical, morphological and antibacterial properties, quercetin would be the main involved for the reduction of Ag⁺ ions [69]. Pradeep *et al.* [68] performed a systematic study to unveil the mechanism of synthesis of AgNP using extract of *Hypericum perforatum* and concluded that flavonoids and phenolic acids are involved in the reduction of Ag⁺ ions, phloroglucinols and xanthenes act as capping agents and naphthodianthrones were responsible in both steps. Ghoreishi *et al.* [70] indicated that the –OH group of flavonoids (myricetin and quercetin) can be oxidized to carbonyl groups (–C=O) during the bioreduction of metal ions.

The mechanism of biological nanoparticle synthesis needs to be clarified through more detailed studies [68].

4.1.4 CONCLUSIONS

Natural resources have created numerous opportunities for the green synthesis of MNP. Leaves from *Eucalyptus globulus*, a raw plant in Portugal are inexpensive, locally available, abundant and eco-friendly. These ELE revealed to be an excellent resource for the synthesis of stable AgNP with a significant impact on the environment by reducing waste and producing benefits for the MNP. The reaction temperature and concentration of the ELE affected the AgNP synthesis and the best results

were obtained at 50 °C and a ratio 1:2. AgNP_{50°C1:2} showed a spherical shape with high stability and a pure crystalline nature with an average crystallite size of 25.42 nm. Biomolecules identified as being in ELE as catechin, ellagic acid, rutin, gallic acid, quercetin and kaempferol were used as reducing and/or capping agents in the synthesis of AgNP.

4.1.5 REFERENCES

- [1] H. Sawalha, R. Abiri, R. Sanusi, N.A. Shaharuddin, A.A. Noor, N.A. Ab Shukor, H. Abdul-Hamid, S.A. Ahmad, Toward a Better Understanding of Metal Nanoparticles, a Novel Strategy from Eucalyptus Plants, *Plants*. 10 (2021). <https://doi.org/10.3390/plants10050929>.
- [2] A.K. Chauhan, N. Kataria, V.K. Garg, Green fabrication of ZnO nanoparticles using Eucalyptus spp. leaves extract and their application in wastewater remediation, *Chemosphere*. 247 (2020) 125803. <https://doi.org/https://doi.org/10.1016/j.chemosphere.2019.125803>.
- [3] N. Ramezani, Z. Ehsanfar, F. Shamsa, G. Amin, H.R. Shahverdi, H.R.M. Esfahani, A. Shamsaie, R.D. Bazaz, A.R. Shahverdi, Screening of Medicinal Plant Methanol Extracts for the Synthesis of Gold Nanoparticles by Their Reducing Potential, 63 (2008) 903–908. <https://doi.org/doi:10.1515/znb-2008-0715>.
- [4] B. Siripireddy, B.K. Mandal, Facile green synthesis of zinc oxide nanoparticles by Eucalyptus globulus and their photocatalytic and antioxidant activity, *Adv. Powder Technol.* 28 (2017) 785–797. <https://doi.org/https://doi.org/10.1016/j.appt.2016.11.026>.
- [5] Y. Liu, X. Jin, Z. Chen, The formation of iron nanoparticles by Eucalyptus leaf extract and used to remove Cr(VI), *Sci. Total Environ.* 627 (2018) 470–479. <https://doi.org/https://doi.org/10.1016/j.scitotenv.2018.01.241>.
- [6] M. Rabeea, M. Owaid, R. Muslim, Synthesis and characterization of silver nanoparticles by natural organic compounds extracted from Eucalyptus leaves and their role in the catalytic degradation of methylene blue dye, *Songklanakarin J. Sci. Technol.* 43 (2021) 14–23. <https://doi.org/10.14456/sjst-psu.2021.3>.
- [7] M. Hafeez, A. Ghazal, J. Khan, P. Ahmad, M.U. Khandaker, H. Osman, S. Alamri, Eucalyptus globulus Extract-Assisted Fabrication of Copper Oxide/Zinc Oxide Nanocomposite for Photocatalytic Applications, *Crystals*. 12 (2022). <https://doi.org/10.3390/cryst12081153>.
- [8] A.K. Chauhan, N. Kataria, R. Gupta, V.K. Garg, Biogenic fabrication of ZnO@EC and MgO@EC using Eucalyptus leaf extract for the removal of hexavalent chromium Cr(VI) ions from water, *Environ. Sci. Pollut. Res.* (2023). <https://doi.org/10.1007/s11356-022-24967-6>.
- [9] X. Weng, M. Guo, F. Luo, Z. Chen, One-step green synthesis of bimetallic Fe/Ni nanoparticles by eucalyptus leaf extract: Biomolecules identification, characterization and catalytic activity, *Chem. Eng. J.* 308 (2017) 904–911. <https://doi.org/https://doi.org/10.1016/j.cej.2016.09.134>.
- [10] Y. Lin, X. Jin, N.I. Khan, G. Owens, Z. Chen, Efficient removal of As (III) by calcined green synthesized bimetallic Fe/Pd nanoparticles based on adsorption and oxidation, *J. Clean. Prod.* 286 (2021) 124987. <https://doi.org/https://doi.org/10.1016/j.jclepro.2020.124987>.
- [11] R.D. Wouters, P.C.L. Muraro, D.M. Druzian, A.R. Viana, E. de Oliveira Pinto, J.K.L. da Silva, B.S. Vizzotto, Y.P.M. Ruiz, A. Galembeck, G. Pavoski, D.C.R. Espinosa, W.L. da Silva, Zinc oxide nanoparticles: Biosynthesis, characterization, biological activity and photocatalytic degradation

- for tartrazine yellow dye, *J. Mol. Liq.* 371 (2023) 121090. <https://doi.org/https://doi.org/10.1016/j.molliq.2022.121090>.
- [12] E. Coelho, M. Lemos, Z. Genisheva, L. Domingues, M. Vilanova, J.M. Oliveira, Validation of a LLME/GC-MS Methodology for Quantification of Volatile Compounds in Fermented Beverages, *Molecules*. 25 (2020). <https://doi.org/10.3390/molecules25030621>.
- [13] P. Ferreira-Santos, R. Nunes, F. De Biasio, G. Spigno, D. Gorgoglione, J.A. Teixeira, C.M.R. Rocha, Influence of thermal and electrical effects of ohmic heating on C-phycocyanin properties and biocompounds recovery from *Spirulina platensis*, *LWT*. 128 (2020) 109491. <https://doi.org/https://doi.org/10.1016/j.lwt.2020.109491>.
- [14] C.V. Restrepo, C.C. Villa, Synthesis of silver nanoparticles, influence of capping agents, and dependence on size and shape: A review, *Environ. Nanotechnology, Monit. Manag.* 15 (2021) 100428. <https://doi.org/https://doi.org/10.1016/j.enmm.2021.100428>.
- [15] D. Baruah, M. Goswami, R.N.S. Yadav, A. Yadav, A.M. Das, Biogenic synthesis of gold nanoparticles and their application in photocatalytic degradation of toxic dyes, *J. Photochem. Photobiol. B Biol.* 186 (2018) 51–58. <https://doi.org/https://doi.org/10.1016/j.jphotobiol.2018.07.002>.
- [16] M.S. Kiran, V.S. Betageri, C.R.R. Kumar, S.P. Vinay, M.S. Latha, In-Vitro Antibacterial, Antioxidant and Cytotoxic Potential of Silver Nanoparticles Synthesized Using Novel *Eucalyptus tereticornis* Leaves Extract, *J. Inorg. Organomet. Polym. Mater.* 30 (2020) 2916–2925. <https://doi.org/10.1007/s10904-020-01443-7>.
- [17] V. Vilas, D. Philip, J. Mathew, Catalytically and biologically active silver nanoparticles synthesized using essential oil, *Spectrochim. Acta Part A Mol. Biomol. Spectrosc.* 132 (2014) 743–750. <https://doi.org/https://doi.org/10.1016/j.saa.2014.05.046>.
- [18] L.M. Liz-Marzán, Tailoring surface plasmons through the morphology and assembly of metal nanoparticles., *Langmuir*. 22 (2006) 32–41. <https://doi.org/10.1021/la0513353>.
- [19] I. Alghoraibi, C. Soukkarieh, R. Zein, A. Alahmad, J.-G. Walter, M. Daghestani, Aqueous extract of *Eucalyptus camaldulensis* leaves as reducing and capping agent in biosynthesis of silver nanoparticles, *Inorg. Nano-Metal Chem.* 50 (2020) 895–902. <https://doi.org/10.1080/24701556.2020.1728315>.
- [20] R.T. V Vimala, G. Sathishkumar, S. Sivaramakrishnan, Optimization of reaction conditions to fabricate nano-silver using *Couroupita guianensis* Aubl. (leaf & fruit) and its enhanced larvicidal effect, *Spectrochim. Acta Part A Mol. Biomol. Spectrosc.* 135 (2015) 110–115. <https://doi.org/https://doi.org/10.1016/j.saa.2014.06.009>.
- [21] S. Patil, R. Chandrasekaran, Biogenic nanoparticles: a comprehensive perspective in synthesis, characterization, application and its challenges, *J. Genet. Eng. Biotechnol.* 18 (2020) 67. <https://doi.org/10.1186/s43141-020-00081-3>.
- [22] M.F. Zayed, W.H. Eisa, Phoenix *dactylifera* L. leaf extract phytosynthesized gold nanoparticles; controlled synthesis and catalytic activity, *Spectrochim. Acta Part A Mol. Biomol. Spectrosc.* 121 (2014) 238–244. <https://doi.org/https://doi.org/10.1016/j.saa.2013.10.092>.
- [23] R.J.B. Pinto, J.M.F. Lucas, M.P. Morais, S.A.O. Santos, A.J.D. Silvestre, P.A.A.P. Marques, C.S.R. Freire, Demystifying the morphology and size control on the biosynthesis of gold nanoparticles using *Eucalyptus globulus* bark extract, *Ind. Crops Prod.* 105 (2017) 83–92. <https://doi.org/https://doi.org/10.1016/j.indcrop.2017.05.003>.
- [24] M. Valodkar, P.S. Nagar, R.N. Jadeja, M.C. Thounaojam, R. V Devkar, S. Thakore,

- Euphorbiaceae latex induced green synthesis of non-cytotoxic metallic nanoparticle solutions: A rational approach to antimicrobial applications, *Colloids Surfaces A Physicochem. Eng. Asp.* 384 (2011) 337–344. <https://doi.org/https://doi.org/10.1016/j.colsurfa.2011.04.015>.
- [25] P. Ferreira-Santos, Z. Genisheva, C. Botelho, J. Santos, C. Ramos, J.A. Teixeira, C.M.R. Rocha, Unravelling the Biological Potential of Pinus pinaster Bark Extracts, *Antioxidants* (Basel, Switzerland). 9 (2020) 334. <https://doi.org/10.3390/antiox9040334>.
- [26] A.C. Dong, P. Huang, B. Caughey, W.S. Caughey, Infrared Analysis of Ligand- and Oxidation-Induced Conformational Changes in Hemoglobins and Myoglobins, *Arch. Biochem. Biophys.* 316 (1995) 893–898. <https://doi.org/https://doi.org/10.1006/abbi.1995.1120>.
- [27] P. Rani, V. Kumar, P.P. Singh, A.S. Matharu, W. Zhang, K.-H. Kim, J. Singh, M. Rawat, Highly stable AgNPs prepared via a novel green approach for catalytic and photocatalytic removal of biological and non-biological pollutants, *Environ. Int.* 143 (2020) 105924. <https://doi.org/https://doi.org/10.1016/j.envint.2020.105924>.
- [28] N. Esmaili, P. Mohammadi, M. Abbaszadeh, H. Sheibani, Green synthesis of silver nanoparticles using Eucalyptus comadulensis leaves extract and its immobilization on magnetic nanocomposite (GO-Fe₃O₄/PAA/Ag) as a recoverable catalyst for degradation of organic dyes in water, *Appl. Organomet. Chem.* 34 (2020) e5547. <https://doi.org/https://doi.org/10.1002/aoc.5547>.
- [29] K.J. Brobbey, J. Haapanen, M. Gunell, M. Toivakka, J.M. Mäkelä, E. Eerola, R. Ali, M.R. Saleem, S. Honkanen, J. Bobacka, J.J. Saarinen, Controlled time release and leaching of silver nanoparticles using a thin immobilizing layer of aluminum oxide, *Thin Solid Films.* 645 (2018) 166–172. <https://doi.org/https://doi.org/10.1016/j.tsf.2017.09.060>.
- [30] J.F. Moulder, *Handbook of X-ray Photoelectron Spectroscopy: A Reference Book of Standard Spectra for Identification and Interpretation of XPS Data*, Physical Electronics Division, Perkin-Elmer Corporation, 1992.
- [31] A.M. Fonseca, I.C. Neves, Study of silver species stabilized in different microporous zeolites, *Microporous Mesoporous Mater.* 181 (2013) 83–87. <https://doi.org/https://doi.org/10.1016/j.micromeso.2013.07.018>.
- [32] A.V. Naumkin, A. Kraut-Vass, S.W. Gaarenstroom, C.J. Powell, NIST X-ray Photoelectron Spectroscopy Database, NIST Stand. Ref. Database 20, Version 4.1. (2012).
- [33] J.P.Z. Gonçalves, J. Seraglio, D.L.P. Macuvelle, N. Padoin, C. Soares, H.G. Riella, Green synthesis of manganese based nanoparticles mediated by Eucalyptus robusta and Corymbia citriodora for agricultural applications, *Colloids Surfaces A Physicochem. Eng. Asp.* 636 (2022) 128180. <https://doi.org/https://doi.org/10.1016/j.colsurfa.2021.128180>.
- [34] M. Sivagami, I. V Asharani, Catalytic reduction of nitroarenes by Cucumis maderaspatanus L. leaves extract mediated silver nanoparticles, *J. Taiwan Inst. Chem. Eng.* 149 (2023) 104981. <https://doi.org/https://doi.org/10.1016/j.jtice.2023.104981>.
- [35] Z. Gharari, P. Hanachi, H. Sadeghinia, T.R. Walker, Eco-Friendly Green Synthesis and Characterization of Silver Nanoparticles by Scutellaria multicaulis Leaf Extract and Its Biological Activities, *Pharmaceuticals.* 16 (2023). <https://doi.org/10.3390/ph16070992>.
- [36] J. Jiang, G. Oberdörster, A. Elder, R. Gelein, P. Mercer, P. Biswas, Does nanoparticle activity depend upon size and crystal phase?, *Nanotoxicology.* 2 (2008) 33–42. <https://doi.org/10.1080/17435390701882478>.
- [37] Y. Mo, Y. Tang, S. Wang, J. Lin, H. Zhang, D. Luo, Green synthesis of silver nanoparticles using

- eucalyptus leaf extract, *Mater. Lett.* 144 (2015) 165–167. <https://doi.org/https://doi.org/10.1016/j.matlet.2015.01.004>.
- [38] S.A.O. Santos, R.J.B. Pinto, S.M. Rocha, P.A.A.P. Marques, C.P. Neto, A.J.D. Silvestre, C.S.R. Freire, Unveiling the Chemistry behind the Green Synthesis of Metal Nanoparticles, *ChemSusChem*. 7 (2014) 2704–2711. <https://doi.org/https://doi.org/10.1002/cssc.201402126>.
- [39] M. Khatun, Z. Khatun, M.R. Karim, M.R. Habib, M.H. Rahman, M.A. Aziz, Green synthesis of silver nanoparticles using extracts of *Mikania cordata* leaves and evaluation of their antioxidant, antimicrobial and cytotoxic properties, *Food Chem. Adv.* 3 (2023) 100386. <https://doi.org/https://doi.org/10.1016/j.focha.2023.100386>.
- [40] S.M. Roopan, Rohit, G. Madhumitha, A.A. Rahuman, C. Kamaraj, A. Bharathi, T. V Surendra, Low-cost and eco-friendly phyto-synthesis of silver nanoparticles using *Cocos nucifera* coir extract and its larvicidal activity, *Ind. Crops Prod.* 43 (2013) 631–635. <https://doi.org/https://doi.org/10.1016/j.indcrop.2012.08.013>.
- [41] S. Jebri, A. Fdhila, C. Dridi, Nanoengineering of eco-friendly silver nanoparticles using five different plant extracts and development of cost-effective phenol nanosensor, *Sci. Rep.* 11 (2021) 22060. <https://doi.org/10.1038/s41598-021-01609-4>.
- [42] D. Ben Hassine, R. Rahmani, J.P. Souchard, M. Abderrabba, J. Bouajila, *Eucalyptus brevifolia* F. Muell and *Eucalyptus stricklandii* Maiden leaves extracts: HPLC-DAD, GC-MS analysis and in vitro biological activities, combined with the principal component analysis, *South African J. Bot.* 147 (2022) 826–839. <https://doi.org/https://doi.org/10.1016/j.sajb.2022.03.027>.
- [43] A. Ashraf, R.A. Sarfraz, A. Mahmood, M. ud Din, Chemical composition and in vitro antioxidant and antitumor activities of *Eucalyptus camaldulensis* Dehn. leaves, *Ind. Crops Prod.* 74 (2015) 241–248. <https://doi.org/https://doi.org/10.1016/j.indcrop.2015.04.059>.
- [44] G. Dogan, N. Kara, E. Bagci, S. Gur, Chemical composition and biological activities of leaf and fruit essential oils from *Eucalyptus camaldulensis*., *Z. Naturforsch. C.* 72 (2017) 483–489. <https://doi.org/10.1515/znc-2016-0033>.
- [45] K. Wang, Y. Liu, X. Jin, Z. Chen, Characterization of iron nanoparticles/reduced graphene oxide composites synthesized by one step eucalyptus leaf extract, *Environ. Pollut.* 250 (2019) 8–13. <https://doi.org/https://doi.org/10.1016/j.envpol.2019.04.002>.
- [46] L. Zhou, J. Li, Q. Kong, S. Luo, J. Wang, S. Feng, M. Yuan, T. Chen, S. Yuan, C. Ding, Chemical Composition, Antioxidant, Antimicrobial, and Phytotoxic Potential of *Eucalyptus grandis* × *E. urophylla* Leaves Essential Oils., *Molecules*. 26 (2021). <https://doi.org/10.3390/molecules26051450>.
- [47] D. Ben Hassine, M. Abderrabba, Y. Yvon, A. Lebrihi, F. Mathieu, F. Couderc, J. Bouajila, Chemical composition and in vitro evaluation of the antioxidant and antimicrobial activities of *Eucalyptus gillii* essential oil and extracts., *Molecules*. 17 (2012) 9540–9558. <https://doi.org/10.3390/molecules17089540>.
- [48] Z. Obeizi, H. Benbouzid, S. Ouchenane, D. Yilmaz, M. Culha, M. Bououdina, Biosynthesis of Zinc oxide nanoparticles from essential oil of *Eucalyptus globulus* with antimicrobial and anti-biofilm activities, *Mater. Today Commun.* 25 (2020) 101553. <https://doi.org/https://doi.org/10.1016/j.mtcomm.2020.101553>.
- [49] I. Almas, E. Innocent, F. Machumi, W. Kisinza, Chemical composition of essential oils from *Eucalyptus globulus* and *Eucalyptus maculata* grown in Tanzania, *Sci. African.* 12 (2021)

- e00758. <https://doi.org/https://doi.org/10.1016/j.sciaf.2021.e00758>.
- [50] S. Diloksumpun, N. Wongkattiya, K. Buaban, T. Saleepochn, P. Suttiarporn, S. Luangkamin, Variation in the Antibacterial and Antioxidant Activities of Essential Oils of Five New *Eucalyptus urophylla* S.T. Blake Clones in Thailand, *Molecules*. 27 (2022). <https://doi.org/10.3390/molecules27030680>.
- [51] V. Aleksic Sabo, P. Knezevic, Antimicrobial activity of *Eucalyptus camaldulensis* Dehn. plant extracts and essential oils: A review., *Ind. Crops Prod.* 132 (2019) 413–429. <https://doi.org/10.1016/j.indcrop.2019.02.051>.
- [52] K. Ali, B. Ahmed, S.M. Ansari, Q. Saquib, A.A. Al-Khedhairi, S. Dwivedi, M. Alshaeri, M.S. Khan, J. Musarrat, Comparative in situ ROS mediated killing of bacteria with bulk analogue, *Eucalyptus* leaf extract (ELE)-capped and bare surface copper oxide nanoparticles, *Mater. Sci. Eng. C*. 100 (2019) 747–758. <https://doi.org/https://doi.org/10.1016/j.msec.2019.03.012>.
- [53] K. Sebei, F. Sakouhi, W. Herchi, M.L. Khouja, S. Boukhchina, Chemical composition and antibacterial activities of seven *Eucalyptus* species essential oils leaves, *Biol. Res.* 48 (2015) 7. <https://doi.org/10.1186/0717-6287-48-7>.
- [54] Y. Huang, M. An, A. Fang, O.J. Olatunji, F.N. Eze, Antiproliferative Activities of the Lipophilic Fraction of *Eucalyptus camaldulensis* against MCF-7 Breast Cancer Cells, UPLC-ESI-QTOF-MS Metabolite Profile, and Antioxidative Functions., *ACS Omega*. 7 (2022) 27369–27381. <https://doi.org/10.1021/acsomega.2c02389>.
- [55] M. Pan, Q. Lei, H. Zhang, Prediction and confirmation of active ingredients in *Eucalyptus globulus* Labill leaves, *Ind. Crops Prod.* 154 (2020) 112631. <https://doi.org/https://doi.org/10.1016/j.indcrop.2020.112631>.
- [56] Z.-R. Mashwani, M.A. Khan, T. Khan, A. Nadhman, Applications of plant terpenoids in the synthesis of colloidal silver nanoparticles, *Adv. Colloid Interface Sci.* 234 (2016) 132–141. <https://doi.org/https://doi.org/10.1016/j.cis.2016.04.008>.
- [57] J.Y. Song, B.S. Kim, Rapid biological synthesis of silver nanoparticles using plant leaf extracts, *Bioprocess Biosyst. Eng.* 32 (2009) 79–84. <https://doi.org/10.1007/s00449-008-0224-6>.
- [58] Y. AMAKURA, M. YOSHIMURA, N. SUGIMOTO, T. YAMAZAKI, T. YOSHIDA, Marker Constituents of the Natural Antioxidant *Eucalyptus* Leaf Extract for the Evaluation of Food Additives, *Biosci. Biotechnol. Biochem.* 73 (2009) 1060–1065. <https://doi.org/10.1271/bbb.80832>.
- [59] Ștefan Dezsi, A.S. Bădărău, C. Bischin, D.C. Vodnar, R. Silaghi-Dumitrescu, A.-M. Gheldiu, A. Mocan, L. Vlase, Antimicrobial and Antioxidant Activities and Phenolic Profile of *Eucalyptus globulus* Labill. and *Corymbia ficifolia* (F. Muell.) K.D. Hill & L.A.S. Johnson Leaves, *Molecules*. 20 (2015) 4720–4734. <https://doi.org/10.3390/molecules20034720>.
- [60] C. Ferreira, A. Pereyra, A. Patriarca, M. Mazzobrea, T. Polak, V. Abram, M. Buera, N. PoklarUlrihd, Phenolic Compounds in Extracts from *Eucalyptus globulus* Leaves and *Calendula officinalis* Flowers, *J. Nat. Prod. Res.* www.jacsd.com (2016).
- [61] A. Nasr, T. Saleem Khan, G.-P. Zhu, Phenolic compounds and antioxidants from *Eucalyptus camaldulensis* as affected by some extraction conditions, a preparative optimization for GC-MS analysis, *Prep. Biochem. Biotechnol.* 49 (2019) 464–476. <https://doi.org/10.1080/10826068.2019.1575860>.
- [62] E. Al-Sayed, A.-N. Singab, N. Ayoub, O. Martiskainen, J. Sinkkonen, K. Pihlaja, HPLC–PDA–ESI–MS/MS profiling and chemopreventive potential of *Eucalyptus gomphocephala* DC, *Food Chem.* 133 (2012) 1017–1024.

- <https://doi.org/https://doi.org/10.1016/j.foodchem.2011.09.036>.
- [63] F. Gomes, N. Martins, L. Barros, M.E. Rodrigues, M.B.P.P. Oliveira, M. Henriques, I.C.F.R. Ferreira, Plant phenolic extracts as an effective strategy to control *Staphylococcus aureus*, the dairy industry pathogen, *Ind. Crops Prod.* 112 (2018) 515–520. <https://doi.org/https://doi.org/10.1016/j.indcrop.2017.12.027>.
- [64] L. Boulekbache-Makhlouf, E. Meudec, J.-P. Mazauric, K. Madani, V. Cheynier, Qualitative and Semi-quantitative Analysis of Phenolics in *Eucalyptus globulus* Leaves by High-performance Liquid Chromatography Coupled with Diode Array Detection and Electrospray Ionisation Mass Spectrometry, *Phytochem. Anal.* 24 (2013) 162–170. <https://doi.org/https://doi.org/10.1002/pca.2396>.
- [65] M.A. Ghareeb, M.R. Habib, H.S. Mossalem, M.S. Abdel-Aziz, Phytochemical analysis of *Eucalyptus camaldulensis* leaves extracts and testing its antimicrobial and schistosomicidal activities, *Bull. Natl. Res. Cent.* 42 (2018) 16. <https://doi.org/10.1186/s42269-018-0017-2>.
- [66] T.J.I. Edison, M.G. Sethuraman, Instant green synthesis of silver nanoparticles using *Terminalia chebula* fruit extract and evaluation of their catalytic activity on reduction of methylene blue, *Process Biochem.* 47 (2012) 1351–1357. <https://doi.org/https://doi.org/10.1016/j.procbio.2012.04.025>.
- [67] A.K. Mittal, S. Kumar, U.C. Banerjee, Quercetin and gallic acid mediated synthesis of bimetallic (silver and selenium) nanoparticles and their antitumor and antimicrobial potential, *J. Colloid Interface Sci.* 431 (2014) 194–199. <https://doi.org/https://doi.org/10.1016/j.jcis.2014.06.030>.
- [68] M. Pradeep, D. Kruszka, P. Kachlicki, D. Mondal, G. Franklin, Uncovering the Phytochemical Basis and the Mechanism of Plant Extract-Mediated Eco-Friendly Synthesis of Silver Nanoparticles Using Ultra-Performance Liquid Chromatography Coupled with a Photodiode Array and High-Resolution Mass Spectrometry, *ACS Sustain. Chem. Eng.* 10 (2022) 562–571. <https://doi.org/10.1021/acssuschemeng.1c06960>.
- [69] S. Jain, M.S. Mehata, Medicinal Plant Leaf Extract and Pure Flavonoid Mediated Green Synthesis of Silver Nanoparticles and their Enhanced Antibacterial Property, *Sci. Rep.* 7 (2017) 15867. <https://doi.org/10.1038/s41598-017-15724-8>.
- [70] S.M. Ghoreishi, M. Behpour, M. Khayatkashani, Green synthesis of silver and gold nanoparticles using *Rosa damascena* and its primary application in electrochemistry, *Phys. E Low-Dimensional Syst. Nanostructures.* 44 (2011) 97–104. <https://doi.org/https://doi.org/10.1016/j.physe.2011.07.008>.

4.2 ANTIBACTERIAL AND PHOTOCATALYTIC BEHAVIOR OF OPTIMIZED AgNP

4.2.1 INTRODUCTION

A variety of toxic dyes are used in the manufacture of leather, foodstuffs, paint, textile, plastic, paper, cosmetics, rubber and pharmaceuticals as a result of their exploitation leading to pollution of water resources which is dangerous for humans and the environment [1]. It is estimated that around 10,000 different types of synthetic and natural dyes are produced worldwide each year, weighing somewhere between 7×10^5 and 1×10^6 tons, with a significant amount of dyes wasted during the manufacturing and application processes [2,3]. The fixation of reactive dyes during the dyeing process is extremely inefficient, almost 50% released directly into the environment [4]. The IC or Acid Blue 74 dye is extensively used as blue food additive, E132, and in the textile industry, and it is present as a pollutant in the major industrial effluents contaminating freshwater bodies [5]. The presence of two sulfonic acid groups in the molecule enhances its solubility in water [3]. IC dye is considered a highly toxic compound of the indigoid class of dyes and its direct contact causes skin and eye irritations, with permanent injury to the cornea and conjunctiva. It is also responsible for gastrointestinal irritations with nausea, diarrhea and vomiting [6,7]. As IC dye is very harmful to the environment even at low quantities, its removal from contaminated water is crucial.

Advanced oxidative processes (AOP) have been applied for wastewater treatment since the production of reactive free radicals allows to degraded organic pollutants by redox reactions [8]. Heterogeneous photocatalysis distinguishes out among AOP because involves redox reactions induced by irradiation in the presence of catalysts. The ability to incorporate renewable sunlight energy in the form of solar photons is the main advantage of heterogeneous photocatalysis, which adds significant environmental value to the degradation process. In particular, for large-scale aqueous-phase applications, the use of solar light to photodegrade wastewater contaminants can make it a competitive method [9]. Recent reviews describe various catalysts that have been synthesized and used in wastewater treatment for degradation of dyes [10], PAH (Polycyclic Aromatic Hydrocarbons) [11], antibiotics [12] or herbicides [13]. IC was effectively degraded (87%) under visible light by a heterostructured composite of borosilicate glass containing CdS/ZnS quantum dots [7]. Also, silver-attached reduced graphene oxide nanocomposite exhibited notable photocatalytic degradation ability

towards both IC and methylene blue [14]. Sun *et al.* [15] studied the anthracene degradation by AgBr/BiOBr/TiO₂ catalyst and founded a high photocatalytic activity, stability and adaptability of the new material.

Due to their excellent optical absorption over a broad range of the sunlight spectrum, including both visible light and UV light, noble MNP have been recognized as a type of effective material suitable for harvesting light energy for chemical processes [16]. AgNP have gained much attention due to their excellent conductivity, stability and multiple applications as catalysts, antiviral, antifungal or/and antibacterial agents [17–20]. These remarkable properties of AgNP are attractive for heterogeneous catalysis, so they may be used as an efficient catalyst for remove pollutants in liquid effluents. In this context, in the present subchapter, the obtained AgNP were evaluated as environmental remediation agents, i.e., as photocatalyst for the degradation of pollutants and as antimicrobial agents.

4.2.2 MATERIALS AND METHODS

4.2.2.1 Chemicals

Indigo Carmine (IC, C₁₆H₈N₂Na₂O₈S₂) was purchased from Merck. Other reagents were acquired from Sigma-Aldrich and utilized as received. Ultrapure water (Milli-Q system, Millipore) was used to prepare all aqueous solutions.

4.2.2.2 Evaluation of antibacterial activity

The antibacterial activity of the biosynthesized AgNP was evaluated using a traditional disc diffusion method. *Escherichia coli* (ATCC 25922) and *Staphylococcus aureus* (ATCC 6538) were first cultured in nutrient broth for 24 h at 37 °C. The AgNP at various amounts (1-10 mg.mL⁻¹) were placed on sterile paper discs of 5 mm diameter on cultured plates with nutrient agar. After 24 h of incubation at 37 °C, the diameter of the growth prevention halo was measured to determine the antibacterial activity against both bacteria (inhibition zone in mm).

Results from each experiment were expressed as the mean ± standard deviation (SD), with three independent replicates. Statistically significant differences in concentrations of AgNP in the antibacterial assay were evaluated by a Two-Way Anova followed by Sidak using the GraphPad Prism® software (version 8.0). *P* values < 0.05 were considered to be statistically significant.

4.2.2.3 Evaluation of photocatalytic activity

The photocatalytic activity of biosynthesized AgNP on the degradation of IC dye as a wastewater pollutant model under UV light, visible light and sunlight irradiation was evaluated during 2 h of reaction. First, the photocatalytic degradation was assessed at a laboratory scale, using a visible LED lamp (Lexman, 24.5W) and a UV Hg-lamp (Philips TL BLB 1FM, 6x8W). The photodegradation reactions were carried out in a magnetically stirred photoreactor with a capacity of 250 mL with an aqueous solution of IC dye (10 mg.L⁻¹) with 1 g.L⁻¹ of AgNP at RT, in dark conditions over 30 min. Thereafter, the solution was exposed to UV light irradiation (1.6-1.7 mW.cm² measured by lux meter UV34 Lux Meter-PCE) and visible light irradiation (60,000 lux measured by an illuminance meter, Konica Minolta) placed outside the reactor. The photocatalytic experiments under sunlight irradiation were conducted in an open space where it was possible to gather the solar radiation on a sunny day, between 12 a.m. and 2 p.m. (1.1-0.4 mW.cm² of UV irradiation and 69-62,000 lux of visible irradiation). Dye samples were withdrawn at fixed times, AgNP were separated from the dye solution through centrifugation and the supernatant was analyzed at 610 nm using a UV-Vis spectrophotometer. All the experiments were carried out in triplicate.

The toxicity of the IC solution after 2 h of photodegradation under different irradiation was assessed by the germination of grains of corn kernels, based on a procedure adapted from Sancey *et al.* [21] and Tanji *et al.* [22]. 15 healthy grains of corn were placed in a Petri dish with two paper filters and 5 mL of each aqueous solution was added every day: (A) Ultrapure water (control); (B) IC untreated solution at 10 mg.L⁻¹; (C) IC solution after photodegradation under UV light irradiation; (D) IC solution after photodegradation under visible light irradiation and (E) IC solution after photodegradation under direct sunlight irradiation, after 2 h of reaction. Petri dishes were covered and seeds were germinated in a growth chamber at RT in the February of 2023. Three replicates were prepared for the assays.

The following equation is used to estimate germination after counting the number of seeds that have germinated after 7 days (equation 4-4):

$$\text{Germination (\%)} = \frac{(\% \text{ of germination control} - \% \text{ of germination test})}{\% \text{ of germination control}} \times 100 \quad (\text{Equation 4-4})$$

4.2.3 RESULTS AND DISCUSSION

The environmental applications of green AgNP are focused in their potential as antimicrobial agents and as heterogeneous catalysts for the photodegradation of contaminants in aqueous effluents.

The antibacterial potential of MNP has been assessed and it may result from the production of ROS, which destroy cell biomolecules and disrupt nuclear membranes and cells [23]. AgNP provide a broad spectrum of antimicrobial coverage, including bacteria, fungi and viruses. The antibacterial properties of synthesized AgNP_{50°C:1:2} against two types of bacteria were investigated: *E. coli* (gram-negative) and *S. aureus* (gram-positive). The concentrations of AgNP in both cases ranged from 1.0 to 10.0 mg.mL⁻¹ (**Figure 4-8**).

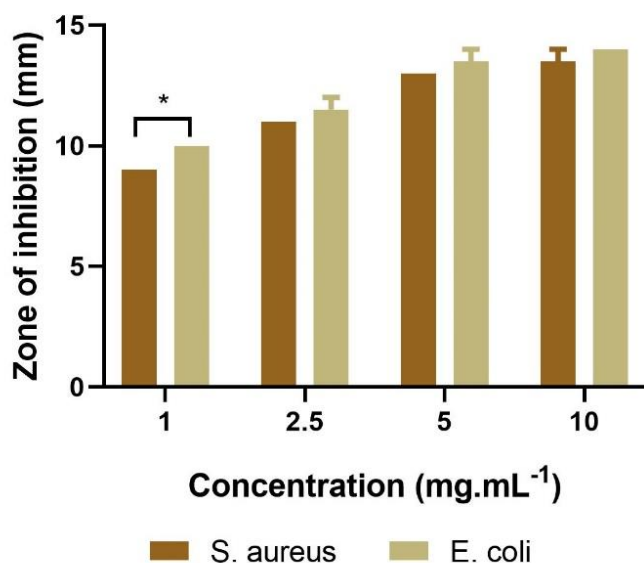


Figure 4-8. Antibacterial activity of AgNP_{50°C:1:2} at range concentration 1-10 mg.mL⁻¹. The symbol * shows significant differences ($p < 0.05$) between inhibition zone of the same concentration of AgNP in different bacteria.

The antibacterial activity of the AgNP_{50°C:1:2} against *E. coli* and *S. aureus* can be evidenced in both cases and the bacterial inhibition depends on AgNP concentration. The significant difference in the diameter of the zone of inhibition of the *S. aureus* and *E. coli* is detected with 1.0 mg.mL⁻¹ of AgNP. The lower effect of AgNP against *S. aureus* is attributed to the difference in the bacteria membrane structure, distinctively: Gram-positive bacteria have a thicker cell wall made of peptidoglycan proteins, which allows them to gain resistance to AgNP, in contrast to Gram-negative bacteria have weaker cell walls. Since Gram-positive bacteria have negatively charged cell walls that can draw silver ions to their

surface, it is possible to reduce the number of silver ions that reach the plasma membrane [24]. Bhuyan *et al.* [25] reported that the superficial contact of AgNP with the cell membrane can inhibit enzymatic systems of the respiratory chain, the replication of bacterial DNA is reduced and the inactivation of protein occurs. The results obtained with green synthesized AgNP are consistent with the well-known powerful antibacterial properties of AgNP.

Recent studies have shown that green AgNP can be used as heterogeneous catalyst in the photodegradation of a variety of dyes [5,26]. The mechanism of photodegradation of dyes by MNP is attributed to the formation of surface plasmons in the MNP under photonic excitation. This photo absorption process is followed by the creation of electrons, transfer of charge carriers and recombination of charge carriers with the organic dye molecules after this excitation step activates the dye [27]. The band gap energy (E_g) is an essential parameter determining the performance of the photocatalyst [28,29]. The corresponding band gap value of AgNP_{50°C-1.2} could be estimated according to equation 4-5:

$$E_g = \frac{1240}{\lambda_g} \quad (\text{Equation 4-5})$$

where E_g is the band gap of the semiconductor and λ_g is the threshold wavelength, the one of the corresponding absorbance edge [28]. The estimated E_g was 2.67 eV, making it able to participate effectively in the photodegradation of pollutants [30].

Here, the photodegradation activity of biosynthesized AgNP_{50°C-1.2} is evaluated using a model dye molecule, IC (**Figure 4-9**).

This performance parameter was monitored over time by UV-visible spectroscopy at 610 nm, during 2 h of reaction. To demonstrate the efficiency of biosynthesized AgNP and the impacts of different irradiations on the IC degradation, control experiments were carried out.

The results indicate that the removal of IC is insignificant under UV light, visible light and sunlight irradiations without the presence of AgNP in line with other works [31]. In addition, no significant changes are observed during the dye degradation experiment conducted in the dark in the presence of AgNP.

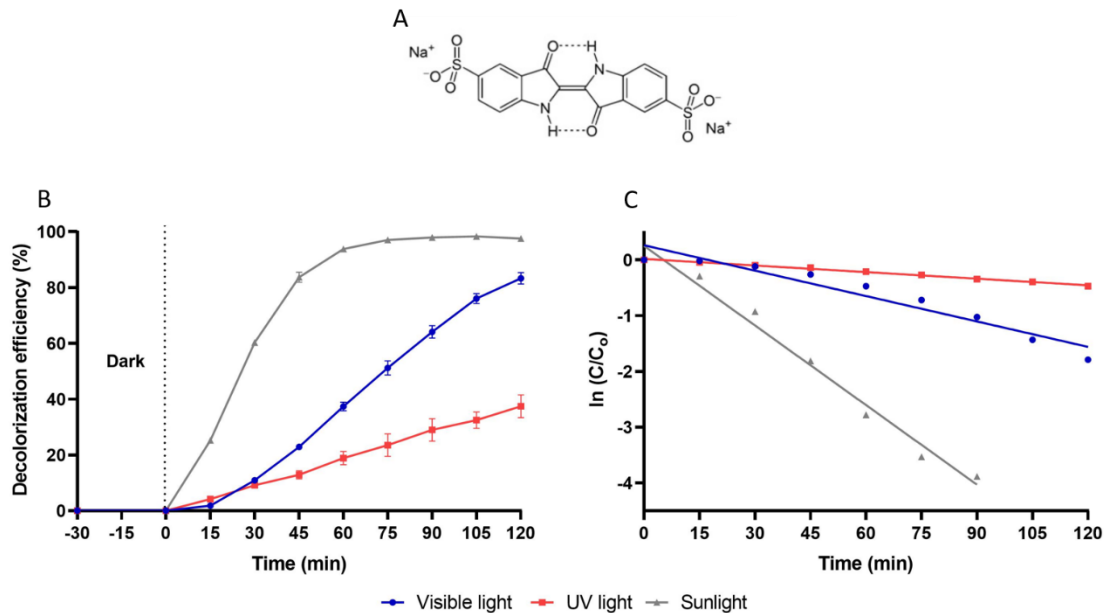


Figure 4-9. Evaluation of photocatalytic efficiency of $\text{AgNP}_{50^{\circ}\text{C}:1.2}$ under different irradiations (A) Indigo Carmine (IC) dye, (B) Decolorization efficiency *vs* time and (C) $\ln(C/C_0)$ *vs* time.

These data confirm that the dye degradation rely on both the presence of AgNP and the irradiation, as in a typical heterogeneous photocatalysis. The absorption peak of IC dye (610 nm) decrease with the increase in irradiation time and almost disappears at the end of reaction (**Figure 4-10**), evidencing the extinction of the molecular structure of the IC dye by an attack on the exocyclic double bond [31,32].

After 60 min, $93.8 \pm 0.6\%$ of the IC dye is degraded under sunlight irradiation, whereas only 27.4 ± 1.5 and $18.8 \pm 2.4\%$ degradations are reached under visible and UV light, respectively. These results are also confirmed by the kinetic analysis where the photocatalytic decolorization of IC is fitted by a pseudo-first-order kinetic model (equation 3-4).

The plot of $\ln(C/C_0)$ *vs* time for the photocatalytic degradation of the IC dye solution using $\text{AgNP}_{50^{\circ}\text{C}:1.2}$ is shown in **Figure 4-9B**. The k calculated is found to be 0.0476, 0.0152 and 0.0039 min^{-1} for sunlight, visible and UV light, respectively, and confirms that sunlight is the best radiation to promote the photodegradation. The regression coefficient values are higher than 0.933, which indicates that the experimental data are well fitted by the pseudo-first-order model (**Table 4-6**).

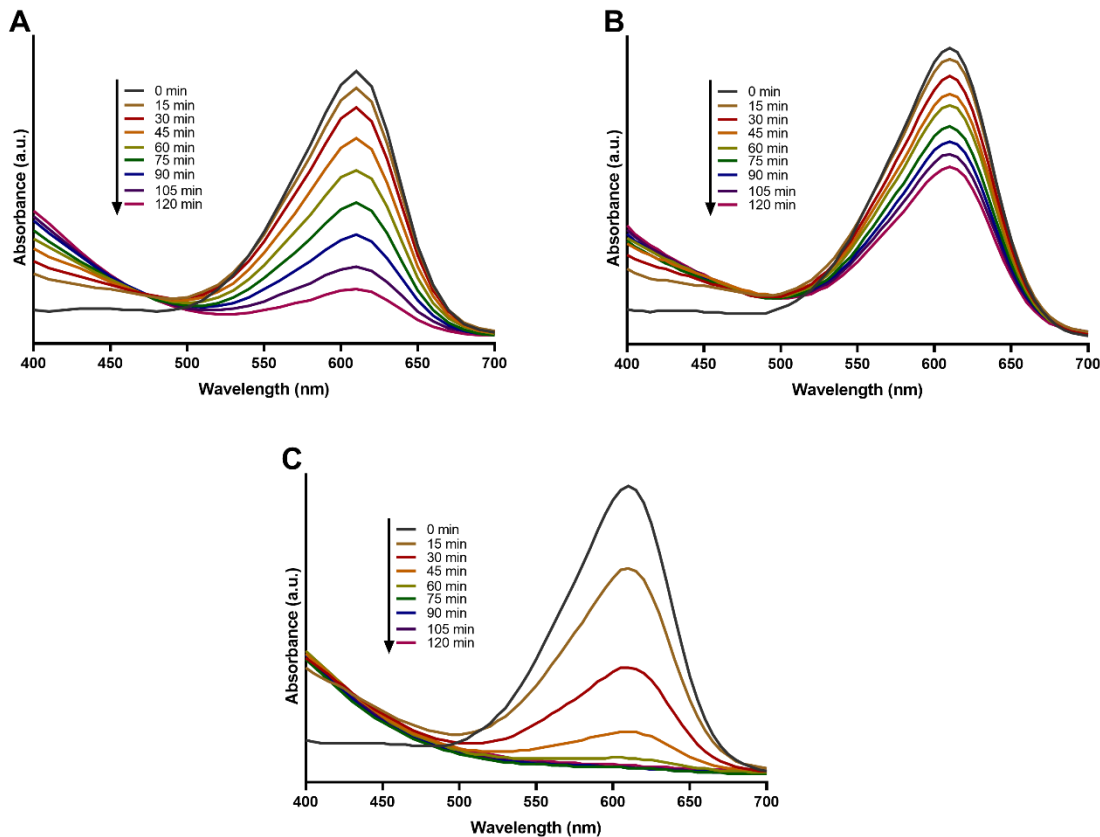


Figure 4-10. UV-visible spectra of Indigo Carmine (IC) degradation in the presence of AgNP_{50°C:1:2} under (A) Visible irradiation, (B) UV irradiation and (C) Sunlight.

Table 4-6. Values of decolorization efficiency (%), kinetic constant ($k = \text{min}^{-1}$) and linear correlation coefficient (R^2) for IC photodegradation under UV, visible and sunlight irradiation.

Radiation type	Decolorization efficiency %	Rate constant (k, min^{-1})	Squared R (R^2)
UV	37.41±4.12	0.0039	0.9942
Visible	83.30±2.03	0.0152	0.9311
Sunlight	97.58±0.51	0.0476	0.9821

The half-life ($t_{1/2}$) of the decolorization is calculated using equation 4-6:

$$t_{1/2} = \frac{0.693}{k} \quad \text{(Equation 4-6)}$$

The half-life is found to be 14.6, 45.6 and 177.7 min for IC decolorization under sunlight, visible and UV light, respectively.

The total mineralization is not confirmed in this work. However, some previous investigations [33,34] showed the photodegradation of IC dye into isatin sulfonic acid up to 2-amine-5-sulfo-benzoic acid formation via oxidation.

These comparative evaluations demonstrated that direct sunlight irradiation is the optimum condition for the photocatalytic reduction of IC dye in presence of AgNP. Solar energy for the degradation of pollutants by photocatalysis is an economic and sustainable solution.

For the evaluation of the phytotoxic effect of the treated solution after photodegradation, germination tests with corn kernels were performed (**Figure 4-11**).

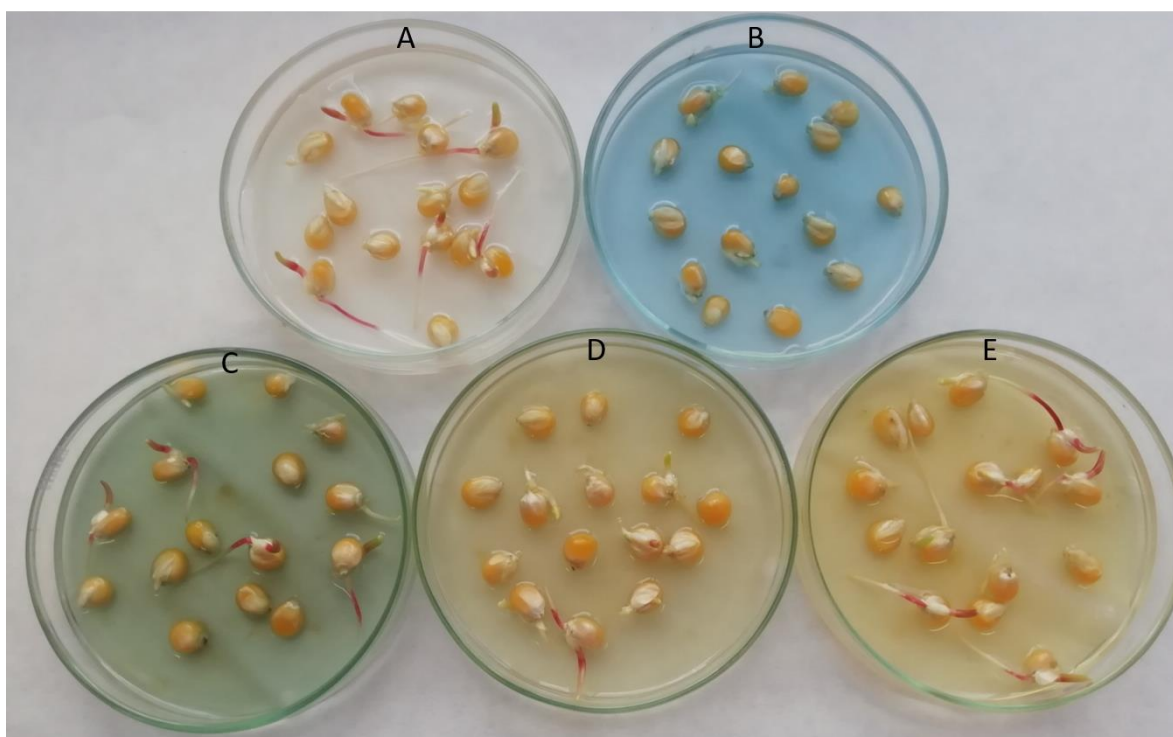


Figure 4-11. Germination test results. (A) Ultrapure water, (B) IC solution at 10 mg.L^{-1} untreated, (C) IC solution after 120 min of photodegradation in the presence of $\text{AgNP}_{50^\circ\text{C}1:2}$ under: UV light irradiation, (D) visible light irradiation and (E) direct sunlight irradiation.

There is a significant difference between the untreated solution (control) and treated IC solutions by photodegradation using $\text{AgNP}_{50^\circ\text{C}1:2}$ catalyst. The germination of corn kernels was assessed in Petri dishes irrigated with ultra-pure water during 7 days at RT. The assays were performed in February

2023 and the temperature of the water was 15 °C. The germination of corn kernels was successful in control (70%).

On the other hand, the germination was minor for untreated aqueous solutions containing IC dye at 10 mg.mL⁻¹, which did not exceed 13%, and treated solutions under UV, visible light and sunlight irradiation reached in 7 days 40, 53 and 73%, respectively. In presence of sunlight irradiation, the germination is similar to the control. This confirms low phytotoxicity after the photocatalytic degradation processes mainly with sunlight radiation, the results of phytotoxicity being in agreement with the results of photodegradation. Consequently, degradation catalyzed by AgNP and under sunlight irradiation reached the best combination for preventing or decreasing the environmental impact of the contaminated effluents by dyes.

4.2.4 CONCLUSIONS

The AgNP exhibited efficient antibacterial activity against both gram-positive and gram-negative bacteria: *Escherichia coli* (15 mm maximum zone of clearance) and *Staphylococcus aureus* (14 mm maximum zone of clearance). High photodegradation of IC dye under UV, Visible light and sunlight radiation was successfully achieved with sunlight as the best option. In addition, germination tests confirmed the efficiency of the IC photodegradation using AgNP with sunlight radiation. This work is promoting the development of a dual-in-one platform for cleaning up wastewater systems.

4.2.5 REFERENCES

- [1] F. Luo, D. Yang, Z. Chen, M. Megharaj, R. Naidu, One-step green synthesis of bimetallic Fe/Pd nanoparticles used to degrade Orange II, *J. Hazard. Mater.* 303 (2016) 145–153. <https://doi.org/https://doi.org/10.1016/j.jhazmat.2015.10.034>.
- [2] E. Errais, J. Duplay, F. Darragi, I. M'Rabet, A. Aubert, F. Huber, G. Morvan, Efficient anionic dye adsorption on natural untreated clay: Kinetic study and thermodynamic parameters, *Desalination*. 275 (2011) 74–81. <https://doi.org/https://doi.org/10.1016/j.desal.2011.02.031>.
- [3] M.F. Chowdhury, S. Khandaker, F. Sarker, A. Islam, M.T. Rahman, M.R. Aual, Current treatment technologies and mechanisms for removal of indigo carmine dyes from wastewater: A review, *J. Mol. Liq.* 318 (2020) 114061. <https://doi.org/https://doi.org/10.1016/j.molliq.2020.114061>.
- [4] A. Telke, D. Kalyani, J. Jadhav, S. Govindwar, Kinetics and Mechanism of Reactive Red 141 Degradation by a Bacterial Isolate *Rhizobium radiobacter* MTCC 8161, *Acta Chim Slov.* 55 (2007).
- [5] P. Rani, V. Kumar, P.P. Singh, A.S. Matharu, W. Zhang, K.-H. Kim, J. Singh, M. Rawat, Highly

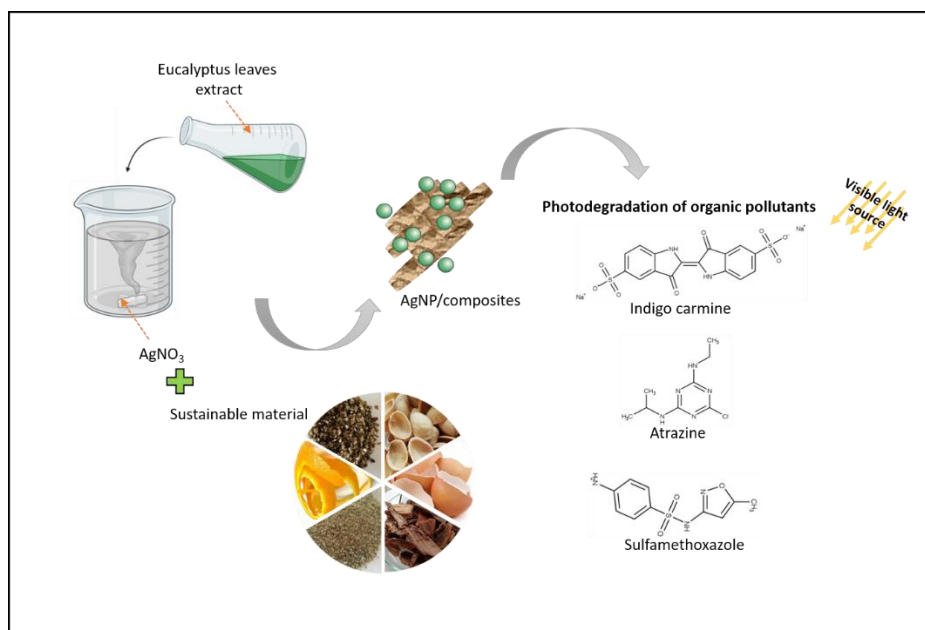
- stable AgNPs prepared via a novel green approach for catalytic and photocatalytic removal of biological and non-biological pollutants, *Environ. Int.* 143 (2020) 105924. <https://doi.org/https://doi.org/10.1016/j.envint.2020.105924>.
- [6] M.F. Abdel Messih, M.A. Ahmed, A. Soltan, S.S. Anis, Facile approach for homogeneous dispersion of metallic silver nanoparticles on the surface of mesoporous titania for photocatalytic degradation of methylene blue and indigo carmine dyes, *J. Photochem. Photobiol. A Chem.* 335 (2017) 40–51. <https://doi.org/https://doi.org/10.1016/j.jphotochem.2016.11.001>.
- [7] S.Y. Janbandhu, S. CT, S.R. Munishwar, J.R. Jayaramaiah, R.S. Gedam, Borosilicate glasses containing CdS/ZnS QDs: A heterostructured composite with enhanced degradation of IC dye under visible-light, *Chemosphere.* 286 (2022) 131672. <https://doi.org/https://doi.org/10.1016/j.chemosphere.2021.131672>.
- [8] S.O. Ganiyu, S. Sable, M. Gamal El-Din, Advanced oxidation processes for the degradation of dissolved organics in produced water: A review of process performance, degradation kinetics and pathway, *Chem. Eng. J.* 429 (2022) 132492. <https://doi.org/https://doi.org/10.1016/j.ccej.2021.132492>.
- [9] M.E. Borges, M. Sierra, E. Cuevas, R.D. García, P. Esparza, Photocatalysis with solar energy: Sunlight-responsive photocatalyst based on TiO₂ loaded on a natural material for wastewater treatment, *Sol. Energy.* 135 (2016) 527–535. <https://doi.org/10.1016/j.solener.2016.06.022>.
- [10] V. Gadore, S.R. Mishra, M. Ahmaruzzaman, Metal sulphides and their heterojunctions for photocatalytic degradation of organic dyes-A comprehensive review, *Environ. Sci. Pollut. Res.* 30 (2023) 90410–90457. <https://doi.org/10.1007/s11356-023-28753-w>.
- [11] O. Samuel, M.H.D. Othman, R. Kamaludin, H. Dzinun, A. Imtiaz, T. Li, T. El-badawy, A.U. Khan, M.H. Puteh, E. Yuliwati, T.A. Kurniawan, Photocatalytic degradation of recalcitrant aromatic hydrocarbon compounds in oilfield-produced water: A critical review, *J. Clean. Prod.* 415 (2023) 137567. <https://doi.org/https://doi.org/10.1016/j.jclepro.2023.137567>.
- [12] A. Azimi-Fouladi, P. Falak, S.A. Hassanzadeh-Tabrizi, The photodegradation of antibiotics on nano cubic spinel ferrites photocatalytic systems: A review, *J. Alloys Compd.* 961 (2023) 171075. <https://doi.org/https://doi.org/10.1016/j.jallcom.2023.171075>.
- [13] M.H. Hazaraimi, P.S. Goh, W.J. Lau, A.F. Ismail, Z. Wu, M.N. Subramaniam, J.W. Lim, D. Kanakaraju, The state-of-the-art development of photocatalysts for the degradation of persistent herbicides in wastewater, *Sci. Total Environ.* 843 (2022) 156975. <https://doi.org/https://doi.org/10.1016/j.scitotenv.2022.156975>.
- [14] P.P.A. Jose, M.S. Kala, N. Kalarikkal, S. Thomas, Silver-attached reduced graphene oxide nanocomposite as an eco-friendly photocatalyst for organic dye degradation, *Res. Chem. Intermed.* 44 (2018) 5597–5621. <https://doi.org/10.1007/s11164-018-3443-8>.
- [15] X. Sun, W. He, X. Hao, H. Ji, W. Liu, Z. Cai, Surface modification of BiOBr/TiO₂ by reduced AgBr for solar-driven PAHs degradation: Mechanism insight and application assessment, *J. Hazard. Mater.* 412 (2021) 125221. <https://doi.org/https://doi.org/10.1016/j.jhazmat.2021.125221>.
- [16] S. Sarina, E.R. Waclawik, H. Zhu, Photocatalysis on supported gold and silver nanoparticles under ultraviolet and visible light irradiation, *Green Chem.* 15 (2013) 1814–1833. <https://doi.org/10.1039/C3GC40450A>.

- [17] S.S. Salem, A. Fouda, Green Synthesis of Metallic Nanoparticles and Their Prospective Biotechnological Applications: an Overview., *Biol. Trace Elem. Res.* 199 (2021) 344–370. <https://doi.org/10.1007/s12011-020-02138-3>.
- [18] A.A. Yaqoob, K. Umar, M.N.M. Ibrahim, Silver nanoparticles: various methods of synthesis, size affecting factors and their potential applications—a review, *Appl. Nanosci.* 10 (2020) 1369–1378. <https://doi.org/10.1007/s13204-020-01318-w>.
- [19] N. Esmaili, P. Mohammadi, M. Abbaszadeh, H. Sheibani, Green synthesis of silver nanoparticles using *Eucalyptus comadulensis* leaves extract and its immobilization on magnetic nanocomposite (GO-Fe₃O₄/PAA/Ag) as a recoverable catalyst for degradation of organic dyes in water, *Appl. Organomet. Chem.* 34 (2020) e5547. <https://doi.org/https://doi.org/10.1002/aoc.5547>.
- [20] A.M. El Shafey, Green synthesis of metal and metal oxide nanoparticles from plant leaf extracts and their applications: A review, *Green Process. Synth.* 9 (2020) 304–339. <https://doi.org/doi:10.1515/gps-2020-0031>.
- [21] B. Sancey, G. Trunfio, J. Charles, J.-F. Minary, S. Gavaille, P.-M. Badot, G. Crini, Heavy metal removal from industrial effluents by sorption on cross-linked starch: Chemical study and impact on water toxicity, *J. Environ. Manage.* 92 (2011) 765–772. <https://doi.org/https://doi.org/10.1016/j.jenvman.2010.10.033>.
- [22] K. Tanji, J.A. Navio, A. Chaqroune, J. Naja, F. Puga, M.C. Hidalgo, A. Kherbeche, Fast photodegradation of rhodamine B and caffeine using ZnO-hydroxyapatite composites under UV-light illumination, *Catal. Today.* 388–389 (2022) 176–186. <https://doi.org/https://doi.org/10.1016/j.cattod.2020.07.044>.
- [23] A. Abdal Dayem, M.K. Hossain, S.B. Lee, K. Kim, S.K. Saha, G.-M. Yang, H.Y. Choi, S.-G. Cho, The Role of Reactive Oxygen Species (ROS) in the Biological Activities of Metallic Nanoparticles, *Int. J. Mol. Sci.* 18 (2017). <https://doi.org/10.3390/ijms18010120>.
- [24] M.M.K. Peiris, S.S.N. Fernando, P.M. Jayaweera, N.D.H. Arachchi, T.D.C.P. Guansekara, Comparison of Antimicrobial Properties of Silver Nanoparticles Synthesized from Selected Bacteria, *Indian J. Microbiol.* 58 (2018) 301–311. <https://doi.org/10.1007/s12088-018-0723-3>.
- [25] B. Bhuyan, A. Paul, B. Paul, S.S. Dhar, P. Dutta, *Paederia foetida* Linn. promoted biogenic gold and silver nanoparticles: Synthesis, characterization, photocatalytic and in vitro efficacy against clinically isolated pathogens, *J. Photochem. Photobiol. B Biol.* 173 (2017) 210–215. <https://doi.org/10.1016/j.jphotobiol.2017.05.040>.
- [26] M. Rabeea, M. Owaid, R. Muslim, Synthesis and characterization of silver nanoparticles by natural organic compounds extracted from *Eucalyptus* leaves and their role in the catalytic degradation of methylene blue dye, *Songklanakar J. Sci. Technol.* 43 (2021) 14–23. <https://doi.org/10.14456/sjst-psu.2021.3>.
- [27] M. Mehta, M. Sharma, K. Pathania, P.K. Jena, I. Bhushan, Degradation of synthetic dyes using nanoparticles: a mini-review, *Environ. Sci. Pollut. Res.* 28 (2021) 49434–49446. <https://doi.org/10.1007/s11356-021-15470-5>.
- [28] W.M. Shume, H.C.A. Murthy, E.A. Zereffa, A Review on Synthesis and Characterization of Ag₂O Nanoparticles for Photocatalytic Applications, *J. Chem.* 2020 (2020) 5039479. <https://doi.org/10.1155/2020/5039479>.
- [29] S. Jain, M.S. Mehata, Medicinal Plant Leaf Extract and Pure Flavonoid Mediated Green

- Synthesis of Silver Nanoparticles and their Enhanced Antibacterial Property, *Sci. Rep.* 7 (2017) 15867. <https://doi.org/10.1038/s41598-017-15724-8>.
- [30] Aryan, Ruby, M.S. Mehata, Green synthesis of silver nanoparticles using *Kalanchoe pinnata* leaves (life plant) and their antibacterial and photocatalytic activities, *Chem. Phys. Lett.* 778 (2021) 138760. <https://doi.org/https://doi.org/10.1016/j.cplett.2021.138760>.
- [31] S.Y. Janbandhu, U. Patra, G.K. Sukhadeve, R. Kumar, R.S. Gedam, Photocatalytic performance of glasses embedded with Ag-TiO₂ quantum dots on photodegradation of indigo carmine and eosin Y dyes in sunlight, *Inorg. Chem. Commun.* 148 (2023) 110317. <https://doi.org/https://doi.org/10.1016/j.inoche.2022.110317>.
- [32] G.K. Sukhadeve, S.Y. Janbandhu, R. Kumar, D.H. Lataye, D.D. Ramteke, R.S. Gedam, Visible light assisted photocatalytic degradation of Indigo Carmine dye and NO₂ removal by Fe doped TiO₂ nanoparticles, *Ceram. Int.* 48 (2022) 29121–29135. <https://doi.org/https://doi.org/10.1016/j.ceramint.2022.05.053>.
- [33] T.T. Guaraldo, T.B. Zanoni, S.I.C. de Torresi, V.R. Gonçalves, G.J. Zocolo, D.P. Oliveira, M.V.B. Zanoni, On the application of nanostructured electrodes prepared by Ti/TiO₂/WO₃ “template”: A case study of removing toxicity of indigo using visible irradiation, *Chemosphere.* 91 (2013) 586–593. <https://doi.org/https://doi.org/10.1016/j.chemosphere.2012.12.027>.
- [34] A. Hernández-Gordillo, V. Rodríguez-González, S. Oros-Ruiz, R. Gómez, Photodegradation of Indigo Carmine dye by CdS nanostructures under blue-light irradiation emitted by LEDs, *Catal. Today.* 266 (2016) 27–35. <https://doi.org/https://doi.org/10.1016/j.cattod.2015.09.001>.

CHAPTER 5 RECYCLING OF SUSTAINABLE MATERIALS AS SUPPORTS FOR GREEN SILVER NANOPARTICLES

The use of a sustainable technology to synthesize green AgNP from renewable resources is very appealing. In this chapter, a green protocol for the production AgNP/composites is introduced, via *in situ* reduction of Ag⁺ ions on sustainable materials (clays and waste materials) using eucalyptus leaves extract (ELE) as a reducing and stabilizing agent, without adding any toxic or expensive organic solvent, surfactant or hazardous chemicals. The synthesized AgNP/composites were evaluated as photocatalysts to degrade Indigo Carmine (IC), atrazine (ATZ) and sulfamethoxazole (SMX) under visible light.



This chapter was adapted from:

Rocha, V., Franco, S., Bertão, A.R., Neves, I.C., Tavares, T., *Recycling of natural and waste materials as supports for green-AgNP as efficient catalysts in photodegradation of organic pollutants* (under revision).

5.1 INTRODUCTION

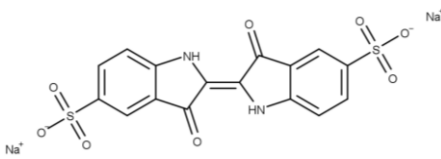
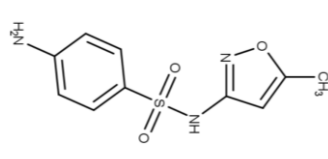
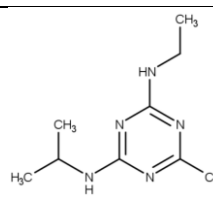
One of the sources of water pollution are organic compounds that are part of everyday life. In addition to dyes, such as IC, herbicides are another type of dangerous compounds that farmers frequently utilize on a large scale. Atrazine, 2-chloro-4-(ethylamine)-6-(isopropylamine)-s-triazine (ATZ), is an s-triazine herbicide introduced as a priority hazard substance by the European Union in 2004 due to its poor biodegradability, toxicity and water solubility [1]. Although this herbicide does not typically bioaccumulate, its persistence in the environment and mobility in some soils may result in the contamination of surface and groundwater [1] and ATZ is suspected to be both endocrine disruptor and carcinogenic [2]. Antibiotics are famously one of the most important kinds of environmental contamination. Besides different antibiotics, sulfonamide antibiotic, with a concentration level of ng.L^{-1} to mg.L^{-1} , sulfamethoxazole (SMX) has been consistently found in surface water, groundwater, seawater and WWTP effluents [3]. It is imperative to develop sustainable, effective and affordable techniques for effective reduction or elimination of these types of pollutants and microorganisms from wastewater and drinking water.

Presently, there is significant research efforts in utilizing green MNP as catalysts in photocatalysis. This approach aims to contribute to environmental remediation by effectively eliminating harmful and toxic substances, as well as pollutants like dyes and organic compounds [4]. Most studies of photocatalytic degradation using green MNP have been carried out adding suspensions of fine powdered MNP into the contaminated solution [5–7]. The utilization of powder MNP in photocatalytic reactors shows several limitations, including the challenge of filtering the final suspensions due to the small particles size. This difficulty renders the application of photocatalytic slurry reactors impractical. Agglomeration is another drawback of suspended MNP in their catalytic applications. In most instances, MNP aggregation results in catalytic deactivation because fewer surfaces are available [8]. Furthermore, after being used as intended, MNP buildup in the environment causes ongoing pollution and may have detrimental impacts on living organisms [9]. Recent reviews are focused on transformation fate and biological toxicity of MNP in aquatic environments [10–12]. The immobilization of MNP on solid supports, including carbon, activated carbon, metal oxides, graphene, polymers, glass and zeolites, could be used to address these issues [13,14].

The utilization of economic materials for manufacturing purposes could involve either recycling waste or employing natural materials from renewable sources that are abundant on Earth. This approach is particularly applicable in the context of wastewater treatment. Due to their non-toxic nature, affordability, porosity, layered morphology, large abundance in the earth's crust, chemical inertness and mechanical stability, clays have become one of these materials that has attracted a lot of attention [15–17]. Likewise, waste materials have been applied as effective support for green MNP [18,19]. At the moment, large quantities of waste are released at the end of the line, which cause serious environmental issues. Various studies have shown good photocatalytic activity using natural and waste materials as supports for MNP. For example, Sohrabnezhad and Seifi [20] reported that green Ag/ZnONP immobilized onto a natural material (montmorillonite) showed an effective photocatalytic activity for dye degradation under visible light. Honarmand *et al.* [8] explored the photocatalytic ability of SnO₂-bentonite nanocomposites synthesized via a green and simple route for the degradation of organic dyes. Biosynthesized ZnONP supported on powdered wastes of eggshells was described as a promising material for the photocatalytic degradation of diazinon [18]. Rashidi and Islami [19] immobilized Ag@AgClNP on the surface of biowaste *Elaeagnus angustifolia* seed and investigated its photocatalytic degradation of methylene blue under sunlight with excellent photoactivity without any agglomeration. Green MNP immobilization on different supports decreases the agglomeration of NP, increases their stability and facilitates their separation and recovery [14].

The aim of this chapter is the recycling of clays and waste materials as solid supports for AgNP synthesized *in situ* using eucalyptus leaves extract (ELE) as a reducing and stabilizing agent. AgNP/composites based in clays (bentonite, kaolin, sepiolite and vermiculite) or waste materials (eggshell, orange peel, peanuts shell, pine bark, pistachio shell and walnut shell) were evaluated as photocatalysts for degradation of IC dye under visible light. The best photocatalyst, the nanocomposite of AgNP/kaolin, was selected and investigated again on the photocatalytic degradation of IC but under different spectra, wavelengths and intensities of visible light emitted by a light-emitting-diode lamp (LED). The nanocomposite of AgNP/kaolin was also used to degrade ATZ and SMX in an aqueous solution under visible light. The physicochemical properties of selected pollutants are shown in **Table 5-1**.

Table 5-1. Physicochemical properties of selected pollutants [21].

Compound	Indigo Carmine (IC, dye)	Sulfamethoxazole (SMX, antibiotic)	Atrazine (ATZ, herbicide)
Structure			
Molecular formula	C ₁₆ H ₈ N ₂ Na ₂ O ₈ S ₂	C ₁₀ H ₁₁ N ₃ O ₃ S	C ₈ H ₁₄ ClN ₅
Molecular weight (g.mol ⁻¹)	466.4	253.3	215.7
Surface Area (Å ²)	197	107	63
Log K _{ow}	-	0.89	2.61
Dissociation constant	-	pKa1 = 1.6; pKa2 = 5.7	pKa = 1.60, very weak base

5.2 MATERIAL AND METHODS

5.2.1 Chemicals

Silver nitrate (AgNO₃, 99.8%) was purchased from PanReac AppliChem. IC, Atrazine (ATZ), Ethylenediaminetetraacetic acid disodium salt dehydrate (EDTA-2Na), Isopropyl Alcohol (IPA) and 1,4-benzoquinone (BQ) were purchased from Merck, Sigma-Adrich. Sulfamethoxazole (SMX) was obtained from TCI. All aqueous solutions were prepared with ultrapure water, obtained from a Milli-Q system (Millipore, USA), with a resistivity of 18.2 MΩcm⁻¹.

The bentonite clay was collected in Alentejo, Portugal (Brunauer–Emmett–Teller (BET) surface area of 11.9 m².g⁻¹ and porosity of 11%); the kaolin was obtained from Minas de Barqueiros, S.A. (Apúlia, Portugal) (BET surface area of 13.7 m².g⁻¹ and porosity of 46%); the sepiolite was obtained from Tolsa, S.A. (Spain) (BET surface area of 108 m².g⁻¹ and porosity of 49%) and vermiculite was obtained from Sigma-Aldrich (BET surface area of 39 m².g⁻¹ and porosity of 10%) [22]. These clays were washed and dried at 50 °C and reduced to fine powder (< 1 mm) in a mechanical grinder before use. The collected

waste materials (eggshell, orange peel, peanuts shell, pine bark, pistachio shell and walnut shell) were extensively washed and dried at 50 °C and then converted to fine powder (< 1 mm). Orange peel was lyophilized.

5.2.2 Biosynthesis of AgNP/composite

2 g of powder of each material: clays (bentonite, kaolin, sepiolite and vermiculite) and waste materials (eggshell, orange peel, peanuts shell, pine bark, pistachio shell and walnut shell) were individually added to 20 mL of 60 mM of AgNO₃ and the mixtures were stirred for 60 min at RT. Meanwhile, ELE was prepared as described in previous chapters. Then, the filtered extract was added dropwise to the mixture at a volume ratio of 1:1, at 50 °C with constant stirring. The suspension formed was centrifuged and washed and the resulting precipitate was dried overnight at 50 °C. Different volumes of AgNO₃ and ELE (20, 50 and 100 mL), and biosynthesis temperatures (RT and 50 °C) were tested with one of the supports.

5.2.3 Characterization of the nanocomposites

FTIR-ATR was used to investigate the structural characteristics of AgNP/composites and an optical study of biosynthesized nanocomposites was also undertaken using a UV–Vis spectrophotometer, as described in previous chapters. The morphology of the synthesized Ag nanocomposites was observed and recorded using a transmission electron microscope, TEM (JEM-2100-HT, Cryo & Tomography) which operated at an accelerating voltage of 200 kV. A small quantity of the aqueous dispersion of the sample was deposited onto a 400-mesh copper grid that had been coated with a carbon film. Subsequently, the grid was dried under vacuum to prepare for microscope observation. Chemical compositions of AgNP/composites were analyzed by X-ray photoelectron spectroscopy, XPS (ESCALAB 250XI, Thermo Fisher Scientific) with Al K_α X-rays (1486.6 eV) using 650 μm spot size under the base pressure below 10⁻¹⁰ mbar. Thermo Scientific Avantage software fitting by Voight function with a Smart background mode was used to carry out the XPS analyses.

5.2.4 Photocatalytic activity

The photocatalytic activity of the different AgNP/composite samples was evaluated using IC as a model pollutant, under visible light. 100 mL of an aqueous IC solution at 10 mg.L⁻¹ was mixed with the

biosynthesized Ag nanocomposite (1g.L^{-1}) in the dark for 30 min. After this initial time for adsorption, the LED lamp (Lexman, 24.5 W) at 12.5 cm of distance was switched on and aliquots were withdrawn at different reaction times. The quantification of IC dye was monitored by UV–Vis spectrophotometry.

Different scavengers, such as 1,4-benzoquinone (BQ), isopropyl alcohol (IPA) and ethylenediaminetetraacetic acid disodium salt dehydrate (EDTA-2Na), were used to trap superoxide radical anions ($\text{O}_2^{\cdot-}$), hydroxyl radicals ($\cdot\text{OH}$) and electron holes (h^{\cdot}), respectively to obtain more information about photodegradation mechanism. The assay conditions were the following: 100 mL of an aqueous IC solution at 10 mg.L^{-1} with 1 g.L^{-1} of photocatalyst and concentration of scavenger 0.1 mM during 120 min. The impact of the scavenger on the photocatalytic efficiency was monitored by using UV-Vis for IC dye.

After the selection of the best AgNP/composite, the photodegradation of ATZ and SMX was also evaluated as described above. The quantification of ATZ and SMX was performed by ultra high-performance liquid chromatography (UHPLC-DAD) using a Shimadzu Nexera X2 and a Kinetex C18 column (Phenomenex, Torrance) ($1.7\ \mu\text{m} \times 100\ \text{\AA} \times 2.1\ \text{mm}$), operating in gradient mode. For ATZ quantification, a mixture of acetonitrile and ultrapure water (45:55 v/v %) was used as the mobile phase, at the flow rate of $0.2\ \text{mL.min}^{-1}$. The chromatograms were registered at ATZ maximum adsorption wavelength at 225 nm. For SMX quantification, a mixture of ultrapure water and 0.1% formic acid in acetonitrile (20:80 v/v %) was used as the mobile phase, at the flow rate of $0.2\ \text{mL.min}^{-1}$. The chromatograms were registered at SMX maximum adsorption wavelength at 268 nm. In both cases, an injection volume of $5\ \mu\text{L}$ was used and the autosampler and column temperatures were kept at $25\ ^\circ\text{C}$.

5.2.4.1 Effect of spectrum, wavelength and intensity of visible light

A Ledigma lamp (Ledigma Ltd) was used to perform the measurements, under different lighting conditions to evaluate the effect of spectrum, wavelengths and intensities of visible light on the photocatalytic degradation of IC, using the best photocatalyst selected. That consists of an LED light source composed of 10 individual LED. The combination of the spectral energy distribution of each LED, which can be individually and independently controlled, provides a total spectral energy distribution ranging from 380 to 720 nm. These assays used three different light wavelengths: one LED with a peak at 440 nm, another at 460 nm and a third one at 630 nm. The white LED was used

as in the assay above (Lexman). **Figure 5-1** shows the radiance spectra of the different visible lights emitted by the LED lamps used in this work. The white light gives a full spectrum light with output at every wavelength, while the single spectrum blue LED has the maximum wavelength at 440 nm, another one at 460 nm and the single spectrum red LED has the maximum wavelength at 630 nm. The intensity was adjusted by changing the distance between the light source and the sample, 32.5 (l_1) to 12.5 cm (l_2).

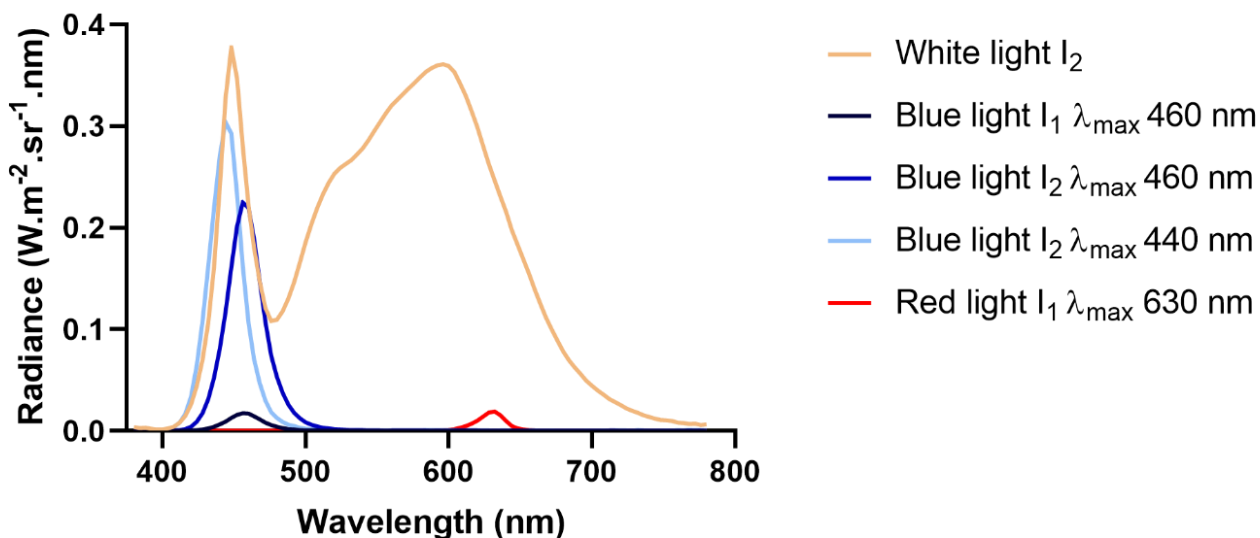


Figure 5-1. Radiance spectra of the different visible light emitted by LED lamps.

5.2.5 Statistical analysis

All experiments were carried out with three independent replicates and results were expressed as mean \pm standard deviation (SD). The significance of the data was statistically determined with One-way ANOVA followed by Tukey's multiple comparisons tests using GraphPad Prism® software (version 8.0). P values < 0.05 were considered to be statistically significant.

5.3 RESULTS AND DISCUSSION

Here, a green protocol for the production AgNP/composites is introduced, via *in situ* reduction of Ag^+ ions on sustainable materials using ELE as a reducing and capping agent without the use of toxic or expensive organic solvent, surfactant or harmful chemicals.

The layered phyllosilicate minerals, which occur naturally in the earth's crust and are important components of soils, were used to prepare AgNP/composites [23]. Due to their natural abundance, low-cost, non-toxic nature, layered morphology, porosity, chemical inertness and mechanical stability, these inorganic materials have gained significant interest to act as solid supports for MNP [15,16]. The clays used in this work, bentonite, sepiolite and vermiculite have two tetrahedral (SiO_4) layers that are bonded together by one octahedral (Al_2O_3) layer and the structure is often referred to as 2:1 phyllosilicate. Kaolin differs from the others as it has a 1:1 of tetrahedral and octahedral layers [24]. The structure of kaolin is fixed due to the hydrogen bonding and consequently, there is no expansion between the layers, presenting a low shrink-swell capacity when it is wetted [24].

The use of waste materials as supports for biogenic MNP, with focus on the removal of contaminants from aqueous environments, has seen a great increase in interest in recent years [18,25–27]. Fruit shells such as pistachio shell, peanuts shell, walnut shell and orange peel are abundant agricultural residues obtained in huge quantities, which could help to overcome the raw material shortage [27–30]. For instance, eggshells waste is one of the most prevalent types of food processing waste and it is mainly composed of calcium carbonate [31], while pine bark is a by-product of global lumber industry and is produced in large quantities in some regions of the world [32].

These different materials were used to prepare several AgNP/composites synthesized in the same conditions (2 g of support material with 20 mL of AgNO_3 and 20 mL of ELE at 50 °C) and were evaluated as a photocatalyst to degrade IC dye as a model pollutant in aqueous solutions under visible light, as a screening catalytic study.

Previously, photolysis and dark experiments were performed. The concentration of IC in the absence of nanocomposite has not changed within 120 min under visible light, confirming that IC dye is very steady and, on the other hand, no degradation of dye occurred in dark experiments. **Table 5-2** shows the results obtained on the decolorization of IC dye under visible light within 120 min catalyzed by biosynthesized nanocomposites as well as the final pH of photodegradation. Clays seem to be a better support for the AgNP than waste materials. Among the clays tested as supports for green AgNP, AgNP/kaolin showed a higher decolorization efficiency of approximately 48%, while only 11% and 3% of decolorization were achieved by AgNP/bentonite and AgNP/sepiolite, respectively. The AgNP/vermiculite was unable to degrade the dye. These results seem to be also related with pH and structure of the clays as clays with acid pH enhance the reaction, the initial pH of IC solution was

6.71±0.20. In addition, the specific structural characteristics of kaolin may have a positive impact on the formation of AgNP on the surface and improve the decolorization efficiency.

Table 5-2. Screening tests of IC photodegradation with AgNP/composites synthesized in identical conditions (2 g of sustainable material with 20 mL de AgNO₃ and 20 mL of ELE at 50 °C).

AgNP/Clays	Decolorization efficiency (%) after 120 min	Final pH after 120 min of photodegradation
Bentonite	10.8±3.8 ^a	8.06±0.17
Kaolin	47.8±1.3 ^b	3.89±0.01
Sepiolite	3.1±1.1 ^a	7.44±0.05
Vermiculite	n.d.	8.22±0.06
AgNP/Waste materials		
Eggshell	>1 ^a	8.01±0.19
Orange peel	4.6±2.3 ^a	4.01±0.08
Peanuts shell	>1 ^a	4.06±0.05
Pine bark	6.4±2.3 ^a	3.68±0.09
Pistachio shell	15.2±1.3 ^b	3.77±0.03
Walnut shell	>1 ^a	3.90±0.04

not detected (n.d.); Values are expressed as mean ± SD. Different letters indicate significant differences ($p < 0.05$) in decolorization efficiency between tested sustainable materials (clays or waste materials).

In terms of waste materials applied as supports for green AgNP, AgNP/pistachio shell reaches the best results (15%), followed by AgNP/pine bark (6%) and AgNP/orange peel (5%). The eggshell, peanuts shell and walnut shell samples showed a decolorization efficiency lower than 1% (**Table 5-2**). With these supports, the pH seems to have slightly effect on the catalytic activity that rather depends on the characteristics of the shells. Since the best results were obtained with the pistachio shell, this support

was used in the following characterization and in further catalytic assays to be compared with the clay supports.

FTIR spectra (**Figure 5-2**) from clays (A) and pistachio shell (B) as supports show the different functional groups.

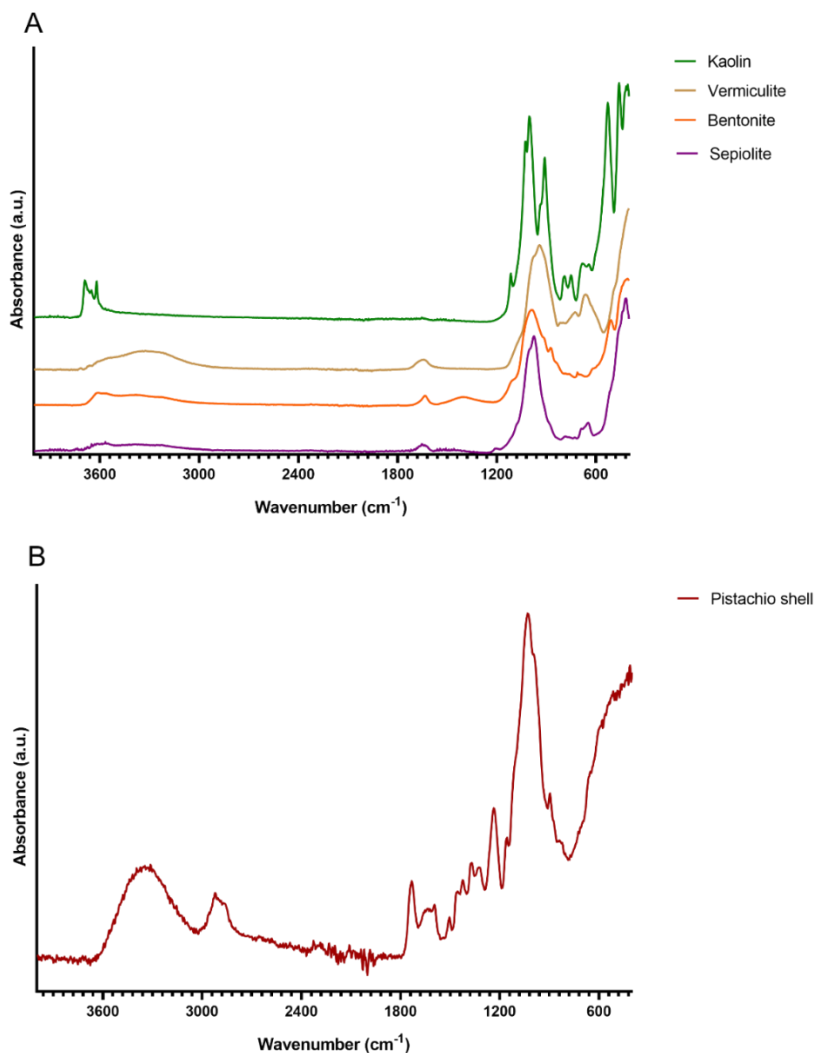


Figure 5-2. FTIR spectra of (A) different clays (kaolin, vermiculite, bentonite and sepiolite) and (B) pistachio shell used as a sustainable supports for AgNP.

Natural kaolin with rich surface hydroxyl groups has been extensively utilized in the field of environmental applications due to its ability to act as multi-functional carrier [15]. The FTIR spectrum of raw kaolin reveals the four characteristic absorption bands at 3700, 3670, 3650 and 3620 cm⁻¹ assigned to OH stretching vibrations [33]. When these characteristics bands are well defined, the

structure of kaolin is ordered, which was further evidenced by the P_0 index (the quotient of the absorbance at 3620 and at 3700 cm^{-1}), $P_0 = 1.112 > 1$, confirming that kaolin has an ordered structure [34]. Further, absorption bands assigned to Si–O stretching vibrations (1115, 1032, 1009, 470 and 430 cm^{-1}), Al–OH stretching vibration (939, 913 cm^{-1}), Si–O–Al stretching vibrations (789, 754, 538 cm^{-1}) and Mg/Al–OH stretching vibrations (696 cm^{-1}) were identified [33,35].

FTIR spectrum of raw pistachio shell (**Figure 5-2B**) reveals the broad peaks at around 3430 cm^{-1} , usually observed in raw materials, corresponding to the OH stretching associated with inter and intramolecular H-bonding of phenolic, alcoholic and carboxyl groups present in cellulose and cellulose components of the pistachio shell [27]. Aliphatic C–H deforming vibrations are attributed to the absorption bands at 2950 and 2850 cm^{-1} . The band at 2397 cm^{-1} is assigned with atmospheric carbon dioxide. The bands around 1740 and 1601 cm^{-1} are attributed to aromatic C=O ring and C=O stretching (probably –COOH) or C=C of aromatic groups in lignin [36]. Moreover, the presence of CH, CH₂ and CH₃ groups in cellulose, hemicellulose and in lignin of the pistachio shell is indicated by the absorption bands at 1376 cm^{-1} and 1459 cm^{-1} . The peak at 1042–1073 cm^{-1} probably belongs to the stretching vibration of OH functional groups of carboxylic acids and alcohols. These findings are in accordance with the previous studies with pistachio shell used as effective support for green AgNP [14] and green CuNP [27].

Since sustainable materials have many different functional groups across their surface and green AgNP are charged negatively (**Figure 4-5B**), NP may be loaded onto those materials by a combination of electrostatic and functional group interactions.

Considering the preliminary screening using the photocatalytic degradation of IC dye by different AgNP/composites, kaolin and pistachio shell were selected as promising supports for those NP. A new biosynthesis of AgNP/composites was performed by increasing the amount of AgNO₃ and ELE, 100 mL of each one, at RT. The photocatalytic efficiency of both systems was evaluated and the results are shown in **Figure 5-3**.

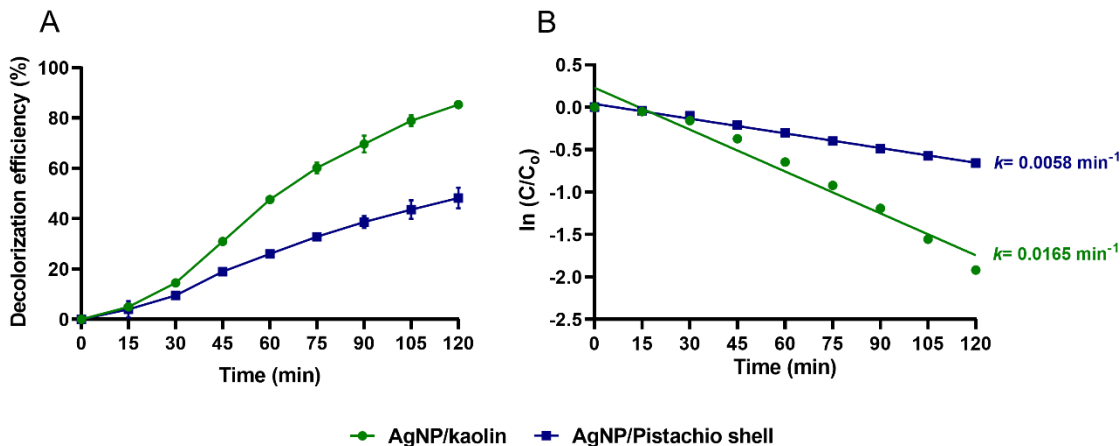


Figure 5-3. Evaluation of photocatalytic efficiency of AgNP/kaolin and AgNP/pistachio synthesized with 2 g of kaolin or pistachio shell with 100 mL de AgNO_3 and 100 mL of ELE at RT: (A) Decolorization efficiency (%) vs time and (B) $\ln(C/C_0)$ vs time.

The best catalytic results were obtained with the clay as support and the decolorization efficiency grew with time. A maxima of 85.3 (± 1.8)% and 48.3 (± 4.1)% were achieved with AgNP/kaolin and AgNP/pistachio shell, respectively (**Figure 5-3A**). This indicates that as the amount of AgNP increases, the decolorization efficiency rises, compare to **Table 5-2**.

The degradation profiles were fitted by a first-order, equation 3-4 (**Figure 5-3B**). It is evident that the photodegradation rate constant of was higher with AgNP/kaolin than with AgNP/pistachio shell, 0.0165 and 0.0058 min^{-1} , respectively. Considering these catalytic results, kaolin was selected as the best support for green AgNP. Furthermore, because of its low cost, abundance, thermal and mechanical stability, kaolin has received much attention as a promising support for green MNP, such as nZVI [34], AgNP [37], Ag/AgCl [35] and TiO_2 [38]. Kaolin is a suitable support and an excellent material that can go through several cycles of recycling because it is resistant to oxidative degradation in the presence of hydroxyl radicals and this inertness towards chemical and physical changes in the presence of $\cdot\text{OH}$ [34].

5.3.1 Influence of biosynthesis experimental parameters for AgNP/kaolin on the rate of degradation

Since the best catalytic results were obtained with kaolin as support for the NP, the influence of different synthesis parameters were evaluated. Kaolin was moistured with increasing volumes of AgNO₃ and of ELE, at RT or 50 °C, and the experimental conditions used are displayed in **Table 5-3**.

Table 5-3. Experimental conditions tested for the synthesis of AgNP/kaolin composite.

Sample	AgNO ₃ (mL)	ELE (mL)	Reaction temperature (°C)	Decolorization efficiency (%) after 120 min	Rate constant <i>k</i> (min ⁻¹)	Squared R (R ²)
AgNP/kaolin _{20:20 50 °C}	20	20	50	47.8±1.3	0.0042	0.9192
AgNP/kaolin _{20:20 RT}	20	20	RT	57.6±0.7	0.0079	0.9630
AgNP/kaolin _{50:50 50 °C}	50	50	50	67.6±1.5	0.0095	0.8702
AgNP/kaolin _{50:50 RT}	50	50	RT	77.4±1.5	0.0115	0.9632
AgNP/kaolin _{100:100 50 °C}	100	100	50	86.8±0.3	0.0162	0.8763
AgNP/kaolin _{100:100 RT}	100	100	RT	85.3±1.8	0.0165	0.9628

Figure 5-4 displays the photocatalytic IC degradation results using different AgNP/kaolin composites. The catalytic results showed that increasing the amounts of AgNO₃ and ELE, thus fabricating more AgNP, the photocatalytic performance increases, with 58% and 77% IC degradation for AgNP/kaolin_{20:20 RT} and AgNP/kaolin_{50:50 RT}, respectively. However, among the synthesized photocatalysts, AgNP/kaolin_{100:100} synthesized with 100 mL of AgNO₃ and 100 mL of ELE showed high decolorization of IC dye under visible irradiation, regardless of the temperature used in the synthesis. These results support that the biosynthesis of AgNP/kaolin composites at RT delivers a catalyst as efficient as the one obtained at higher temperature, which favors a more sustainable synthesis.

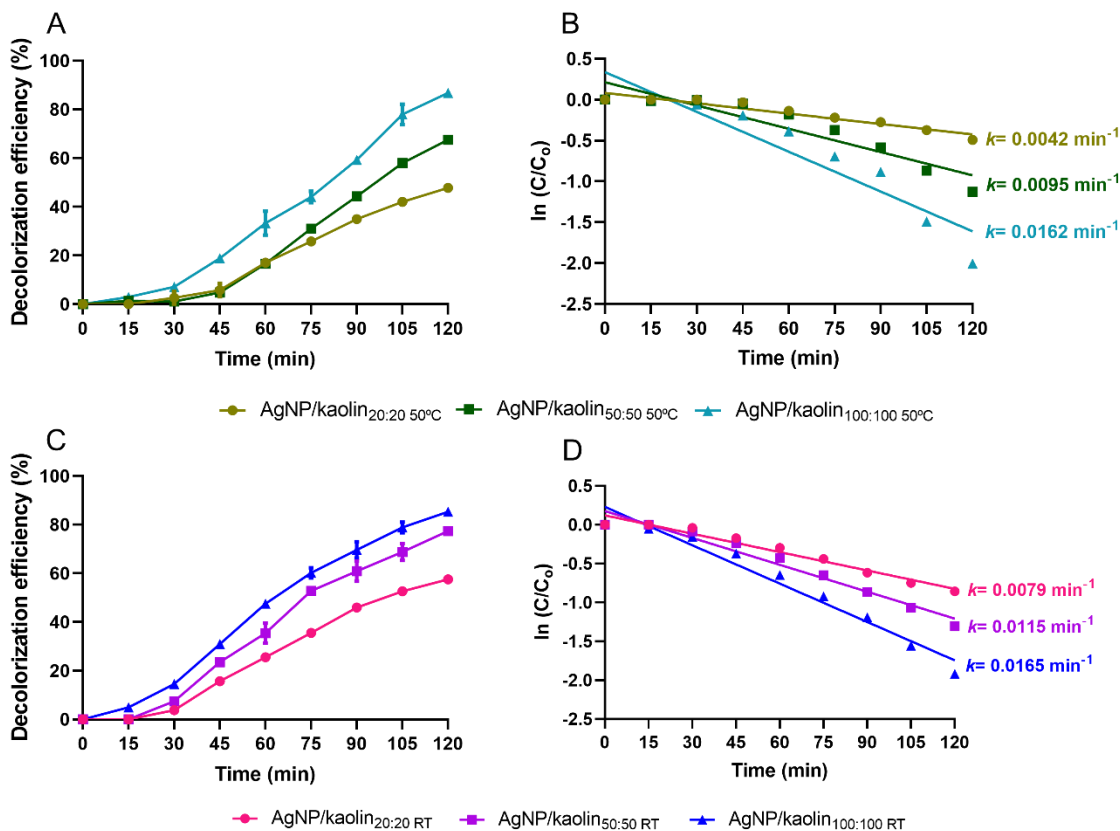


Figure 5-4. Photocatalytic efficiency of AgNP/kaolin composites synthesized with different volumes of AgNO₃ and ELE, at 50 °C and RT: (A and C) Decolorization efficiency (%) vs time and (B and D) ln(C/C₀) vs time.

The optical properties of the nanocomposites were evaluated in order to understand the interactions/locations of the AgNP with the kaolin. The green AgNP/kaolin composites were analyzed in the wavelength range from 300 to 700 nm by UV-Vis.

Figure 5-5 shows the optical spectra of the nanocomposites and it can be seen that AgNP/composites obtained at 50 °C showed the characteristic SPR, whereas the nanocomposites obtained at RT do not show that SPR. This behavior could indicate a different distribution of the AgNP on the surface of the kaolin particles.

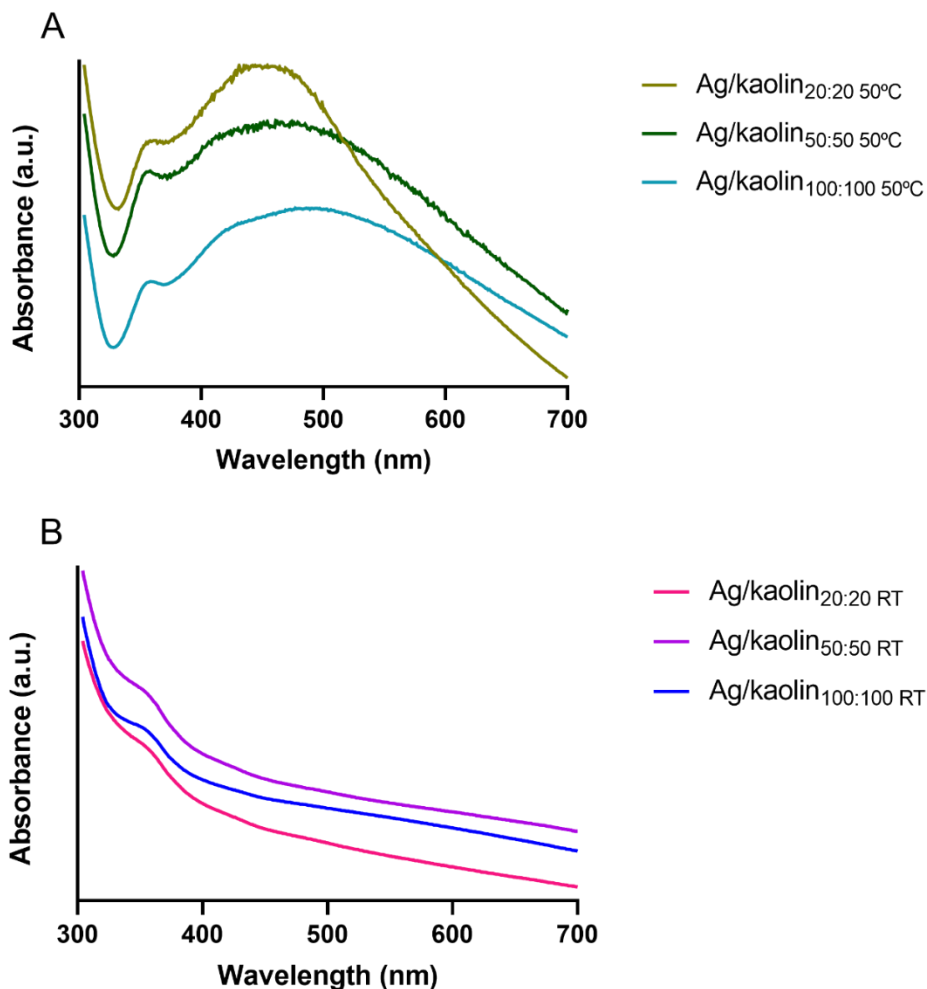


Figure 5-5. Evaluation of optical properties by UV-Vis of AgNP/kaolin composites synthesized at (A) 50 °C and (B) RT.

For environmental and economic reasons, the nanocomposites of AgNP/kaolin_{50:50 RT} and AgNP/kaolin_{50:50 50 °C} were selected for further evaluations.

In order to understand the catalytic behavior of AgNP/kaolin, transmission electron microscopy (TEM) and X-ray photoelectron spectroscopy (XPS) were carried out. **Figure 5-6** shows TEM images of typical AgNP/kaolin_{50:50 RT} and AgNP/kaolin_{50:50 50 °C}, in which the NP are visible as dark spots over the surface of kaolin.

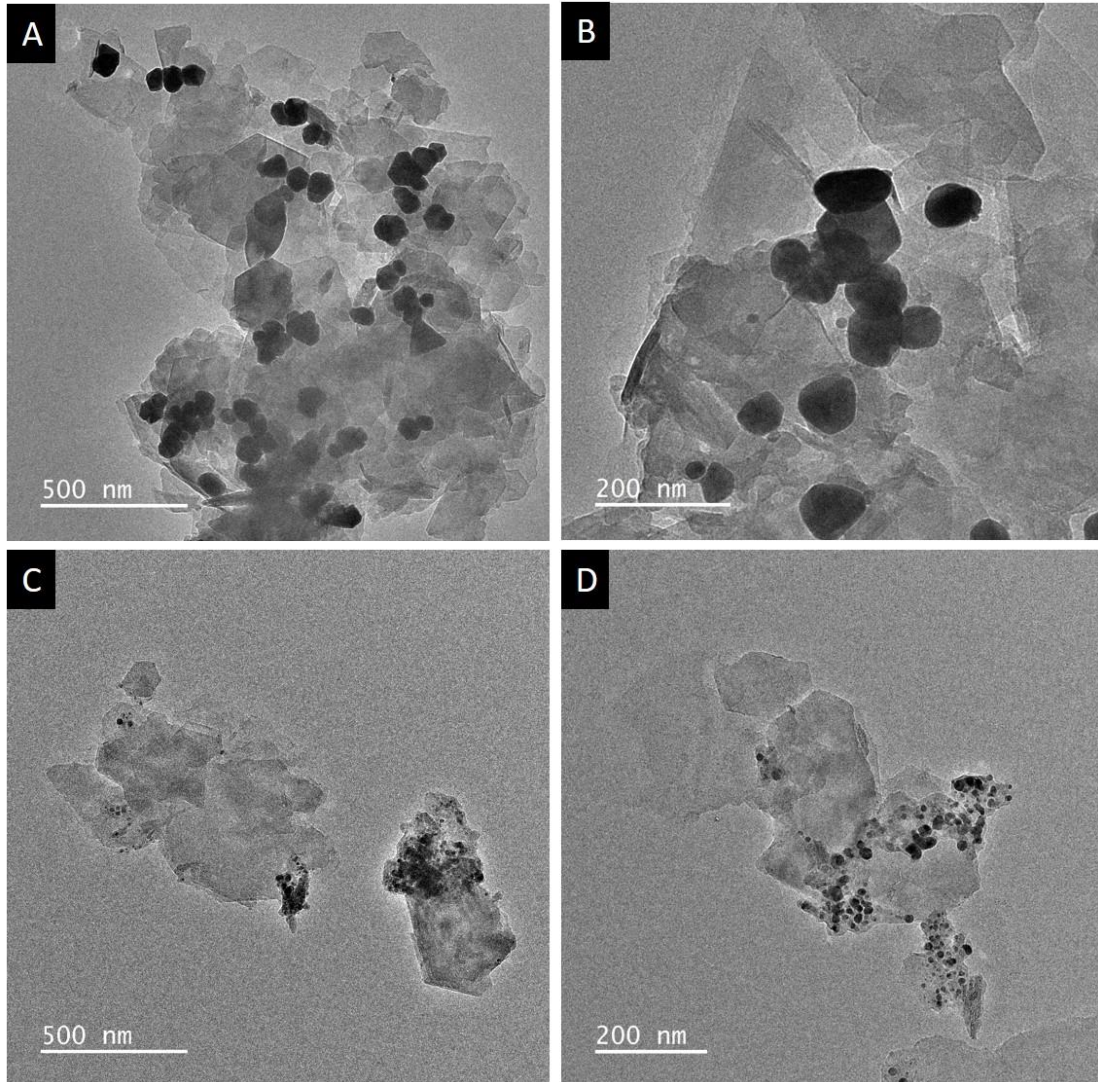


Figure 5-6. Images of TEM of AgNP/kaolin_{50:50:50°C} (A-B) and AgNP/kaolin_{50:50:RT} (C-D) with different scales.

These images show that the temperature of the synthesis affects the size of the particles, in this case, the AgNP dispersed in the kaolin support. The AgNP supported on kaolin and produced at 50 °C are spherical with diameters ranging from 29 to 127 nm. The spherical AgNP synthesized at RT show diameters ranging from 5 to 25 nm. The images reveal that by increasing the temperature of biosynthesis, the AgNP appear to cluster and to spread out more throughout the clay support. At RT the AgNP are much smaller than their counterpart, but they are more aggregated with the kaolin material.

The AgNP/kaolin_{50:50 RT} exhibited a higher decolorization efficiency compared with AgNP/kaolin_{50:50 50°C}, probably due to its relatively smaller particle size and better dispersion on the support which enhance the photocatalytic activity. The high number of small AgNP provides larger surface areas and thus more catalytically active sites for heterogeneous catalysis [38].

The surface composition and the relative distribution of the surface elements present in the Ag nanocomposites samples prepared at two different temperatures were carried out by XPS measurements. Both samples revealed the presence of oxygen (O 1s), carbon (C 1s), silicon (Si 2p), iron (Fe 2p) and aluminum (Al 2p) in their survey XPS resolution spectra, typical from kaolin clay, as well as, of silver in the region of Ag 3d that belongs to the AgNP. In addition, small amounts of certain elements were identified at the surface, as potassium (K 2p, 293.43 eV, 0.73 wt% for AgNP/kaolin_{50:50 RT}) and magnesium (Mg 1s, 1304.72 eV, 0.53 wt% for AgNP/kaolin_{50:50 50 °C}) attributed to the clay and chloride (Cl 2p) from the green AgNP (**Figure 5-7**).

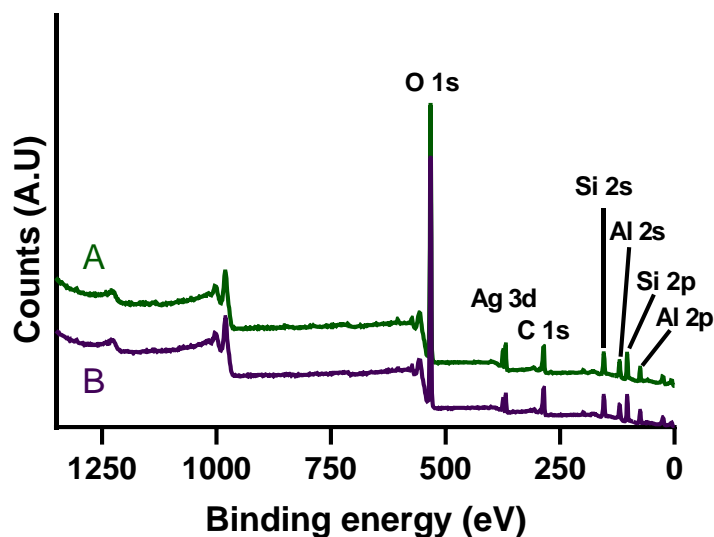


Figure 5-7. Survey XPS spectra of (A) AgNP/kaolin_{50:50 RT} and (B) AgNP/kaolin_{50:50 50 °C}.

The BE of the principal elements as well as their relative amount (wt%) in the surface identified by XPS are shown in **Table 5-4**.

Table 5-4. Binding energies (BE) and the relative amount of the surface elements (wt%) from the XPS spectra in the Si 2p, Al 2p, Cl 2p, O 1s, C 1s, Ag 3d and Fe 2p regions of AgNP/kaolin samples.

Photoelectrons Peaks	Si 2p		Al 2p		Cl 2p		O 1s		C 1s		Ag 3d		Fe 2p	
	BE (eV)	wt (%)	BE (eV)	wt (%)	BE (eV)	wt (%)	BE (eV)	wt (%)	BE (eV)	wt (%)	BE (eV)	wt (%)	BE (eV)	wt (%)
Samples														
AgNP/kaolin_{50:50 50°C}	102.93	22.26	74.64	16.85	198.26	1.11	532.25	53.56	286.42	13.57	368.33	6.22	712.63	1.58
AgNP/kaolin_{50:50 RT}	102.89	22.73	74.60	17.02	198.21	1.12	532.09	54.78	286.30	14.77	368.16	4.34	712.67	1.70

The BE of each element identified in both nanocomposites is similar, suggesting that the immobilization of the AgNP does not affect the kaolin structure. This statement is proved by the equivalent Si/Al ratio found for both samples, 1.32 and 1.34 for AgNP/kaolin_{50:50 50°C} and AgNP/kaolin_{50:50 RT}, respectively. The typical elements Si 2p, Al 2p and O 1s from the kaolin show a single peak attributed to them in their XPS survey from the Si and Al atoms in the tetrahedral and octahedral sites in the layer silicates [39]. Both samples show a peak Al 2p at 74.64 (AgNP/kaolin_{50:50 50°C}) and at 74.60 eV (AgNP/kaolin_{50:50 RT}), characteristic of the chemical bonds Si-O-Al in octahedral Al coordination, where the Si atoms at 102.9 eV are in tetrahedral coordination, typical of kaolinite materials [39].

The peaks at 286.42 or 286.30 eV, attributed to C 1s for AgNP/kaolin_{50:50 50°C} and AgNP/kaolin_{50:50 RT}, respectively, confirm the presence of the biomolecules. In addition, the close BE values (368.33 and 368.16 eV), for Ag 3d, despite the temperature, show that the immobilization does not affect the oxidation state of the silver in the nanoparticle compared to the same BE values obtained for the AgNP in suspension, 368.44 for RT and 368.90 for 50 °C. These BE values are consistent with Ag⁰. The silver surface quantified in both samples is different, with 6.22 and 4.34 wt% for AgNP/kaolin_{50:50 50°C} and for AgNP/kaolin_{50:50 RT}, respectively, and these results suggest that the increase in temperature discloses more particles to the surface, consequently more silver is detected at 50 °C. A stronger presence of AgNP in the surface defined at 50 °C does not enhance the catalytic activity of the composite, which increases only with the Ag:ELE volumes (**Table 5-3**).

5.3.2 Evaluation of photocatalytic performance

Different active species such as $\cdot\text{OH}$ and $\text{O}_2\cdot^-$ radicals and h^+ were generated during the photodegradation reaction of IC in the presence of the nanocomposites. To identify these active species responsible for the photocatalytic degradation of IC under visible light, various scavengers like EDTA-2Na (h^+ scavenger), IPA ($\cdot\text{OH}$ radical scavenger) and BQ ($\text{O}_2\cdot^-$ radical scavenger) were introduced into the aqueous solution of IC dye containing 100 mg of AgNP/kaolin_{50:50 RT}. After being trapped, the main reactive species will be quenched in the pollutant degradation process and the degradation efficiency will decrease, which would indirectly prove the importance of the referred active species. **Figure 5-8** shows the effect of different scavengers on the photodegradation activity of AgNP/kaolin_{50:50 RT} to degrade IC dye.

The primary reactive species will be quenched in the pollutant degradation process after being trapped, and the degradation efficiency will decrease, which will imply the significance of the mentioned active species.

When adding IPA to the dye solution, the decolorization occurs similarly to the control indicating that bulk $\cdot\text{OH}$ radicals were not used in the degradation process of IC dye. The decolorization rate decreased 31.5% when BQ was added to the IC solution, indicating that $\text{O}_2\cdot^-$ radicals were used in the degradation process. The decolorization rate of IC dye also decreased 37.5% when EDTA-2Na was added to the solution, which means that h^+ has taken part in the degradation process. Similar results were obtained by other authors [40,41].

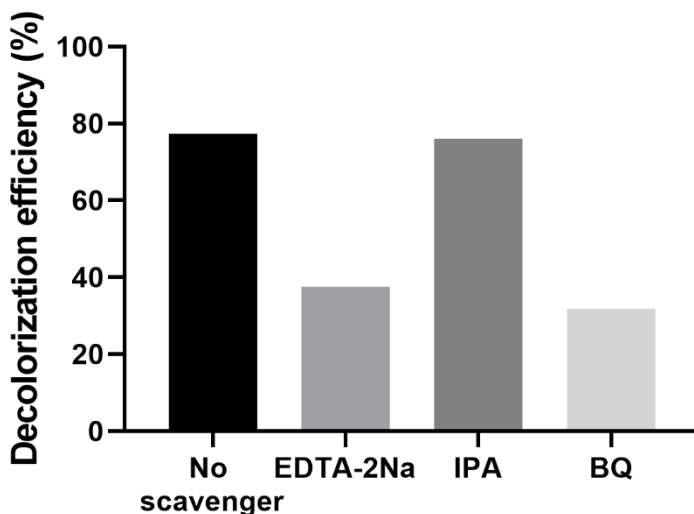


Figure 5-8. Photocatalytic degradation of IC dye with $\text{AgNP}/\text{kaolin}_{50:50 \text{ RT}}$ in the absence and presence of scavengers (EDTA-2Na, IPA and BQ) under visible light irradiation.

These results show that the mechanism of the photodegradation catalyzed by the nanocomposites involves $\text{O}_2\cdot^-$ and h^+ radical species.

The photocatalytic activity of $\text{AgNP}/\text{kaolin}_{50:50 \text{ RT}}$ was also evaluated on the degradation process of SMX and ATZ under visible light. Since some pollutants are degraded in the presence of visible light or completely adsorbed on the photocatalyst surface, it is necessary to perform control tests. Photolysis experiments performed in the absence of a photocatalyst led to no degradation of the organic pollutants within 120 min, suggesting the high stability of selected molecules against photolysis. Results from

dark experiments indicate that the adsorption of each pollutant onto the nanocomposite is negligible under the conditions tested.

As demonstrated in **Figure 5-9**, both ATZ and SMX were degraded by visible light-induced photocatalysis with AgNP/kaolin_{50:50 RT}. The rate constants for the degradation of those compounds were estimated considering a pseudo-first order rate equation, based on the linear plot of $\ln(C/C_0)$ versus the radiation time (**Figure 5-9B**).

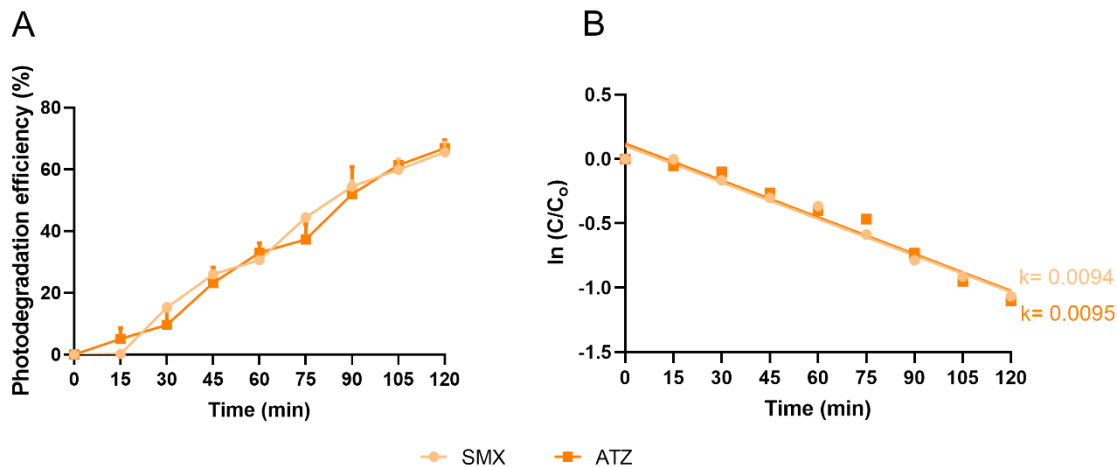


Figure 5-9. Photocatalytic efficiency of AgNP/kaolin_{50:50 RT} on the degradation of both organic compounds: (A) Photocatalytic efficiency vs time and (B) $\ln(C/C_0)$ vs time.

The photodegradation of SMX and ATZ increased over time. The nanocomposite is efficient to degrade both compounds and the reactional path is similar between SMX and ATZ, with 65.6% and 66.8% of degradation at 120 min, respectively. These results suggest that the same catalytic mechanism as in IC degradation is followed during the degradation of both compounds.

The catalytic assays revealed that after 120 min of reaction, the degradation under visible light irradiation and in the presence of AgNP/kaolin_{50:50 RT} follows the sequence: SMX \approx ATZ < IC. TOC analysis indicated that after 120 min, 44.0%, 42.8% and 14.6% mineralization were achieved for ATZ, SMX and IC, respectively. The difference between degradation and mineralization is the presence of intermediates during the photodegradation of pollutants that can be mineralized by the continuing the process for a longer period of time. The high mineralization efficiency obtained for ATZ and for SMX, shows that the nanocomposite was very effective to mineralize these pollutants, with similar ratio degradation:mineralization, 1.5.

The stability of the catalyst, after the photodegradation reaction of IC, SMX and ATZ, was studied by FTIR and compared with the fresh catalyst, AgNP/kaolin_{50:50 RT} (**Figure 5-10**).

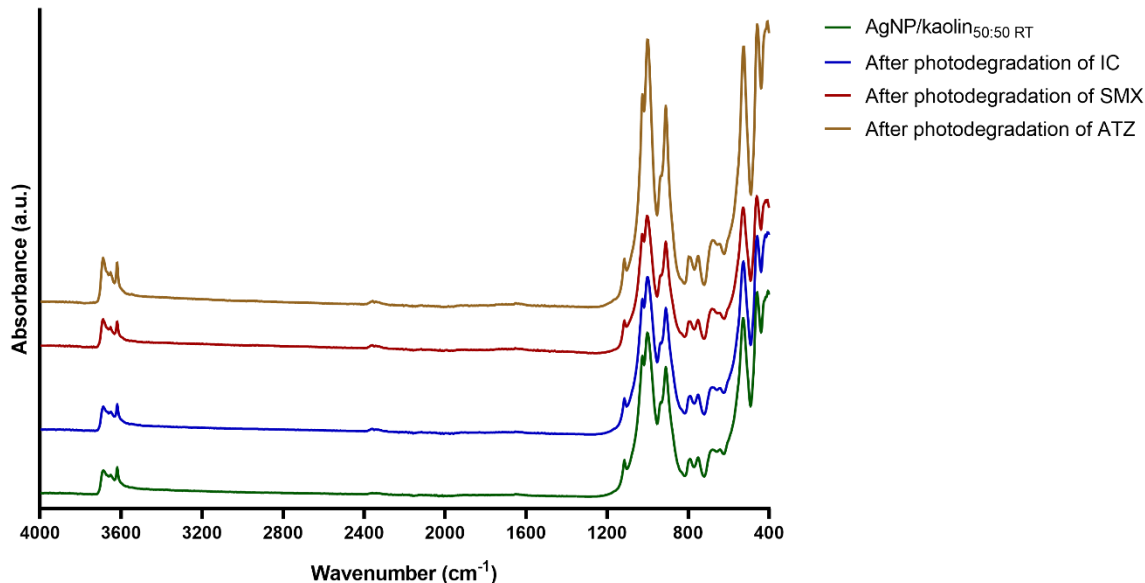


Figure 5-10. FTIR spectra of AgNP/kaolin_{50:50 RT} before and after the photodegradation of ATZ, SMX and IC.

All the FTIR spectra of the catalysts after the photodegradation of ATZ, SMX and IC are very similar between them and present the same absorbance bands typical of the pristine material, which suggest that the catalysts are stable after the degradation reaction.

5.3.3 Effect of spectrum, wavelength and intensity of visible light

For effective visible light-driven photocatalysis, the choice of the light source is of utmost importance. In this study, the photocatalytic activity of AgNP/kaolin_{50:50 RT} was evaluated by the degradation of a model pollutant, IC dye, under different visible light emitted by LED lamps. Compared to traditional visible light sources like fluorescent tubes and xenon lamps, LED lamps have a long lifespan and relatively low energy usage [42]. LED can emit powerful single-colored light in a relatively restricted range of wavelengths that can be used to assess the effect of spectrum, wavelength and intensity on photocatalytic degradation [43]. The effects of spectrum, wavelength and intensity of visible light on the decolorization efficiency and mineralization of IC are shown in **Table 5-5**.

Table 5-5. Spectrum, wavelength and intensity of visible light on the decolorization efficiency and mineralization of IC dye using AgNP/kaolin_{50:50 RT} as photocatalyst.

Visible light emitted by LED lamps λ_{max} (nm)	Radiance (W.m ⁻² .sr ⁻¹) 400 to 500 nm	Decolorization efficiency after 120 min (%)	Mineralization after 120 min (%)
White light I ₂	14.21	77.4±1.5	14.6
Blue light I ₁ , 460	0.560	9.1±1.1	4.0
Blue light I ₂ , 460	7.170	84.9±2.6	14.4
Blue light I ₂ , 440	8.770	85.9±2.4	13.6
Red light I ₁ , 630	0.001	n.d.	n.d.

not detected (n.d.)

The results indicate that the spectrum of white light is effective to degrade the IC dye, achieving 77% of decolorization and 15% of mineralization. To understand the effect of the spectrum it was decided to test blue light with λ_{max} at 460 nm and red light with λ_{max} at 630 nm at the same intensity light. The results showed low photocatalytic performance, in which 9% of IC was degraded and only 4% was mineralized after 120 min under blue light at 460 nm, and no degradation was found under red light. Increasing the light intensity, the blue light at 460 nm was able to degrade 85% and mineralize 14% of initial IC. So, a positive relationship is obtained between the decolorization efficiency and visible light intensity. Changing the λ_{max} of blue light to 440 nm, the results were similar, that is 86% of IC degradation and 14% of IC mineralization.

5.4 CONCLUSIONS

The use of sustainable alternatives to present water treatment methods is highly desirable. In this work, it is proposed to use a sustainable material as efficient support for green AgNP synthesis using ELE. The existing phytochemicals in ELE convert the silver ions to AgNP on a natural support. The AgNP/kaolin reached the best catalytic results on the degradation of IC, ATZ and SMX molecules under visible light. This study encourages the use of natural and waste materials as efficient supports for

green AgNP and the respective optimization of the biosynthetic process in order to make it sustainable, efficient and cost-effective. Additional studies on the recycling and the leaching rate of nanocomposite should be performed.

5.5 REFERENCES

- [1] H. Zhang, X. Liu, J. Ma, C. Lin, C. Qi, X. Li, Z. Zhou, G. Fan, Activation of peroxymonosulfate using drinking water treatment residuals for the degradation of atrazine, *J. Hazard. Mater.* 344 (2018) 1220–1228. <https://doi.org/10.1016/j.jhazmat.2017.11.038>.
- [2] A. Shawky, R.M. Mohamed, I.A. Mkhallid, M.A. Youssef, N.S. Awwad, Visible light-responsive Ag/LaTiO₃ nanowire photocatalysts for efficient elimination of atrazine herbicide in water, *J. Mol. Liq.* 299 (2020) 112163. <https://doi.org/10.1016/j.molliq.2019.112163>.
- [3] M. Chen, C. Guo, S. Hou, L. Wu, J. Lv, C. Hu, Y. Zhang, J. Xu, In-situ fabrication of Ag/P-g-C₃N₄ composites with enhanced photocatalytic activity for sulfamethoxazole degradation, *J. Hazard. Mater.* 366 (2019) 219–228. <https://doi.org/10.1016/j.jhazmat.2018.11.104>.
- [4] B. Pant, M. Park, J.H. Lee, H.-Y. Kim, S.-J. Park, Novel magnetically separable silver-iron oxide nanoparticles decorated graphitic carbon nitride nano-sheets: A multifunctional photocatalyst via one-step hydrothermal process, *J. Colloid Interface Sci.* 496 (2017) 343–352. <https://doi.org/10.1016/j.jcis.2017.02.012>.
- [5] A.Q. Malik, T. ul G. Mir, D. Kumar, I.A. Mir, A. Rashid, M. Ayoub, S. Shukla, A review on the green synthesis of nanoparticles, their biological applications, and photocatalytic efficiency against environmental toxins, *Environ. Sci. Pollut. Res.* 30 (2023) 69796–69823. <https://doi.org/10.1007/s11356-023-27437-9>.
- [6] J. Chaudhary, G. Tailor, M. Yadav, C. Mehta, Green route synthesis of metallic nanoparticles using various herbal extracts: A review, *Biocatal. Agric. Biotechnol.* 50 (2023) 102692. <https://doi.org/10.1016/j.cbab.2023.102692>.
- [7] N. Rani, P. Singh, S. Kumar, P. Kumar, V. Bhankar, K. Kumar, Plant-mediated synthesis of nanoparticles and their applications: A review, *Mater. Res. Bull.* 163 (2023) 112233. <https://doi.org/10.1016/j.materresbull.2023.112233>.
- [8] M. Honarmand, M. Golmohammadi, A. Naeimi, Green synthesis of SnO₂-bentonite nanocomposites for the efficient photodegradation of methylene blue and eriochrome black-T, *Mater. Chem. Phys.* 241 (2020) 122416. <https://doi.org/10.1016/j.matchemphys.2019.122416>.
- [9] T. Parandhaman, M.D. Dey, S.K. Das, Biofabrication of supported metal nanoparticles: exploring the bioinspiration strategy to mitigate the environmental challenges, *Green Chem.* 21 (2019) 5469–5500. <https://doi.org/10.1039/C9GC02291K>.
- [10] J. Zhao, X. Wang, S.A. Hoang, N.S. Bolan, M.B. Kirkham, J. Liu, X. Xia, Y. Li, Silver nanoparticles in aquatic sediments: Occurrence, chemical transformations, toxicity, and analytical methods, *J. Hazard. Mater.* 418 (2021) 126368. <https://doi.org/10.1016/j.jhazmat.2021.126368>.
- [11] M. Gao, J. Chang, Z. Wang, H. Zhang, T. Wang, Advances in transport and toxicity of

- nanoparticles in plants, *J. Nanobiotechnology*. 21 (2023) 75. <https://doi.org/10.1186/s12951-023-01830-5>.
- [12] J. Kang, N. Zhou, Y. Zhang, Y. Wang, C. Song, X. Gao, G. Song, J. Guo, L. Huang, T. Ma, X. Yu, Synthesis, multi-site transformation fate and biological toxicity of silver nanoparticles in aquatic environment: A review, *Environ. Technol. Innov.* 32 (2023) 103295. <https://doi.org/https://doi.org/10.1016/j.eti.2023.103295>.
- [13] A. Kumar, G. Sharma, M. Naushad, A.H. Al-Muhtaseb, A. García-Peñas, G.T. Mola, C. Si, F.J. Stadler, Bio-inspired and biomaterials-based hybrid photocatalysts for environmental detoxification: A review, *Chem. Eng. J.* 382 (2020) 122937. <https://doi.org/https://doi.org/10.1016/j.cej.2019.122937>.
- [14] M. Bordbar, N. Mortazavimanesh, Biosynthesis of waste pistachio shell supported silver nanoparticles for the catalytic reduction processes, *IET Nanobiotechnology*. 12 (2018) 939–945. <https://doi.org/https://doi.org/10.1049/iet-nbt.2017.0266>.
- [15] C. Li, N. Zhu, S. Yang, X. He, S. Zheng, Z. Sun, D.D. Dionysiou, A review of clay based photocatalysts: Role of phyllosilicate mineral in interfacial assembly, microstructure control and performance regulation, *Chemosphere*. 273 (2021) 129723. <https://doi.org/https://doi.org/10.1016/j.chemosphere.2021.129723>.
- [16] G. Gopal, H. Sankar, C. Natarajan, A. Mukherjee, Tetracycline removal using green synthesized bimetallic nZVI-Cu and bentonite supported green nZVI-Cu nanocomposite: A comparative study, *J. Environ. Manage.* 254 (2020) 109812. <https://doi.org/https://doi.org/10.1016/j.jenvman.2019.109812>.
- [17] T. Baran, M. Nasrollahzadeh, Facile fabrication of magnetically separable palladium nanoparticles supported on modified kaolin as a highly active heterogeneous catalyst for Suzuki coupling reactions, *J. Phys. Chem. Solids*. 146 (2020) 109566. <https://doi.org/https://doi.org/10.1016/j.jpcs.2020.109566>.
- [18] F. Lashkarizadeh, Green synthesis of ZnO/eggshell nanocomposite using ferulago macrocarpa extract and its photocatalytic and antimicrobial activity in water disinfection, *Inorg. Nano-Metal Chem.* (2021) 1–12. <https://doi.org/10.1080/24701556.2021.1983837>.
- [19] M. Rashidi, M.R. Islami, Green synthesis of Ag@AgCl/Elaeagnus angustifolia seed nanocomposite using Elaeagnus angustifolia leaves: an amazing nanophotocatalyst with highly photocatalytic activity under sunlight irradiation, *Environ. Sci. Pollut. Res.* 27 (2020) 21455–21467. <https://doi.org/10.1007/s11356-020-08598-3>.
- [20] S. Sohrabnezhad, A. Seifi, The green synthesis of Ag/ZnO in montmorillonite with enhanced photocatalytic activity, *Appl. Surf. Sci.* 386 (2016) 33–40. <https://doi.org/https://doi.org/10.1016/j.apsusc.2016.05.102>.
- [21] PubChem, (n.d.). <https://pubchem.ncbi.nlm.nih.gov/> (accessed May 2, 2023).
- [22] C. Quintelas, F. Costa, T. Tavares, Bioremoval of diethylketone by the synergistic combination of microorganisms and clays: uptake, removal and kinetic studies, *Environ. Sci. Pollut. Res.* 20 (2013) 1374–1383. <https://doi.org/10.1007/s11356-012-1055-1>.
- [23] C. de S.F. Gomes, J.B.P. Silva, Minerals and clay minerals in medical geology, *Appl. Clay Sci.* 36 (2007) 4–21. <https://doi.org/https://doi.org/10.1016/j.clay.2006.08.006>.
- [24] N. Kumari, C. Mohan, Basics of Clay Minerals and Their Characteristic Properties, in: 2021. <https://doi.org/10.5772/intechopen.97672>.
- [25] W. Chang, S. Liu, A. Qileng, W. Liu, Y. Liu, In-situ synthesis of monodispersed Au nanoparticles

- on eggshell membrane by the extract of *Lagerstroemia speciosa* leaves for the catalytic reduction of 4-nitrophenol, *Mater. Res. Express.* 6 (2018) 15002. <https://doi.org/10.1088/2053-1591/aae2f0>.
- [26] M. Rashidi, M.R. Islami, A.M. Tikdari, Green synthesis of Pd nanoparticles supported on modified Nonpareil almond shell using almond hull extract: a beneficial nanocatalyst for convenient reduction of organic dyes, *J. Mater. Sci. Mater. Electron.* 30 (2019) 18111–18122. <https://doi.org/10.1007/s10854-019-02164-5>.
- [27] A. Taghizadeh, K. Rad-Moghadam, Green fabrication of Cu/pistachio shell nanocomposite using *Pistacia Vera L.* hull: An efficient catalyst for expedient reduction of 4-nitrophenol and organic dyes, *J. Clean. Prod.* 198 (2018) 1105–1119. <https://doi.org/https://doi.org/10.1016/j.jclepro.2018.07.042>.
- [28] Z. Dolatkah, A. Mohammadkhani, S. Javanshir, A. Bazgir, Peanut shell as a green biomolecule support for anchoring Cu₂O: a biocatalyst for green synthesis of 1,2,3-triazoles under ultrasonic irradiation, *BMC Chem.* 13 (2019) 97. <https://doi.org/10.1186/s13065-019-0612-9>.
- [29] M. Bordbar, N. Mortazavimanesh, Green synthesis of Pd/walnut shell nanocomposite using *Equisetum arvense L.* leaf extract and its application for the reduction of 4-nitrophenol and organic dyes in a very short time, *Environ. Sci. Pollut. Res.* 24 (2017) 4093–4104. <https://doi.org/10.1007/s11356-016-8183-y>.
- [30] T.F. Akinhanmi, E.A. Ofudje, A.I. Adeogun, P. Aina, I.M. Joseph, Orange peel as low-cost adsorbent in the elimination of Cd(II) ion: kinetics, isotherm, thermodynamic and optimization evaluations, *Bioresour. Bioprocess.* 7 (2020) 34. <https://doi.org/10.1186/s40643-020-00320-y>.
- [31] M. Baláž, E. V Boldyreva, D. Rybin, S. Pavlović, D. Rodríguez-Padrón, T. Mudrinić, R. Luque, State-of-the-Art of Eggshell Waste in Materials Science: Recent Advances in Catalysis, Pharmaceutical Applications, and Mechanochemistry., *Front. Bioeng. Biotechnol.* 8 (2020) 612567. <https://doi.org/10.3389/fbioe.2020.612567>.
- [32] F. Sessa, G. Merlin, P. Canu, Pine bark valorization by activated carbons production to be used as VOCs adsorbents, *Fuel.* 318 (2022) 123346. <https://doi.org/https://doi.org/10.1016/j.fuel.2022.123346>.
- [33] A. Tironi, M. Trezza, E. Irassar, A.N. Scian, Thermal Treatment of Kaolin: Effect on the Pozzolanic Activity, *Procedia Mater. Sci.* 1 (2012) 343–350. <https://doi.org/10.1016/j.mspro.2012.06.046>.
- [34] W. Moyo, T.T.I. Nkambule, Green synthesis of kaolin-supported nanoscale zero-valent iron using *camellia sinensis* extract for effective adsorption of dissolved organic matter: Preparation, adsorption, and Fenton regenerative valorization of “spent” adsorbent, *Environ. Nanotechnology, Monit. Manag.* 18 (2022) 100697. <https://doi.org/https://doi.org/10.1016/j.enmm.2022.100697>.
- [35] N. Rakhshan, M. Mansournia, F. Jookar Kashi, Plant Extract-Strategy Using *Teucrium Polium* Stems to Green Synthesize Ag/AgCl Bionanocomposite Imprinted on Fe₃O₄/kaolinite and Potentials in Catalytic and Chemosensor Applications, *Arab. J. Chem.* (2022) 103719. <https://doi.org/https://doi.org/10.1016/j.arabjc.2022.103719>.
- [36] M. Konsolakis, N. Kaklidis, G.E. Marnellos, D. Zaharaki, K. Komnitsas, Assessment of biochar as feedstock in a direct carbon solid oxide fuel cell, *RSC Adv.* 5 (2015) 73399–73409. <https://doi.org/10.1039/C5RA13409A>.

- [37] Y. Dou, F. Tu, Y. Wu, X. Wang, G. Lu, L. Zhao, Facile preparation of Kaolin supported silver nanoparticles mediated by *Thymbra spicata* extract and investigation of the anti-human lung cancer properties, *J. Saudi Chem. Soc.* 25 (2021) 101303. <https://doi.org/https://doi.org/10.1016/j.jscs.2021.101303>.
- [38] M.O. Alfred, M.O. Omorogie, O. Bodede, R. Moodley, A. Ogunlaja, O.G. Adeyemi, C. Günter, A. Taubert, I. Iermak, H. Eckert, I.D.A. Silva, A.S.S. de Camargo, A. de Jesus Motheo, S.M. Clarke, E.I. Unuabonah, Solar-active clay-TiO₂ nanocomposites prepared via biomass assisted synthesis: Efficient removal of ampicillin, sulfamethoxazole and artemether from water, *Chem. Eng. J.* 398 (2020) 125544. <https://doi.org/https://doi.org/10.1016/j.cej.2020.125544>.
- [39] C. Elmi, S. Guggenheim, R. Gieré, Surface Crystal Chemistry of Phyllosilicates Using X-Ray Photoelectron Spectroscopy: A Review, *Clays Clay Miner.* 64 (2016) 537–551. <https://doi.org/10.1346/CCMN.2016.064033>.
- [40] P.P.A. Jose, M.S. Kala, N. Kalarikkal, S. Thomas, Silver-attached reduced graphene oxide nanocomposite as an eco-friendly photocatalyst for organic dye degradation, *Res. Chem. Intermed.* 44 (2018) 5597–5621. <https://doi.org/10.1007/s11164-018-3443-8>.
- [41] A.P. Chowdhury, B.H. Shambharkar, BiOBr-Ag₈SnS₆ heterostructured nanocomposite photocatalysts: Synthesis, characterization, and photocatalytic application, *Asia-Pacific J. Chem. Eng.* 13 (2018) e2182. <https://doi.org/https://doi.org/10.1002/apj.2182>.
- [42] T. Pulli, T. Dönsberg, T. Poikonen, F. Manoocheri, P. Kärhä, E. Ikonen, Advantages of white LED lamps and new detector technology in photometry, *Light Sci. Appl.* 4 (2015) e332–e332. <https://doi.org/10.1038/lssa.2015.105>.
- [43] Y. Chen, A. Lu, Y. Li, H.Y. Yip, T. An, G. Li, P. Jin, P.-K. Wong, Photocatalytic inactivation of *Escherichia coli* by natural sphalerite suspension: Effect of spectrum, wavelength and intensity of visible light, *Chemosphere.* 84 (2011) 1276–1281. <https://doi.org/https://doi.org/10.1016/j.chemosphere.2011.05.055>.

CHAPTER 6 GENERAL CONCLUSIONS AND FUTURE PERSPECTIVES

The final chapter of this PhD thesis provides a comprehensive summary of the main results, along with the most pertinent conclusions. Additionally, some suggestions for potential future research directions are forwarded in this topic.

6.1 GENERAL CONCLUSIONS

This thesis aims at the definition and development of an efficient nanocomposite based on eco-friendly nanoparticles supported on natural materials to be used for the removal of pollutants from water. Thus, defining a clean technology that may rehabilitate water without resort to dangerous chemicals and with low waste generation.

Silver nanoparticles (AgNP) were the nano-entities of choice, as they are known to have excellent catalytic and antibacterial properties and were exploited through sustainable synthesis and subsequent immobilization in environmental friendly materials. Among other bio-resources, plant extracts have shown their effectiveness in the biosynthesis of AgNP.

In this thesis, the importance of the selection of plant extracts as well as their chemical characterization before the synthesis of AgNP is proved. A screening involving a range of different aqueous plant extracts obtained from *Eucalyptus globulus*, *Pinus pinaster*, *Citrus sinensis*, *Cedrus atlantica* and *Camellia sinensis* was performed to select the best extracts to synthesize highly stable AgNP. Optimal conditions of extraction (raw material, extraction time and temperature) were determined using as a basis the total phenolic and flavonoid content of each extract. Water was used as the extraction solvent as it is the safest, cheapest and most environmental friendly solvent. From all plant by-products tested, the eucalyptus leaves (ELE), green tea (GTE) and black tea (BTE) extracts obtained at 50 °C for 30 min, were the ones with lower associated energy costs and were selected as promising candidates to biosynthesize AgNP. Here the importance of the previous optimization of the extraction process was emphasized, guaranteeing the extraction's efficiency and reducing energetic costs, making the process more sustainable.

For the green synthesis of AgNP with the different pre-selected plant by-products, we started with a ratio of 1:1 (metal:extract) at 50 °C for 60 min. The results showed the formation of AgNP with a wide range of particle sizes (40.6 to 86.4 nm), confirming that the amounts and types of phenolic compounds are two of the main reasons for the variability in the sizes of AgNP. The Energy-dispersive X-ray (EDX) spectra of the biosynthesized AgNP showed the presence of silver as well as magnesium, oxygen and chloride, resulting from the organic compounds present in the extracts. The quantities determined by EDX analysis revealed that AgNP obtained with GTE retained 83.2% of silver (4.90 mmol of Ag), in concordance with the obtained by the ferric reducing antioxidant power (FRAP) method, indicating that the GTE shows stronger reducing activity. The AgNP showed high negative values of zeta potential (-31.8 to -36.3 mV), meaning the coordination

with anionic stabilizing agents and the stability of the AgNP colloidal solution, as a result to electrostatic repulsion between the negative charges. Fourier transform infrared spectroscopy (FTIR) results support that the functional groups of each extract play essential roles in the reduction of Ag⁺ ions to biosynthesize AgNP.

The antibacterial activity of selected extracts and biosynthesized AgNP was investigated against both Gram-negative bacteria, *Escherichia coli*, *Pseudomonas putida* S12 and *Vibrio spp.* and Gram-positive bacteria, *Bacillus megaterium*, *Staphylococcus aureus* and *Streptococcus equisimillis*. The extracts were only effective against *Vibrio spp.* and the ELE showed the highest inhibition action (11.5±0.5 mm). ELE-AgNP, GTE-AgNP and BTE-AgNP were potentially effective in suppressing bacterial growth within a range of inhibition zones from 7.3±0.4 to 14±1 mm. This antibacterial screening confirmed that green AgNP possess efficient antimicrobial potential against bacteria and could be used as alternative disinfectants in wastewater remediation.

The photocatalytic potential of biosynthesized ELE-AgNP was assessed by evaluating the photodegradation of a model dye compound, Indigo carmine (IC) dye, under direct sunlight and with different dosages of ELE-AgNP (0.5 and 1.0 g.L⁻¹). The kinetics assessment confirmed that the photocatalytic reaction follows a pseudo-first-order model, with an apparent rate constant (k) of 0.0178 and 0.03612 min⁻¹ using 0.5 and 1.0 g.L⁻¹ of ELE-AgNP, respectively. The increase of the dosage of the catalyst led to higher photocatalytic activity, indicating that the amount of ELE-AgNP influences the degradation rate, as more electron-pairs are formed which increases the rate of reaction.

The synthesis of AgNP from ELE, a raw plant in Portugal, was optimized and characterized. Different temperatures (RT and 50 °C) and ratios, between AgNO₃ and ELE (1:1 and 1:2), were tested. The results indicated that AgNP obtained at 50 °C presents the characteristic Surface Plasmon Resonance (SPR) with a λ_{max} at 458 and 464 nm for AgNP_{50°C:1:1} and AgNP_{50°C:1:2}, respectively. These results confirm in a first approach, the successful synthesis of ELE-AgNP. On the other hand, ELE-AgNP obtained at RT, ELE-AgNP_{RT:1:1}, does not show the characteristic SPR. Also from scanning electron microscope (SEM) analysis is not possible to confirm the synthesis of ELE-AgNP at RT. The synthesis at 50 °C showed the formation of ELE-AgNP with different shapes and sizes. With a low amount of extract (ELE-AgNP_{50°C:1:1}), the particles are irregularly shaped, while the higher amount of extract (ELE-AgNP_{50°C:1:2}) results in the formation of particles with more defined shapes, mostly spherical. From X-ray photoelectron spectroscopy (XPS) measurements was possible to conclude that the increase of the preparation temperature of ELE-AgNP affects the quantity of the elements on the surface. For the sample ELE-AgNP_{RT:1:1}, Ag⁺ species is dominant with 64.3% contribution, suggesting

that the reduction of silver is not completed at this temperature, followed by 20.2% of metallic Ag and 15.5% of AgO. The increase in temperature changes the oxidation state of the same silver species and the presence of the silver oxide is improved with 38.2% of AgO and Ag₂O, followed by only 19.3% of Ag⁺ and 42.6% of Ag. At 50 °C, the silver reduction occurs and this indicates that increasing the amount of extract in the synthesis of ELE-AgNP at 50 °C can be sufficient to reduce the Ag⁺ ions. Thermal stability of ELE-AgNP_{50°C:1:1} and ELE-AgNP_{50°C:1:2} showed a weight loss smaller than 24% and 22%, respectively, up to 800 °C. These results suggest that the amount of ELE to biosynthesize ELE-AgNP does not influence their thermal properties. The zeta potential showed that ELE-AgNP have a negatively charged surface, which implies strong repellent forces among the particles leading to aggregation prevention and stabilization of the ELE-AgNP in the medium. After 3 months, the zeta potential values were -32.0±0.5 mV and -31.5±0.3 mV for ELE-AgNP_{50°C:1:1} and ELE-AgNP_{50°C:1:2}, respectively, and this proved that the nanoparticles are stable. The XRD patterns of ELE-AgNP_{50°C:1:2} revealed a good crystallinity of the biosynthesized AgNP (83.3%) and using the Debye-Scherrer formula the average crystallite size of ELE-AgNP_{50°C:1:2} is found to be 25.42 nm.

In the results of the eucalyptus leaves extraction, the yield was 18.4% and the major constituents of the extract were 1,8-cineole or eucalyptol (72.3%), followed by pinocarveol (7.9%) and pinocarpone (2.1%). Also, twelve phenolic compounds were detected, including flavonoids and phenolic acids. Some phenolic compounds of the ELE, before and after biosynthesis of AgNP_{50°C:1:2}, were quantified and after synthesis of AgNP_{50°C:1:2}, the amount of the catechin, ellagic acid, rutin, gallic acid, quercetin and kaempferol decreased and this drop was more accentuated for gallic acid, kaempferol and catechin, with a reduction of 51, 31 and 26%, respectively, indicating that these compounds can be used as reducing and/or capping agents in the reaction of synthesis of ELE-AgNP.

The antibacterial activity of the biosynthesized ELE-AgNP_{50°C:1:2} at different concentrations (1-10 mg.mL⁻¹) was evaluated and the AgNP exhibited efficient antibacterial activity against both gram-positive and gram-negative bacteria: *Escherichia coli* (15 mm maximum zone of clearance) and *Staphylococcus aureus* (14 mm maximum zone of clearance) and the bacterial inhibition depends on ELE-AgNP concentration.

The photocatalytic activity of biosynthesized ELE-AgNP_{50°C:1:2} on the degradation of IC dye as a wastewater pollutant model under ultraviolet (UV) light, visible light and sunlight irradiation was evaluated during 120 min of reaction. High photodegradation of IC dye under UV, visible light and sunlight radiation was successfully achieved with sunlight as the best compromise. The *k* calculated is found to be 0.0476, 0.0152 and 0.0039 min⁻¹ for sunlight, visible and UV light, respectively, and confirms that sunlight is the best radiation to promote

the photodegradation. The phytotoxicity effect of the treated solution after photodegradation germination tests with corn kernels were performed. The results confirm low phytotoxicity after the photocatalytic degradation processes mainly with sunlight radiation.

Finally, it is proposed to use a sustainable material (clays and waste materials) as efficient support for green ELE-AgNP synthesis. The existing phytochemicals in ELE convert the silver ions to AgNP on sustainable support without adding any toxic or expensive organic solvent, surfactant or hazardous chemicals. AgNP/composites based in clays (bentonite, kaolin, sepiolite and vermiculite) or waste materials (eggshell, orange peel, peanuts shell, pine bark, pistachio shell and walnut shell) were evaluated as photocatalysts for degradation of IC dye under visible light. The best photocatalyst, the nanocomposite of AgNP/kaolin, was selected and the influence of biosynthesis experimental parameters for AgNP/kaolin on the rate of degradation was studied. The catalytic results showed that increasing the amounts of AgNO₃ and ELE, thus fabricating more AgNP, the photocatalytic performance increases, with 58% and 77% IC degradation for AgNP/kaolin_{20:20 RT} and AgNP/kaolin_{50:50 RT}, respectively, after 120 min of reaction. The evaluation of active species responsible for the photocatalytic degradation of IC showed that O₂^{•-} radical and H[•] are species involved in the reaction. The UV/Vis study displayed that AgNP/composites obtained at 50 °C showed the characteristic SPR, whereas the nanocomposites obtained at RT do not show SPR. This behavior could indicate a different distribution of the ELE-AgNP on the surface of the kaolin particles. TEM images revealed that the temperature of the synthesis affects the size of the particles, in this case, the ELE-AgNP dispersed in the kaolin support. The ELE-AgNP supported on kaolin and produced at 50 °C are spherical with diameters ranging from 29 to 127 nm. The spherical ELE-AgNP synthesized at RT show diameters ranging from 5 to 25 nm. The images reveal that by increasing the temperature of biosynthesis, the ELE-AgNP appear to cluster and to spread out more throughout the clay support.

The photocatalytic performance of AgNP/kaolin_{50:50 RT} nanocomposite was evaluated on the degradation process of sulfamethoxazole (SMX) and atrazine (ATZ) under visible light. The nanocomposite is efficient to degrade both compounds and the reactional path is similar between SMX and ATZ, with 65.6% and 66.8% of degradation at 120 min of reaction, respectively.

Comparing the performance of photodegradation of IC at 10 mg.L⁻¹ with ELE-AgNP in suspension and ELE-AgNP immobilized on kaolin, the *k* calculated is found to be 0.0152 and 0.0115 min⁻¹, respectively, confirming that the immobilization of nanoparticles can be a solution for efficient photodegradation of aqueous pollutants.

6.2 FUTURE WORK

This thesis may close the existing literature gaps on the use of sustainable materials as supports for biogenic metal nanoparticles (MNP) to be applied on wastewater treatment, aside from the benefits to be taken on future developments in this field. This study encourages the application of bio-resources in the synthesis of AgNP as well as the use of sustainable alternatives as efficient supports for green AgNP and the respective optimization of the biosynthetic process in order to make it sustainable, efficient and cost-effective.

Although the obtained results seem to be promising in this research field, some aspects need further research. The present thesis explores the application of ELE as a promising source of biomolecules to synthesize AgNP, but for the future, the application of other plant extracts may be tested. A viable alternative material may be evergreen plants, which can circumvent seasonal time constraints. These plant resources have a high practicability for green synthesis in terms of availability because their collections are not restricted by time or season. Agricultural wastes, which complies with the waste usage concept for environmental preservation, are another appropriate raw material. Future studies should take into account the seasonal and geographical availability and consider the material extraction procedure with the aim of streamlining the extraction process as much as possible.

Future work should focus on the specific mechanism of green synthesis of AgNP in order to establish the best strategy for its industrial application. This thesis focused specifically on phenolic compounds participating in the biosynthesis of AgNP however, several other biomolecules are in the aqueous extract and may participate in the production of AgNP. Carbohydrates and proteins should be the focus of future studies, as they are may contribute to the stability of MNP.

Immobilization of MNP on sustainable materials opened a new perspective for use of wastes or low-cost materials. A preliminary study regarding the potential of different sustainable materials as support for AgNP was conducted in this thesis. However, low photodegradation efficiency was obtained with some materials probably due to their specific features. Therefore, further evaluations of the optimal relative amount of extract, metal and temperature reaction should be explored in order to optimize the process of immobilization and to explore the potential of the photodegradation of water pollutants. Some more sustainable materials may be considered as support for green MNP and material surface treatments should be explored to enhance the quality of the support of AgNP.

The obtained results showed the efficient photodegradation of indigo carmine dye, of the herbicide atrazine and of the antibiotic sulfamethoxazole at lab-scale. In the future it is important to contemplate the degradation of other hazardous and persistent pollutants as well as to conduct research at pilot-scale in order to evaluate the system efficiency in real effluents coming from wastewater treatment plants (WWTP), industry or agricultural runoffs and the process economic feasibility.

In addition, stability, reusability and leaching rate of green nanomaterial should be considered. The ideal nanocomposite ought to be easily separated from the reaction medium, recycled and reused for other runs without marked loss of activity. Also the storage of nano-entities needs to be considered.